CRANFIELD UNIVERSITY
LIBRARY

CRANFIELD UNIVERSITY

SCHOOL OF MECHANICAL ENGINEERING

Ph.D. Thesis

Academic Year 1997-98

Ian Bennett

The Design and Analysis of Pipe Diffusers for Centrifugal Compressors

Supervisor: Prof. Robin. L. Elder

December 1997

ProQuest Number: 10820897

All rights reserved

INFORMATION TO ALL USERS
The quality of this reproduction is dependent upon the quality of the copy submitted.

In the unlikely event that the author did not send a complete manuscript
and there are missing pages, these will be noted. Also, if material had to be removed,
a note will indicate the deletion.



ProQuest 10820897

Published by ProQuest LLC (2018). Copyright of the Dissertation is held by Cranfield University.

All rights reserved.
This work is protected against unauthorized copying under Title 17, United States Code
Microform Edition © ProQuest LLC.

ProQuest LLC.
789 East Eisenhower Parkway
P.O. Box 1346
Ann Arbor, MI 48106 – 1346

CRANFIELD UNIVERSITY
LIBRARY

ABSTRACT

Diffusers are necessary to convert the high velocity head of centrifugal compressor discharge flow into useful static pressure. One diffuser type that has shown a great deal of promise, particularly at high pressure ratios, are pipe diffusers. These have been successfully incorporated into centrifugal compressor stages in North America since the early 1970's. With their commercial sensitivity, however, little design or detailed flow information has been published, and most of this literature is old, dating back twenty years to the design's conception.

This thesis is a compilation of pipe diffuser information, formed from the limited literature works and an intensive experimental parametric study. Two themes run through this thesis and are brought about by different reader needs. The first need is for design information. This must show the strengths and weakness of pipe diffusers and be of sufficient accuracy to potentially produce designs at the first attempt. The second need is to understand the flows within the diffuser itself, in order that through this knowledge further improvements can be made. Both of these requirements are addressed in this thesis.

The studies are centred on, what was originally, a Rolls-Royce research centrifugal compressor impeller of 6:1 pressure ratio operating at 35,000 rpm with a tip speed of 533ms^{-1} consuming up to a nominal 1MW of power. Significant modifications to the original compressor assembly were made to allow modular changes of diffuser and permit detailed measurement access. Initially, a vaneless diffuser investigation was carried out with the primary aim of determining the flow entering the diffusers. This was followed by a diffuser throat sizing exercise as it is well recognised that the diffuser throat has a governing control over the complete stage performance. An exercise in changing the number of diffuser pipes was then undertaken, followed by a hybrid diffuser investigation incorporating an oval, rather than circular, cross-section. In all of these cases, detailed flow measurements were carried out using both conventional pneumatic instrumentation and a purposely developed unsteady pressure measurement data acquisition system. This system enabled detailed traverses of the diffuser throats to be undertaken. These unique measurements shed new light on the flow 'seen' by the pipe diffuser channel.

Computational investigations using computational fluid dynamics (CFD) codes are carried out to compliment the experimental investigations.

ACKNOWLEDGEMENTS

The author is indebted to staff within the University, and in particular to Prof. Robin Elder and Dr Tony Tourlidakis, both of whom volunteered important advice and guidance. In addition, the author wishes to give thanks for support given from external sources; in particular from Roger Wells (European Gas Turbines) and Mike Coney (National Power). They both contributed a great deal of industrial experience and practicality into the research.

In order to carry out the high speed experiments, a great deal of engineering support was required. For this I would like to thank, amongst others, Dick Dewar and Bob Wilson for their design and manufacturing input. In particular, much of the success of the experimental studies is due to Dick Lutley. Dick, as the project's principal technician, was able to ensure the safe and reliable running of the test facility.

Finally, thanks must go to my spouse, Sue, and son Max, both of whom allowed me to indulge in further education, and it is to them that I dedicate this work.

Ian Bennett

CONTENTS

Chapter 1 Introduction 1

1.1. OUTLINE OF THESIS 2

1.2. VANELESS DIFFUSERS 3

1.3. CASCADE DIFFUSERS 9

1.4. CHANNEL DIFFUSERS 10

1.4.1 VANELESS SPACE 11
1.4.2 SEMI-VANELESS SPACE 12
1.4.3 CHANNEL REGION 15

1.5. PIPE DIFFUSERS 17

1.5.1 REVIEW OF EXPERIMENTAL INVESTIGATIONS INTO PIPE DIFFUSERS 18
1.5.2 REVIEW OF EXISTING DESIGN INFORMATION FOR PIPE DIFFUSERS 24

1.6. CLOSURE 26

Chapter 2 Impeller Flow Studies 29

2.1. DESCRIPTION OF THE 35D TEST COMPRESSOR 30

2.2. GENERAL DESCRIPTION OF FLOWS WITHIN CENTRIFUGAL COMPRESSORS 31

2.2.1 PRIMARY FLOWS 31
2.2.2 SECONDARY FLOWS 33
2.2.3 RESULTANT FLOW 37

2.3. OVERALL PERFORMANCE OF THE 35D COMPRESSOR 38

2.4. UNSTEADY TOTAL PRESSURE TRAVERSES 41

2.4.1 ACCURACY OF MEASUREMENTS 41
2.4.2 UNSTEADY TOTAL PRESSURE READINGS 42
2.4.3 OVERALL PERFORMANCE CORRELATION 54

2.5. PNEUMATIC TRAVERSES 54

2.5.1 DETAILED FLOW MEASUREMENTS AND DISCUSSION 55
2.5.2 OVERALL PERFORMANCE FROM PNEUMATIC TRAVERSES 58

2.6. COMPUTATIONAL INVESTIGATIONS 58

2.6.1 1-D DESIGN PROGRAM 58
2.6.2 FLUENT 60
2.6.3 TURBO 3D 61
2.6.4 RAMPANT 62

2.7. CONCLUSIONS 74

Chapter 3 Pipe Diffuser Area Expansion 77

3.1. DESIGNING THE FIRST PIPE DIFFUSER TO BE TESTED **78**

3.1.1 General Philosophy 78
3.1.2 Selection of a 'Diffuser-Design' Mass Flow for Throat Sizing 79
3.1.3 Choosing the Number of Pipes 81
3.1.4 Calculating The Prominent Geometric Features 81
3.1.5 Computing the Throat Mach Number 82
3.1.6 The Geometry of the 31 Pipe Diffuser Tested 83

3.2. EXPERIMENTAL ARRANGEMENT **84**

3.3. RANGE **85**

3.4. THROAT BLOCKAGE **86**

3.4.1 Blockage Variation with Throat Area 88

3.5. STAGE PERFORMANCE AND RANGE **89**

3.6. COMPARISON WITH ROLLS-ROYCE DATA **91**

3.7. CLOSURE **92**

Chapter 4 Pipe Diffuser Sidewall Expansion 95

4.1. PIPE DIFFUSER GEOMETRIC DESIGN CONSIDERATIONS **96**

4.2. DESCRIPTION OF THE DIFFUSERS TESTED **99**

4.3. OPERATIONAL RANGE **100**

4.3.1 Effect of Operational Speed on Range 102
4.3.2 Effect of Wetted Diffuser Area on Range 103
4.3.3 Effect of Diffuser leading Edge Incidence on Range 106
4.3.4 Effect of the Number of Diffuser Passages (or Pipes) on Range 108
4.3.5 Concluded Primary Range Enhancing parameters 108

4.4. LOSSES WITHIN THE PSEUDO- AND SEMI- VANELESS SPACES **109**

4.5. THROAT BLOCKAGE **110**

4.5.1 Discrepancies in Blockage Measurements 110
4.5.2 Blockage Variation with Pipe Diffuser Design 112
4.5.3 Effect of Incidence on Throat Blockage 113

4.6. STAGE PERFORMANCE **114**

4.7. FLOW DISTORTION AND UNSTEADINESS **116**

4.8. CLOSURE **118**

Chapter 5 Detailed Flow within Pipe Diffusers 119

5.1. IMPELLER TIP 120

5.2. VANELESS, PSEUDO- AND SEMI-VANELESS SPACES 120

5.2.1 LEADING EDGE WEDGE ANGLE 126
5.2.2 IMPELLER TIP STATIC PRESSURE FIELD DISTORTION 128
5.2.3 UNSTEADY STATIC-PRESSURE MEASUREMENTS WITHIN THE PSEUDO- AND SEMI- VANELESS SPACES 129

5.3. DIFFUSER THROAT 131

5.4. COMPUTATIONAL MODELS 139

5.4.1 DISCUSSION OF PREDICTED FLOWS WITHIN THE PSEUDO- AND SEMI-VANELESS SPACES 140
5.4.2 USING RAMPANT AS A DIFFUSER DESIGN TOOL 143

5.5. CLOSURE 145

Chapter 6 Conclusions and Further Work 147

6.1. CONCLUSIONS 146

6.2. FURTHER WORK 147

References 151

APPENDIX A Overall Performance Instrumentation

A.1. PRIMARY PERFORMANCE INSTRUMENTATION A.1

A.2. PERFORMANCE DATA ACQUISITION AND ANALYSIS A.6

A.3. ACCURACY AND ERROR ESTIMATES A.14

A.4. LOCATION OF DETAILED STATIC PRESSURE TAPPINGS A.14

A.5. MEASUREMENT LOCATIONS A.18

APPENDIX B Detailed Instrumentation

B.1. PNEUMATIC PRESSURE PROBE B.1

B.2. HIGH SPEED TOTAL PRESSURE TRANSDUCERS PROBES B.10

B.3. TRAVERSE GEAR B.20

B.4. WEDGE PROBE B.28

APPENDIX C **Engineering Drawings**

APPENDIX D **Impeller Measurements at 80% Speed**

APPENDIX E **Overall Performance Data for Traverses**

APPENDIX F **Details of CFD Solver and Equations Solved**

APPENDIX G **Pipe Diffuser Geometry**

APPENDIX H **Unsteady Static Pressure Measurements within Pseudo- and Semi- Vaneless Spaces**

APPENDIX I **Pneumatic Diffuser Throat Traverses**

APPENDIX J **Unsteady Diffuser Throat Measurements**

NOMENCLATURE

A	flow area
A_g	geometric flow area
A_w	wetted flow area
B	blockage factor (define as B= flow blockage /geometric flow area)
C_f	vaneless diffuser wall friction coefficient
$C_{p,\,i\text{-}j}$	static pressure recovery coefficient $=\left(\frac{p_j - p_i}{p_{oi} - p_i}\right)$
D_h	hydraulic diameter
f( )	a function of
I	rothalpy
m	mass flow
M	Mach number
N_I	number impeller passages
N_D	number diffuser passages
p	pressure
pvs	pseudo-vaneless-space
R	gas constant
Re	Reynolds number
r	radius
s	streamline direction
svs	semi-vaneless-space
T	temperature
t	thickness
tip	impeller tip
u	blade tip velocity
v	gas velocity
w	passage width
W	relative gas velocity
X_{svs}	pathlength within semi-vaneless-space

Greek

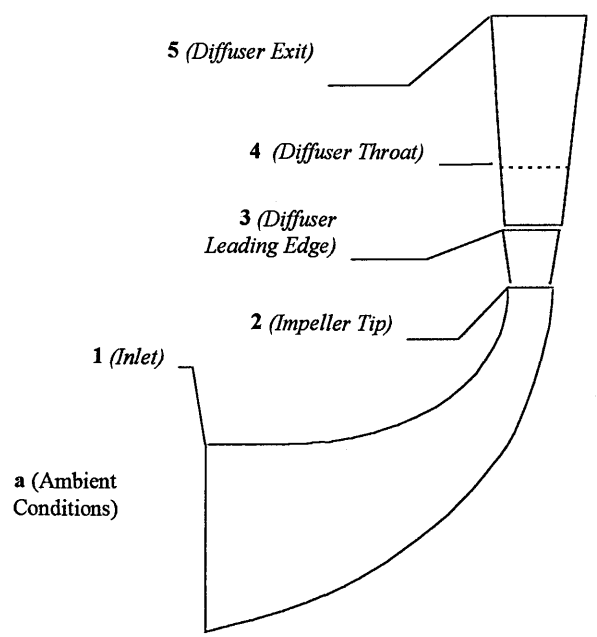
α	angle of incidence
γ	ratio of specific heats
η	isentropic efficiency
μ	viscosity

ρ	density
τ_w	wall friction
ω	impeller rotational speed
ξ	wall friction coefficient

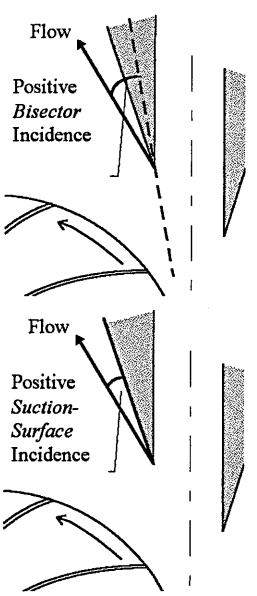
Subscripts

eff	effective
jet	jet term at impeller exit
le	diffuser leading edge
pipe	pipe bisector
ps	pressure surface
rad	radial component of velocity
ss	suction surface
tan	tangential component of velocity
th	diffuser throat
wake	wake term at impeller exit
o	total or stagnation conditions

other subscripts refer to measurement planes as defined below:



In addition, the following incidence definitions are used throughout:



CHAPTER 1
Introduction

Diffusers are necessary to regain the high kinetic energy of the discharged flow from centrifugal compressors and convert it into useful static pressure. In most practical applications they are required to operate over a wide range of incidence angles and Mach numbers, together with handling a periodic unsteady inlet flow. Despite being the least 'dynamic' aspect of the compressor assembly, they have a controlling influence over the stage performance and operational range. Approximately one third of the total system losses occurs within the diffuser (see Figure 1.1) but more importantly, surge and/or choke may be induced prematurely by poor design [e.g. Pampreen (1993)].

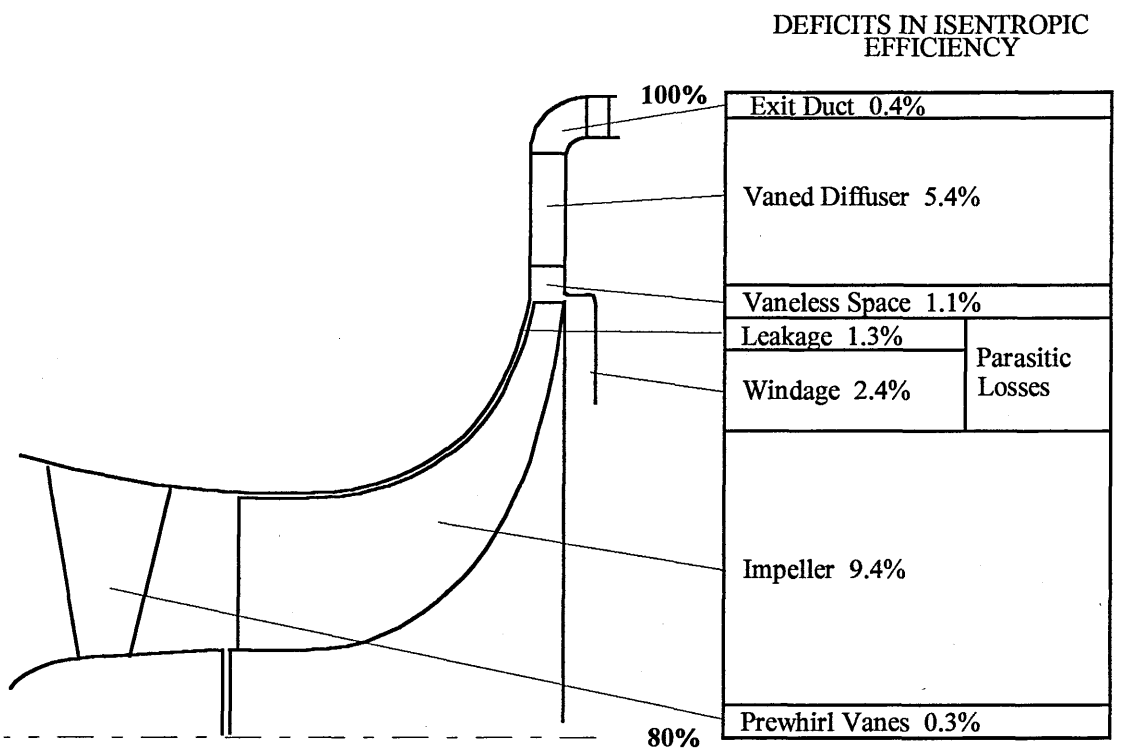


Figure 1.1 *Loss Breakdown within an 8:1 Pressure Ratio Compressor [Came (1977)]*

Over the years many types of diffusing system have been developed, each with its own advantages and disadvantages. One particular type that has had great commercial impact, but for which there is little published information, is the pipe diffuser. The limited literature on pipe diffusers has presented them as giving superior performance when operating with high leading edge Mach numbers, making the design particularly suitable for high pressure ratio centrifugal compressors. In addition, it has been argued that the elliptic leading edge of the pipe diffuser is superior to alternative vaned designs due to better incidence matching across the blade width. Predominantly, this information came from literature that originated from the USA and Canada in the late 1960's and early 1970's [initially by Kenny (1969)] and it would seem that shortly after their commercial value became evident, the rate of publication diminished. In response to claims by the US gas turbine industry of performance enhancements in adopting pipe diffusers, the Engineering and Physical Sciences Research Council (UK), together with European Gas Turbines and National Power, presented Cranfield University with a research grant totaling £450K to carry out an investigation into pipe diffusers. The objectives of the resulting research project were to design and analyse a series of pipe diffusers which included detailed experimental traverses and associated computational modeling. This thesis reports the work undertaken to achieve these objectives and was covered by approximately 90% of the total grant award.

1.1. Outline of Thesis

Immediately following this section are the results of a literature survey. Emphasis is placed on reviewing design methodologies for pipe diffusers but with only a small database of published articles to refer to, the author has decided to widen his search to encompass other diffuser designs. The aim of the generalisation was to make best use of all available information and perhaps adopt existing and proven techniques used for other diffuser types and adapt them for the pipe geometry. After all, despite the conceptual difference, pipe diffusers still have many of the features associated with alternative designs.

Chapter 2 concentrates on the impeller flows with emphasis on determining the flow that is 'seen' by the diffuser. Detailed flow measurements, using uniquely developed instrumentation, were made at the discharge of a high speed compressor.

Chapters 3 and 4 each deal with a parametric study of a salient geometric feature of pipe diffusers. Chapter 3 deals with the effect of area expansion; defined here as the effective flow area variation between impeller tip and diffuser throat (an alternative description is 'the effect of throat area' as the impeller tip effective flow area is fixed). Chapter 4 is an investigation into sidewall expansion. This occurs when, given a fixed throat area, the number of pipes is reduced resulting in a step in the meridional plane. In

both Chapters 3 and 4, the author attempts to restrict discussion to information of interest to designers. This includes measurements of throat blockage, impeller tip flow distortion, losses and flow unsteadiness together with full descriptions of the design philosophy used to initially specify the diffusers tested.

In Chapter 5 the author attempts to correlate all detailed measurements to provide the reader with an understanding of the flow between the impeller tip and the diffuser throat. Associated CFD studies are presented to supplement the detailed unsteady flow measurements.

Finally, in Chapter 6, the significant findings of this thesis are highlighted and conclusions drawn.

LITERATURE REVIEW

A literature review follows that is broken down into parts defined by diffuser type, each of which describes the main flow features together with cited design procedures. The diffuser types discussed are:

I) Vaneless Diffusers
II) Cascade Diffusers
III) Channel Diffusers
IV) Pipe Diffusers

The last of these, the section on pipe diffusers, is additionally sub-divided into separate reviews of experimental investigations and design methodologies. Finally, on the basis of information contained within the review, a design algorithm was assembled and implemented successfully in Chapter 3.

1.2. VANELESS DIFFUSERS

Vaneless diffusers are the simplest of all the designs examined in this report with variables limited to those that effect the shape of the meridional section. For conical sideplates (more complicated alternatives are possible) this means that only W_5, R_5 and W_3 require prescription, see Figure 1.2.

Disadvantages of the vaneless diffuser include

- the large frontal area required for effective diffusion
- the limited pressure recovery due to instability of the radial velocity profile, particularly for flows with M>2 (Kenny 1970)
- the long pathline which gives rise to high wall frictional losses

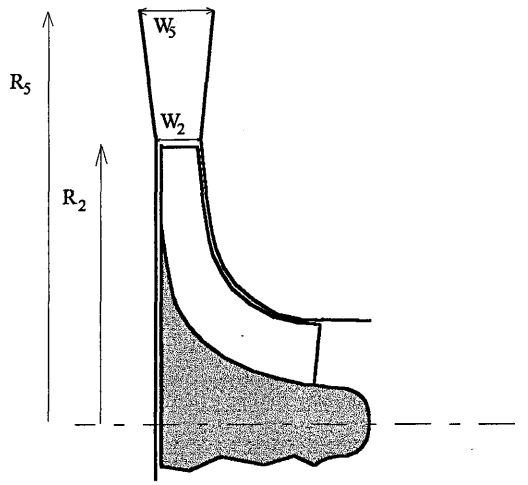


Figure 1.2 Designation of Vaneless Diffuser Geometry

A crucial advantage of the vaneless diffuser configuration is its ability to operate free from strong shocks, and their subsequent losses, for supersonic inlet velocities. It is for this reason that many vaned diffuser designs incorporate a small section of vaneless space specifically to diffuse the flow to subsonic conditions prior to vane inlet.

At first thought, vaneless diffusers may be envisaged as to operate in a fashion analogous to 2-D diverging-duct flow: the increase in normal flow area reduces the flow velocity with a consequential rise in static pressure. However, this hypothesis fails when considering supersonic discharge velocities where the flow within the diffuser, despite the increasing flow area, still slows. This seems to contradict our understanding of compressible gas dynamics where to diffuse supersonic flows we require a converging duct. This anomaly may be explained by the conservation of angular momentum. For high pressure centrifugal compressors, most of the flow diffusion is not achieved through flow area variation but through the dominant flow angular momentum term with the increase in tangential flow radius enforcing a reduction in tangential velocity.

Cohen et al (1987) gives a worked example of how, given impeller discharge conditions, the flow at exit of a vaneless space may be evaluated. An iterative procedure using successive approximations for the discharge radial velocity was employed. Such a simple equation set neglecting losses is acceptable for first approximation purposes, but for detailed examination and optimisation of possible geometric designs further enhancements are necessary. These must be able to account for wall frictional losses and consequential boundary layer growth on the sidewalls, together with a method to calculate the losses due to jet/wake mixing. It is these two aspects that the literature has sought to resolve in developing an analytic technique for the general vaneless diffuser application.

It should be emphasised at this stage that the methods reported here are dependent on the quality of the inlet boundary conditions i.e. the impeller discharge fluid properties and velocity. Methods of calculating these are beyond the scope of this report. They range from 1-D methods (e.g. Frigne and van den Braembussche (1978) and Herbert (1980)) to fully 3-D Navier Stokes solutions using Computational Fluid Dynamic techniques (reviews of which include Lakshminarayana (1991), McNally and Sockol(1985), Japikse (1976) and Whitfield and Baines (1990)). Here the author will restrict his discussion to calculations within the vaneless and semi-vaneless spaces together with a particular emphasis to those calculation methods which may be enhanced and/or adapted for pipe diffuser design.

To model the effects of wall friction, Senoo and Kyushu (1984) introduced a non-dimensional wall friction term into their equation set. This was of the form:

$$\tau_w = \frac{1}{2}\xi\rho v^2 \qquad \text{-(1.1)}$$

and was resolved into radial and circumferential contributions for each respective momentum equation (the radial momentum equation was needed to solve an additional unknown, the total pressure loss). Unfortunately, it was necessary to use an empirical value for the friction coefficient, ξ. This directly affected not only the velocities predicted but also the total pressure loss and therefore its accurate assignment was of primary importance. As a first guess Senoo and Kyushu (1984) indicate that it is commonplace in diffuser design to use pipe flow friction factor data, but taking double the passage width as the hydraulic diameter. Using the standard equation for hydraulic diameter (e.g. Fox and McDonald (1985)) we have:

Hydraulic Diameter, $$D_h = \frac{4A}{P} \qquad \text{-(1.2)}$$

Where A= cross-sectional area , P= wetted perimeter

For a radial diffuser we have

$$D_h = \frac{4.\pi D_5 w_5}{2\pi D_5}$$

Hence, $$D_h = 2w_5 \qquad \text{-(1.3)}$$

Senoo and Kyushu (1984) therefore recommend that no special treatment is necessary.

There are difficulties associated with this approach. It has been shown experimentally [Brown (1947)] that the wall friction coefficient varies significantly in the radial direction with a peak near impeller discharge, falling to values similar to those in pipes when reaching diffuser discharge. See Figure 1.3.

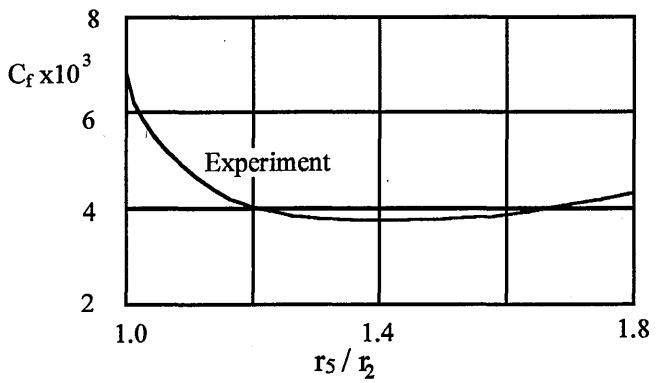


Figure 1.3 Variation of Friction Coefficient with Radius [Brown (1947)]

Therefore great care must be taken when utilising constant values for wall friction as it is envisaged that these experimentally derived vaneless diffuser average values are functions of discharge radius. As the vaneless space within vaned diffuser configurations only extend to radius ratios of 1.05 -1.10, additional caution is merited due to the local steep gradient in C_f.

To solve the 1-D equations of flow, incorporating a friction term, Senoo and Kyushu (1984) iteratively solved the flow using a series of thin annular rings, each of which was regarded as a separate control volume. This procedure was necessary to account for the non-linear pressure loss which affected the radial momentum equation.

These above methods were limited due to the 1-D simplification and through practical use Senoo and Kyushu (1984) recommended that their method should only be used when the impeller discharge flow is not too distorted. To allow for flow distortion in the axial direction, Senoo et al (1977) proposed a 2-D method. This, despite the solution of eleven simultaneous differential equations still required an empirical relation for wall friction coefficient. This was assigned a function of Mach number and therefore did allow for some radial variation.

Instead of using C_f data derived from pipe flow experiments, Dou (1989) used a 2-D boundary layer formulation to calculate the wall friction. Like Senoo et al (1977) this approach also departed from the use of constant values for C_f and allowed a variation with radius qualitatively similar to that shown earlier by Brown (1942). Theory was based on a momentum integral approach utilising the fully turbulent form of a momentum thickness equation derived by Truckenbrodt and given in Schlichting (1960). i.e.

$$C_f = G.f(\bar{r}) \qquad \text{-(1.4)}$$

where $\bar{r} = \dfrac{r_5}{r_2}$

$$G = 0.07\left(\frac{\mathrm{Re}_{r_2}}{\sin\alpha_2}\right)^{-\frac{1}{5}} \qquad \text{-(1.5)}$$

Re_{r_2} = Reynolds number based on inlet conditions and diffuser inlet radius

and $$f(\bar{r}) = \bar{r}^{-\frac{1}{2}}\left(1-\bar{r}^{-\frac{1}{5}}\right)^{-\frac{1}{5}} \qquad \text{-(1.6)}$$

The function $f(\bar{r})$ is plotted below.

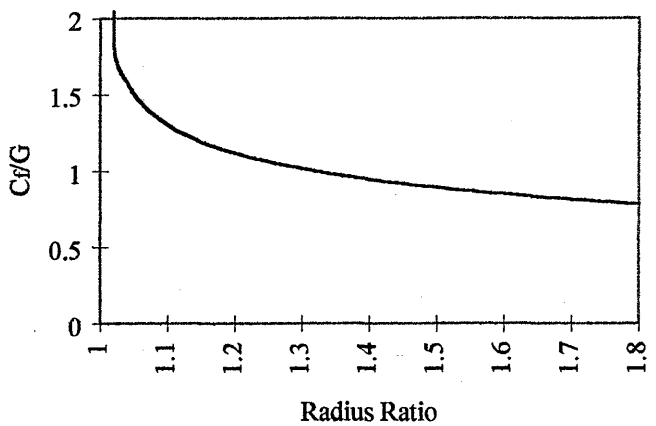


Figure 1.4 Friction factor -v- radius ratio correlation [Dou (1989)]

Dou (1989) correlated this relationship with published vaneless diffuser data to produce an empirical equation relating the diffuser loss against the passage width and inlet flow angle. This was introduced as a correction term in the loss equation. Unfortunately, the analysis was unable to model the flow near the impeller discharge [Dou (1989)] making it unsuitable for modeling the flow within the vaneless space of a vaned diffuser arrangement. This limitation is due to the following:

- *The flow angle was presumed constant throughout.*

If this procedure was to be used for designing the vaneless space of a vaned configuration the variation in flow angle with respect to radius would be required.

- *The inlet flow was presumed uniform.*

An inlet mixing loss was not included in the calculation procedure and therefore the complete calculation algorithm has not been proven.

- *Method assumes parallel walls.*

This severely limits the applicability of the method.

- *Correlation with experiment only outside $\bar{r}>1.06$.*

The method has not been assessed against measurements taken near impeller.

An alternative design approach was completed by Herbert (1980). Wall friction was computed using a long empirical equation with Mach number, boundary layer thickness and boundary layer momentum thickness as independent variables. As the formulation required boundary layer information prior to wall friction calculation, it was necessary to use an iterative solution procedure. A series of annular control volumes, much like Senoo and Kyushu (1984), were constructed within the vaneless space, and each was solved in turn from diffuser inlet to discharge. The approach was limited in that it assumed an impeller "mixed out state" at diffuser inlet, did not allow any core flow asymmetry or predict a total pressure loss until the hub and shroud boundary layers met.

Frigne and van den Braembussche (1978) made a fundamental contribution to this field by allowing a gradual mixing of the impeller jet/wake structure through the diffuser. They showed, through a worked example, that the mixing is not instantaneous and takes place over a measurable radial distance. By modeling these two regions of flow, they were able to account for the mixing losses through the application of a jet/wake shear force coefficient. The shear force between the jet and wake was proportional to the difference in their respective velocities, squared. i.e.

$$\tau_M = \frac{1}{2} c_M \rho (v_{jet} - v_{wake})^2 \qquad \text{-(1.7)}$$

where $c_M = 0.094$

Despite the relatively high value for the shear force coefficient (when compared against wall friction terms), Frigne and van den Braembussche (1978) explain that the

mixing term does not completely dominate the flow at impeller discharge. This is because the large constant value of coefficient is off-set by a relatively small velocity squared term. In conjunction, the wall friction term was calculated empirically using the Reynolds number and a relative roughness term, the latter accounting for surface finish. The constant value of c_M is accepted here, as it was shown by Dean and Senoo (1960) that its influence on the flow field was limited. It should be noted that this attempt at modeling the gradual mixing of flow within a vaneless diffuser was limited by assumption of incompressible flow and neglected boundary layer blockage effects due to growth on the sidewalls.

Unlike other diffuser types, there is only a small database of isolated diffuser performance data available and designers lack the design-type performance charts found for other diffuser types (e.g. the Rundstadler and Dolan (1973) channel diffuser effectiveness charts) [Japikse (1984)]. Consequently, aerodynamic designers are normally forced to use techniques similar to those cited above [Japikse (1984)]. This approach is partially justified as there is some evidence that vaneless diffusers, unlike channel diffusers, are relatively insensitive to inlet blockage [Japikse (1984)]. However, even if this latter point was generally true, vaneless diffuser performance charts would still be required with meridional aspect ratio and diffusion angle (or equivalent parameters specifying the geometry) as independent variables.

1.3. CASCADE DIFFUSERS

Cascade diffusers, or cambered vane, comprise aerofoil-type or curved plate sections placed at impeller discharge, see Figure 1.5.

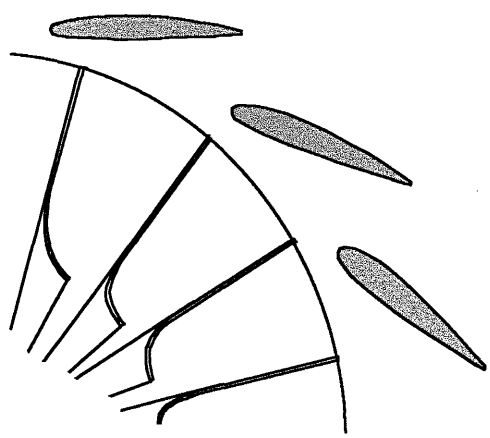


Figure 1.5 Sketch of an Aerofoil Type Cascade Diffuser Arrangement

Their action is to remove swirl from the flow and direct the gas to an optimum flow angle, aiding downstream vaneless diffusion and are described by Kenny (1970) to act in a manner similar to axial stator cascades. Whitfield and Baines (1990), in their brief review of the subject, state that the main advantage of this type of arrangement is the wide flow range possible. Disadvantages include high manufacturing costs and a relatively small design base. A design quandary that also arises is the lack of a throat for low solidity cascades. This causes problems as the flow rate corresponding to throat choking is traditionally an important parameter in vane design and is used to help select a design flow.

A common design method for cascade diffusers is based around the application of conformal transformations to aerofoil cascade data (Whitfield and Baines (1990)) although alternatives exist and are reviewed by Kenny (1970).

1.4. CHANNEL DIFFUSERS

Channel diffusers may be split into three distinct regions (See Figure 1.6):

(i) The Vaneless Space
(ii) The Semi-Vaneless Space
(iii) The Flow Channel

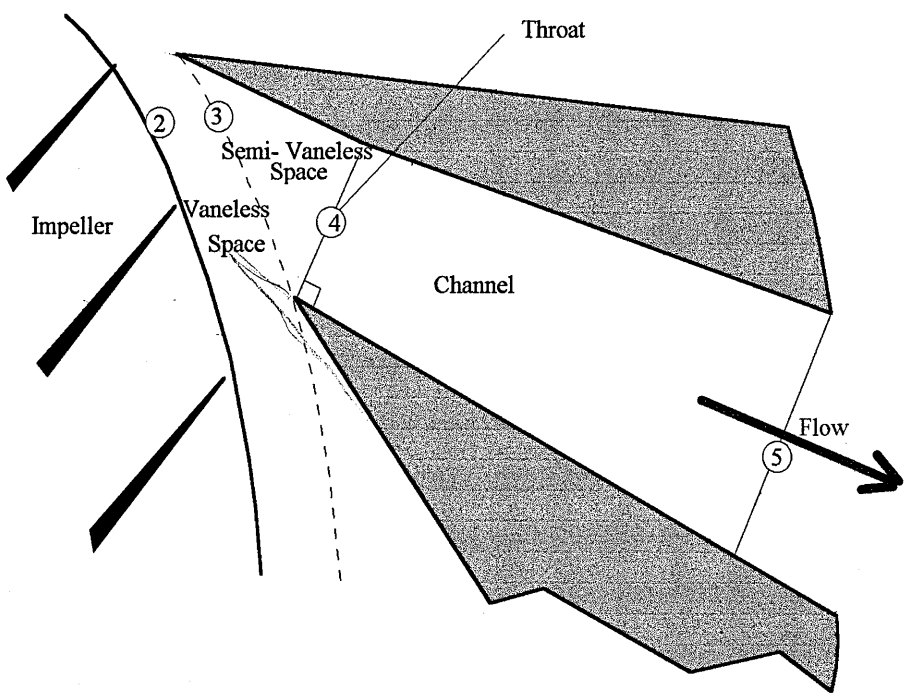


Figure 1.6 Sketch of a Channel or Vane-Island Type Diffuser

All design methods reported here do not allow the upstream components to be influenced by those downstream and therefore it is convenient to examine each of these regions in the order seen by the flow. However, it should be noted that in a comparative experimental investigation between vaneless and vaned configurations, Inoue and Cumpsty (1984) were able to demonstrate that the vanes did influence the impeller discharge flow, particularly at low flow rates for a diffuser with a small vaneless space (vane leading edge radius ratio of 1.04). This may not be generally true and is apparently contradicted in the work of Krain (1981) who showed that no downstream diffuser influence propagated upstream into the impeller. However Krain (1981) tested a stage with a vane leading edge radius ratio of 1.1. This slightly larger vaneless space could clearly be of significance.

1.4.1 VANELESS SPACE

As already discussed in the section on vaneless diffusers, it is apparent that authors have either opted to continue impeller jet/wake calculations into the diffuser or have assumed instantaneous flow mixing at impeller discharge and continued the calculation using averaged conditions with a mixing loss incorporated. A method based on the former was proposed by Frigne and van den Braembussche (1978) and was an extension of their method for modeling vaneless diffuser flow. The calculation procedure was complicated in that the inlet boundary conditions for their semi-vaneless space calculation required "mixed-out" conditions. As the leading edge (start of the semi-vaneless space calculation domain) is normally within a radius ratio of 1.1, problems arise due to the high probability that the mixing procedure will not be fully completed until much larger radii. The example below (Figure 1.7) shows how the jet wake velocities (designated by subscripts j and w respectively) do not merge until reaching a radius ratio of 1.22.

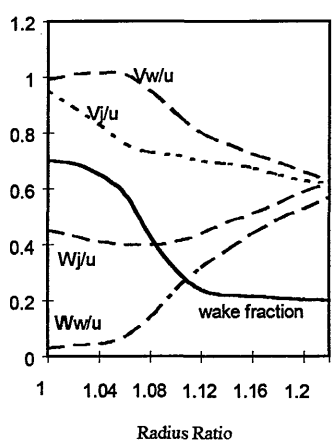


Figure 1.7 Jet/Wake Mixing within Vaneless Space [Frigne and van den Braembussche (1978)]

To ensure that the mixing loss was properly accounted for, Frigne and van den Braembussche (1978) calculated the total losses up to the mixed state, as for a vaneless diffuser, then subtracted a wall friction loss between the vane leading edge and the calculated mixed-out radius. Using this technique the loss associated with the complete jet/wake mixing was incorporated.

The design procedure of Herbert (1980) assumes a calculated mixed out state at impeller exit and therefore the method is equally applicable, without change, to be used for the vaneless space within vaned diffusers as well as for vaneless diffusers described earlier.

1.4.2 SEMI-VANELESS SPACE

It is within this region that the unsteady flow from the impeller strongly interacts with the stationary blades. To compute this unsteadiness is currently outside the capability of design programs but work has been completed using CFD [e.g. Dawes (1994)]. Here we will restrict ourselves to methods that use time averaged quantities. This simplification allows designers to use methods developed for steady flows, including boundary layer theory. Despite this crudeness, the importance of the flow within this region should never be underestimated. Rogers (1982) demonstrated that the stall surge limit was intimately connected with the diffusion between impeller discharge and diffuser throat. Such a correlation was confirmed by Elder and Gill (1984), and was extended to show how a reduced number of diffuser vanes enabled higher pressure recovery within the semi-vaneless space. As the static pressure recovery is a function mass flow, this meant that a reduced number of blades allowed increased operational range. This is reflected in the overall performance map, Figure 1.8. Note that the lack of flow range variation at low speeds was attributed to inducer mismatch.

It is within the semi-vaneless space that previous investigators have perceived that the deleterious throat blockage is accumulated. Diffuser performance is very sensitive to throat blockage as is shown in a sample performance plot, Figure 1.9 [Whitfield and Baines (1990)].

For designers, the primary reason for detailed calculations in this region is to accurately evaluate the throat blockage. Ideally these methods should be able to cope with variations in inlet vane shape, and in particular, the suction surface curvature. The latter was investigated by Clements and Artt (1989). They showed that a concave suction surface was detrimental to diffuser performance and that an optimum stage performance was achieved with a straight edge combined with a vaneless space extending up to between 1.06 and 1.1 times the impeller diameter. Earlier, Clements and Artt (1987) used the calculation method documented by Herbert (1980) to properly match a diffuser

and an impeller. The momentum integral formulation employed to model the flow within the vaneless and semi-vaneless spaces was found suitable.

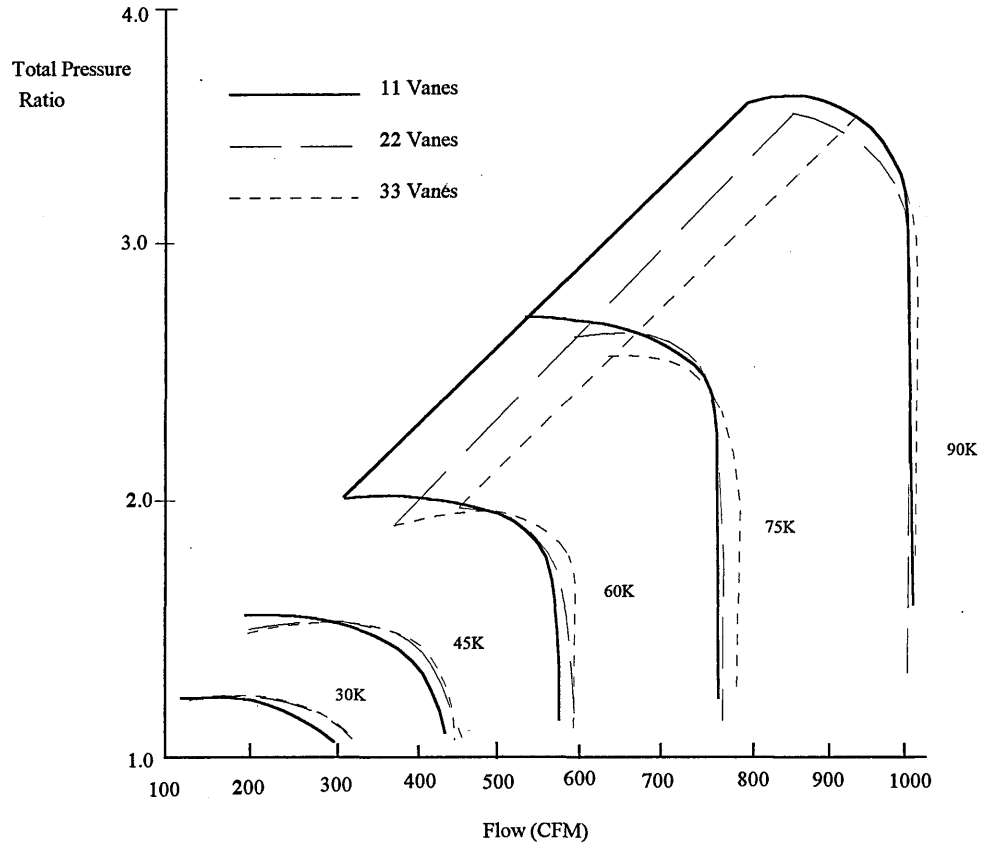


Figure 1.8 *Sensitivity of Flow Range To Number of Vanes [Elder and Gill (1984)]*

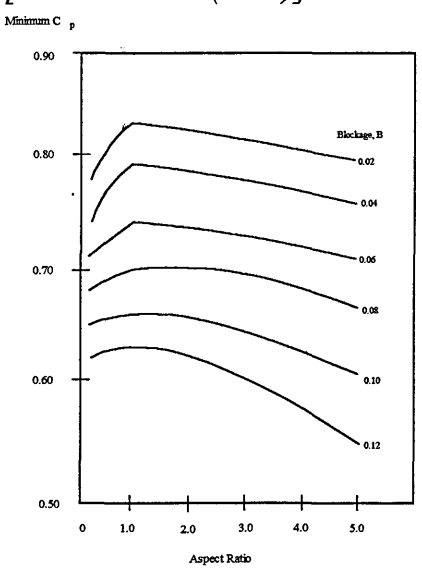


Figure 1.9 *Sample Diffuser Channel Performance Chart (Whitfield and Baines (1990))*

Despite being a comprehensive calculation scheme, Herbert's semi-vaneless space analysis suffers from the following limitations:

I) It is unable to model the unsteady flow.
ii) Its boundary layer analysis requires empirical input.
iii) No account is taken of the vane inlet suction surface shape.
iv) An empirical equation relating throat blockage to the total pressure loss is required for closure.

The first three deficiencies can be justified given that the analysis is based on 1-D flow relations and is only for preliminary design purposes. All of the methods documented here are restricted in this way. It is the last point that gives the most concern, with some doubt cast on the pedigree (as acknowledged by Herbert himself) on the relation utilised i.e.:

$$P_{04} = P_{03}(0.36 + 1.28B_{th} - 0.64B_{th}^2) \qquad -(1.8)$$

No source for this expression is documented in Herbert (1980) and within the text it is described as an "arbitrary relation". To understand its importance it is necessary to have a rudimentary grasp of the calculation procedure. Essentially the method takes the vaneless space discharge values as inputs to the semi-vaneless space control volume. The hub and shroud boundary layers are assumed to continue growing together with an additional boundary layer starting on the leading edge of the vane suction surface. Thus combined, there are three boundary layers which accumulate to form the throat blockage. Once found, the throat total pressure is evaluated using the above equation. This is then used to compute the static pressure gradient, a controlling parameter in any boundary layer analysis. The boundary layer calculation is then repeated using this revised pressure gradient and a new throat blockage is found. Therefore, in an indirect manner, equation (1.8) strongly influences the final value found for blockage.

The method does not require details of geometry apart from inlet and outlet flow area, together with vane angle, the latter being used to evaluate the inlet Mach number. The incident flow may be supersonic, in which case a Prandtl-Meyer type expansion or compression (whichever is appropriate) is incorporated with the default to model a strong shock should a weak solution of the wave equation not exist. As the inlet flow to the vanes is expected to be barely supersonic ($M<1.2$), no total pressure losses are included in the leading edge calculations.

Instead of a relationship between throat blockage and total pressure loss, Frigne and van den Braembussche (1978) used a correlation formed from experimental data

presented by Kenny (1972). This related static pressure regain between vane leading edge and throat, to throat blockage. See Figure 1.10.

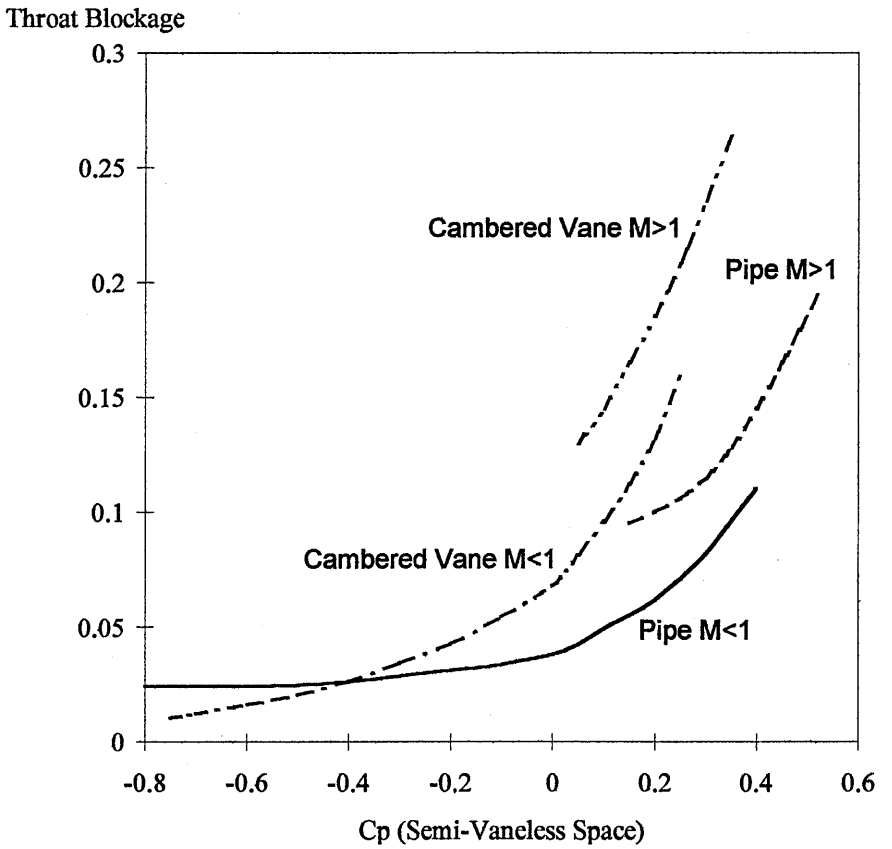


Figure 1.10 *Graph of Throat Blockage -v- Static Pressure Recovery [Kenny (1972)]*

Frigne and van den Braembussche (1978) adopt the published pipe diffuser relationship rather than that designated for cambered vane diffusers by Kenny (1972). No reasons for this are reported in their paper. Kenny (1972) does indicate that the performance of vane-island diffusers "is similar to or better" than cascade types and it would seem that Frigne and van den Braembussche (1978) considered the vane-island diffuser very much superior to the cambered vane one.

1.4.3 CHANNEL REGION

On entering the channel (i.e. just after the throat), in all design methodologies cited here, the flow is assumed to be 1-D and the diffuser effectiveness' are evaluated from performance charts of tested 2-D ducted arrangements with undistorted inlet and discharge. An example of such data was shown earlier in Figure 1.9. The assumption of uniform flow at inlet, entering perpendicular to the inlet plane, is justified in that the flow

and corresponding time averaged pressure contours are suitably arranged by the influence of the vanes. See Figure 1.11.

It should be kept in mind, however, that (confidential) contract studies carried out at Cranfield have shown that the flow at diffuser throat is pulsating and contains a large swirl component [Elder (1995)]. Indeed, studies by Dean and Young (1976) have shown discrepancies between centrifugal compressor throat flows and 2D laboratory data, Figure 1.12.

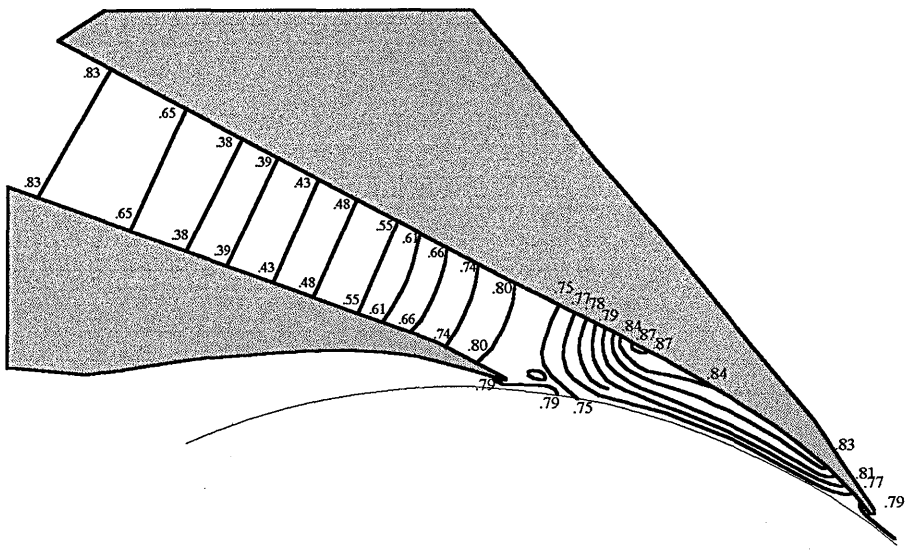


Figure 1.11 *Static Pressure within the Impeller Exit/Diffuser Entrance Region [Verdonk (1978)]*

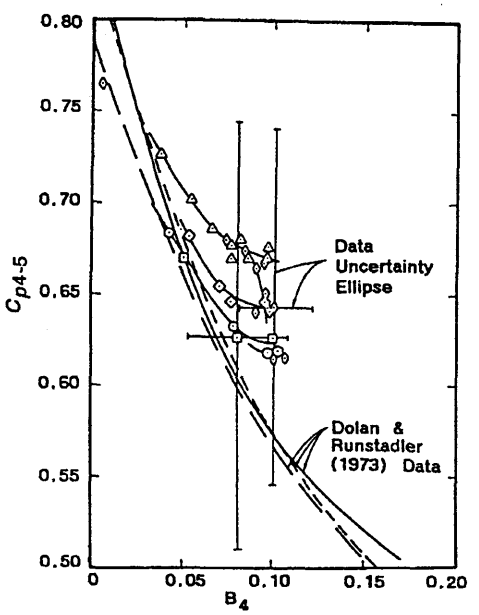


Figure 1.12 *Static Pressure within Diffuser Channel [Dean and Young (1976)]*

1.5. PIPE DIFFUSERS

Pipe diffusers are similar in concept to cascade diffusers in that they comprise of a vaneless space, a semi-vaneless space and a diffusing channel. However, unique to pipe diffusers is a region between the vaneless space and the semi-vaneless space called the pseudo-vaneless space. See Figure 1.13. Passages are formed via a series of discrete pipe drillings that are machined out of a solid annular ring. These drillings are arranged so that they intersect to form a series of elliptic leading edges, the incidence of which varies from 0° at the ridge tangency radius to a maximum at the leading edge cusp. It is the length of this leading edge that defines the pseudo-vaneless space. The cusp is used here, and in the literature, to define the leading edge. Instead of the suction surface as normally used for cascade design, pipe diffuser designers have historically measured from the bisector of the leading edge wedge (see nomenclature).

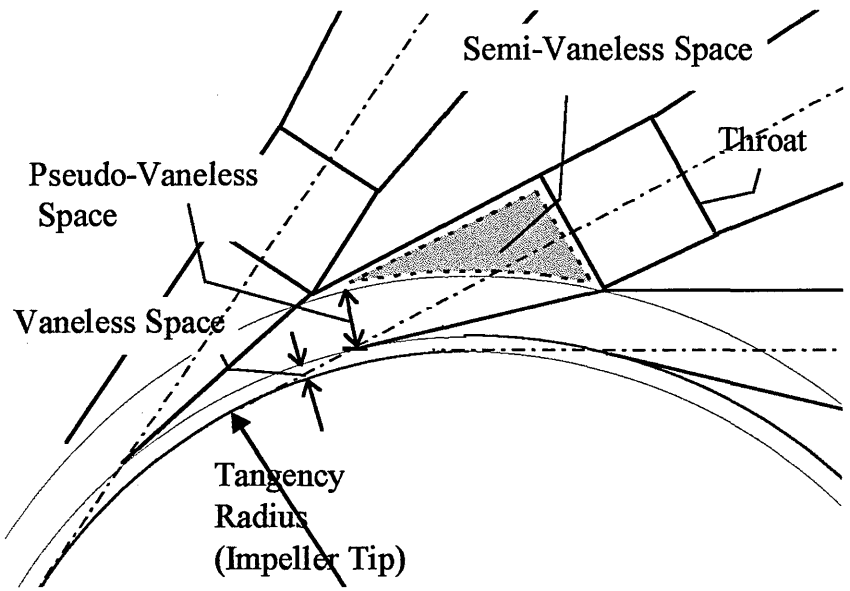


Figure 1.13 Designation of Pipe Diffuser Geometry

The following advantages of pipe diffusers presented in the literature include:

i) Comparatively low cost [Kenny (1969)].
ii) Superior efficiency at supersonic inlet Mach numbers [Kenny (1970)].
iii) Relatively small number of design parameters [Kenny (1969)].
iv) Has nearly the optimum aspect ratio of .75 as obtained for vaned diffusers [Runstadler and Dean (1963)].
v) Better mixing of flow due to twin vortices formed by swept-back leading edges and circular cross-section, Figure 1.14.

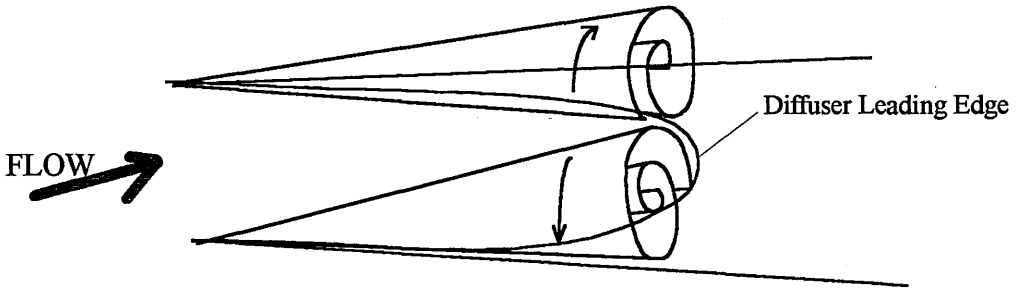


Figure 1.14 *Formation of Twin Vortex Sheets at Pipe Diffuser Leading Edge*

For clarity, this section on pipe diffusers is split into two. The first half reviews published experimental investigations into pipe diffusers. The second reviews associated design information. Descriptions are divided into three geometric areas. The first the vaneless space; the second the pseudo- and semi- vaneless spaces and finally the downstream diffuser channel.

1.5.1 REVIEW OF EXPERIMENTAL INVESTIGATIONS INTO PIPE DIFFUSERS

1.5.1.a Flow in the vaneless space

Some flow measurements were made by Kenny (1972) but these were circumferentially averaged and the profile measured was used to prescribe the inlet boundary of a pseudo-vaneless space calculation.

1.5.1.b Flow in the pseudo-and semi vaneless spaces

In his early investigations, Kenny (1970) did not report anything about the detailed flow within this region but did present experimental evidence that pipe diffusers did operate with smaller throat blockage when compared against alternative designs. Evidence of this is shown below in Figure 1.15.

The deleterious effect of large throat blockage on diffusing passage effectiveness was reflected in the overall performance of the stages. When compared against its vane and flat plate counterparts, the pipe diffuser operated up to 8.8% more efficiently. Kenny postulated that this improvement was due to the elliptic leading edge formed by the intersection of the pipe drillings. It is reported that there is better matching of flow incidence, with the diffuser incidence angle varying from zero at ridge tangency point to a maximum at the leading edge apex. This hypothesis was experimentally confirmed by Kenny (1970). A scallop was cut into the leading edge of a conventional vane diffuser (see Figure 1.16) and the performance compared with its original configuration (see Figure 1.15).

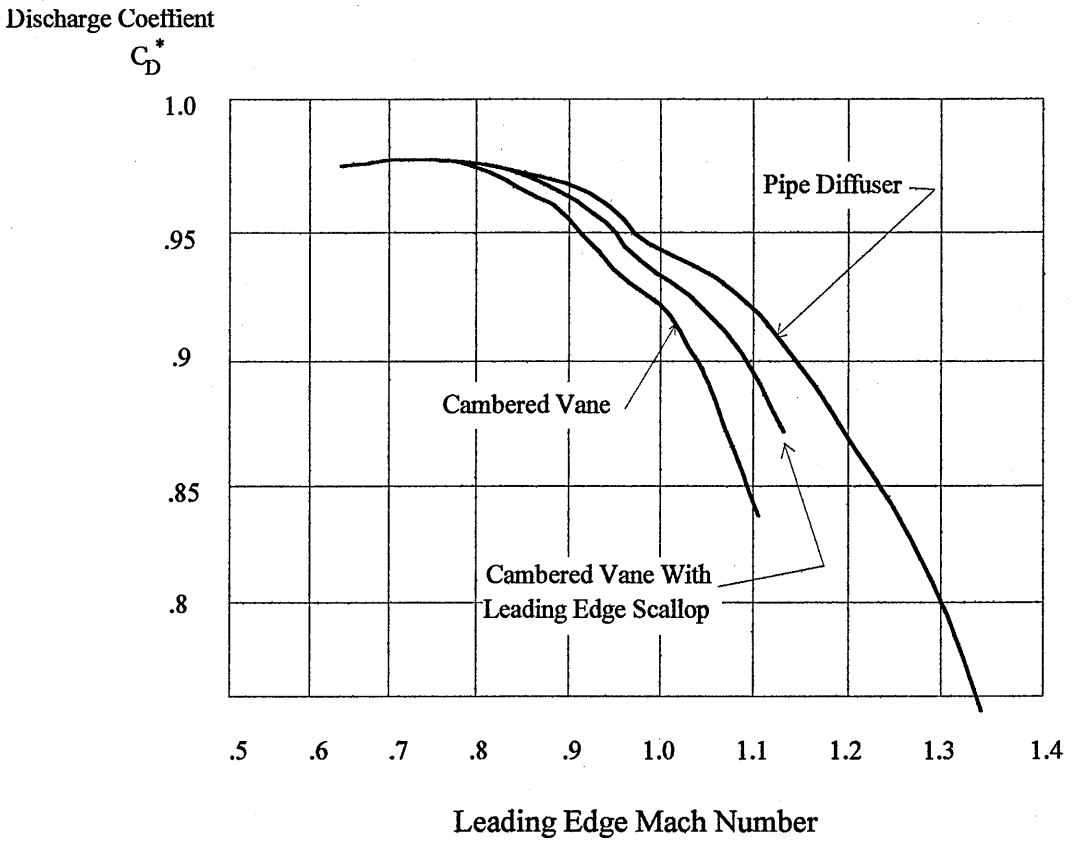


Figure 1.15 *Comparison of Choking Throat Discharge Coefficient for Pipe and Cambered Vane Diffusers [Kenny (1970)].*
[Note $C_D^* = (1-B_{th})$]

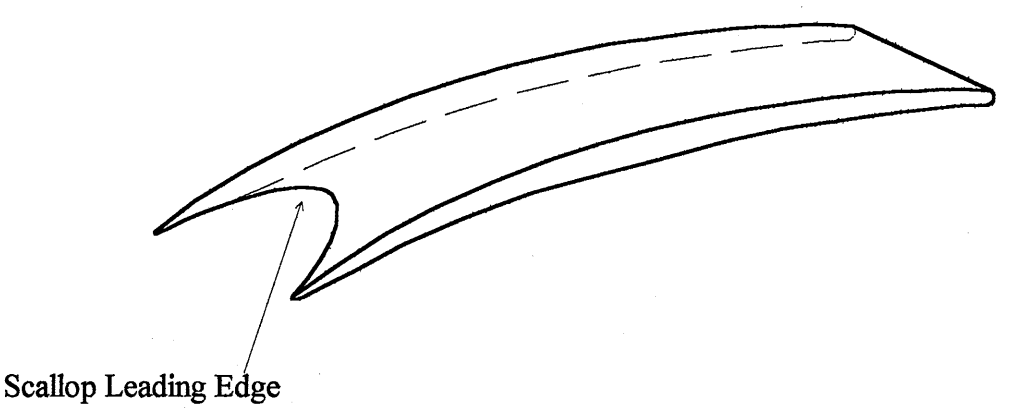


Figure 1.16 *Cambered Vane Diffuser with LE Scallop*

The scallop enhanced both the efficiency and operational range of the stage, and was particularly effective for when the incidence flow was supersonic, Figure 1.17.

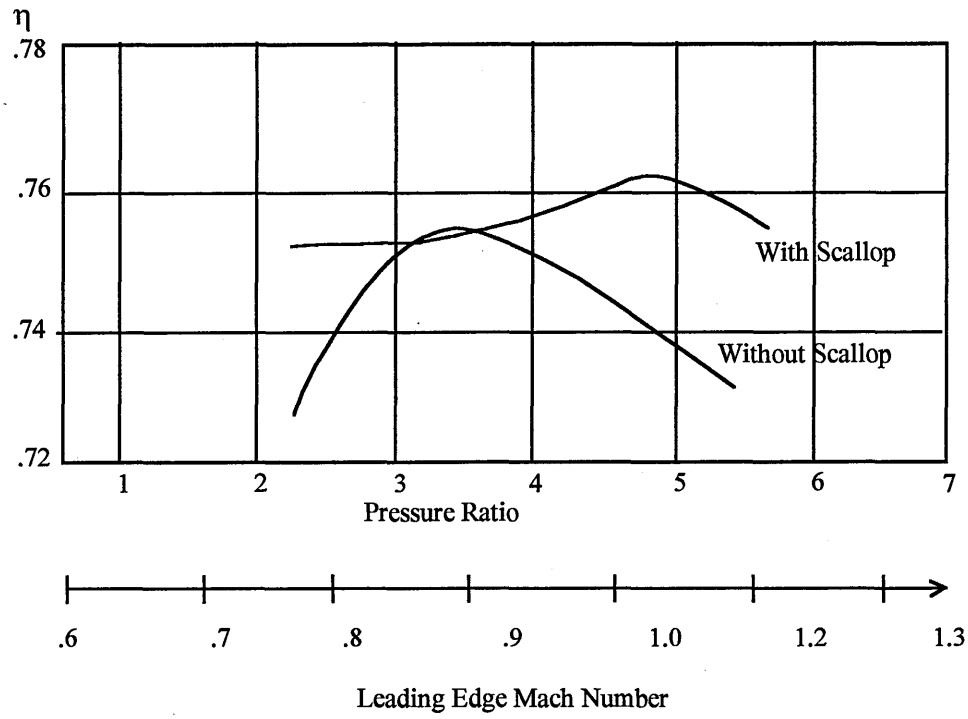


Figure 1.17 *Comparison of Vaned Diffuser Performance With and Without Scallop (Kenny 1970)*

In a similar piece of work, Klassen (1973) compared the performance of various diffuser designs. These included a cambered vane, a flat plate and two pipe diffuser designs; one with a conical diffusing section, the other with a trumpet shape. Of the pipe diffusers, the trumpet configuration proved the most effective, but still was unable to outperform the cambered vane design. Possible reasons for this disappointing result include:

Incidence Mismatch. Following the early Kenny (1969) investigations into pipe diffusers, Klassen (1973) used the impeller tip as the tangency radius for his designs. This was understandable, as Kenny (1969) reports this in a manner that suggests it is an integral part of the design. However, using the published performance chart and geometry given in Klassen (1973), the leading edge incidence of the pipes and flow may be shown to be unmatched, see Table 1.1.

Table 1.1 Calculated Incident Flow and Pipe Diffuser Leading Edge Angles

Corrected Mass flow, (Kg/s)*	0.21	0.23	0.25	0.275	0.295
Flow Angle	75.6°	74.3°	73.1°	71.5°	70.7°
Pipe Leading Edge Angle	66.1°	66.1°	66.1°	66.1°	66.1°
Incidence Mismatch	9.5°	8.2°	7°	5.4°	4.6°

* The design mass flow was 0.263 kg/s

Therefore, instead of a negative, there is a positive incidence angle near choke (0.295 kg/sec) which enforces further mismatch at lower flow rates. This mismatch introduces excessive diffusion in the pseudo- and semi- vaneless spaces, introducing excessive blockage and hence increased diffuser channel total pressure losses. In this particular example, another effect of mismatching was demonstrated, that of prematurely forcing the system into surge. See Figure 1.18. This is attributed to a limiting static pressure rise in the pseudo- and semi- vaneless spaces.

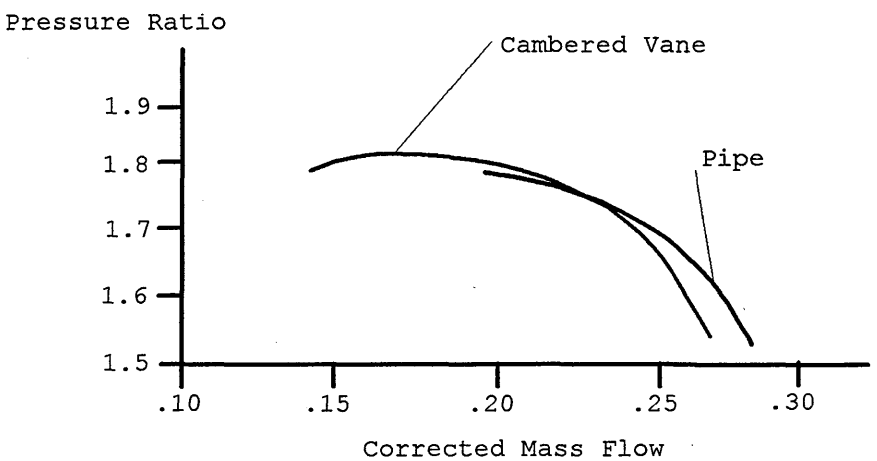


Figure 1.18 Premature Stall of a Mismatched Pipe Diffuser [Klassen (1973)]

Throat Sizing. The pipe designs were not tested with a 'correct' throat size. With the cambered vane size used as the 100% reference , pipe diffusers were tested with 93% and 98% of design throat area. To give an indication of sensitivity, a 2% rise in efficiency was noted with an increase in pipe throat areas.

Leading Edge Mach Number. Following the Kenny (1970) work, as the compressor was of low pressure ratio, it would not be expected to show significant performance enhancement with a pipe diffuser.

Reeves (1977) also investigated the effect of different leading edge shapes. Instead of a cylindrical bore, three alternatives were tried (see Figure 1.19):

i) a square with radiused corners.
ii) two oval type shapes with semi-circular ends and parallel sides.

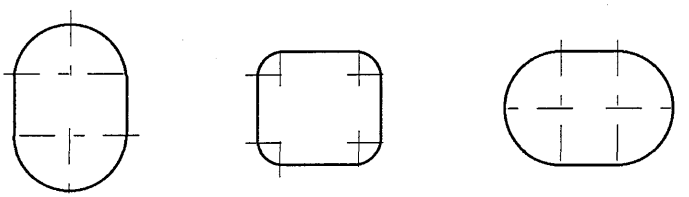


Figure 1.19 Pipe Cross-Sections Tested by Reeves (1977)

Of these tested, the square design suffered from additional throat blockage and subsequently poorer performance when compared against the semi-circular designs. The motivation behind these non-circular variations was to avoid a large step in channel width between impeller and diffuser, thus allowing additional flexibility when designing for a fixed total throat area.

Reeves (1977) hypothesised range incidence correlations in order to help design diffusing systems for maximum flow range. He showed that pipe diffusers should be designed for a -3° incidence at choking flow, Figure 1.20.

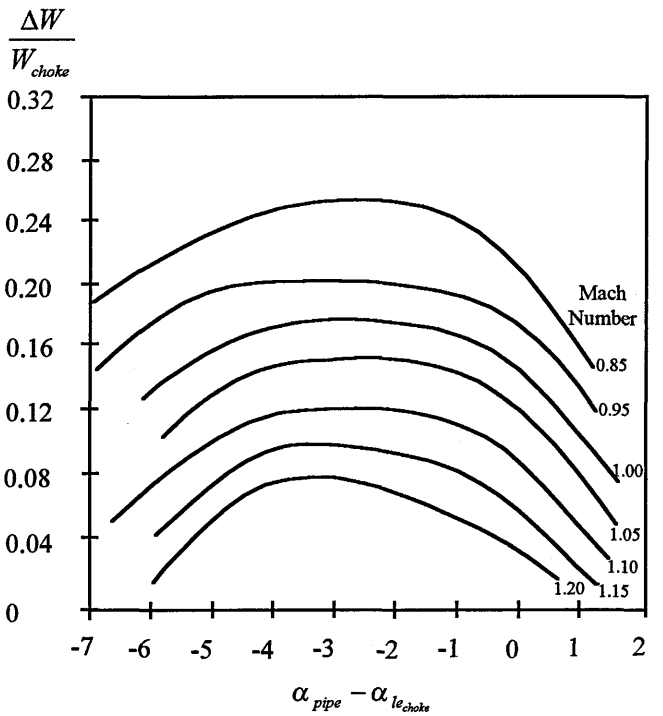


Figure 1.20 Range-Incidence Correlation [Reeves (1977)]

This work confirms the mismatching and poor performance of Klassen's (1973) designs. Groh (1969) showed that a reduction in pipe number (and consequential increase in pipe throat diameter to maintain a constant throat area) caused an increase in the flow range without significantly compromising performance or efficiency. Unfortunately, this work was carried out with a non-typical impeller and of low pressure ratio (2:1). Parallels of this range enhancement may be drawn with the work of Elder and Gill (1984) for channel diffusers. However, for standard pipe diffusers such improvements are limited due to the step size from impeller discharge to diffuser inlet. Unique to the pipe diffuser is a length of constant flow area leading up to the throat, any choking of which occurs at the downstream end due to boundary layer growth reducing the effective flow area. Kenny (1970) showed that a short throat gave the best performance. See Figure 1.21.

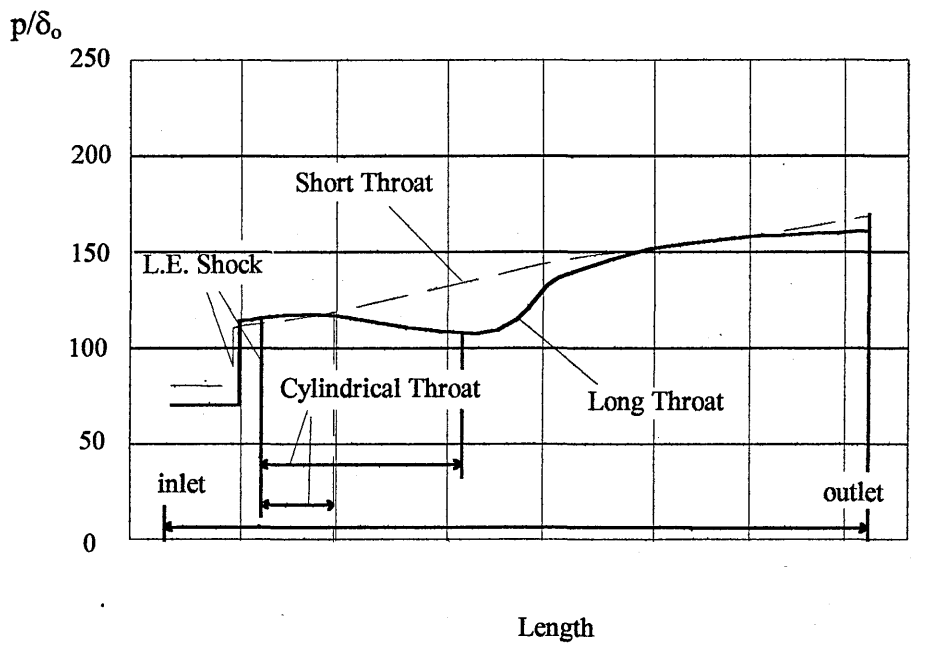


Figure 1.21 *Effect of Throat Length on Static Pressure Distribution within a Pipe Diffuser [Kenny (1970)]*

For high pressure machines and supersonic Mach numbers, Kenny (1972) describes a leading edge bow wave that extends to form a 'weak oblique shock'. However, instead of the abrupt pressure rise shown in the above figure, Kenny (1972) reports a gradual pressure rise. He attributes this smearing to the influence of the thick boundary layer (static pressure tappings were used).

1.5.1.c **Flow in the conical diffuser section**

The flow within this region is normally regarded as too difficult to predict due to large amounts of separation and unsteadiness. Consequently, designers are forced to use empirical data.

Kenny (1972) compared the effects of throat blockage on pipe diffusers and cambered vane diffusers. He showed that pipe diffusers were more resilient to the detrimental effects of throat blockage. See Figure 1.22. Different diffusing systems have been tried for the diffusing section, including single and two stage conical [Groh et al (1969)], and trumpet [Klassen (1973)]. With the success of these setups, the designer is afforded additional design flexibility.

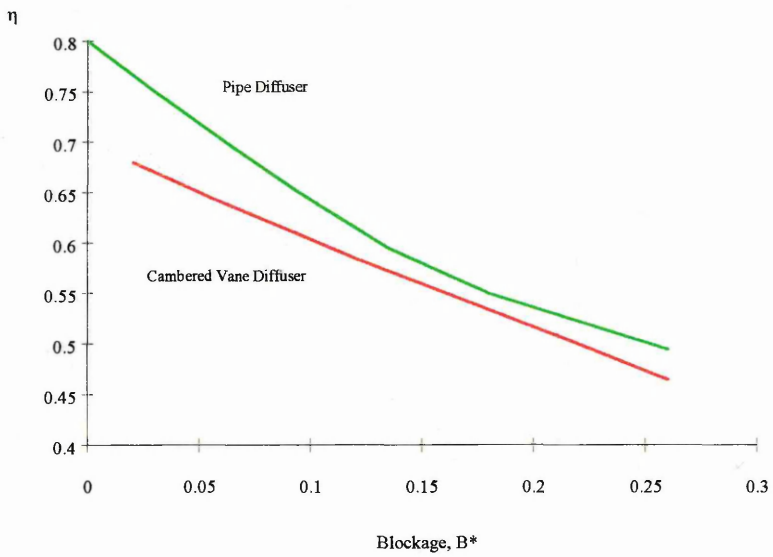


Figure 1.22 *Comparison of Pipe and Cambered Vane Diffuser Effectiveness against a Range of Throat Blockage Conditions [Kenny (1972)]*

From static tappings in the pipe, Kenny (1972) showed how the pressure distribution was essentially 1D after the throat, thus suggesting that the use of Runstadler (1973) type diffuser channel charts is acceptable.

1.5.2 REVIEW OF EXISTING DESIGN INFORMATION FOR PIPE DIFFUSERS

1.5.2.a **Flow in the vaneless space**

Kenny (1972) demonstrated a four wall boundary layer method to predict the near wall flow within an impeller. The resulting flow compared well with detailed experimental flow measurements. The calculation procedure was allowed to continue into the vaneless diffusing section, where the use of a constant wall friction is indicated [Kenny (1972)].

Reeves (1977) in his designs for pipe diffusers, assumed a frictionless vaneless space and prescribed a 2% total pressure drop, the latter based on previous vaneless tests.

1.5.2.b **Flow in the pseudo- and semi- vaneless spaces**

Kenny (1972) used the measured discharge flow to calculate wall friction, C_f. This value showed reasonable correlation over a range of speeds when compared to that calculated via a four wall boundary layer approach. The experimentally derived value for C_f, was used by Kenny (1972) as input to an enhanced version of an integral boundary layer method published by Moses (1964). This was used to calculate the boundary layer growth and subsequent diffuser throat blockage. As the boundary layer theory applied only to 2-D flow, Kenny (1972) required some additional calculations. He used the computed boundary layer build-up on a 2D plane through the pipe centerline as a basis. The boundary layer was then assigned on the smaller chord planes by copying the mean boundary over and removing the chordwise excess from the center, Figure 1.23. Using this procedure good correlation with experiment was obtained.

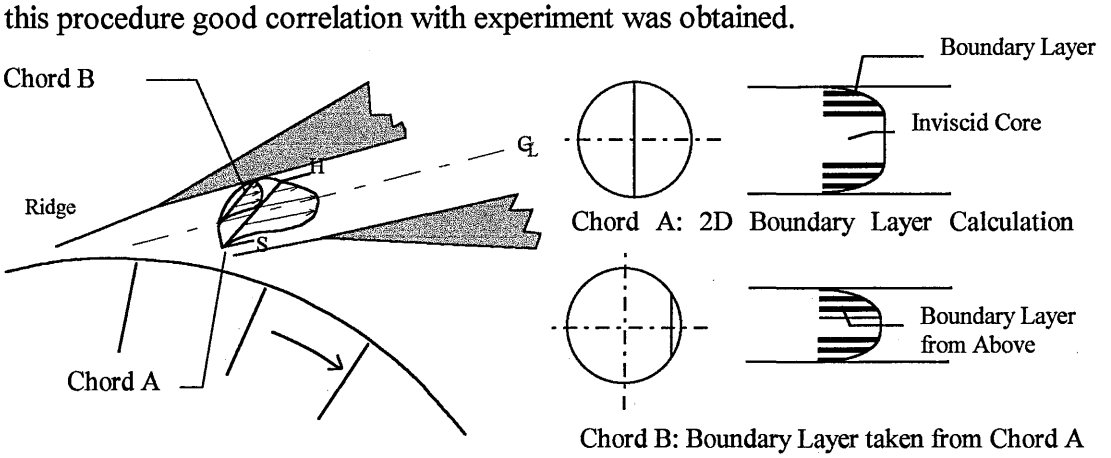


Figure 1.23 *Boundary Layer Calculation within Pseudo Vaneless Space [Kenny (1972)]*

Reeves (1977) in his calculation procedure set the throat total pressure to that measured at impeller exit (this was based on previous experimental experience). Together with throat blockage coefficients (not detailed in his paper) the throat area could be sized. The pipe diffuser incidence was set using Reeves' incidence based correlation.

An incidence-based correlation of a different sort was described by Kenny (1979). In this case, the blockage was plotted against incidence and a curve fit calculated, Figure 1.24. It should be noted that this correspondence is expected to be for one diffuser/impeller configuration only and may not generally hold for all possibilities. A

similar relationship was found when plotting diffuser effectiveness against throat blockage.

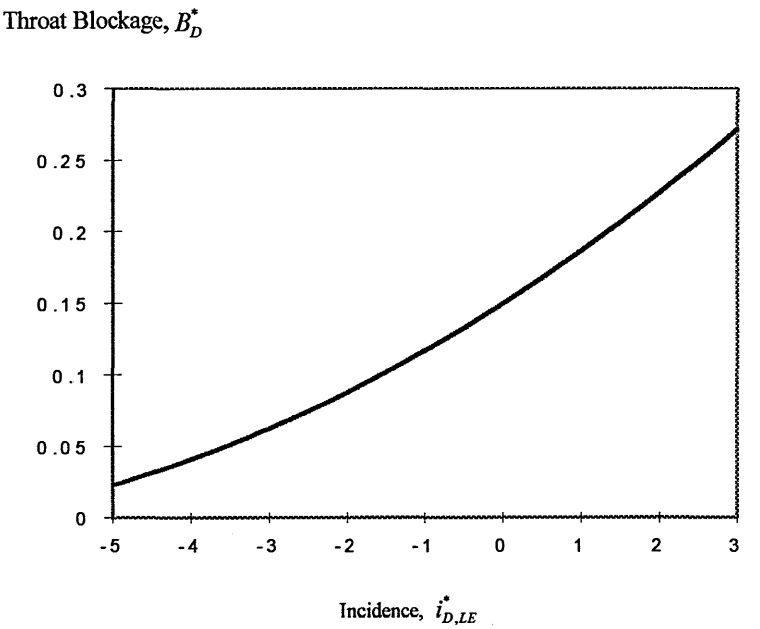


Figure 1.24 *Correlation between Incidence and Throat Blockage [Kenny (1979)]*

1.5.2.c **Flow in the conical diffuser section**

Kenny (1972) attempted to model the flow within the diffusing channel of a pipe diffuser by using the boundary layer approach utilised earlier for pseudo- and semi-vaneless space calculations. The emphasis was to predict the outlet conditions of the channel rather than simulate the actual flow conditions. For this, a total pressure loss mechanism was used which was activated every time separation was predicted by the boundary layer calculation. On reaching this point, the flow was 'reset' to allow the calculation procedure to continue downstream. In practice, if separation took place, it would periodically reoccur until discharge. This resulted in a sawtooth shape when blockage was plotted against distance from throat. Despite not modeling the actual flow physics, the procedure was able to accurately predict the total pressure loss.

1.6. CLOSURE

It has been described how diffusers have a controlling influence on the performance and range of a centrifugal compressor stage. Descriptions of other diffuser types have been given, together with associated experimental observations and design

methodologies. Similarities in geometry between these diffuser types and pipe diffusers have been presented.

Descriptions of pipe diffuser design rules have been summarised. Indications, both from stage performance and individual diffuser performance parameters, are that the pipe diffusers offer significant benefit, particularly at high pressure ratios. Reasons for this improvement are given and can be identified by the reduced throat blockages measured. At lower pressure ratios ($PR \leq 2.5$) there was no advantage noted.

Most vane and pipes diffuser design methods have used integral boundary layer analysis in conjunction with 1-D gas dynamic relations. The Herbert (1980) design program procedure described is typical of these and is utilised later to design some pipe diffusers.

The impressive performance enhancements published by authors from, and associated with, Pratt and Whitney (e.g. Kenny, Reeves, Groh et al) have not been duplicated by others, although there are reasons identified here for this. This highlights the need for an independent and representative series of experiments into these devices and such an investigation is undertaken here.

For completeness, all relevant pipe diffuser references found are summarised in Table 2.

Table 2 Summary of Pipe Diffuser References

Reference	No. of Pipes	Tangency Radius Ratio	Leading Edge Radius Ratio	Pipe Diameter/impeller discharge width	Pipe Throat Length/ Diameter	Impeller Pressure Ratio	Stage Peak Efficiency	Comments
Kenny (1969)	ND	ND	ND	ND	ND	5.4	81.8	First experimental data
Kenny (1970)	ND	ND	ND	ND	ND	10	74.5	Short throat length found to be better
Kenny (1972)	ND	ND	ND	ND	ND	15	72	Supersonic inlet flow
"	ND	ND	ND	ND	ND	12	75	Supersonic inlet flow
"	ND	ND	ND	ND	ND	10	76.8	Supersonic inlet flow
Reeves (1977)	24	0.991	1.097	1.011	0 (tapered passage)	6	ND	 Section
"	20	1.043	1.083	1.14	0.15*	10	ND	 Section
"	24	1.050	1.100	≈1.0	0.38*	10	ND	 Section
Groh(1969)	19	1.0	1.049	1.00	ND	2.5	84.0	Designed for minimum incidence
"	24	1.00	1.062	1.00	ND	2.5	83.6	Designed for minimum incidence
"	31	1.00	1.081	1.00	ND	2.5	83.9	Designed for minimum incidence
Klassen (1973)	28	1.00	1.100	1.00	0.235	1.9	82	Under-performed cascade. Incidence mismatch
"	28	1.00	1.100	1.00	0.235	1.9	80	Under-performed cascade. Incidence mismatch
Japikse	Assorted	ND	ND	ND	ND	Various	ND	Selection tested together with detailed statics

* Based on hydraulic diameter

ND Not Defined in reference

CHAPTER 2
Impeller Flow Studies

This chapter describes experimental and numerical investigations into the flows within and discharging from the Rolls-Royce '35D' research centrifugal compressor impeller whilst in the vaneless diffuser configuration. Such a significant undertaking was felt necessary for the following reasons:

- In order to quantify the flow entering the diffuser, it is necessary to measure the flow discharging from the impeller. The measurements could then be used as prescribed inlet boundary conditions for future CFD diffuser investigations. The accurate implementation of these conditions is thought imperative as it has been well documented earlier in this thesis that the quality of the inlet flow strongly affects the diffuser performance.
- It is important to qualify the impeller flow structure. This would ascertain whether the chosen impeller could be regarded as of a representative design. This could have impact on the range of applicability of the resulting pipe diffuser design rules developed in this thesis.
- The vaneless arrangement was to be used as the comparative baseline configuration
- Detailed traverses would test and confirm the fixed performance instrumentation.

Outline of Chapter

Initially, the pertinent aerodynamic flows found within centrifugal compressors are described in order to define particular features. This helps to render precise the terms used in later discussions.

Following this, the test rig and overall aerodynamic performance of the impeller are presented. Details of the significant rig modifications necessary for the test program are relegated to APPENDIX C, as this information may be omitted without loss of continuity. However, this contribution should not be neglected as these modifications required careful and rigorous specification to exacting standards to ensure safe operation at tip speeds of up to $533ms^{-1}$ (35,000 rpm) and nominal powers up to 1MW. This work amounted to 20-man weeks of machining and the mechanical design and engineering-drawings of over 40 major components. APPENDIX A presents the performance data acquisition and safety monitoring systems. These also required significant design and specification effort.

The detailed flow measurements, taken at the impeller inlet and exit, are then described. The measurement method utilised a combination of pneumatic probes and high speed pressure transducers, the latter capable of resolving the unsteady jet/wake flows. These probes were traversed using a purpose-built 2-Axis stepper system that allowed both movement across the passage width and probe rotation. Together with the high speed ADC card, this resulted in over 350 measurement points per blade passage, each of these ensemble averaged 500 times. In order to measure within a confined and harsh environment, a novel measurement system was specifically developed. In conjunction with the traverse gear, a single ultraminiature pressure transducer took measurements over a range of angular positions and through a curve fitting algorithm the flow angle was evaluated. Details of this measurement system and its development are given in APPENDIX B and represent 6 man-months of specification, development and design.

Following the experimental results, predictions are presented from a centrifugal compressor design and three CFD computer programs. The centrifugal compressor design program, developed by Herbert (1980), was used as a design tool for the diffuser systems and its accuracy and applicability was to be benchmark tested against the simpler vaneless diffuser configuration. Primarily the CFD codes were used to gain additional insight into the impeller blade passage flow, which was not measured in this investigation. Attempts were made using both pressure-based (FLUENT and TURBO3D) and time-marching (RAMPANT) CFD codes.

2.1. DESCRIPTION OF THE 35D TEST COMPRESSOR

The impeller was of centrifugal backswept type and details of its attributes are shown in Table 2.1. The flow discharged at a tip speed of 533ms^{-1} into a parallel walled vaneless diffuser which extended up to a radius ratio of 1.50 (see Figure 2.1). This was followed by an abrupt step from 12.05mm to 21.54mm width at entry into another parallel section. The flow was then turned, at an impeller tip radius ratio of 2.19, by a bend of constant normal flow area. Finally, the flow was diffused by an annular diffuser of area ratio 2 prior to dumping into a large plenum.

The abrupt step and relatively wide discharge width were incorporated to allow simple pipe diffuser modular sections to be inserted later. This configuration was therefore not considered by the author to be an optimum vaneless diffuser design, and indeed, as will be described later, was attributed for premature surge.

Nominal Design Pressure Ratio	5.3
Design Speed (rpm)	34,825
Design Mass Flow ($M\sqrt{\theta}/\delta$) (kg/sec)	4.1
Full Rotor Blades	17
Tip Diameter (m)	0.29253
Tip Width (m)	0.01175
Backsweep (deg)	24°
Rake	8°

Table 2.1 Description of Impeller

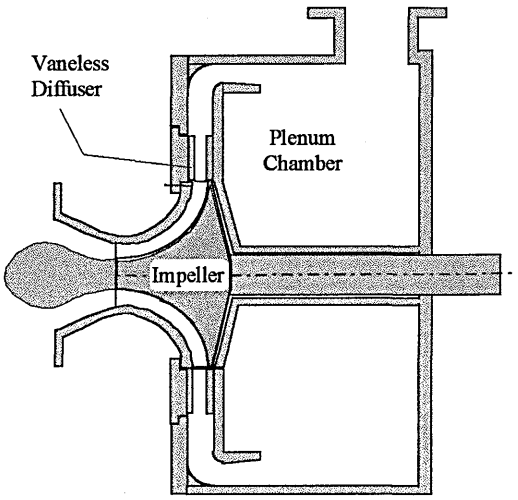


Figure 2.1 35D Impeller Cross-Section

2.2. General Description of Flows within Centrifugal Compressors

The designations used within this thesis are shown in Figure 2.2 for completeness and to avoid ambiguity.

The flows within centrifugal compressors may be divided into primary and secondary streams. The primary are governed by the rotational body forces and the secondary by viscous interactions.

2.2.1 Primary Flows

2.2.1.a Body Rotational Forces

The (inviscid) momentum equations of fluid motion may be written relative to the impeller frame of rotation as thus:

$$\rho\frac{D\overline{w}}{Dt} = -\overline{\nabla}p - 2\rho(\overline{\omega}\times\overline{w}) - \rho\overline{\omega}\times(\overline{\omega}\times\overline{r}) \qquad \text{-(2.1)}$$

where $\overline{\omega}$ and $\overline{w}$ are the rotation of the frame of reference and flow relative velocity respectively.

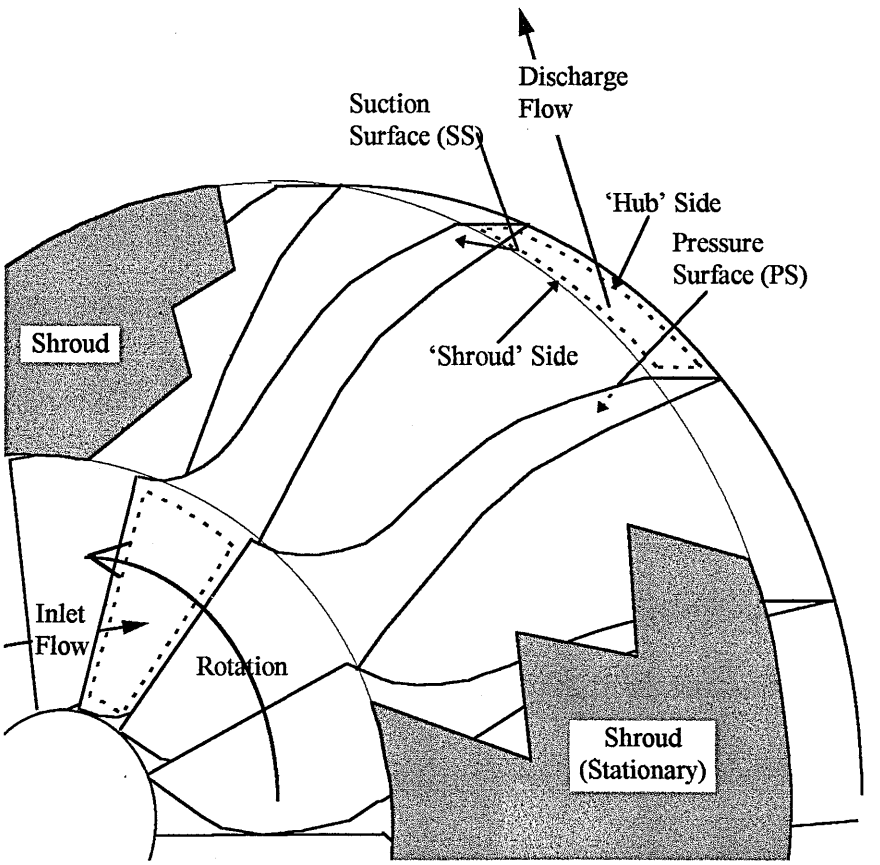


Figure 2.2 Names and Designations of Pertinent Impeller Regions

The last two terms are the coriolis and centrifugal force contributions. For convenience we may now write the above in terms of the streamline direction [Hirsch et al (1996)].

$$\frac{Dw}{Dt} = -\frac{1}{\rho}\nabla p + \frac{w^2}{R_b}\bar{i}_n + \omega^2\bar{r} - 2\omega w \sin\sigma\bar{i}_n \qquad \text{-(2.2)}$$

The second term on the right has been 'added' to account for the restrained reference frame and allows streamline curvature to be properly accounted for. See Figure 2.3

Generally speaking, the streamline curvature term, R_b, is large for centrifugal compressors and therefore, at the impeller exit, it is the coriolis contribution that dominates. Consequently, there is created a negative static pressure gradient from the pressure to the suction blade sides (hence the 'pressure' and 'suction' nomenclature). This phenomenon has been recognised in the past by CFD investigators where, in order to prescribe an impeller static pressure discharge boundary condition, a circumferential distribution of the form below was assumed:

$$\left(\frac{1}{r}\frac{dp}{d\theta}\right)_{exit} = -2\rho\omega w \qquad \text{-(2.3)}$$

In the meridional plane there are forces due to curvature and centrifugal loading. These are balanced by a pressure gradient from hub to shroud (See Figure 2.3)

We therefore have:

$$\frac{1}{\rho}\frac{\partial p}{\partial n_m} = \frac{v_\theta^2}{r}\cos\sigma - \frac{v_m^2}{R_m} \qquad \text{-(2.4)}$$

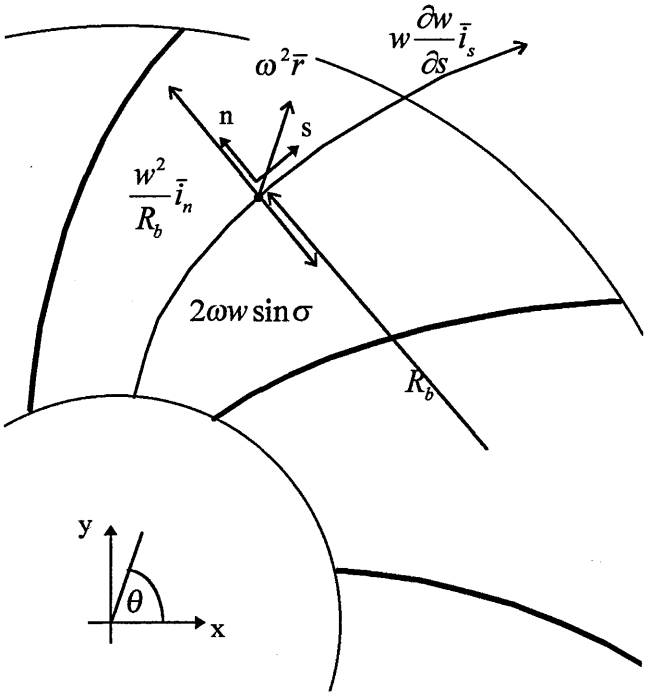


Figure 2.3 Axial Plane Body Forces

As the flow approaches the impeller exit, $\cos\sigma \rightarrow 0$ and there is a positive static pressure gradient created from the shroud to the hub. This balances the body force due to meridional curvature.

2.2.2 SECONDARY FLOWS

The secondary flows in each of the blade passages shown in Figure 2.5 are described below. These have been assembled from (similar but not mutually exclusive) descriptions given by Hirsch (1996), Elder (1994) and Johnson and Moore (1983[1], 1983[2]).

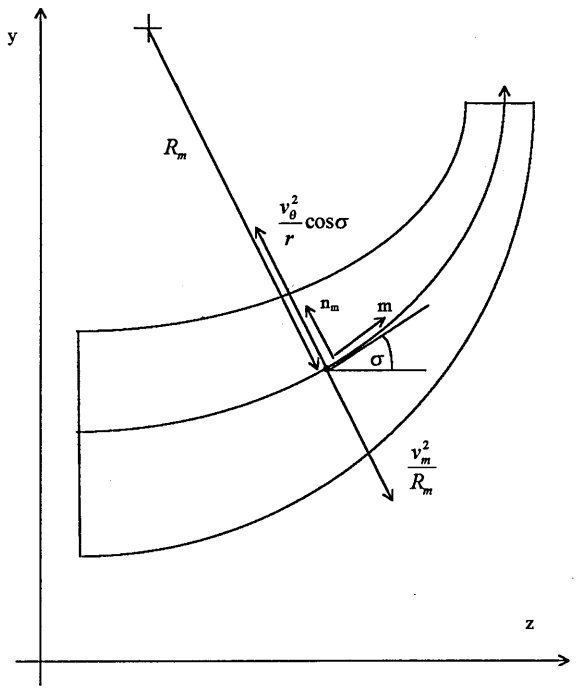


Figure 2.4 Meridional Body Forces
(σ is defined in Figure 2.4)

2.2.2.a FLOW A- WAKE FORMATION

Despite the detailed discussion of the aforementioned inviscid forces, they do not in fact dominate at the impeller discharge. Generally it is agreed (Hirsch et al (1996)) that towards the impeller exit, the viscous forces shape the flow. Primarily, this sensitivity to flow viscosity is due to the increase in flow area and subsequent diffusion within the impeller passage. The developed adverse streamwise pressure gradient invariably causes reverse flow both on the impeller shroud and on the suction surfaces of the blades.

It is the combination of these two areas of separation that is denoted the 'wake' of the familiar two zone jet-wake structure at the impeller discharge. This area of low energy fluid is therefore located near the suction-surface/shroud corner region of the blade passage, Flow 'A' in Figure 2.5.

The reader should note that the 'wake' region is not completely attributed to the separated boundary layer flow. The losses in this region are also thought to be made up from the destructive interaction of counter-rotating passage vortices, as described later, and its location is effected by a combination of these rotational forces and tip clearance flows (e.g. Skoch et al, 1997). The identification of these two flow regions also clouds the jet/wake model picture. Although a popular model and well accepted in the 1960's and 1970's, the two flows are not generally easily distinguishable, particularly for impellers with backward curved blades. Eckhart (1980), from his comparative

measurements between a radial and comparable backward swept impeller, was unable to distinguish a distinct wake in the latter. Clearly one of the difficulties with such a complex flow is that a wake is not necessarily just low momentum fluid, rather it is by definition a region of separated flow. To determine whether a flow is a wake, it is therefore necessary to trace a suspect region back to an original separation. Even with comprehensive measurements and CFD, this is not trivial due to the complex 3-D flows within typical radial turbomachinery.

Measurements by Krain (1988) showed an extreme case for a highly backward curved impeller with uniform discharge flow. Until Krain's work, the closest to a uniform exit flow was a smeared jet/wake. However, it is undisputed that the majority of radial impellers exhibit a region of low momentum fluid near the shroud/suction surface.

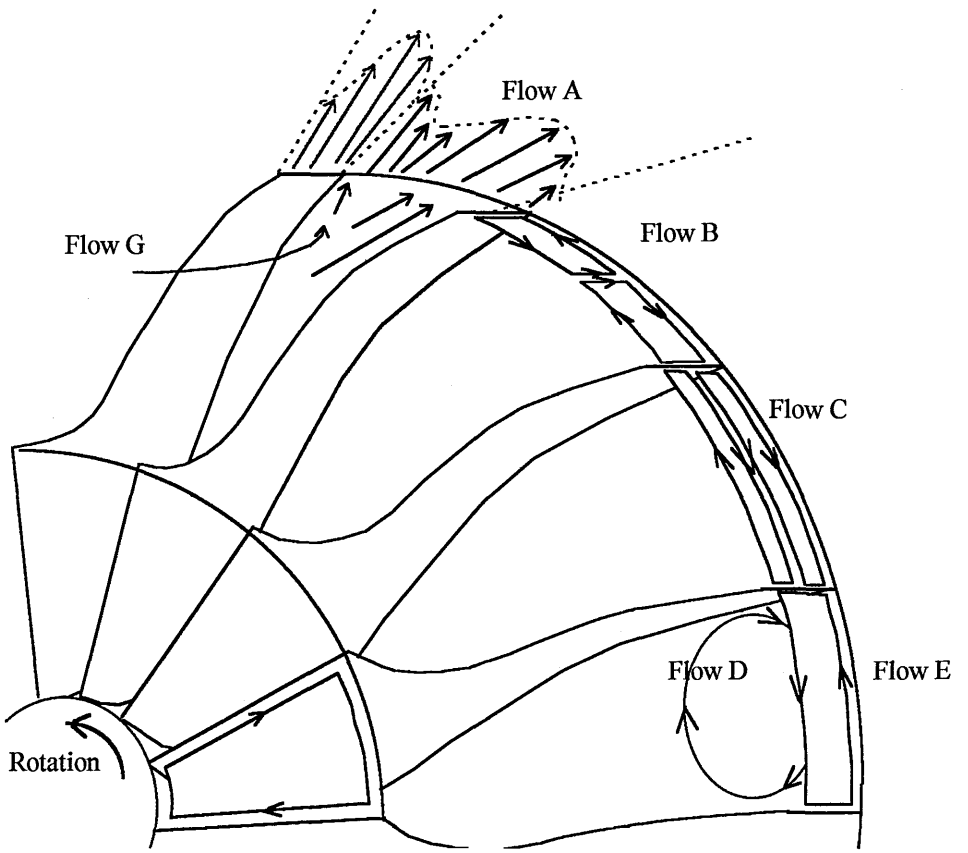


Figure 2.5 Flows within Centrifugal Impeller Blade Passages

2.2.2.b FLOW 'B'- MERIDIONAL TURNING VORTEX PAIR

These passage vortices are formed by turning in the meridional plane. The rotation is created by the relative velocity between the core and the near wall flow. This difference

is due to the near-wall boundary layer that decelerates the flow in the axial direction. Their presence is therefore independent of impeller rotation and consequently their form is also found in simple duct bends.

2.2.2.c FLOW 'C'- CASCADE TURNING VORTEX PAIR

These are formed by turning in the circumferential direction and are commonly named cascade vortices due to their similarity with the dominant vortices found in axial turbomachinery blade passages. Generation of these vortices are like the meridional vortex turning pair, but are turned in a different plane.

2.2.2.d FLOW 'D'- 'IRROTATIONAL' VORTEX

If we assume a uniform inlet flow into the impeller then, relative to the rotating frame, there is a counter-rotating inlet vortex formed at the blade passage inlet. This vortex is sometimes used to explain the impeller 'slip'. Calculation is based on the vortex peripheral speed. The diameter of the vortex is equal to the blade circumferential pitch (i.e. impeller tip circumference divided by the number of blades) and it rotates at the impeller speed.

2.2.2.e FLOW 'E'- PIPE VORTEX

If we consider the blade passage as a series of thin control volumes with viscous interaction between each, then if the inlet disk is rotated, so will the discharge disk. In the rotating reference frame, as discussed, we have such an inlet rotation. This therefore creates the vortex in the impeller discharge plane as shown in Figure 2.5.

2.2.2.f FLOW 'D' AND 'E'- CORIOLIS CONTRIBUTION

In addition to the physics described in the last two sections, contributions from the coriolis body forces will also be present. These forces will be generated when the flow is inclined to the axis of impeller rotation i.e. away from inlet and discharge. The component of vorticty created may then be projected onto the planes shown in Figure 2.5 to give rotation in the same sense as Flows 'D' and 'E'.

2.2.2.g FLOW 'F' AND 'G'- TIP CLEARANCE FLOWS

For an unshrouded impeller there is a running clearance gap (approximately 0.025 to 0.04 of the blade height at tip) between the impeller tip and the shroud (see Figure 2.6). Two flow phenomena are then present. The first is due to the pressure difference across the blades encouraging tip leakage. This flow pushes the shroud/suction-surface wake away from the corner. The second flow distortion is caused due the shroud wall friction. This induces a passage vortex in the same direction as Flow 'E'.

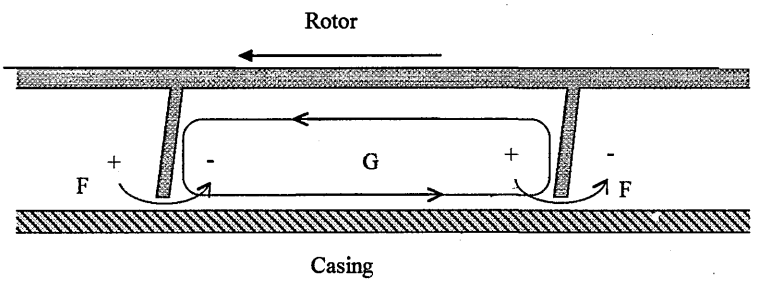


Figure 2.6 Tip Clearance and Shroud Induced Flows

2.2.3 RESULTANT FLOW

The combination of all these primary and secondary flows yields a complex resultant flow-field. Despite the wide range of radial turbomachinery of varying specific speed and backsweep, contrasting regions of high and low velocity flows are invariably detected. These are conventionally denoted as the 'jet' and 'wake' regions respectively, although their form and relative sizes and strengths have some dependency, as already noted, with backsweep. Early distinction was two-dimensional in the axial plane (e.g. Dean and Senoo, 1960) with the wake portion of flow trailing the blade rotation. However, with the advent of further intrusive impeller measurements (particularly Eckardt (1980)), the wake term was redefined to reside in the blade-suction/shroud corner. Of particular note was the appearance of a 'jet' or a region of high throughflow velocity on the shroud/hub corner. Measurements by Johnson and Moore (1983) are a representative example of this flow pattern, Figure 2.7(a). The wake term is seen to occupy 3/4 of the shroud and 1/2 of the suction surface. A high velocity region, defined as the jet, may be seen near the hub/suction region.

It is interesting to note the associated relative total pressure distribution shown in Figure 2.7(b). Two distinct triangular regions of flow separate the pressure/hub and suction/shroud surfaces. These regions could also be defined as 'jet' and 'wake' regions (as done by Dean (1973)). To avoid any confusion, the former or Eckardt (1976) definition will be used. The highlighted region of elevated relative total pressure in the pressure/hub region will henceforth not be given special designation..

The resultant secondary pattern shown in Figure 2.8 (Eckardt (1976)) shows the complex interaction between the secondary flows described earlier. Strong blade to blade flows are present. These, near the shroud are seen to be of sufficient strength to oppose the cavity derived direction. The wake flow is visible, as expected, in the shroud/suction corner.

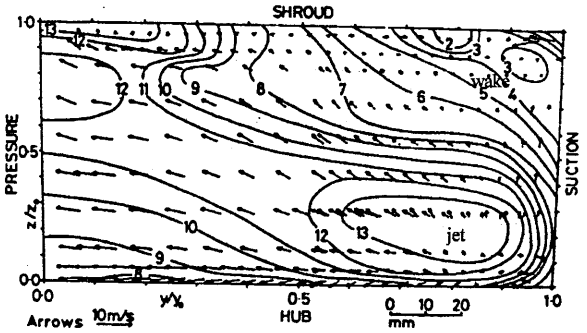


Figure 2.7(a) Relative Velocities at Impeller Discharge

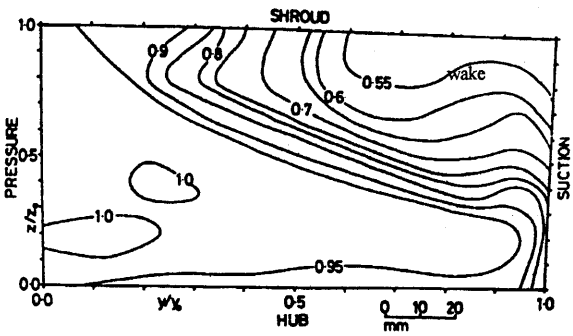


Figure 2.7(b) Relative (Non-Dimensional) Total Pressure at Impeller Discharge

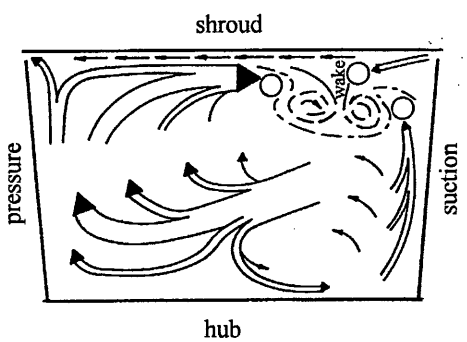


Figure 2.8 Sample Resultant Relative Impeller Exit Flow Pattern (Eckardt (1976))

2.3. Overall Performance of The 35D Compressor

The compressor overall performance, with vaneless diffuser, was measured using the set-up shown below in Figure 2.9(a) and (b).

Mass flow was measured using a calibrated bellmouth flare and all inlet conditions were measured via pressure and temperature rakes. Upstream of these was a throttling gauze that allowed operation with a depressed inlet. This reduced the compressor power requirement and enabled running at 100% design speeds.

The impeller exit temperature was measured within the vaneless diffuser, again utilising rakes. However, instead of total pressure rakes, the discharge total pressure was calculated from static tappings at the impeller tip. This calculation and details of the

all instrumentation was remotely controlled from a control room protected by steel plate and armoured glass. Accelerometers and velocitimeters monitored all bearings together with capacitance and cut-wire devices to monitor tip clearance. Figure 2.10 presents the measured performance of the compressor using the described instrumentation. These results are in agreement to those measured by Pratt (1973) at Rolls-Royce. At the corrected 'design' mass flow of 4.1 kg/sec the impeller total pressure ratio was 6.0 with an impeller total efficiency of 89%.

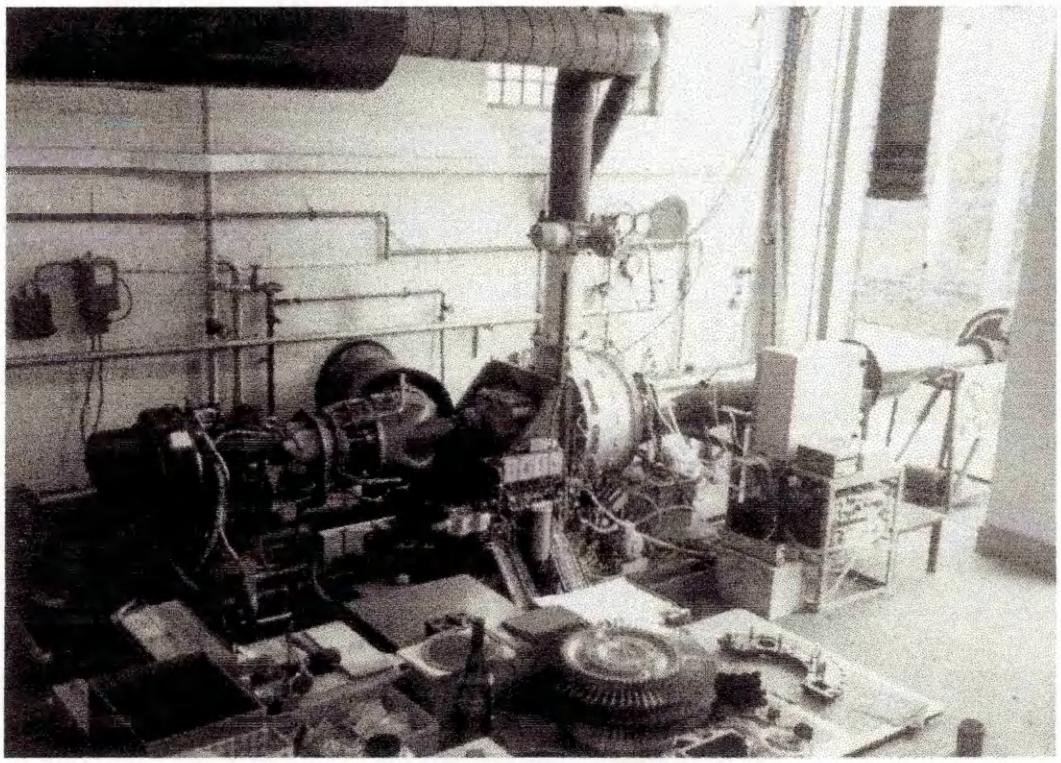


Figure 2.9(a) Picture of Experimental Test Facility

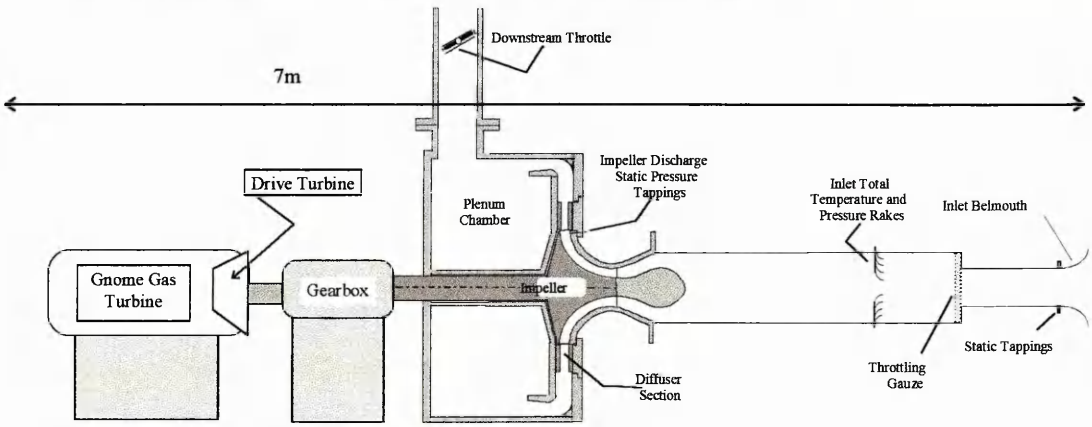


Figure 2.9(b) Sketch of Experimental Test Facility

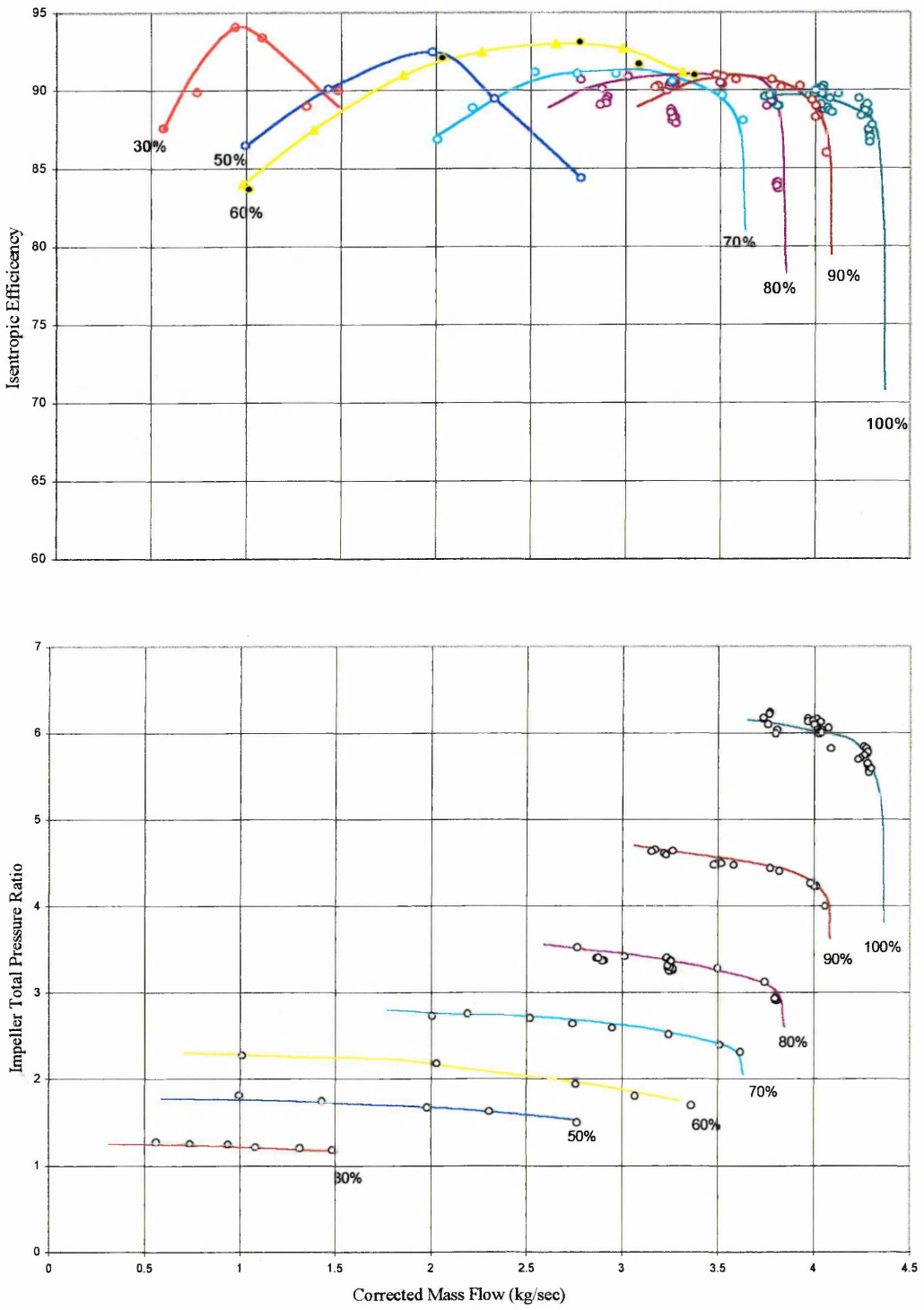


Figure 2.10 Impeller Performance in Vaneless Diffuser Configuration

2.4. UNSTEADY TOTAL PRESSURE TRAVERSES

Detailed traverses were carried out using ultra-miniature pressure transducers at 1.05% of the impeller tip radius. These probes were immersed into the flow and traversed across the passage width (see Figure 2.11), to gain a shroud to tip total pressure distribution. In addition, they were rotated about their axis using a novel technique developed by the author enabling flow angle measurement. Full development, calibration and operational details are described in Appendix B.

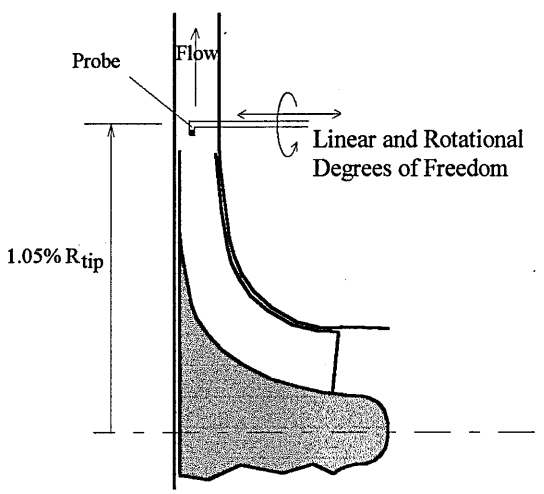


Figure 2.11 Measurement at Impeller Discharge

For this, and in subsequent investigations, six duty points were examined. These corresponded to 'near stall', 'design' and 'near 'choke' at both 80% and 100% speeds. Although the primary interest was in the latter speed, the 80% speed investigations were carried out in order to have an experimental data set that could be compared against proposed pressure-based CFD computations: these were not expected to be able to cope with the high Mach numbers present at full speed within the impeller.

For brevity, only the full speed measurements are discussed here. The 80% measurements are presented in APPENDIX D.

2.4.1 ACCURACY OF MEASUREMENTS

The pressure transducers used (Type: Kulite XCE-062) were shown sensitive to temperature variations and it was necessary to include an additional compensation to correct for these variations. The method used was similar to that outlined by Cherret (1990) and required the calibration of pressure and temperature against transducer supply current and output potential. The electronics and procedure necessary are presented in APPENDIX B.

Traditionally, these types of total pressure transducers are used in conjunction with static-type flush mounted sensors to form wedge or pyramid type arrangement. These

have been used successfully in a variety of applications that require both pressure and flow angle measurement. However, these arrangements have several disadvantages: the large amount of wind tunnel calibration; the increased size of the combined device; and the uncertainty of the probe measurements due to unsteady aerodynamic effects. The latter is particularly prevalent for wedge type devices (e.g. Cherret et al, 1994).

An alternative approach was developed by the author that used an isolated pressure transducer which was yawed over a range of incidences into the flow. From the collection of readings, the flow angle was determined together with the total pressure. This method had the advantage of being small and did not require extensive calibration. In addition, it is expected that these isolated probes are less sensitive to the deleterious influence of unsteady flows.

From APPENDIX B the following errors are apparent:

Total Pressure	± 0.45 Bar
Flow Angle (via curve fit)	± 3°
Total Temperature (from temperature correction)	± 40°C

The above total pressure errors represent the extreme case in that the drift was mainly incurred from resistance changes in the probe due to several immersions into the hot impeller flow- the probes were operating at the stated manufacturer's maximum temperature. However, it should be highlighted that the probe response still remained linear against pressure despite this drift (see APPENDIX B) and therefore the error in fluctuating component of pressure is much less- expected to be over an order of magnitude less, at around 0.03Bar. Therefore the pressure transducer reading should really only be treated as a device to measure the flow unsteadiness, quantifying pressure fluctuation amplitudes.

Traverse gear positional inaccuracies were incurred by a combination of mechanical and human set-up error. These error are estimated as:

Axial Positioning	± 0.1mm (due to the stepper drive free play)
Angular Positioning	± 0.25° (human error on setting up)

2.4.2 Unsteady Total Pressure Readings

Using the 2-axis traverse gear and Kulite pressure transducers, the total pressure, flow angle and a measure of the flow unsteadiness near the impeller tip were recorded. The flow unsteadiness was quantified by taking the standard deviation of total pressure measurement for each spatial location.

2.4.2.a MEASUREMENTS LOCATIONS

In the axial direction measurements were taken at 1.5, 2.2, 3, 4, 5, 6, 7, 8, 9, 9.8 and 10.5 mm from the shroud surface of the 12.05mm wide vaneless diffuser. In the circumferential direction, for the full speed investigations, 40 time steps at 333kHz were recorded. This represented approximately 133% of the time for a blade passage to pass. Together with the large number of axial traverse points, the resulting spatial resolution was very high (see Figure 2.12).

Full design speed results are shown below and represent averages of 500 samples per point. From the measured total pressure, flow angle and total temperature (from the Kulite probe), and together with the static pressure instrumentation within the vaneless space, relative total pressure, radial velocity and relative tangential velocity were all calculated. The main assumption in these calculations was that there were no variations in static pressure across the measurement plane and no circumferential variation in the (Kulite) measured total temperature. The latter values were scaled prior to use by the ratio of Kulite mass weighted temperature to that measured downstream by the thermocouple rakes. This ensured the conservation of thermal energy flux.

It should be noted that the plotted data shows up to 55 time steps, 15 more that measured. The additional points were periodically transposed to ensure that a complete blade passage could be displayed.

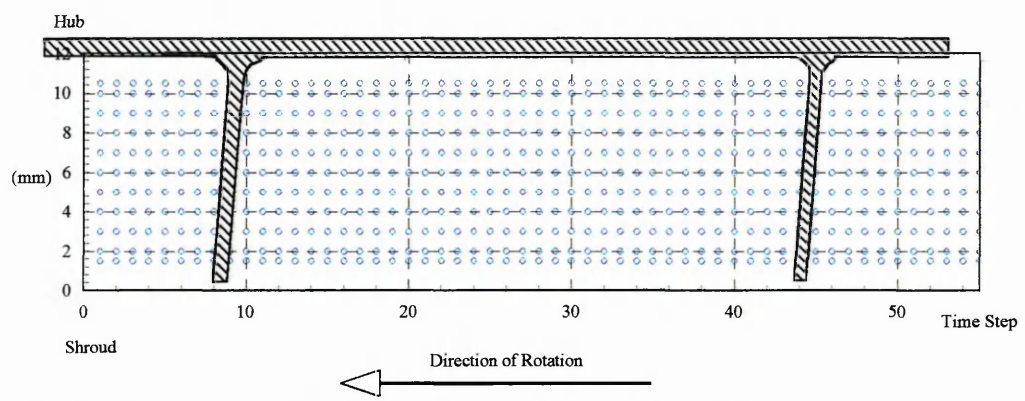


Figure 2.12 *Sketch Showing the High Spatial Resolution of Traverse and Approximate Blade Location*

The location of the suction and pressure surfaces are estimated to be at time steps 11 and 45 respectively, although some caution must be applied to such interpretation since the measurement plane is strictly within the vaneless diffuser and clearly some distortion will occur in the flow from the impeller exit. It is for this reason that the blade locations are not explicitly presented.

2.4.2.b PRESENTATION AND DISCUSSION OF RESULTS

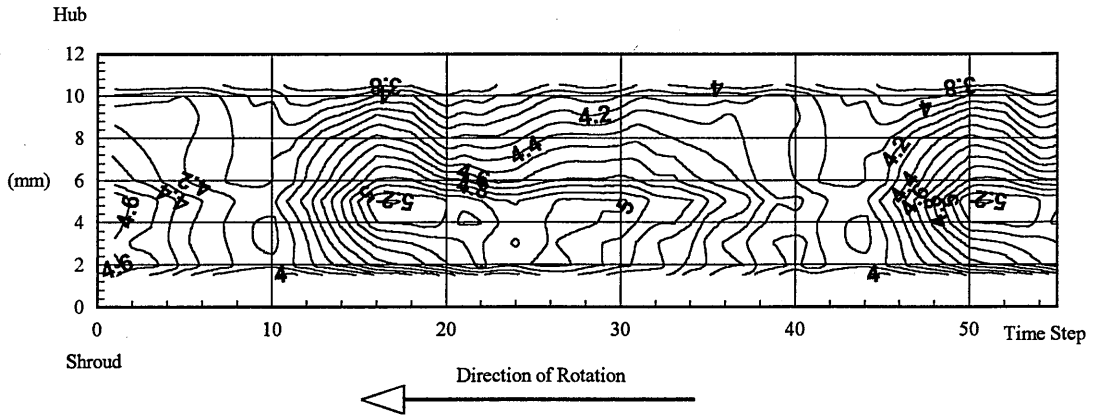
As already introduced, measurements were taken near the impeller discharge (at 1.05 R_{tip}) at 100% and 80% of design speed at three locations on each speed characteristic. For brevity, only the 100% speed results are presented here; the remaining are given in Appendix D).

The 100% speed measured flow properties are presented in Figures 2.13 to 2.15. These are total pressure, flow angle and standard deviation of total pressure.

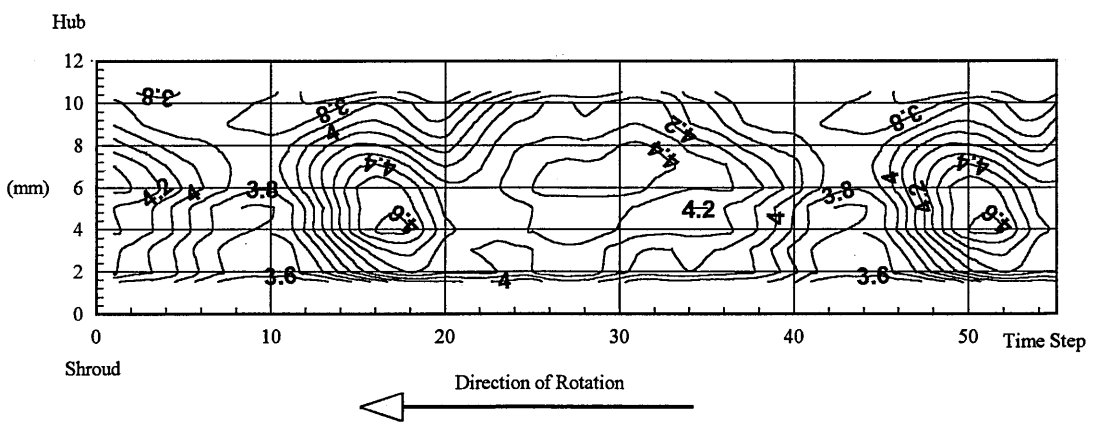
At all measured flow conditions, there are two distinct regions of high total pressure (Figure 2.13). The highest of these is located near the blade suction surface and the other, joined by a small saddle, presents itself almost mid-channel. Of particular interest is the suction surface peak, where a region of low pressure is expected due to blade suction separation. This paradox is explained by examination of the relative total pressure (see Figure 2.16). This perspective gives the more familiar wake picture described earlier. The region of high total pressure, now transposed to the rotating frame, shows itself as a low energy region. A region of high relative total pressure shows itself in the hub/pressure region, separated by diagonal isobars indicating the blade location. These two regions are seen to change in shape over the mass flow range examined. Near surge, the relative total pressure is seen to stratify axially with the wake region occupying almost all of the shroud surface. As the mass flow is increased, this region rotates clockwise to segregate the flow into two triangular zones: the hub/pressure corner dominated by flow of high relative total pressure; and the shroud/suction corner wake, possibly formed from a combination of the shroud and blade separated flow. At all mass flows there is a distinct region of low relative total pressure near the shroud. This region also includes areas of reverse flow, as presented in Figures 2.14 and 2.18.

In Figure 2.17, the profile rotation, pivoted about 4mm from the shroud, indicates that there is a migration of the bulk flow from the centre to the hub side as flow rate is increased. Therefore, instead of the additional mass flow 'filling' the passage, the flow with increased meridional velocity is unable to follow the shroud curvature resulting in further shroud separation. Further evidence of this re-distribution is shown in Figure 2.18. The radial velocity migration from the shroud is clearly visible, together with increased radial velocity gradients in the axial direction.

Near Surge



Design



Near Choke

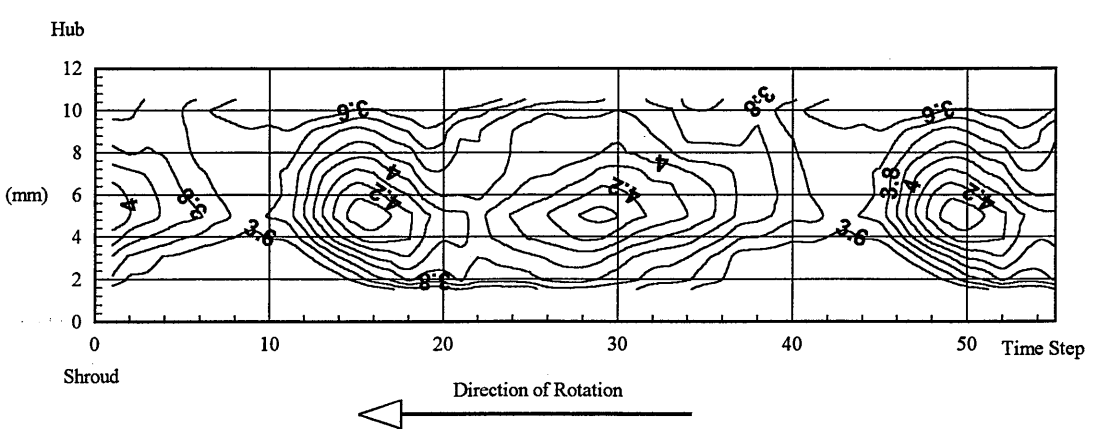
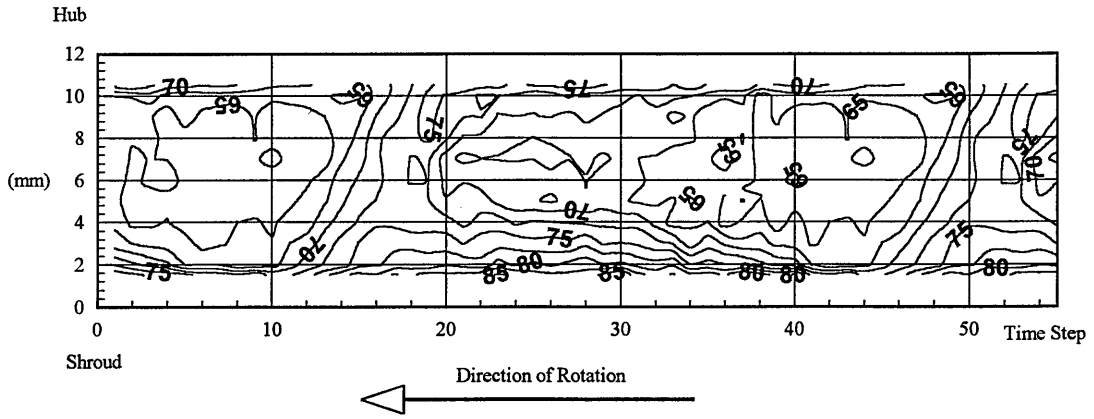
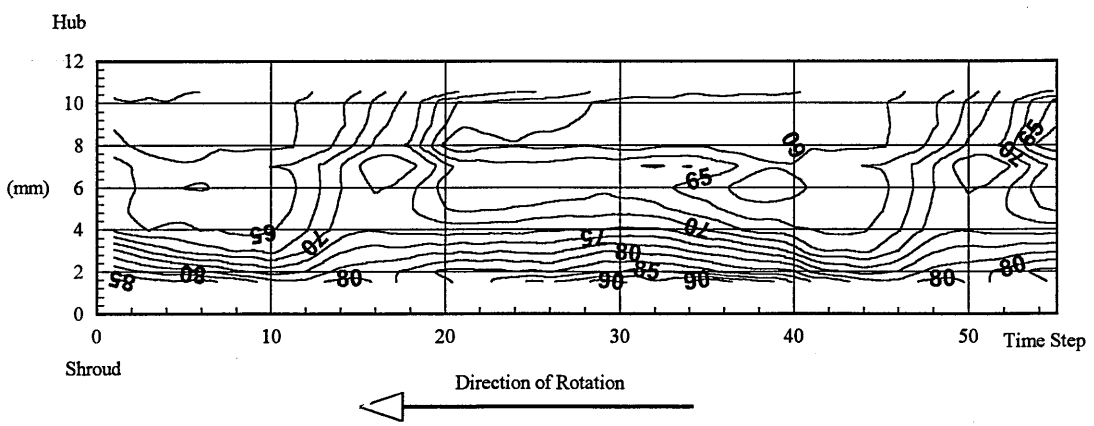


Figure 2.13 Total Pressure at 1.05% R_{tip} at 100% Speed (BarA)

Near Surge



Design



Near Choke

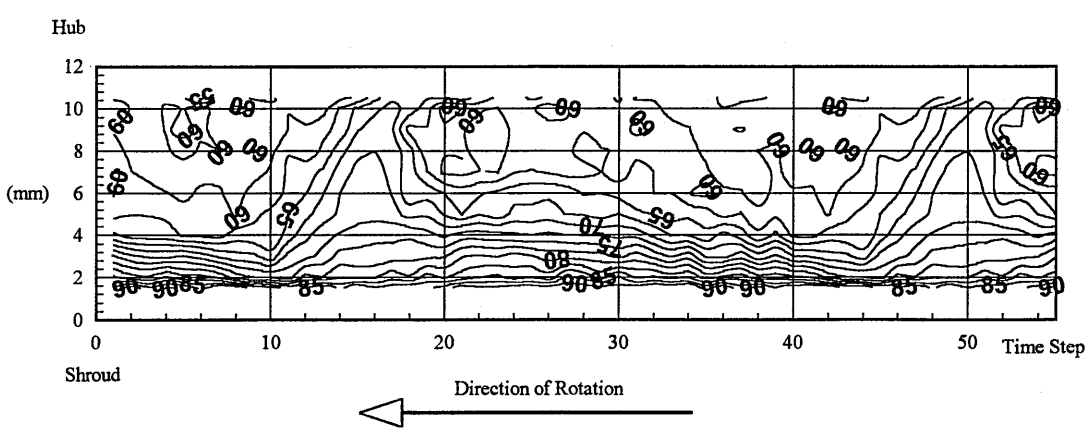
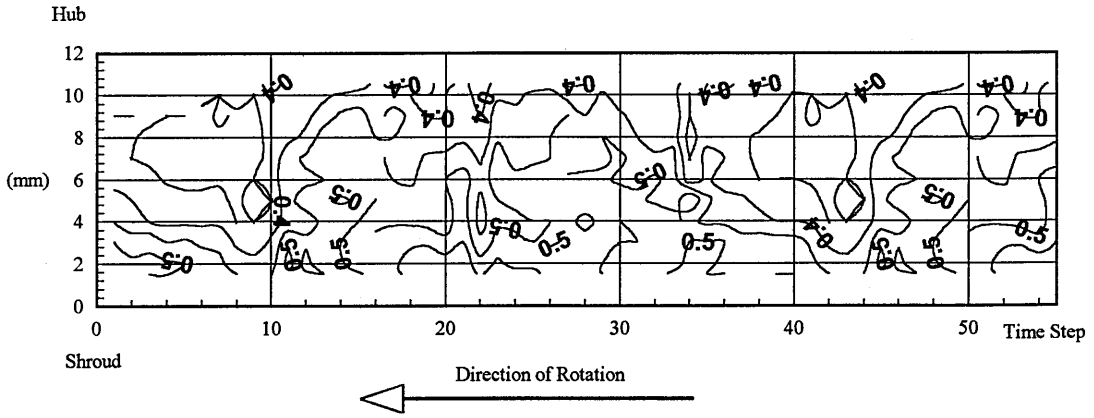
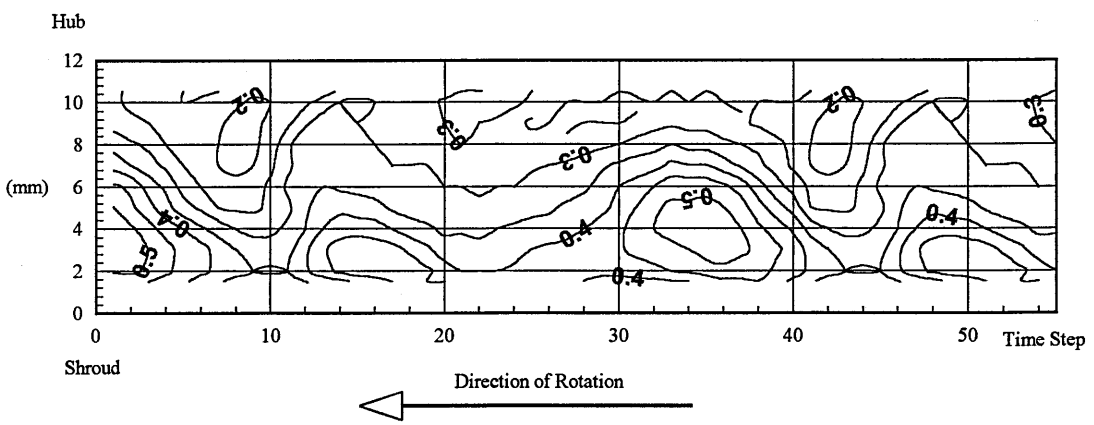


Figure 2.14 Flow Angle (wrt Radial, Degrees) Measured at 1.05% R_{tip} at 100% Speed

Near Surge



Design



Near Choke

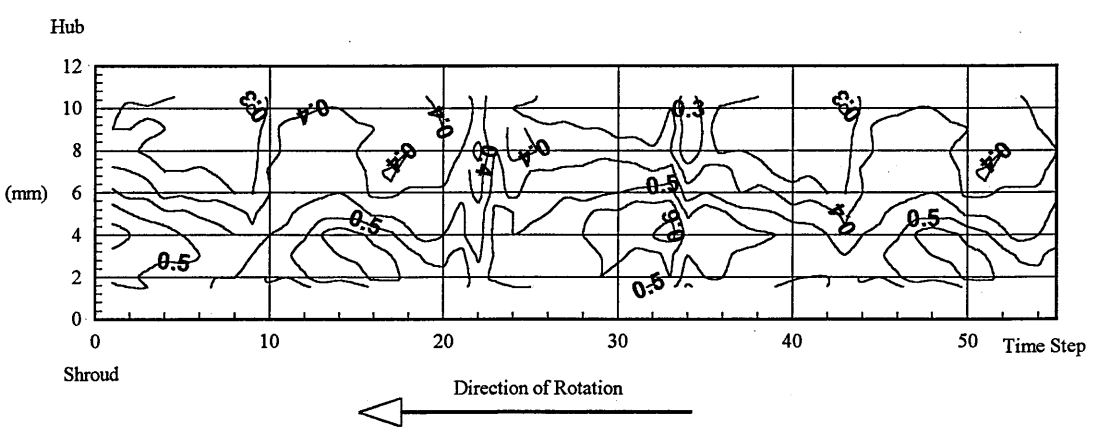
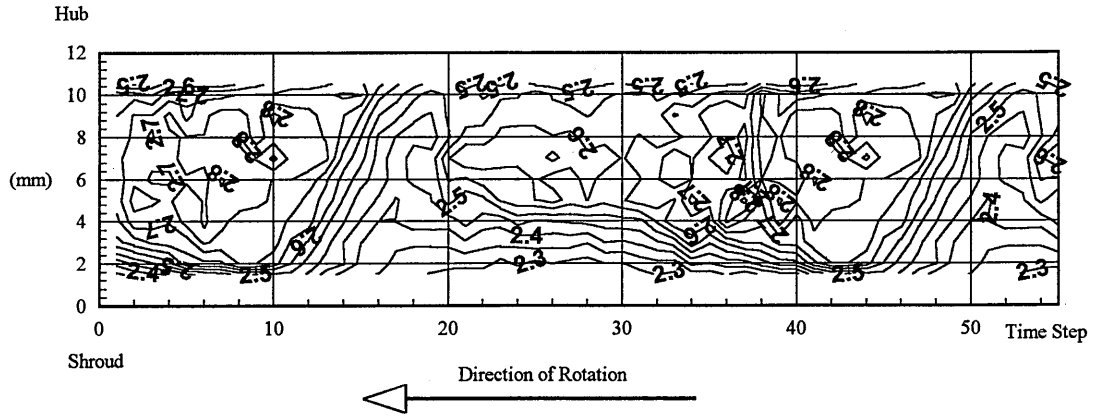
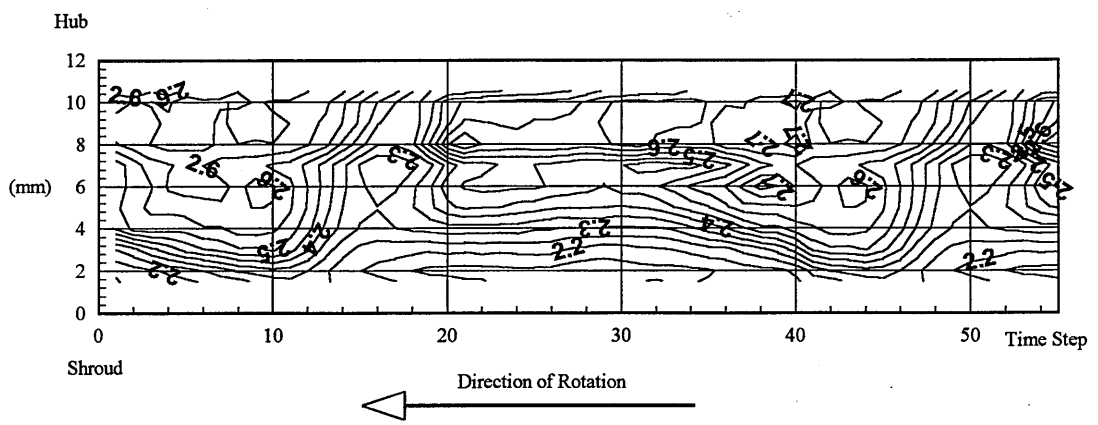


Figure 2.15 Standard Deviation of Total Pressure at 1.05% R_{tip} at 100% Speed (BarA)

Near Surge



Design



Near Choke

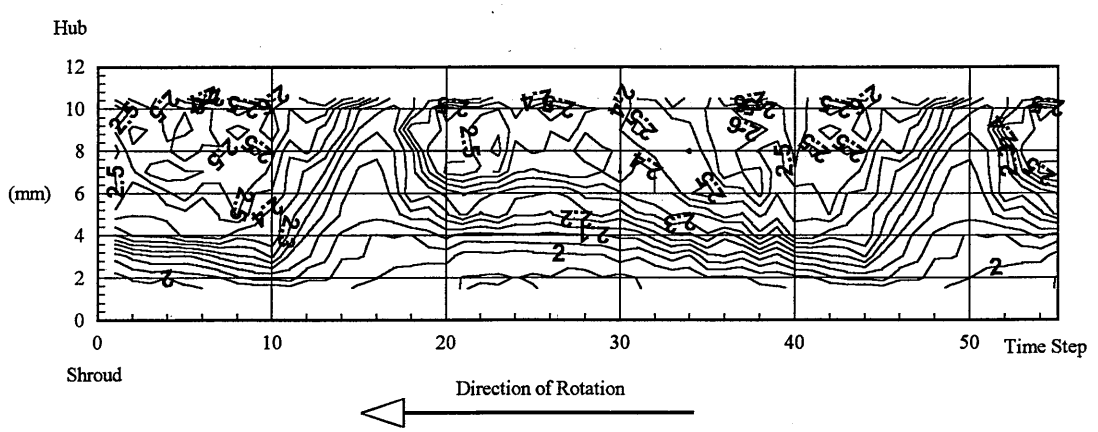
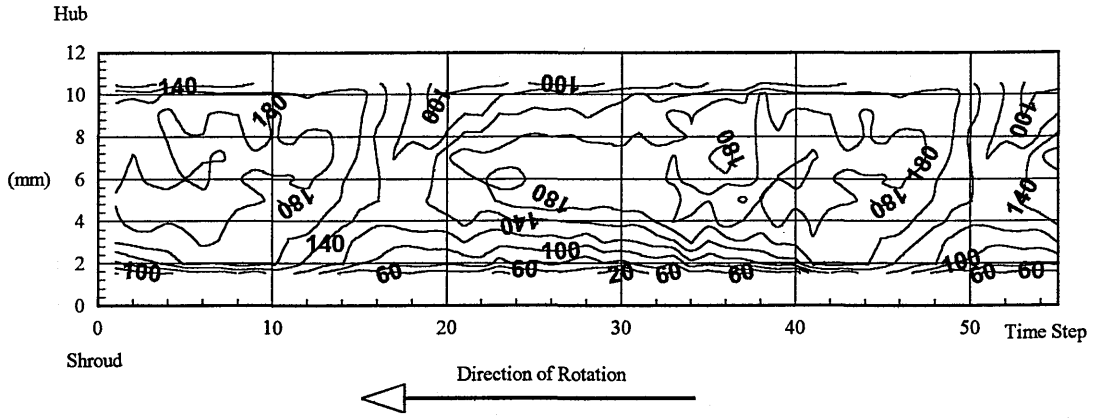
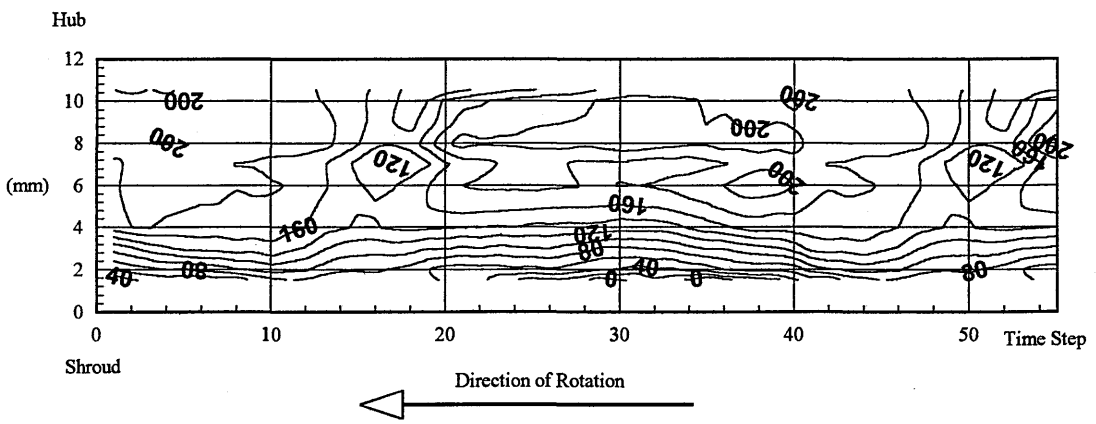


Figure 2.16 Relative Total Pressure at 1.05% R_{tip} at 100% Speed (BarA)

Near Surge



Design



Near Choke

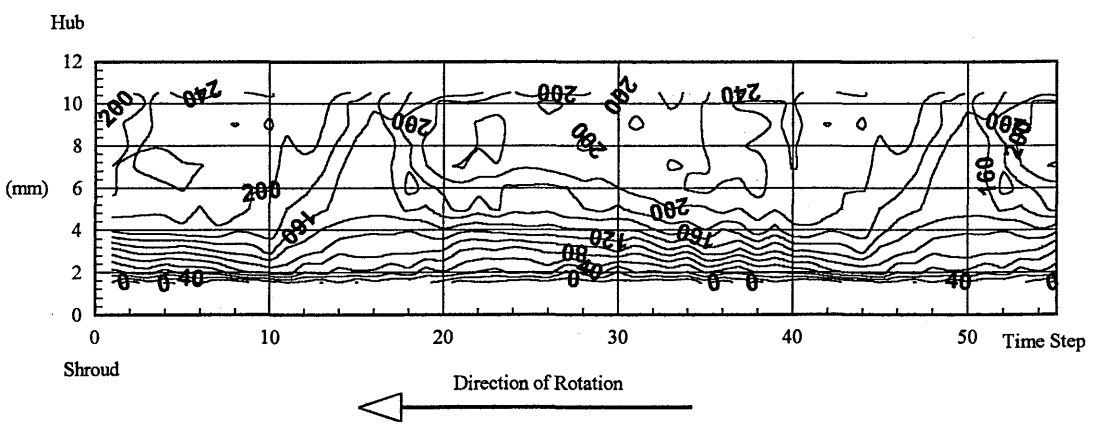
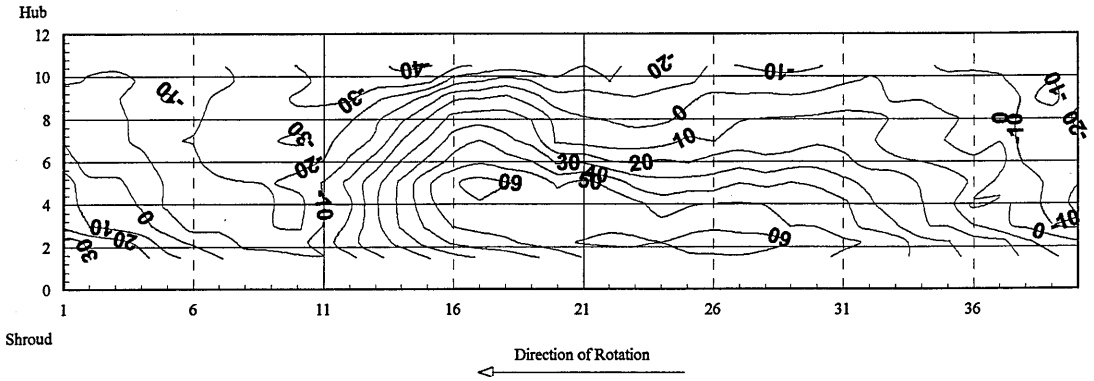
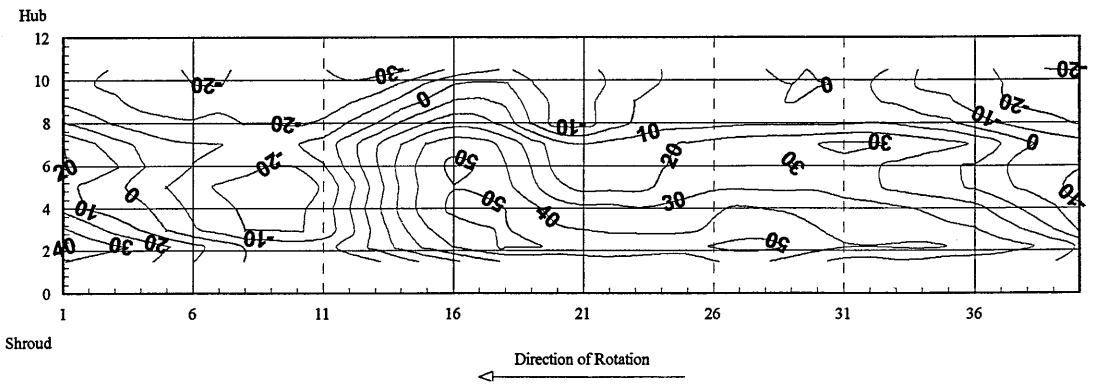


Figure 2.18 Radial Velocity at 1.05% R_{tip} at 100% Speed (ms^{-1})

Near Surge



Design



Near Choke

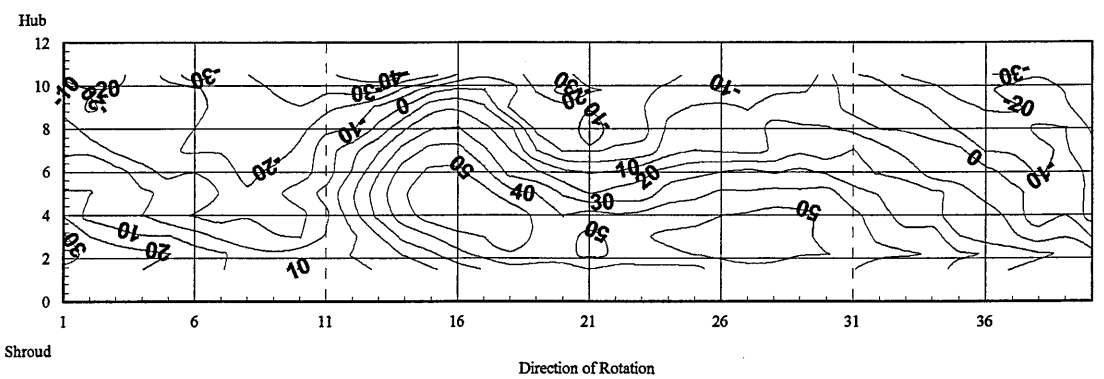
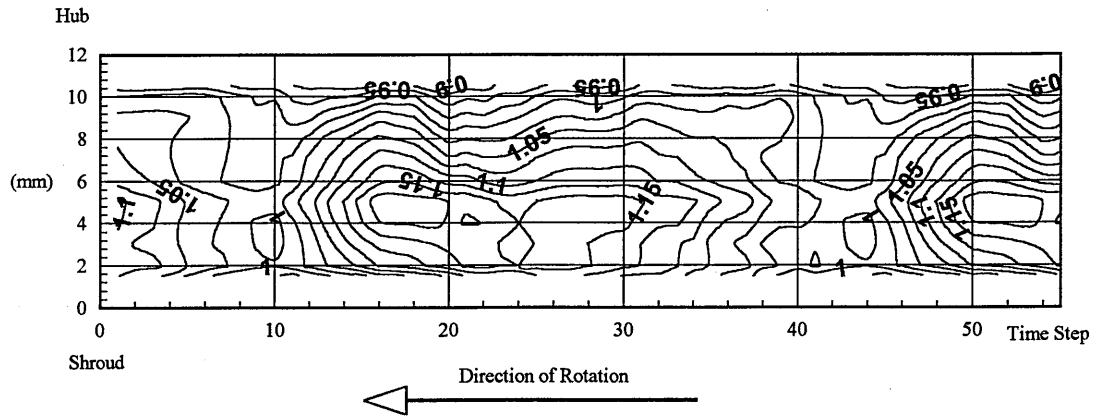
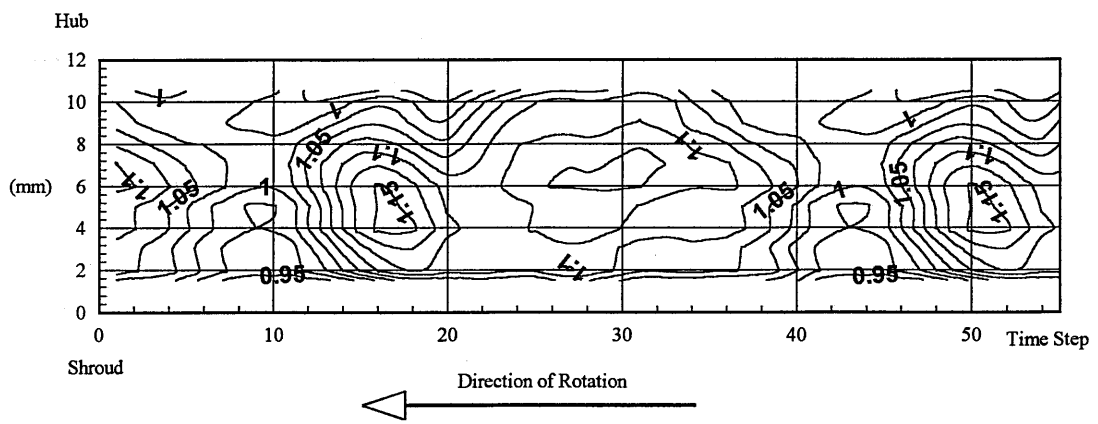


Figure 2.19 Relative Tangential Velocity at 1.05% R_{tip} at 100% Speed (ms^{-1}: positive in direction of impeller rotation)

Near Surge



Design



Near Choke

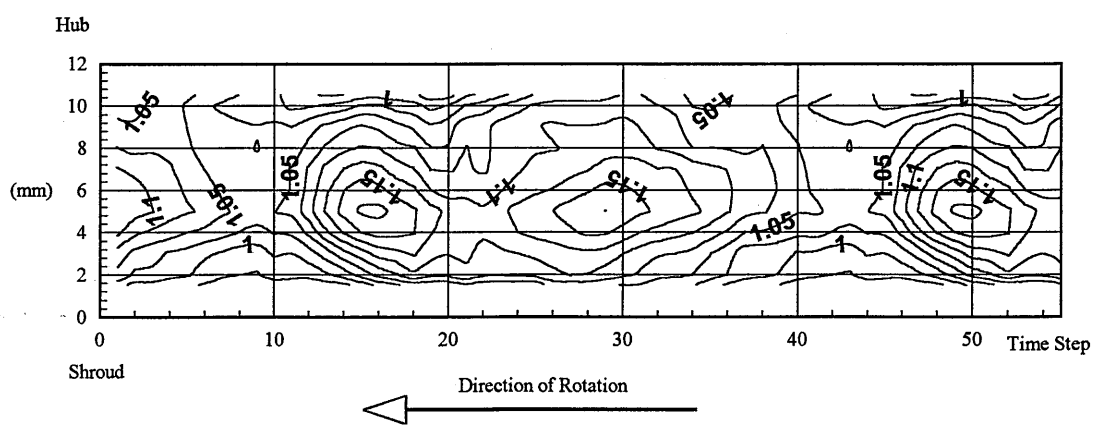


Figure 2.20 Mach Number at 1.05% R_{tip} at 100% Speed

Associated with each time step there is a level of unsteadiness. To give an indication of this, the standard deviation of the raw pressure readings at each spatial measurement point was evaluated. Each standard deviation value was based on 500 samples and the resultant distributions are shown in Figure 2.15. As expected at surge, the distribution is relatively flat with all of the flow showing relatively high unsteadiness. At design mass flow the bulk unsteadiness subsides to reveal the flow is split into a high and a low region. The least turbulent flow is shown in the 'jet' region near the hub/pressure surfaces. The most unsteady region is found near the shroud at a similar location as to where the peak total pressure was measured. Near choke, the flow has again become generally a little more unsteady, expected as we move away from the design condition.

Secondary flows are indicated by consideration of relative (to the mean) tangential velocity contours (see Figure 2.19). These show a strong flow near the shroud surface in the direction of rotation. This is in the opposite direction to a shroud-wall driven cavity flow. The reason for this is again the coincidence with the wake flow position. The core

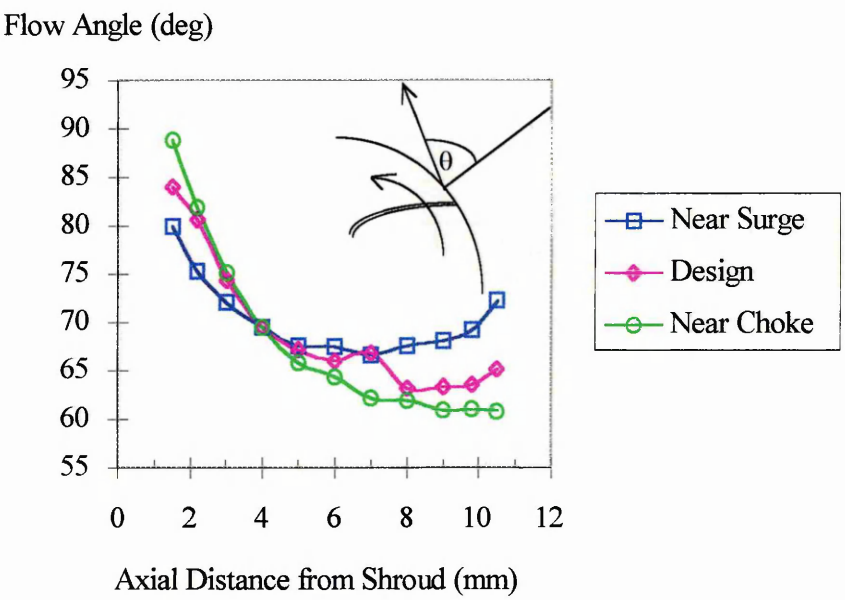


Figure 2.17 Time Averaged Flow Angle across Passage Width

flow follows the curvature of the backward curved blades, but the wake area is relatively stagnant (in the relative frame of reference) and follows the blade rotation more closely. This results in a higher discharge flow angle (i.e. more tangential) and consequently a higher tangential velocity. Using this argument, the flow pattern distortion between the impeller tip and measurement plane may be explained. Plots of relative total pressure at the impeller discharge (Figure 2.16) show a diagonal series of contours that may be extrapolated to intersect at time step 10 on the shroud. These lines are indicative of the blade position but they indicate much larger rake angle (from the axial). This steepening

is therefore due to the elevated tangential flow velocity of the wake in the absolute frame.

The final contour plot, Figure 2.20, shows the Mach number at 1.05 R_{tip}. These show regions of supersonic flow up to Mach 1.2 at choke, with nominal value of Mach number of 1.05 for all flow conditions . As the Mach number was calculated from a mean static pressure, these high Mach number regions coincide with those of high absolute total pressure.

With the temperature sensitivity of the pressure transducer we are also able to determine the total temperature distribution across the passage width. This is shown in Figure 2.21 and therefore it is clear, from this and the preceding arguments, that it is the wake flow that is the high energy flow with the largest absolute total pressure and temperature. This is despite its high loss nature in the relative frame.

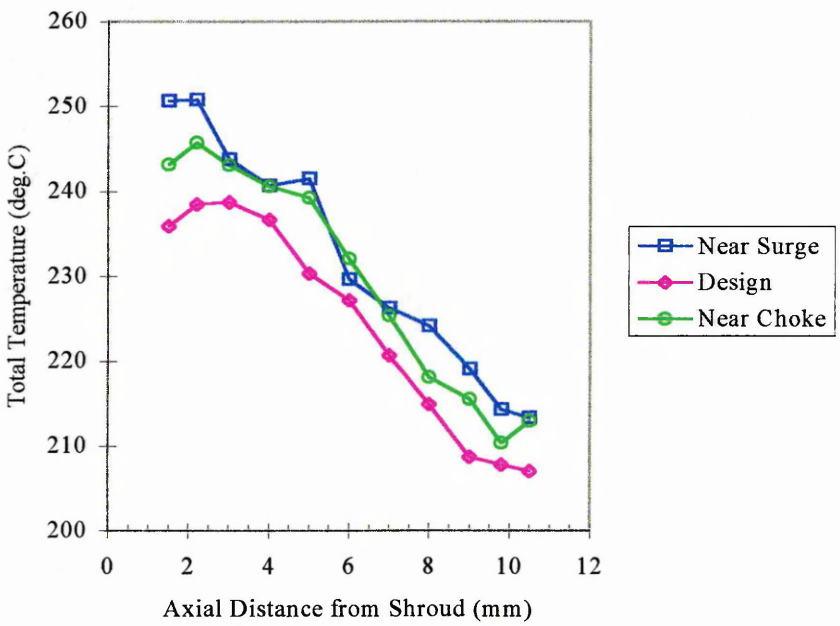


Figure 2.21 Total Temperature Distribution across Impeller Width

Using the evidence presented, it is not completely clear as to the nature of the secondary flow and discussion of this is left until the computational model predictions are considered. Once all of the evidence is collected, a description that conforms to all data is presented.

2.4.3 OVERALL PERFORMANCE CORRELATION

The recorded total pressure and flow angle data were integrated over the impeller exit and compared with the measurements taken by the independent overall-performance data acquisition system. Table 2.2 and Table 2.3 are the collective results from each of these.

Comparison shows that there is a discrepancy of up to 0.15 bar in total pressure and up to 3° in flow angle. Both of these are well within the expected ranges of accuracy.

Table 2.2 Performance Instrumentation Measurements

Percentage of Design Speed	100%	100%	100%	80%	80%	80%
Flow Condition	surge	design	choke	surge	design	choke
Performance Data File	vda122	vda118	vda124	vda142	vda147	vda150
Unsteady Data File Name	3v	2v	4v	9v	10v	11v
Corrected Mass Flow (kg/sec)	3.81	4.07	4.29	2.90	3.25	3.80
Speed (rpm)	34,800	34,560	34,890	28,230	28,110	28,230
Mass Flow (kg/sec)	2.74	2.81	2.82	2.69	2.96	3.35
Impeller Total Pressure Ratio	6.03	5.78	5.57	3.37	3.26	2.93
Isentropic Eff	89.0	88.7	87.0	89.2	88.6	84.0
Tip Speed (m/sec)	532.1	528.4	533.4	431.6	429.8	431.6
Mach Number	1.05	1.04	1.05	0.89	0.90	0.94
Discharge Total Pressure (BarA)	4.39	4.01	3.70	3.21	3.03	2.65
Absolute Flow Angle (wrt radial)	70.6	68.9	67.0	66.6	63.1	54.9

Table 2.3 Unsteady (Kulite) Total pressure Instrumentation Measurements

Percentage of Design Speed		100%	100%	100%	80%	80%	80%
Flow Condition		surge	design	choke	surge	design	choke
Pdischarge	Mass Average	4.28	3.95	3.70	3.07	2.94	2.60
(BarA)	Error (%)	-2.7%	-1.8%	-0.3%	-5.0%	-3.63%	-2.64%
Flow	Mass Average	68.47	67.45	66.42	66.95	63.90	57.74
Angle (Degrees)	Error (degrees)	-2.3°	-1.4°	-0.6°	-0.4°	0.8°	2.8°

2.5. PNEUMATIC TRAVERSES

Measurements of total pressure were also taken using a pneumatic probe near the impeller discharge to provide a check on the Kulite unsteady readings. These were taken at the same operating conditions. The immersed portion of the pneumatic probe

consisted of a simple stainless steel hypodermic tube of 0.75mm outside diameter. As for the Kulite system, the probe was rotated by +/- 30° of the nominal mean flow angle (70°-measured from the radial direction) in steps of 10° and via a curve fit, the total pressure and flow angle were recorded. Details of this instrumentation, including the necessary development, design and calibration are given in Appendix B.

The small probe introduced minimal blockage to the flow and was shown to be, given a sufficient angular traverse range, able to measure pressures to within 0.05 bar and flow angles to within 2° accuracy. It addition, it was sufficiently small to allow measurements within 1mm from the walls. For the results presented, readings were taken at steps of 1mm across the impeller discharge width.

2.5.1 DETAILED FLOW MEASUREMENTS AND DISCUSSION

The 100% speed measurements taken are shown in Figures 2.22 and 2.23. The former presents the total pressure distribution over the measurable flow range. In particular the 'near choke' condition shows a much flatter form as if the larger mass flow has filled the passage width. However, when considering the flow angle plot of Figure 2.23, it becomes clearer that the near shroud flow lacks radial velocity, and the resultant high total pressure is due to the flow being stagnant in the rotating frame. Therefore on discharge it assumes the high impeller tip whirl velocity. These trends were also noticed in post-processing of the unsteady flow measurements when considering the complete exit surface.

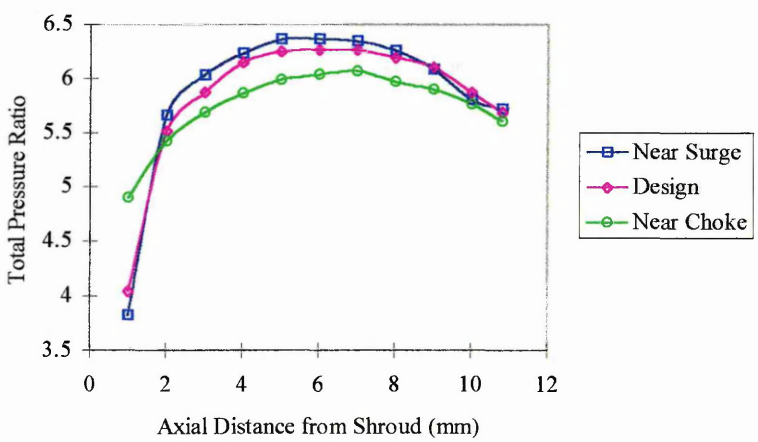


Figure 2.22 Total Pressure Measurements using Pneumatic Probe at 105% R_{tip}

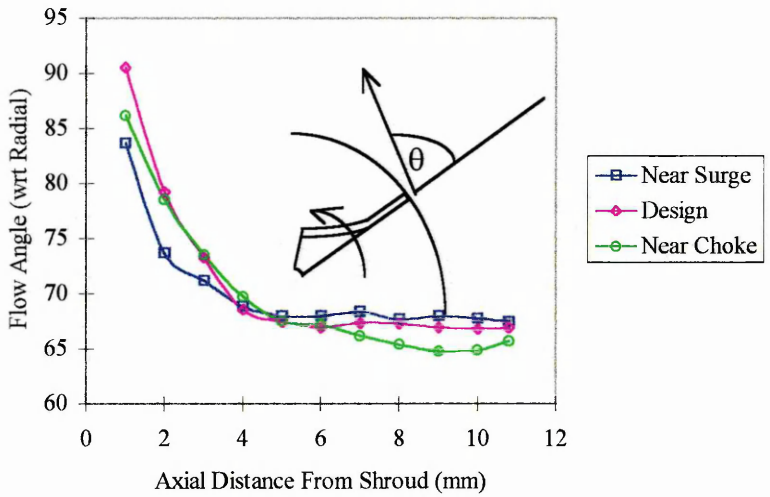


Figure 2.23 Flow Angle Measurements using Pneumatic Probe at 105% R_{tip}

[Note that there is a suspect point on the flow angle distribution plot on figure 2.23. It is expected that the measurement nearest to the shroud gives a reading of approximately 5° too low. In this area the flow is clearly unsteady and also includes areas of reverse flow. Such flows are difficult to measure using a pneumatic device.]

The above measurements may also be compared with mass-flow-averaged unsteady measurements, from which we can get a direct comparison between the two measurement techniques. Flow measurements are compared in Figure 2.24.

Generally the agreement is good with differences in total pressure ratio of up to 0.5 (≡0.35Bar), and flow angle of up to 4°. However there are areas that show discrepancies, where given time, repeat experiments would have been desirable. In particular, the near shroud total pressure measured near surge showed the largest pressure disagreement. It is expected, that the operating point chosen for examination was quasi-stable

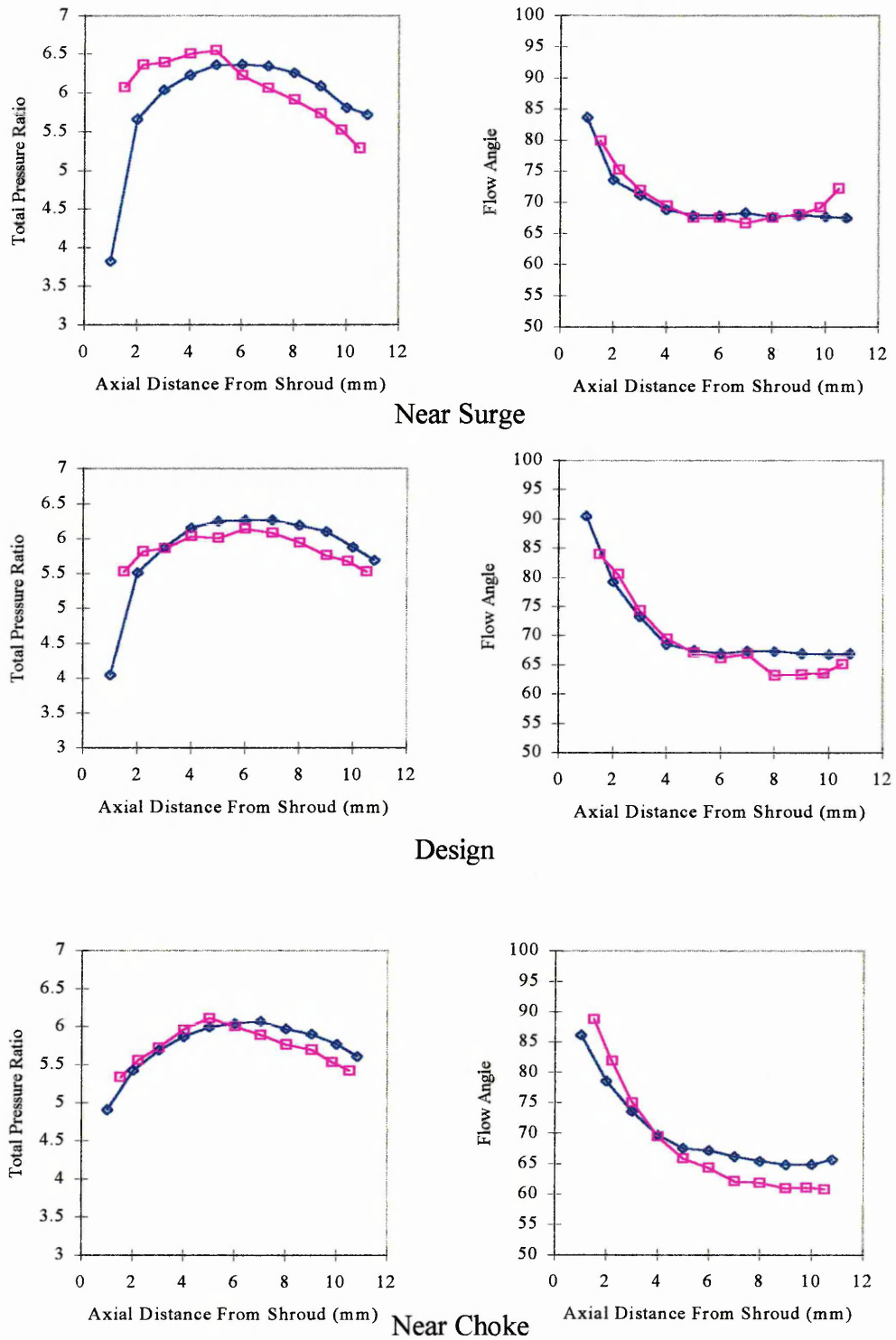


Figure 2.24 Comparison between Kulite and Pneumatic Total Pressure and Flow Angle Measurements at 105% R_{tip}

2.5.2 OVERALL PERFORMANCE FROM PNEUMATIC TRAVERSES

The overall performance calculated from mass weighting the total pressure measurements are tabulate below.

Table 2.4 Impeller Performance Calculated from Discharge Pneumatic Total Pressure Traverse

Speed (%)		100%	100%	100%	80%	80%	80%
Flow Condition		Nr Surge	Design	Nr Choke	Nr Surge	Design	Nr Choke
Pdischarge (BarA)	Overall Instrumentation (P_{dap})	4.39	4.01	3.70	2.87	2.60	2.15
	Traverse (P_{pneu})	4.31	4.07	3.74	2.88	2.61	2.19
	$\Delta(P_{pneu}-P_{dap})$	-0.08	0.06	0.04	0.01	0.01	0.04
	$\Delta(P_{pneu}-P_{dap})/P_{dap}$ %	-1.8%	1.5%	1.1%	0.4%	0.4%	1.9%
Flow Angle (Degrees)	Overall Instrumentation	70.6°	68.9°	67.0°	67.1°	63.1°	60.0°
	Traverse Average	71.7°	70.7°	69.7°	65.6°	63.8°	60.1°
	Δ(Flow Angle)	1.1°	1.8°	2.7°	-1.5°	0.7°	0.1°

Discrepancies are well within the experimental errors expected although there is valid argument which suggests that the integrated detailed measurements are more accurate than those recorded by the static overall instrumentation. The latter relies on static tappings placed on the shroud at the impeller periphery from which, together with energy conservation, the discharge total pressure is calculated. Therefore the static overall instrumentation does not directly measure total pressure. Errors creep in with the assumption that flow variables are assumed planewise constant, particularly the static pressure, which is physically not true. However, both measurements produced suitably accurate measures of performance and no further discussion is merited.

2.6. COMPUTATIONAL INVESTIGATIONS

To complement the experimental work, numerical investigations were carried out using an assortment of computational tools. These computational runs were carried out in order to complement the experimental investigation. Of particular interest was the flow within the blade passage which could not be measured using the fixed instrumentation. It was hoped that the CFD solutions would enhance the understanding of both the primary and secondary flow structure and the way it changed over the flow operating range.

2.6.1 1-D DESIGN PROGRAM

The Herbert (1980) centrifugal compressor design program was used to predict the 1D flow characteristics of the impeller in the vaneless configuration. This program requires the specification of overall geometry (i.e. blade angles, inlet and exit plane dimensions), rotational speed and a prescribed mass flow. The program output gives 1D predictions of flow angles, pressure rise and efficiency. The calculation procedure is complex but well documented in Herbert (1980) and contains a great deal of empiricism.

The main interest in using such a tool was to predict flow inlet conditions into the diffuser. Once confidence was gained in its use, the program was one of the design tools used for pipe diffuser specification later (although some special treatment was necessary as the program was limited to conventional vaned and vaneless diffusers). Of initial interest was the comparison of impeller performance predicted using the Herbert program against experimental measurements. This is shown in Figure 2.25. The graph displays impeller total pressure ratio and impeller isentropic efficiency, both of which are predicted extremely well although there is a minor overprediction of pressure (+3.5%) and underestimation of efficiency (-1.5%). These encouraging results gave the author confidence in the use of the program for the diffuser design later.

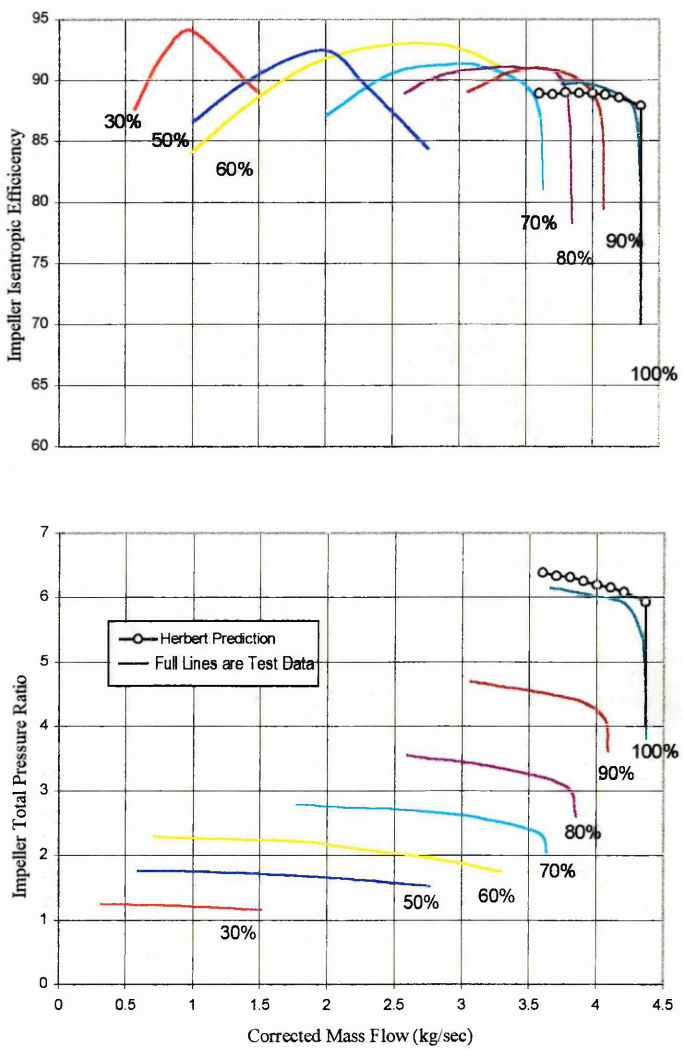


Figure 2.25 Comparison between Herbert(1980) Design Program Predictions and Actual Measurements for the 35D Compressor

2.6.2 FLUENT

Fluent is a commercial CFD (Computational Fluid Dynamics) computer code that numerically solves the 3-D Navier Stokes Equations on generalised structured body-fitted computational meshes. The SIMPLE (Semi-Implicit-Pressure-Linked-Equation) finite volume formulation is utilised together with 2nd order interpolation between cells. A choice of three turbulence models are available, although for the present investigation the standard k-ε model was used.

Details of the wide range of problems and numerical details are documented in Fluent Manuals (1995). The general equation formulation in described in Appendix F.

2.6.2.a COMPUTATIONAL DOMAIN

Initially a mesh of dimensions 24×20×55 (= 26,400 cells) was used to model a single blade passage (see Figure 2.26) . This domain was initially created for TURBO3D by Tourlidakis (1996) and was converted using a filter program written by the author to import it into FLUENT. The mesh included 15 cells upstream of the blade leading edge, and 10 cells downstream of the impeller discharge that extended into the vaneless diffuser to a radius ratio of $1.3R_{tip}$. Although these regions introduced additional cells, they were chosen to prevent the prescribed uniform boundary conditions from propagating into the area of interest and potentially spoiling the solution. Tip clearance was allowed using a 'pinched' arrangement together with prescribed cyclic boundary conditions. The fixed shroud was modelled in the rotating frame via the prescription of a wall with fixed (the same as the impeller) tangential velocity.

Later, in an attempt to improve solver stability, it was necessary to halve the dimensions of the computational domain.

2.6.2.b BOUNDARY CONDITIONS

The boundary conditions used are tabulated below:

Table 2.5 Applied CFD Boundary Conditions

Location	Boundary Condition	Source of Data*
Inlet	Mass Flow	Inlet bellmouth
	Flow Angle	Yaw Probe Traverse
	Turbulent Kinetic Energy	Estimated at 3%
	Dissipation Rate	Estimated from duct hydraulic radius
Discharge	Static Pressure	From vaneless diffuser static tappings

*All the above values, apart from the turbulence quantities, were obtained from actual measurements taken during experimental testing.

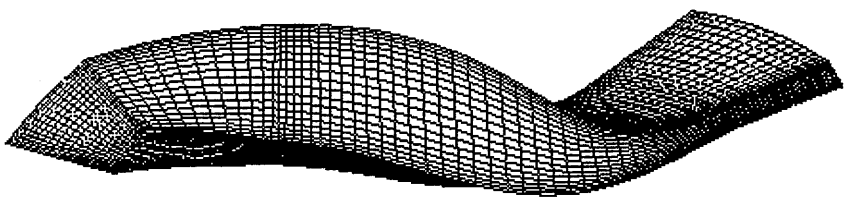


Figure 2.26 Impeller Computational Mesh

During initial trials it became apparent that the stability of the solver was to be a major problem. As already indicated, the initial mesh dimensions were halved in an attempt to improve the situation. A direct solution at full speed proved impossible even with very low relaxation parameters. As guided by the Fluent Users Manual (1995), intermediate solutions were sought at reduced speeds. Starting at 10% of design speed, and together with suitable boundary conditions, such a series of solutions were calculated. At 80% speed however, the author found himself again unable to converge the solution. At this speed the relative Mach number at the inducer exceeded Mach 1 over significant portions of the blade span and FLUENT, unable to cope with the significant density variations, was abandoned for more appropriate codes.

FLUENT's failing lies in the way the solver iterates between the continuity and momentum equations. The main problem with this link is that it does not explicitly include density and subsequently, variations in density are not incorporated into the solution. Particular difficulties occur when density effects to the pressure field exceed those of velocity, and consequently an incorrect solution results. This failing is well known, particularly in turbomachinery fields and methods to overcome this difficulty have been developed (Tourlidakis, 1997)

2.6.3 TURBO 3D

This CFD code was developed at Cranfield by Tourlidakis (1991) specifically for turbomachinery problems. As for Fluent, the SIMPLE algorithm was employed to solve the discretised Navier-Stokes equations on a rotating 3-D structured body-fitted grid and again a k-ε turbulence model was adopted. The programme was run as an independent investigation and is reported, Bennett et al (1997). All computations were carried out against 80% of design speed and these are compared by detailed measurements taken by the author at this reduced condition. Calculation at 100% of the impeller design speed proved impossible due to stability problems similar to those faced by the author when using Fluent.

The conclusion from these particular CFD investigations showed that the impeller demonstrated flows that were representative of centrifugal compressors. These pertinent flows were also found at full speed and are discussed fully in the next section. Despite their relegation to an Appendix, the 80% results are expected to be a useful data set for future CFD investigations and represent as less harsh test for SIMPLE based programs.

2.6.4 RAMPANT

With both FLUENT and TURBO3D failing to converge at 100% impeller speeds, attention was turned to a density based time-marching code, particularly as this type of formulation is regarded as being superior (e.g. Fletcher (1988)) at transonic Mach numbers (albeit problems do occur when the flow is incompressible and artificial compressibility treatment is necessary).

2.6.4.a DESCRIPTION OF COMPUTER PROGRAM

As introduced, RAMPANT is a time-marching code, with the solution explicitly stepped through time to converge to an equilibrium or steady-state solution. The same equations as FLUENT are solved (see APPENDIX F) and second order interpolation schemes were used to enhance accuracy.

In addition to a fundamentally different solution algorithm, RAMPANT allows solution on an unstructured mesh. However for the 35D impeller model this facility was not needed as the earlier structured mesh created was used. The same boundary conditions were again applied (i.e. see Table 2.5) for three design speed operating conditions representing 'near surge', 'design' and 'near choke'. After some familiarisation and optimisation of solution parameters, the author was able to gain convergence for each of the flow conditions. Both residuals and inlet total pressure were monitored during the iterative calculation and it was found that the best convergence indicator was the latter. See Figure 2.27 for a sample monitored output .

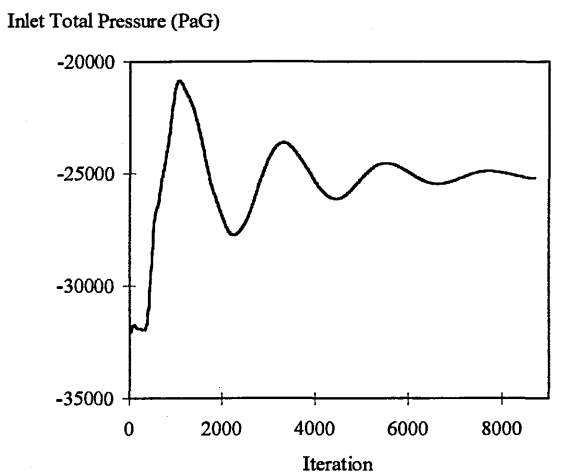


Figure 2.27 Monitoring Inlet Total Pressure to Ensure Solution Convergence

2.6.4.b RESULTS AND DISCUSSION

The Overall Performance is tabulated below and shown graphically in Figure 2.28.

Table 2.6 Overall CFD Performance Predictions

Run Name	35dr30	35dr20	35dr40
Flow Condition	surge	design	choke
Speed (rpm)	34,800	34,560	34,890
Corrected Mass Flow (kg/sec)	3.807	4.072	4.288
Mass Flow (kg/sec)	2.738	2.811	2.816
PR (Mass Weighted)	6.27	6.25	6.14
Isentropic Eff (mass weighted)	91.47	90.54	90.05
Inlet Ttot (K)	287.5	283.9	287.3
Inlet Ptot (Pa)	82,292	76,676	68,484
Disch. Ttot (K)	504.16	499.72	504.2
Disch. Pstatic (Pa)	128,805	123,724	104,218
Disch. Ptot (Pa)	515,605	479,420	420,754
Discharge Angle (deg wrt Radial)	67.44	68.02	66.50

In general the pressure ratio predicted was a little high (approximately +0.2 PR at design) and the corresponding impeller efficiencies also show the same trend. However, the results are encouraging and of sufficient accuracy to give the author confidence in the results. Further discussion now focuses on the detailed flow features.

2.6.4.b.i THE INTERNAL FLOW-FIELD

Figure 2.29 shows the presentation planes that are used to discus the flow. Plane I is the computation domain inlet; Plane II corresponds to the impeller inlet plane; Plane III is approximately one third, and Plane IV two-thirds, into the blade passage; and finally plane V is the exit plane.

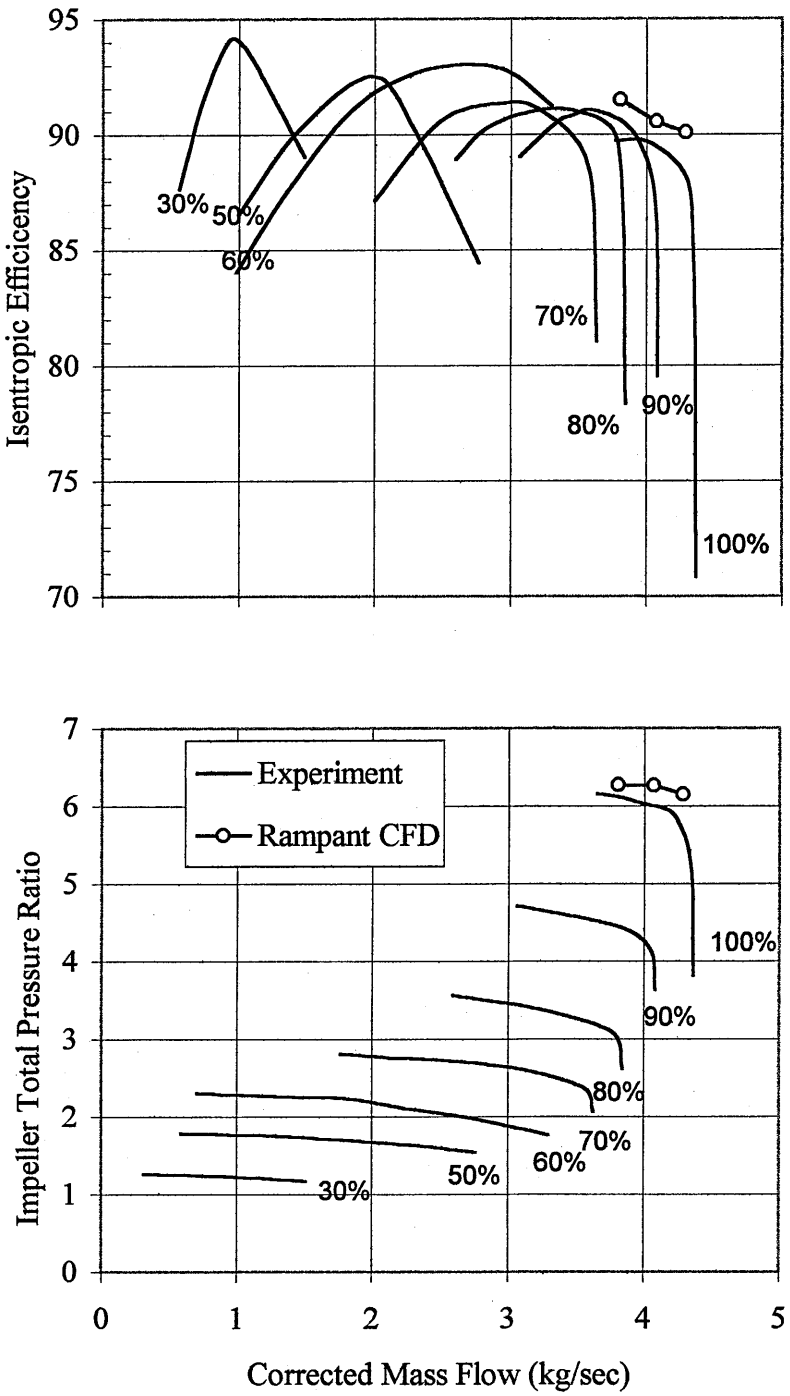


Figure 2.28 *Comparison of CFD Performance Prediction against Experiment*

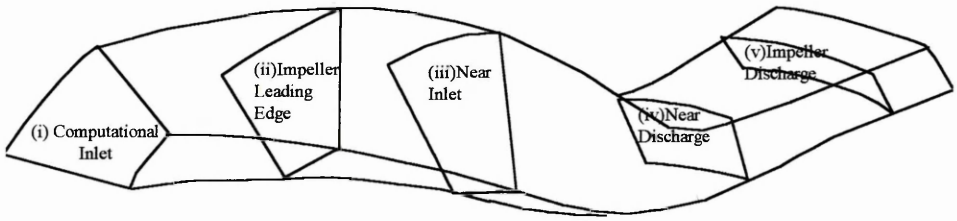


Figure 2.29 Designation of Computational Planes used in Discussion

Figure 2.30 presents a coloured contour plot of the relative (to the impeller rotation) Mach number. At impeller inlet (Plane II) and upstream there is a large radial Mach number gradient. Its presence is due to the rotating reference frame, but it is apparent that this distribution is rapidly distorted by the impeller inducer section. In addition to the radial variation, a low energy region is seen to grow from choke to surge near the shroud region.

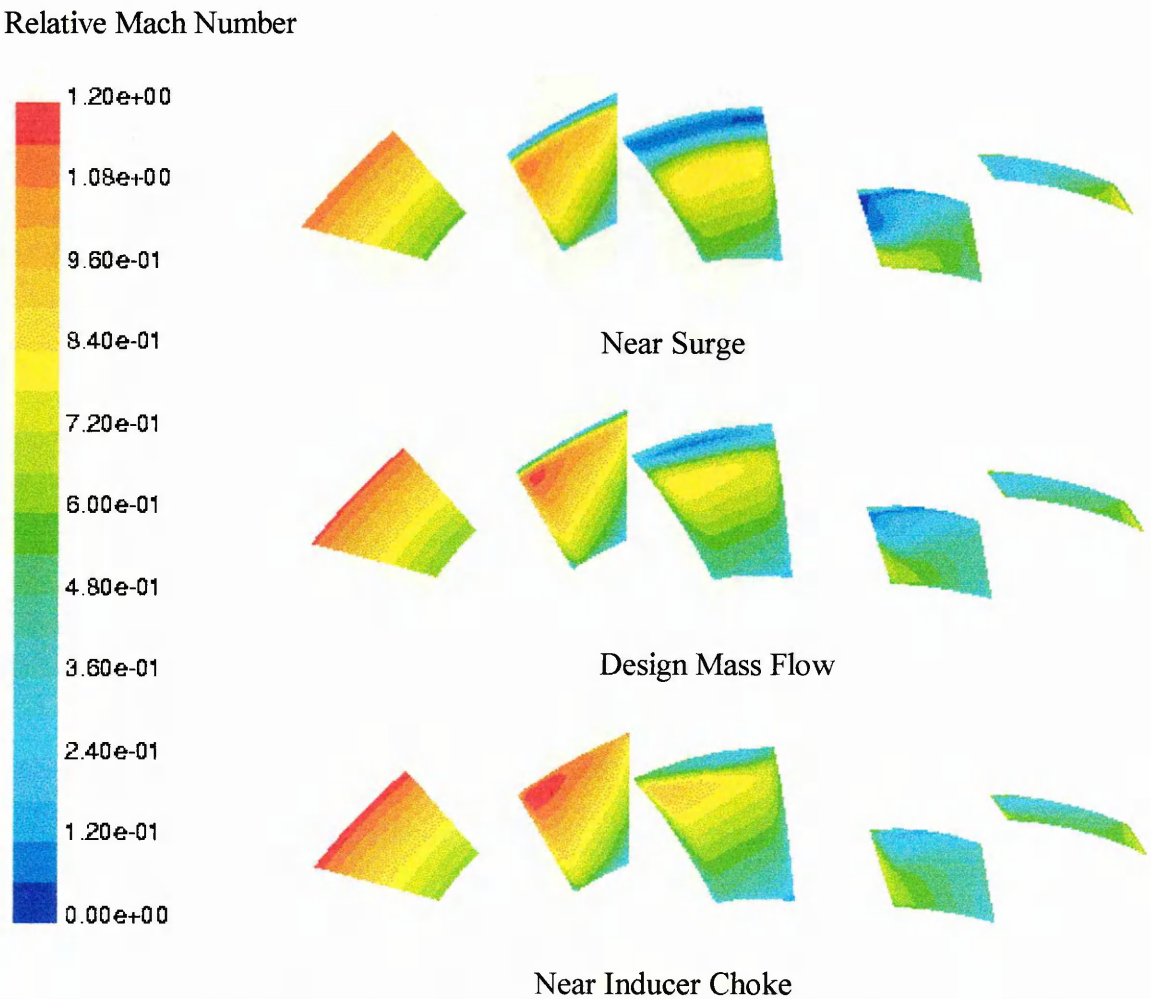


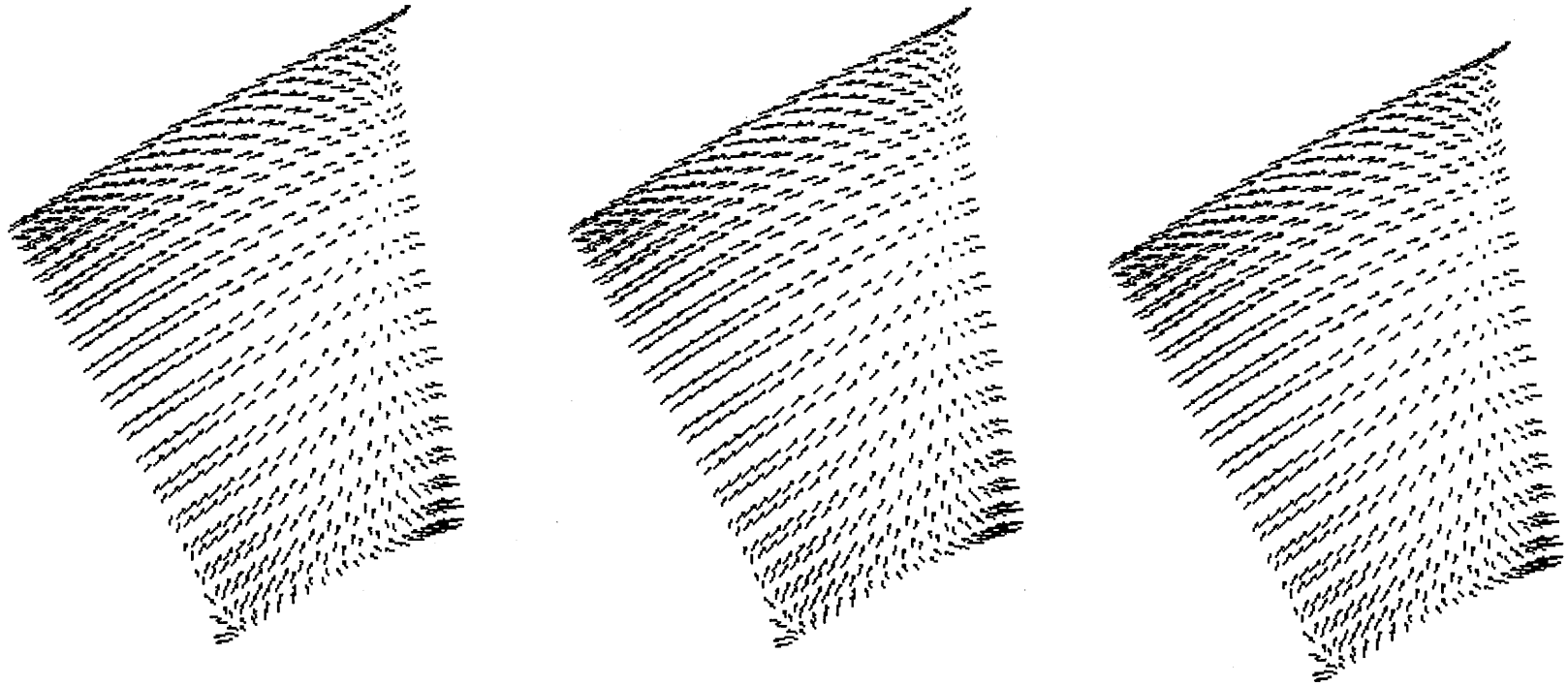
Figure 2.30 RAMPANT Predicted Relative Mach Number Distribution within Blade Passage

As the flow convects to plane III, this region grows to fill almost 20% of the peripheral space. It is hypothesised that this growth is due primarily to the increased adverse static pressure gradient combined with lower speed meridional flow associated with duties near surge. Indeed, reverse flow in this region is well documented (e.g. Bosman (1984), McKenzie (1993)) particularly prior to and during stall. At plane IV near surge, this area of stagnant flow moves to the suction surface of the blades, where from analogy with isolated aerofoil flow separated flow is common. In addition, at all flows, rapid diffusion is shown by the steep drop in Mach number. Finally, at discharge, the flow assumes the anticipated wake formation and, as described earlier, the source of the region of low energy flow is seen to originate from the shroud.

The relative velocity vectors in planes II, III, IV and at the total pressure measuring plane, are shown in Figures 2.31 to 2.34 respectively. Instead of normalising with respect to the rotating frame, a mean-plane velocity was used in order to pick out the secondary flows. It is for this reason that the stationary shroud region, in many of the sections, shows stronger flows in the direction of rotation.

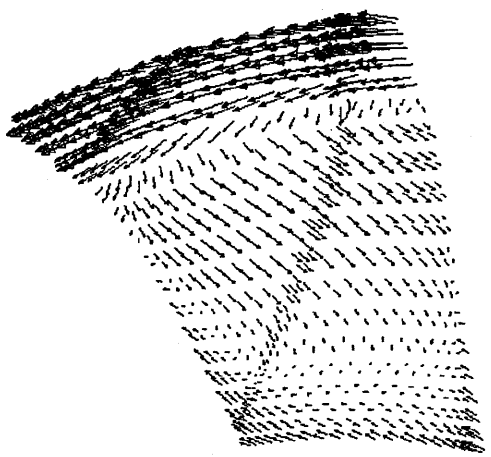
At the impeller inlet (Plane II-Figure 2.31), little difference is observed between the different flow rates. At the tip, some clearance flow are visible (confirming that tip clearance flows were accounted for in the CFD model) but no secondary flows are seen. Further downstream in plane III, the most prominent feature is a band of flow parallel and near to the shroud. Near surge the width of this band becomes larger, and is the region of slow moving fluid seen in the relative Mach Number plot. In addition, there are identifiable secondary flows. The shape of these indicate that the pattern is an amalgam of the meridional and cascade turning vortex pairs. Figure 2.35 shows these two patterns.

Closer to the discharge, these flows are distorted by the influence of viscous forces and the secondary flows become almost indistinguishable. Some remnants of vortices remain in the hub/suction and shroud/pressure regions. These are compressed into their respective corners by slow energy fluid that grows in the shroud/suction corner, particularly towards surge (See Figure 2.36). This triangular area of poor flow is fed by tip clearance leakage, dominating the shroud region and does not migrate towards the hub with the core flow regions. This implies the formation of two distinct regions of flow: the so-called wake flow and a core flow.

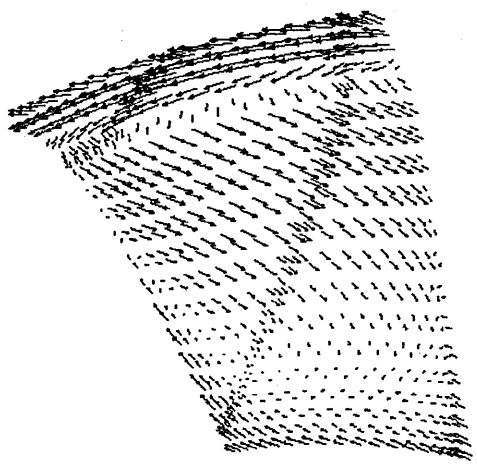


Near Surge | Design Mass Flow | Near Choke

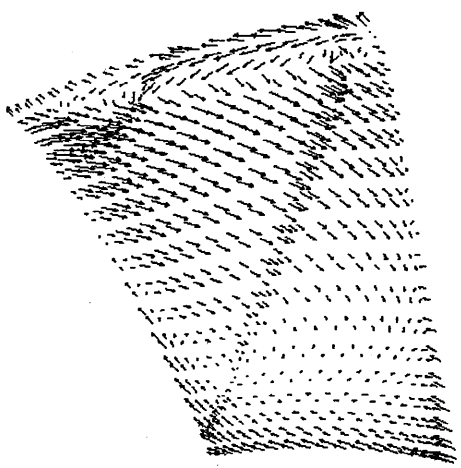
Figure 2.31 RAMPANT Predicted Secondary Flow Velocity Vectors in Plane II (Impeller Inducer)



Near Surge

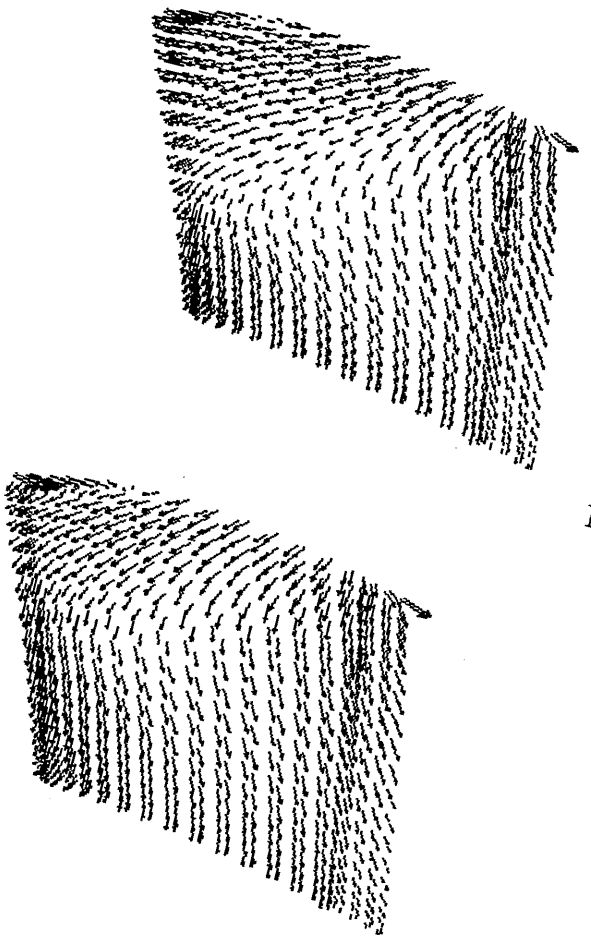


Design Mass Flow



Near Choke

Figure 2.32 RAMPANT Predicted Secondary Flow Velocity Vectors on Plane III (Near Inlet)



Near Surge

Design Mass Flow

Near Choke

Figure 2.33 RAMPANT Predicted Secondary Flow Velocity Vectors on Plane IV (Near Discharge)

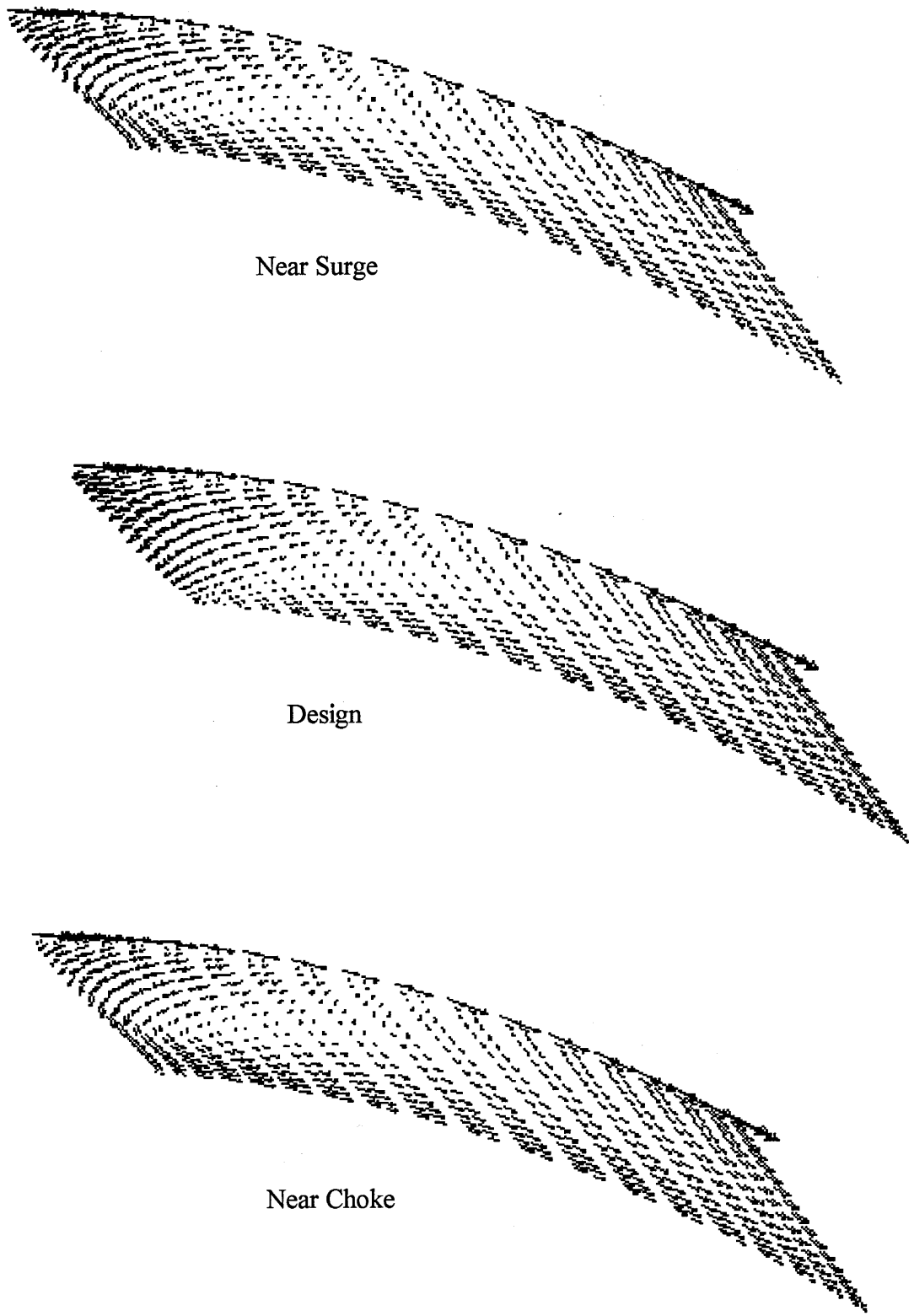


Figure 2.34 RAMPANT Predicted Secondary Flow Velocity Vectors on Plane V (Impeller Discharge)

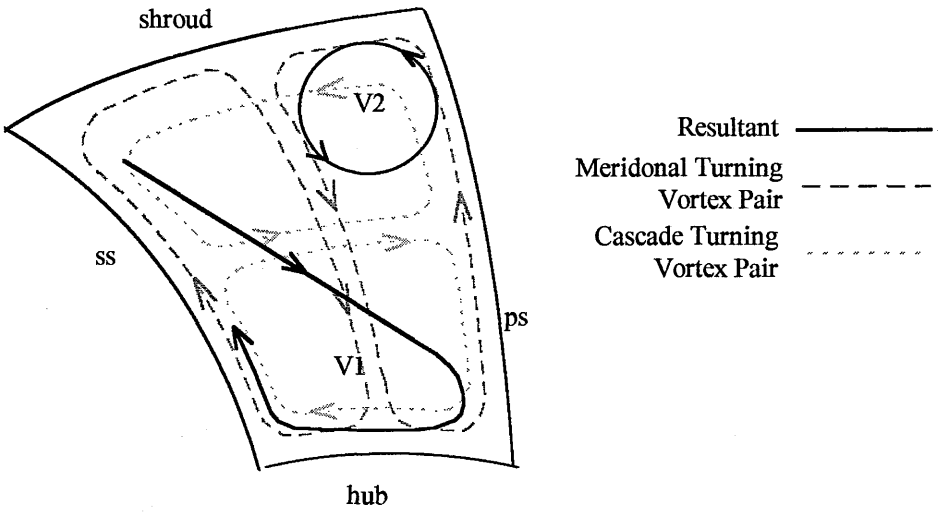


Figure 2.35 Secondary Flows within Plane III (One-third into Impeller Passage)

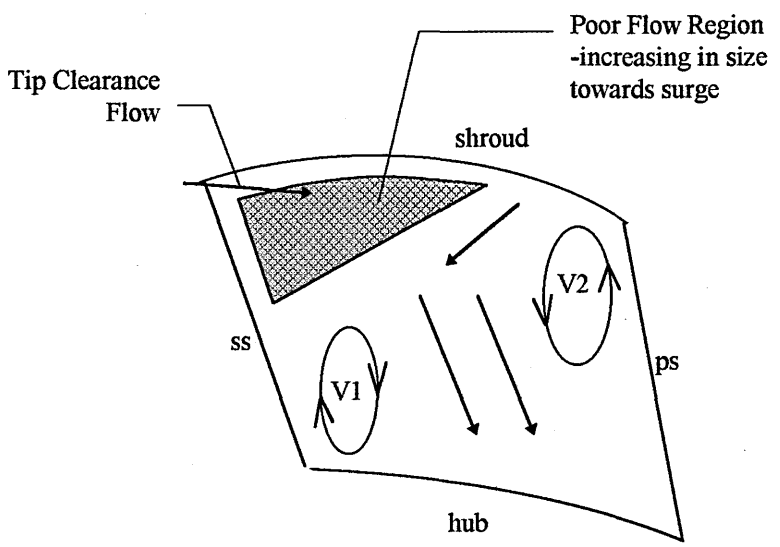
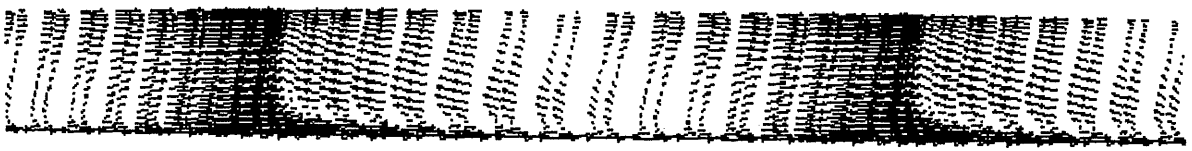
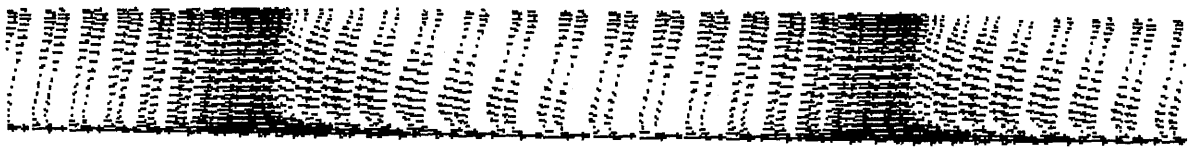


Figure 2.36 Secondary Flows within Plane IV (Two-thirds into Impeller Passage)

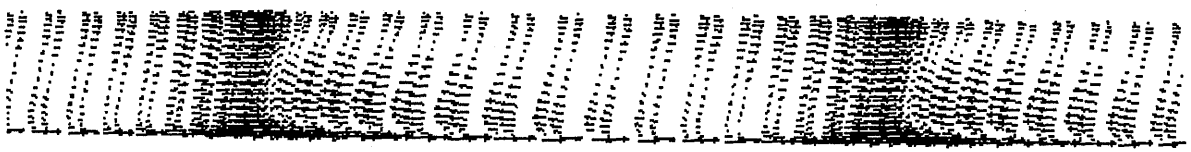
At discharge (see Figure 2.37) the velocity vectors are further distorted. As the mass flow is reduced, the hub/suction vortex V1, is diminished; swallowed by the separated flow region. There still remains evidence of core migration from shroud to tip together with the shroud/pressure vortex V2. Further wake formation appears in Figure 2.38, highlighted by the trough in total pressure. Near choke this area remains close to the shroud and blade suction surface. As we approach surge, the wake zone virtually dominates the complete suction surface and the stratification of total pressure, noted in the experimental results, is visible.



Near Surge



Design Mass Flow



Near Choke

Figure 2.37 RAMPANT Predicted Relative Velocity Vectors in at 1.05% R_{tip}

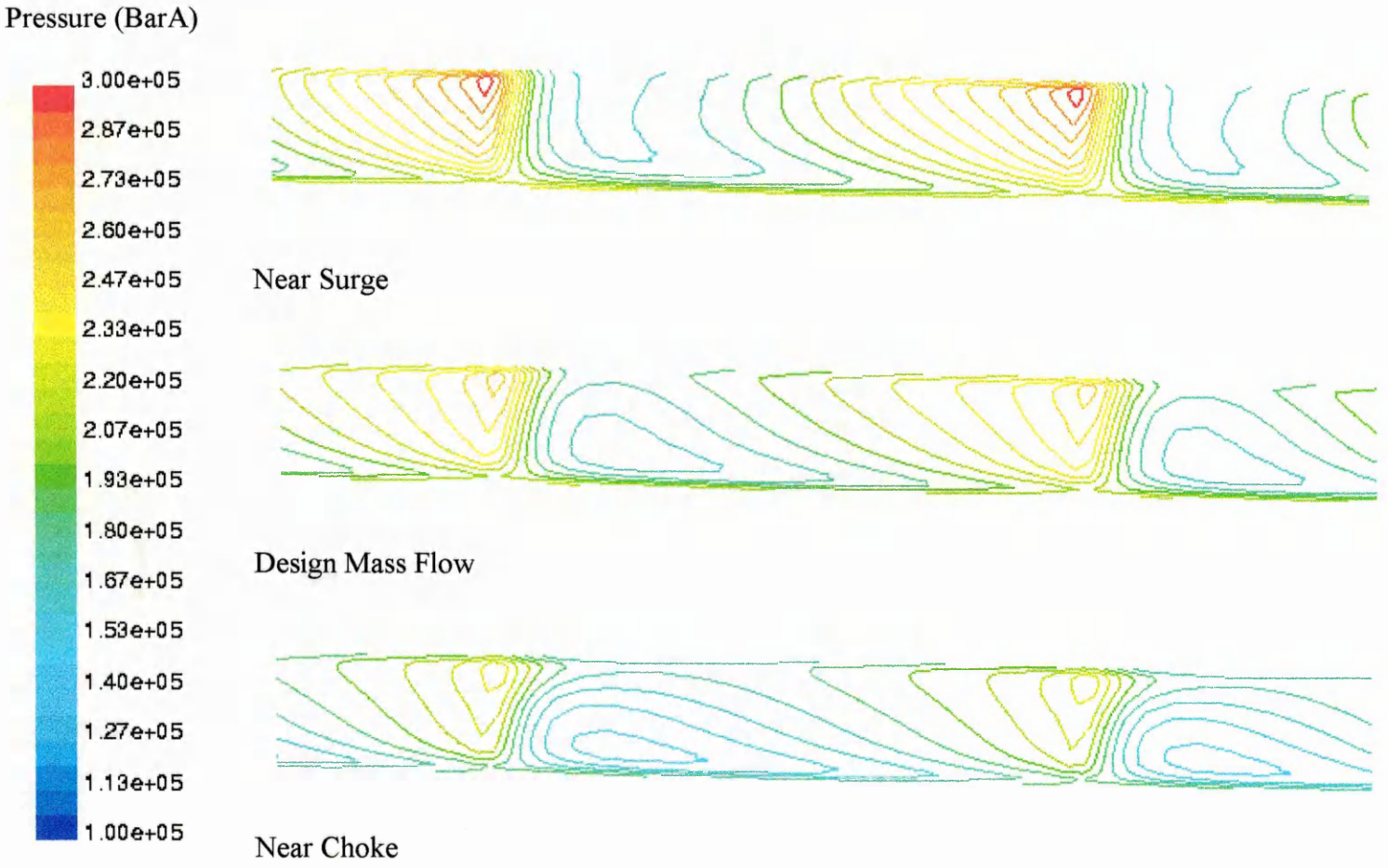


Figure 2.38 RAMPANT Predicted Relative Total Pressure at 1.05% R_{tip}

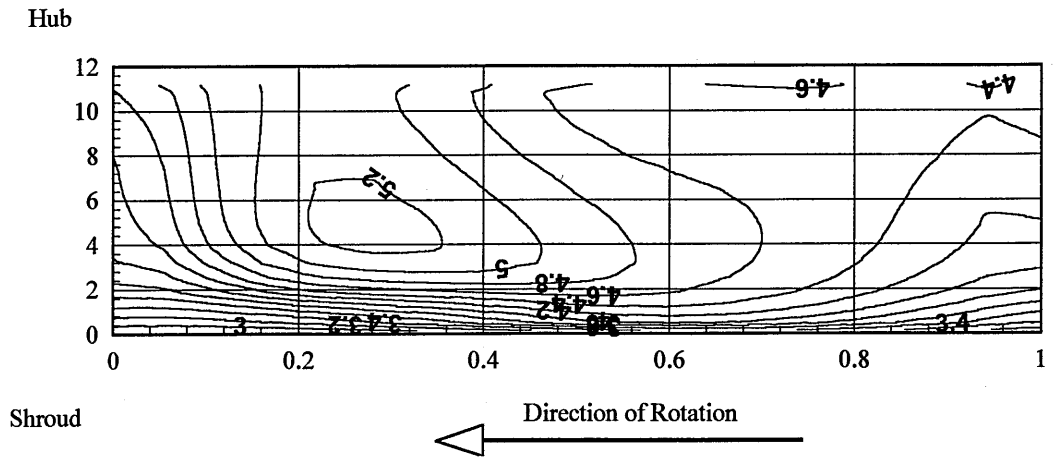
The RAMPANT predicted total pressure and flow angle are presented in Figures 2.38 and 2.39 respectively. These are plotted at 1.05% R_{tip} and show reasonable agreement with experiment. However, one major discrepancy is apparent. The joint regions of high total pressure measurements are not predicted. These two distinct regions have been smoothed out by the numerical scheme to form a single elongated region. This is a little disappointing but could be attributed to the relatively coarse mesh used (24x20x55= 26,400 cells). There is a high probability that further refinement would yield more detail, but this would incur a large amount of computational time without the assurance of success. In addition, during these computations the solution diverged occasionally-increased grid resolution could possible make the solver completely unstable. However, the computations presented a great deal of internal information about the impeller flow and have supplied sufficient detail to construct an understanding of the flow structures.

2.7. CONCLUSIONS

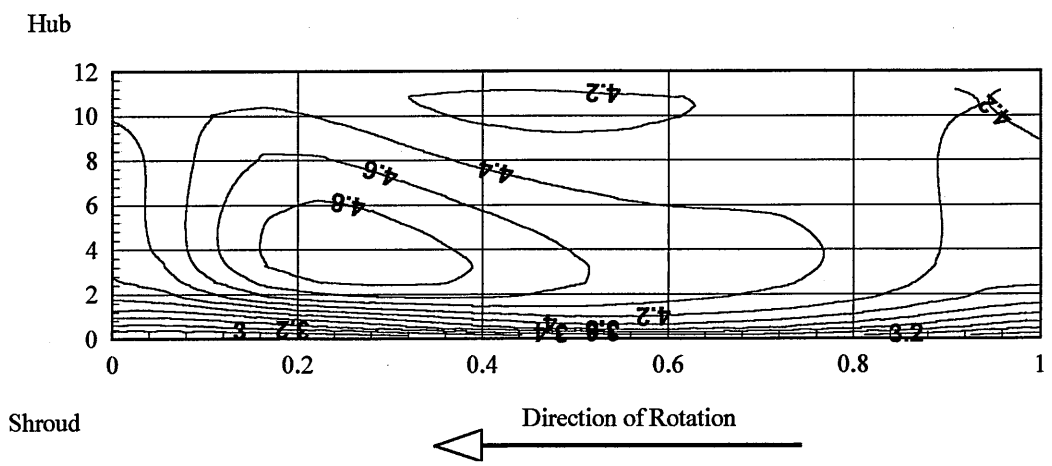
The 35D test compressor has been significantly modified for modular diffuser swapping and incorporated onto Cranfield's high speed test bed. Detailed flow measurements and accompanying computational studies on the 35D compressor in the vaneless diffuser configuration have been presented. These studies have shown the flow discharging from the impeller to be representative of typical centrifugal compressors and therefore a suitable candidate for diffuser studies.

A method developed to measure unsteady total pressure and flow direction has been successfully applied, yielding high quality data that has been further confirmed by conventional pneumatic traverses. Computational success has however been a little patchy although the Herbert (1980) centrifugal compressor design program and the RAMPANT CFD codes have been proved suitable. The former, with modification, is used later as a tool for pipe diffuser design whereas the CFD code is used to predict the full 3D flow field within the diffusers themselves.

Near Surge



Design Flow



Choked Flow

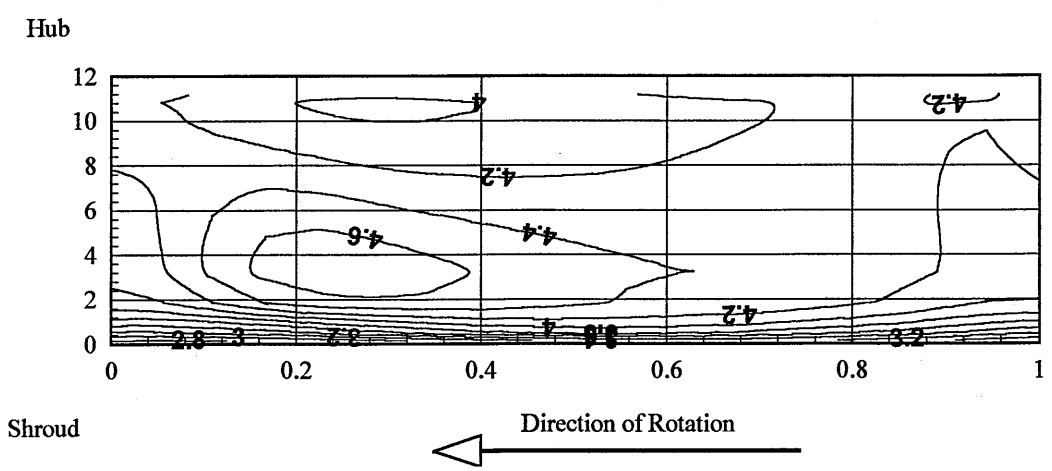
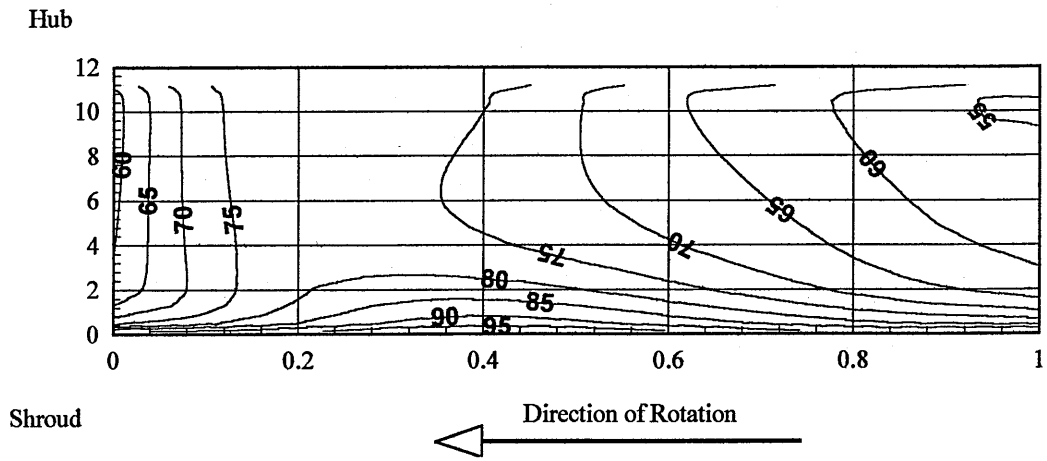
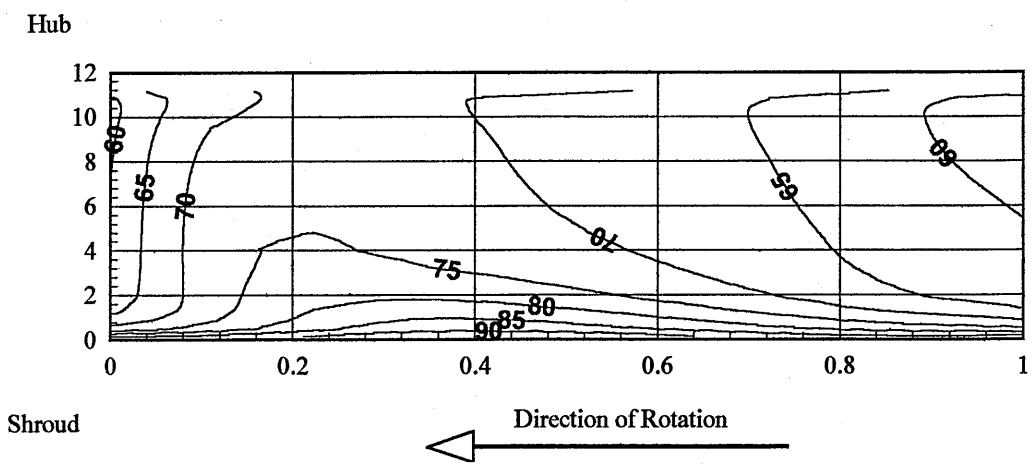


Figure 2.39 *RAMPANT Predicted Absolute Total Pressure at 1.05% R_{tip}*

Near Surge



Design



Near Choke

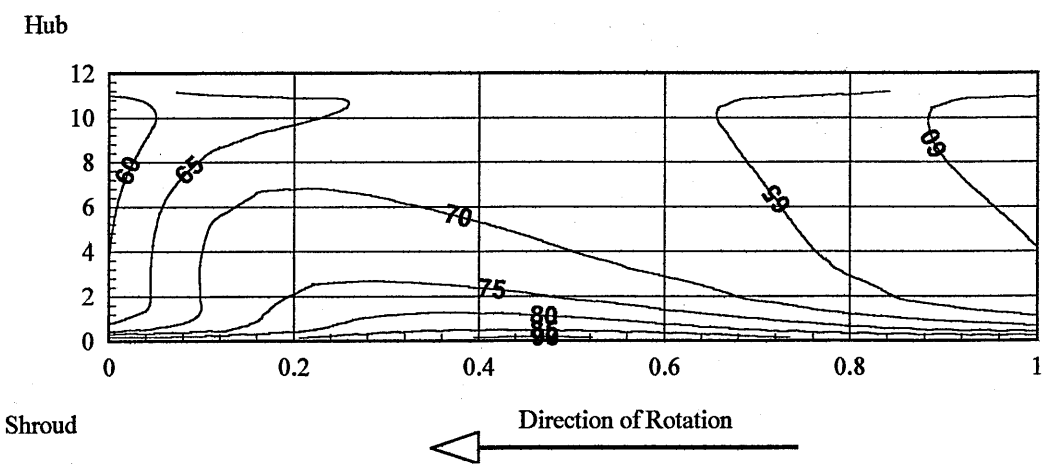


Figure 2.40 RAMPANT Predicted Absolute Flow Angle at 1.05% R_{tip}

CHAPTER 3
Pipe Diffuser Area Expansion

In pipe diffuser configurations, after leaving the impeller, the flow enters a geometrically complex region. Initially, there is a small section of vaneless space (see Figure 1.14) which is then followed by a region called the pseudo-vaneless space where the pipe passages intersect to form elliptic leading edges. This latter region, as discussed in the literature survey, is unique to pipe diffuser configurations as flow in this region is expected to be a combination of vaneless-space type diffusion together with turning due to the influence of the elliptic diffuser leading edges. The flow leaving the pseudo-vaneless space enters a near-triangular zone (when viewed along the impeller axis of rotation) called the semi-vaneless-space. In this region the flow is normally strongly diffused prior to its entry into the diffuser throat. The combination of this diffusion process, together with that occurring in the pseudo-vaneless and vaneless spaces is well known to influence the diffuser throat conditions (e.g. Dean 1974 and Kenny 1970). Excessive diffusion causes the flow into the cone to become poor with large blockage, drastically reducing the performance of the downstream conical diffuser. It is for this reason that designers normally try to minimise this expansion in an attempt to ensure the best possible flow into the cone. However, if the diffuser throat area is reduced excessively it will choke prematurely and this will limit the upper mass flow range of the

complete stage. The throat size therefore has always been a question of compromise, and consequently no diffuser investigation would be complete without some knowledge of how the performance is affected by different sizes. Such an investigation is carried out here and is believed unique, for either pipe or other types of passage diffusers.

In this current investigation, a pipe diffuser was constructed that allowed the throat area to be enlarged by reaming. The conical portion of the pipe diffuser downstream of the throat was not built and instead the flow was dumped into a wide vaneless diffuser. This simplification was necessary because to include the downstream diffusing cones, together with necessary radial-to-axial bends would have incurred too large a burden on the overall project resources. Despite this, the flow between the impeller tip and diffuser throat is still considered representative although it is accepted that this simplification affected stage surge.

Outline of Chapter

The pipe diffuser design philosophy employed is fully outlined, particularly as it proved successful and would be of great use to those requiring practical design information. The experimental investigations into the diffusers are then described. These include comparisons of stage performance and detailed static pressure investigations. Following these experiments, the influence of throat size on range and stage performance is presented and an optimum size is recommended.

3.1. DESIGNING THE FIRST PIPE DIFFUSER TO BE TESTED

3.1.1 GENERAL PHILOSOPHY

It was felt important that the first design tested should follow the geometry presented by the principal developer of the pipe diffuser, Kenny (1969, 1970,1972); his designs were considered successful and would act as a basis for comparison for later pipe diffuser tests. Kenny's philosophy was to use the impeller tip as the pipe drilling tangency radius with the diffuser throat diameter nominally set to equal the impeller discharge width. The combination of these parameters ensured a (near) minimal leading edge radius and avoided a meridional step within the semi-vaneless-space (this is described in detail in section 3.13). By fixing these two key dimensions the geometry could be fully specified with the prescription of a total throat area.

The complete design procedure may best be described with the use of a flow chart (see Figure 3.1). The procedure is iterative and based around finding a diffuser throat (and hence pipe throat diameter) that will choke at the chosen 'diffuser-design' mass flow, the choice of which is described in the next section.

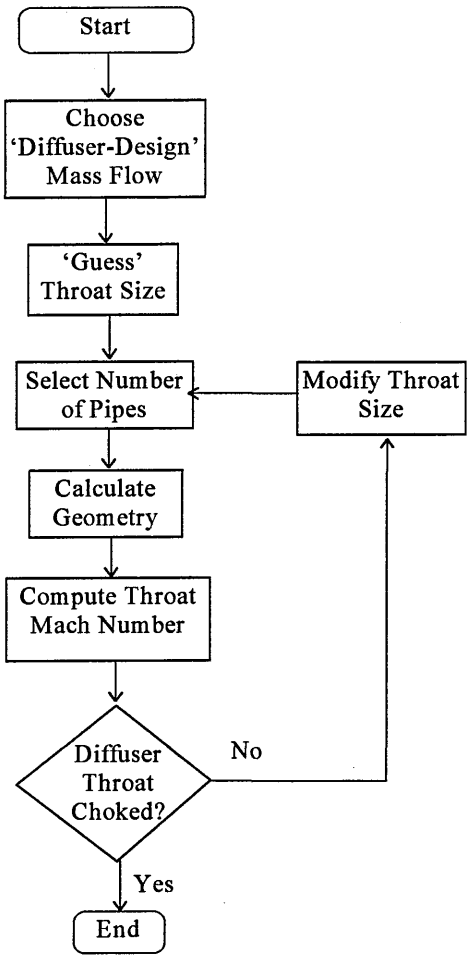


Figure 3.1 Design Procedure Employed

3.1.2 SELECTION OF A 'DIFFUSER-DESIGN' MASS FLOW FOR THROAT SIZING

The performance of the compressor stage can be severely affected by a poorly sized diffuser throat. Discussions with Cranfield staff and Rolls-Royce, who had expertise in this area, concluded that it was the most important and performance sensitive dimension of a diffuser. Privileged information revealed that the diffuser throat was normally sized to choke near the stage design operating point and exactly how close depended on whether the design originated from the UK or North America. Information gathered before and during this research suggested that the ratios of 'design-mass-flow' to 'diffuser-choke-mass-flow' currently used by the gas turbine industry were:

UK : (Design MassFlow)/(Diffuser Choke Mass Flow)≈ 92%
North America: (Design MassFlow)/(Diffuser Choke Mass Flow)≈ 98-100%

These values are sketched below in Figure 3.2 for clarity.

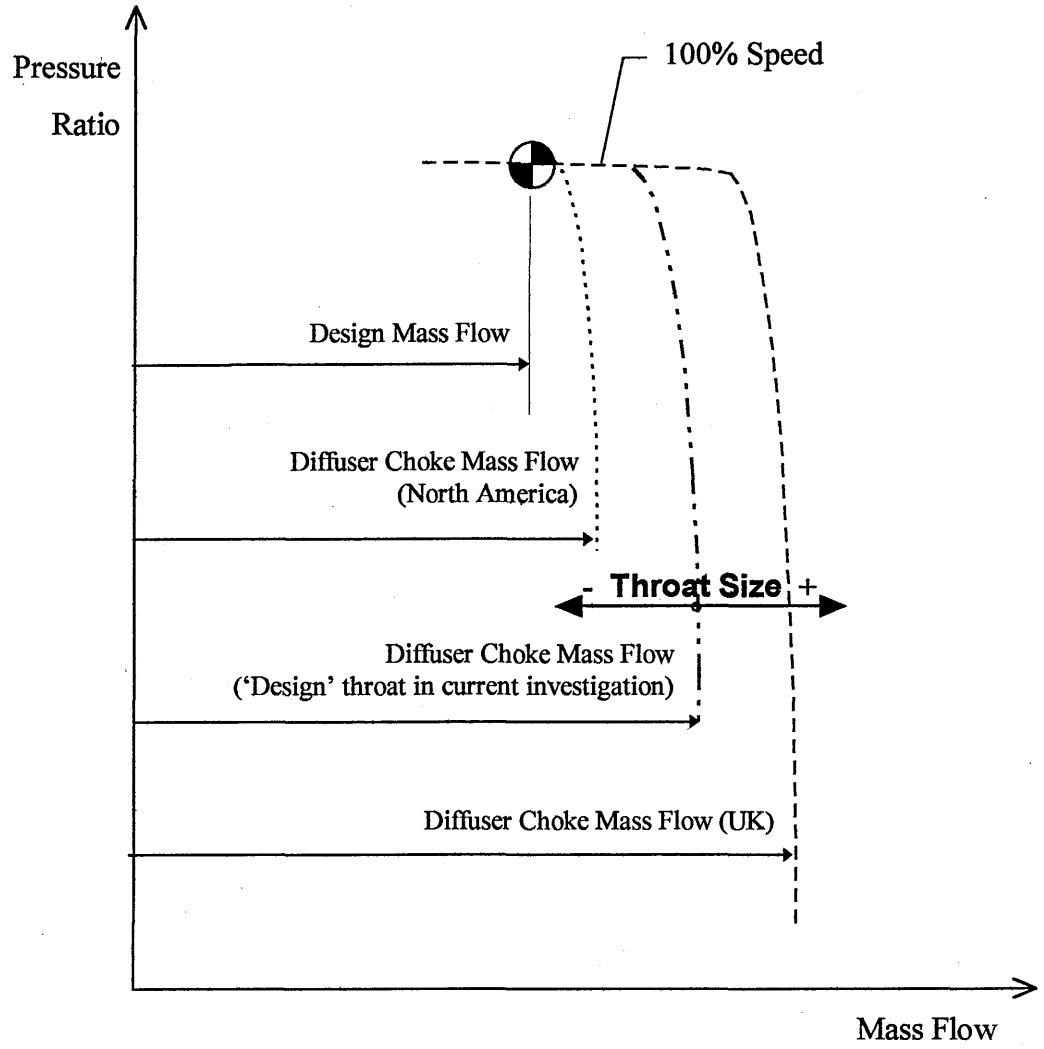


Figure 3.2 Diffuser Throat Sizing Philosophies

For ease of reference this ratio will be called throughout this thesis as the diffuser *design/choke* ratio. After, assuming a corrected stage design mass flow of 4.1kg/sec, a compromise diffuser throat size was designed to choke at mid-way between the mass flows specified by the above two choking criteria. This is designated here as the 'design' throat size. In order to assess the trade-offs between the UK and North American design philosophies, this current study investigated throat sizes to choke at mass lows corresponding to -10%, -5%, 100% and +5% of this compromise 'design' throat size. A performance comparison of these diffusers would then yield the advantages and disadvantages associated with each throat size.

3.1.3 CHOOSING THE NUMBER OF PIPES

Once a total diffuser throat area is prescribed the number of pipes may be selected. Figure 3.3 shows the relationship (after finalising the throat area following several iterations) between the number pipes and the consequential effect on sidewall expansion. Sidewall expansion is a phenomenon particular to pipe diffusers formed from cylindrical drillings: given a design throat size, it is the relationship between the diameter of the pipe drillings and the number of pipes (see Figure 3.3). The Kenny (1970) philosophy is to minimise this expansion. Figure 3.3 therefore indicates that 37 pipe diffuser passages should be used. However, in order to allow the -10% undersized diffuser to be reamed larger for increments in throat area, 31 pipes were chosen. This meant that the 'design' case included a small sidewall expansion step but this was only 1.1 of the impeller tip width and was well below the (believed) industry accepted standard limiting value of 1.3. [In fact, the -10% throat size yielded an optimum 34 pipes- this would have coincided with twice the number of impeller blades (17) and therefore further reduction was necessary.]

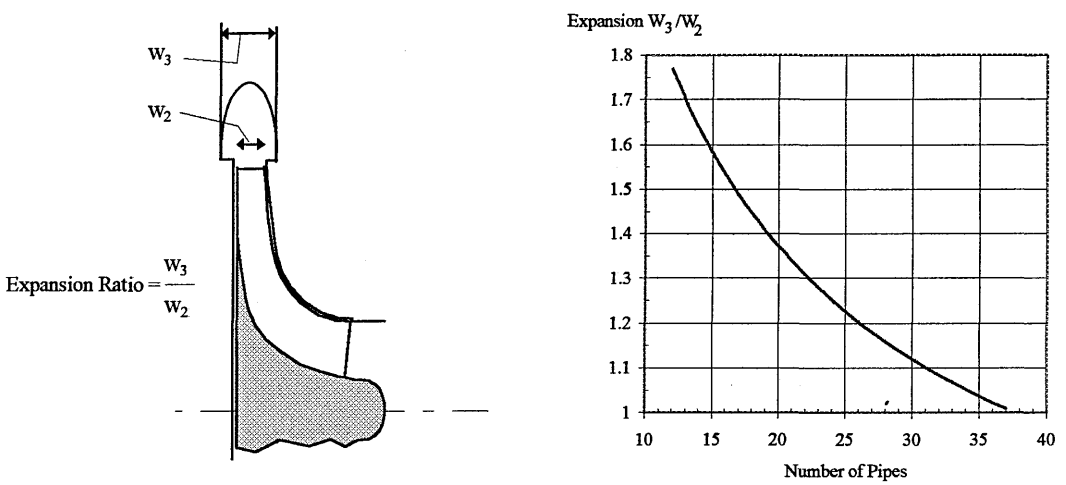


Figure 3.3 Effect of Number of Pipes on Sidewall Expansion Ratio for 'Diffuser-Design' Throat Size

It should be noted that Figure 3.3 would normally be redrawn after each throat size iteration and does not take into account the number of blade passages on blockage. This latter effect however is quite small, as will be shown in Chapter 4.

3.1.4 CALCULATING THE PROMINENT GEOMETRIC FEATURES

Through experience it was found that small perturbations in throat size significantly modified the geometry of the pipe diffuser. Leading edge radius, sidewall expansion (and consequently incidence) and blade angle were all affected. Therefore after each throat area iteration, the complete geometry was re-evaluated prior to the

computation of the throat blockage and throat Mach number. A computer program was developed and utilised for this purpose. The associated geometrical features are presented in APPENDIX G.

3.1.5 COMPUTING THE THROAT MACH NUMBER

To evaluate the 'design' diffuser throat conditions, the Herbert (1980) compressor design program was utilised. This program, having earlier been assessed against the vaneless build, assumes a generalised vane-island diffuser design. The calculation for the semi-vaneless space region is based on a combination of empirical relations for total pressure loss and integral boundary layer equations to account for the blockage formed by the boundary layer growth on the vane suction surface and vaneless diffuser walls up to the diffuser throat. In order to incorporate the lower anticipated blockage of a pipe diffuser, an empirical relationship presented by Kenny (1970), was used. This, as described in Chapter 1, relates blockage to the static pressure recovery (Cp_{svs}) within the semi-vaneless space. The predictions for a 31 pipe diffuser configuration (as eventually tested) at 100% speed over the complete mass flow range are shown superimposed on Kenny's data in Figure 3.4.

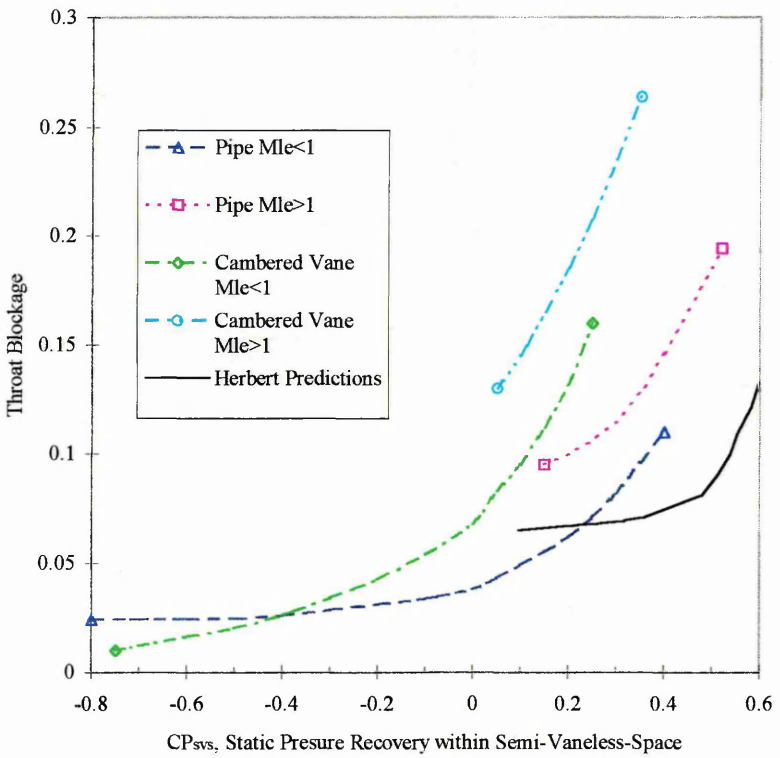


Figure 3.4 Comparison of Calculated and Empirical (Kenny 1970) Pressure Recovery within Semi-Vaneless-Space

Quite clearly the data did not correlate well, and therefore to ensure the best chance of success, a compromise ideology was used. The throat size calculated using the Herbert program was corrected to account for the blockages predicted by Kenny (1970). This rather rough approach was justified at the time as it was thought that any inaccuracy could be compensated for later as initial tests were to be carried out with undersized throats.

The matter of determining the throat blockage was further complicated due to the near sonic conditions predicted near the pipe diffuser leading edge. This could cause ambiguity regarding the use of either the supersonic or the subsonic relationship given by Kenny (1970). The final choice of curve was justified by examination of Rolls-Royce pipe diffuser tests. These suggested much lower blockages than those plotted for supersonic leading edge conditions and therefore the subsonic curves were adopted.

After testing the compressor with the 'design' throat size it was found that imperfections in the design procedure had resulted in undersizing the throat by 1½%. This was regarded as an excellent result considering the limited information available.

3.1.6 THE GEOMETRY OF THE 31 PIPE DIFFUSER TESTED

The pertinent geometric features of the tested 31 pipe diffuser are noted below with complete details given in APPENDIX G.

Table 3.1 Pipe A (31 Pipe) Geometry

±% of Design Throat Size	Diffuser Design/Choke Ratio	Pipe Ø (mm)	R_{le}/R_{tip}	Sidewall Expansion W_6/W_5	Leading Edge (Bisector) Angle*	Bisector Incidence**
-10%	106.8%	12.626	1.092	1.051	67.00°	0.77°
-5%	101.2%	12.938	1.096	1.077	66.49°	1.76°
0%	96.3%	13.274	1.101	1.105	65.95°	2.80°
+5%	91.6%	13.601	1.105	1.132	65.43°	3.79°

* Defined in nomenclature

** Assuming an impeller discharge flow angle corresponding to inducer choke

Historically in the literature, to quantify diffuser incidence, the leading edge bisector angle has always been used for pipe diffusers (see nomenclature at start of thesis for definition) and in particular by Reeves (1977) who demonstrated a bisector-incidence/range relationship. Therefore the bisector, rather than suction surface, incidence definition is adopted here. As Reeves (1977) had shown that the bisector incidence could affect operating range, during this phase of work attempts were made at designing a pipe diffuser arrangement that would allow throat size variations without incurring changes in bisector angle. It became quickly apparent that this could not be

achieved, particularly as the increments in throat sizes, due to project budget restraints, were to be made by reaming-out a single pipe diffuser arrangement. Unfortunately, this incidence variation was amplified further by flow angle deviation due to associated sidewall expansion for the larger bore pipes (making the flow more tangential). The resulting leading edge bisector incidences varied by 3° and according to Reeves (1977) would be expected to significantly alter the operational ranges. Using this philosophy, the undersized throat configurations would be expected to perform with the largest range, although not placed at the optimum incidence indicated by Reeves (1977) to be -3°.

3.2. EXPERIMENTAL ARRANGEMENT

With the annular plates that formed the vaneless diffuser removed, the pipe module could be inserted into the compressor assembly (see Figure 3.5). For consistency, the 'static' thermodynamic instrumentation was arranged to be undisturbed in each of the pipe diffuser tests. This consisted of: the inlet and discharge thermocouple rakes; inlet total pressure probes and impeller discharge static pressure tappings. Further details are given in APPENDIX A and APPENDIX B.

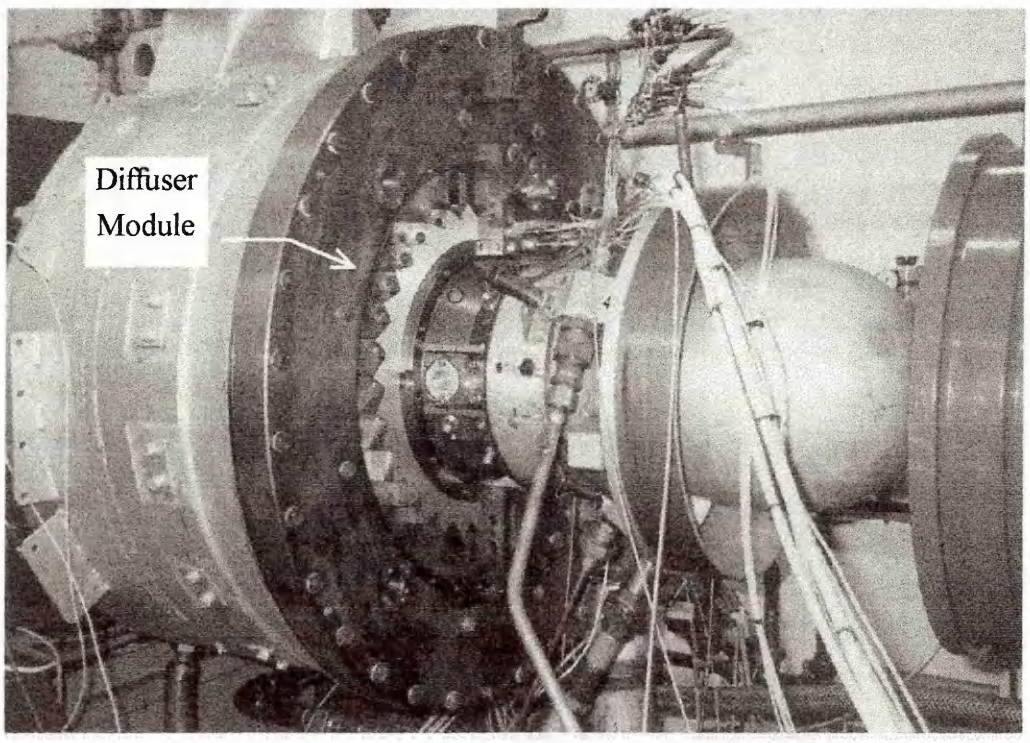


Figure 3.5 Photograph of Compressor with Diffuser Module Inserted (Half of Inner Coverplate is Removed)

3.3. RANGE

It is shown, as expected, in Figures 3.6 and 3.7 that the throat size has a clear influence on both choke and surge. In particular, these figures present the effect on range (surge to choke) for each of the 31 pipe diffuser configurations and it is evident that the largest range was achieved with the 'design' throat area. The poorest performance was that of the -10% undersize example which was unable to operate at 100% speed. An undersized throat may limit the upper mass flow due to choking, together with some stall alleviation. The alternative, that of oversizing, would seem to invite early surge without upper-mass-flow benefit (flow is limited by inducer choke) and therefore should be avoided.

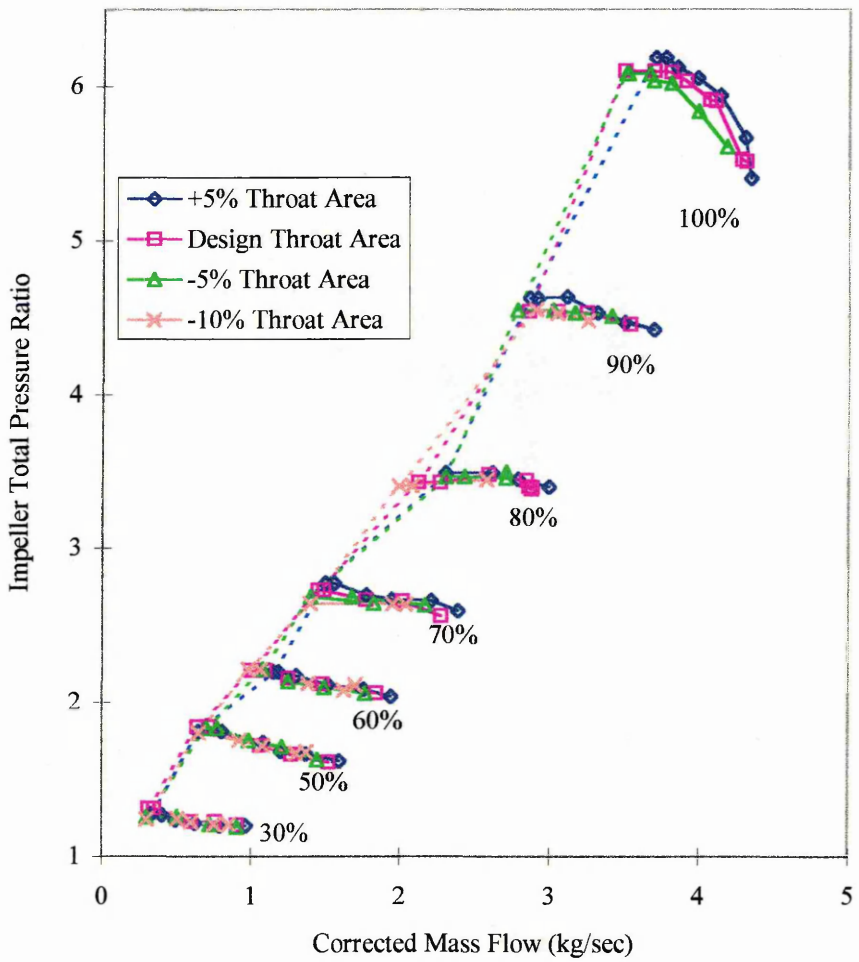


Figure 3.6 Effect of Throat Cross-Sectional-Area on Operating Range

Table 3.2 shows the surge margin (design to surge) for the design speed which already indicates the supremacy of the smaller throat areas. It is clear that if the throat size is made too small (e.g. -10%) the penalty is severe. It is also apparent that that the

conclusions found at the 100% speed case are generally applicable at lower speeds although throat size selection appears to be less critical.

It emerges that the smaller throat sizes, that bring the diffuser choke closer to the design point and reduce the required diffusion upstream of the throat, are more desirable. This tends to support the previously referred to 'North American' practise but also shows that if throat selection is too small the penalty is severe. Referring to section 3.1.2., this suggests that

96% < Diffuser Design/Choke (Flow) ratio < 100%

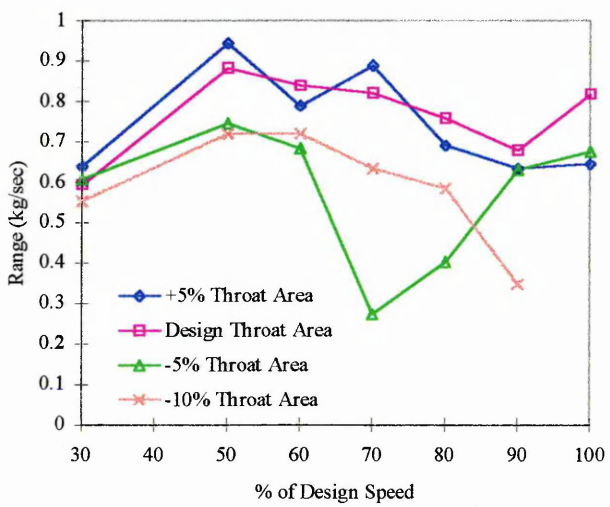


Figure 3.7 Range Variation with Rotational Speed

Table 3.2 Surge Margins at Design Speed

±% of Design Throat Size	Surge Margin (kg/sec)	Comment
-10%	-	Extremely Poor
-5%	0.60	Good
0%	0.59	Good
+5%	0.33	Poor

Note: Surge Margin $= \dot{m}_{design} - \dot{m}_{surge}$

3.4. THROAT BLOCKAGE

Historically (e.g. Dean (1972), Kenny (1970, 1972), Krain (1980)) the static pressure recovery between the impeller tip and diffuser throat has been correlated with throat blockage for most diffuser types, including pipe diffusers. Such correlations are extremely useful as part of a design process as they provide valuable information

required to accurately size the diffuser throat. For the present arrangement, Figure 3.8 shows, that despite the geometric variations between the pipes as shown in Table 3.1, the relationship between the static pressure regain between the impeller tip and the diffuser throat with blockage remained remarkably consistent.

It is important to note that the choice of measurement planes used in Figure 3.8 (and adopted for this thesis) are possibly different from those used by Kenny (1970,1972) in that Kenny quotes blockage to pressure recovery within the *semi-vaneless-space* and not *between impeller tip and throat*. The difference between these is that the latter domain includes the vaneless- and pseudo-vaneless spaces as well as the semi-vaneless space.

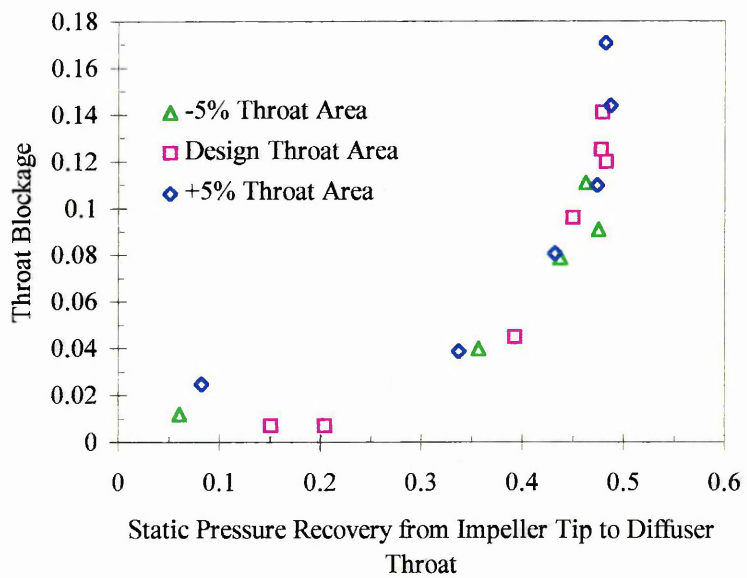


Figure 3.8 Variation of Blockage with Semi-Vaneless-Space Static Pressure Recovery Coefficient (100% Speed)

It was decided to use the pressure recovery between the impeller tip and diffuser throat because:

- There is confusion as to the domain used by Kenny (1970, 1972) to correlate his data. Despite seemingly clear definition in his papers that he uses the semi-vaneless space, reports to the contrary are given by Krain (1980), Japikse (1984) and Japikse and Baines (1994). This must be kept in mind when examining the data.
- The majority of found references, for channel diffusers in general, would tend to use the impeller tip as the inlet measurement plane. Such references include work by Japikse (1984), Krain (1980) and Dean (1974), all of whom have distinguished themselves in centrifugal turbomachinery research.

- In this thesis, the author will make use of data correlated by Dean (1974) for vaned diffusers. As the measurement planes used are unambiguous, with the inlet plane clearly defined as the impeller tip, the data will be used later in Chapter 4 as a basis of comparison between pipe and vane diffusers.
- It is well known that on the diffuser leading edge radii there are strong circumferential static pressure gradients. These are so prominent that this region has often been called 'the region of rapid adjustment' and therefore many static tappings are needed in order to gain a sufficiently accurate planar pressure average. For pipe diffusers in particular, this is extremely difficult to arrange due to the complex leading edge geometry. The alternative option of taking measurements at the impeller tip periphery does make instrumentation much easier to install and, as a bonus, is partially isolated from some of the flow distortions caused by the diffuser vanes.
- Historically, the use of a semi-vaneless-space region in design calculations has been to link the flow from the 'annular' flow of the vaneless-space to the 'linear' flow within the 2D diffuser downstream. Pipe diffuser configurations however, due to the pseudo-vaneless-space region, are not so simple to model as a series of discrete sections. Instead it would seem reasonable to combine the vaneless-, pseudo- and semi- vaneless-spaces together (noting that the vaneless space in conventional pipe diffuser configurations is very small and occupies only approximately 1% of R_{tip}) to form a single control volume for calculations.

3.4.1 BLOCKAGE VARIATION WITH THROAT AREA

It is apparent from Figures 3.8 and 3.6 that the pressure recovery near surge, and the surge-mass-flow-rate are similar for all geometries. This implies that, at surge, the aerodynamic throat areas remain unchanged, despite a 10% geometric variation. This effect may also be seen in Figure 3.9 where the throat blockage generally shows this trend over the complete operating range. Oversizing the geometric throat area would therefore only seem to introduce additional increments in blockage without changing the pseudo- and semi-vaneless-space diffusion. As blockage has a detrimental effect on downstream channel diffusion, oversized diffuser throats should therefore definitely not be used. In addition there is strong argument for sizing the diffuser to choke very near to the design point as would seem to be the North American gas turbine manufacturers' practice. This was discussed in Section 3.3 where the problems associated with making the throat too small were also noted. The conclusion is that it needs to be precisely sized and it has been shown that for this case (using the nomenclature of this study) the optimum lies between 'design' and '-5%'.

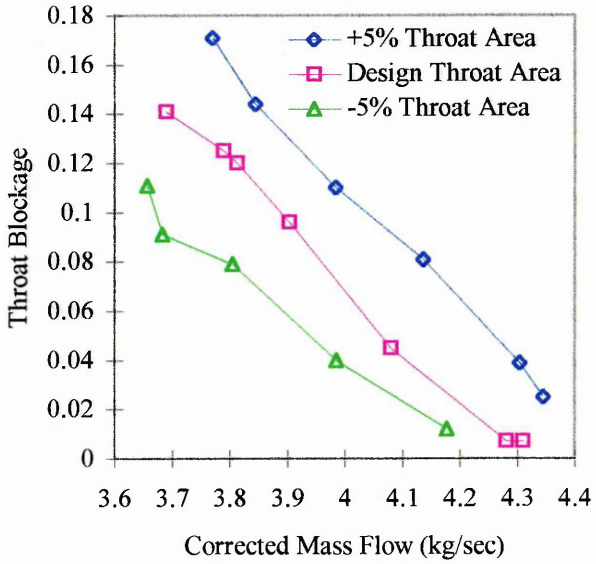


Figure 3.9 Effect of Throat Size Variation on Throat Blockage at 100% Speed

3.5. Stage Performance and Range

The overall stage efficiency and pressure rise were calculated (see Figure 3.10) using the measured throat conditions and applying them to an assumed diffuser of area ratio 4.82 and length/throat-diameter ratio of 13.9 (chosen to allow direct comparison with a previous Rolls-Royce pipe diffuser build). No losses were assumed between the impeller and diffuser throat and therefore the impeller tip total pressure (calculated as described in Appendix A) was used. A throat Mach number was calculated using this total pressure and static pressure measurements on the blade periphery. Diffuser throat blockage was calculated from mass continuity. With the diffuser throat blockage and Mach number, the conical diffuser data from Dolan and Runstadler (1973) was used to predict diffuser losses and hence a hypothetical stage performance. It should be noted that some extrapolation of the Dolan and Runstadler (1973) diffuser data was required as the highest blockage reported there was only 0.12; in this exercise blockages reached almost 0.18.

A Rolls-Royce 31 pipe diffuser test (with all downstream diffusing sections, Pinot (1978)) showed an unstalled operating range less than half of that tested here. This contradicts the literature which has a history blaming the semi-vaneless-space for surge (a brief review of which is given by Elder and Gill, 1984). Arguments for this centre about the strong positive pressure rise characteristic of the semi-vaneless-space, when compared against other components, see Figure 3.11. Despite this, the measurements taken here show that the pseudo- and semi-vaneless spaces, and the conical diffuser flow

stability characteristics are strongly linked and that no stability analysis would be complete without the proper modelling of all. In particular such a model would have to account for the instability in the conical diffuser section brought about by excessive blockage at the diffuser throat.

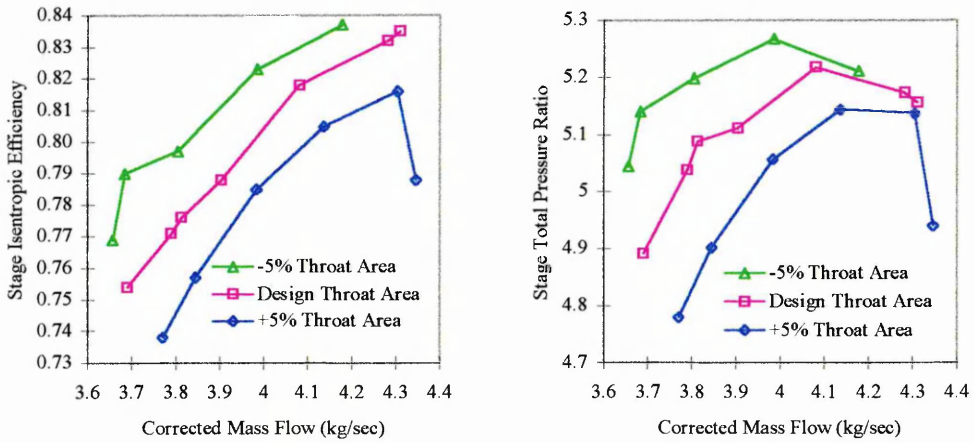


Figure 3.10 *31 Pipe Diffuser, Effect of Throat Size Variation on Stage Performance*

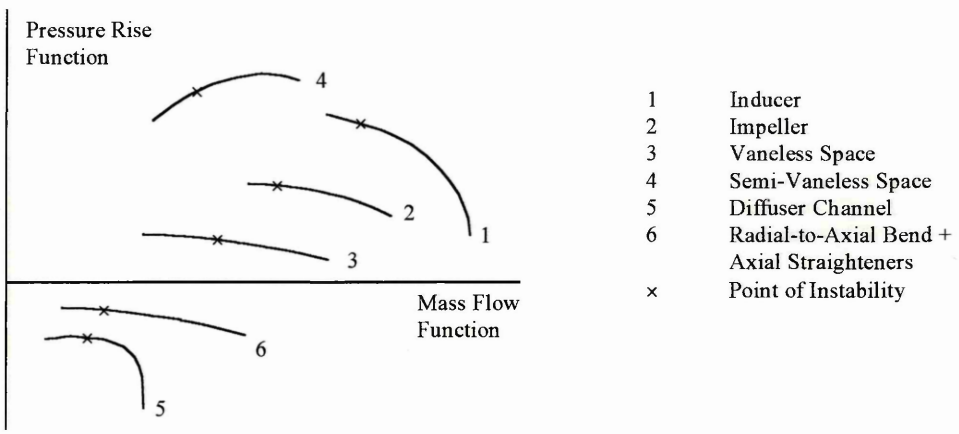


Figure 3.11 *Element Characteristics of a Compressor (Elder and Gill 1984)*

The evaluated stage 100% speed characteristic shown in Figure 3.10 demonstrates that the peak performances of both the design and 5% undersized are similar but with a

marginal increase in pressure rise for the latter. This enhancement is attributed to the reduced throat blockage (see Figure 3.9), which is a governing performance factor for diffusers.

The operational ranges themselves must not be relied upon due to the reasons indicated earlier but it is clear that the throat size strongly influences the stage performance. These studies indicate that a throat size between 'design' and '-5%' is optimum for this stage and all throat sizes of diffusers studied in Chapters 4 and 5 will have the 'design' area. This will ensure a near-optimised and representative throat area that, with a downstream diffusing cone as shown by Pinot (1978), who tested a 31 pipe diffuser with similar throat size to the 'design' case, will operate with reasonable range.

3.6. COMPARISON WITH ROLLS-ROYCE DATA

Some of the 35D Rolls-Royce data is shown in Figure 3.12 (Pinot, 1978) and is a comparison between a 31 pipe and a conventional 29 vane island diffuser. Generally there is a slight pressure-ratio deficit noticed for the pipe diffuser configuration. At 100% speed both diffuser systems yield the same peak efficiency, but at 110% overspeed the pipe diffuser shows a 2% superiority. This is in agreement with the literature (Kenny 1970, Reeves 1977) where pipe designs have been specifically targeted at high pressure compressors. Documentation on the Rolls-Royce experiments indicated that the pipe diffuser tested was slightly oversized (by 1.3%) compared with the 'design' throat size used here. Using Figure 3.10 this equates to an underestimation of 0.55% in efficiency and 0.125 in pressure-ratio. Correcting Figure 3.12 for these differences makes the pipe diffuser design comparable up to 90% speed, and superior beyond. Estimated efficiency enhancements are shown in Table 3.3. In this comparison it has been assumed that the vaned-island throat size was optimum since this had been well researched by Rolls-Royce.

Table 3.3 Pipe Diffuser Performance Enhancement

% of Corrected Design Speed	Mach Number at Impeller Tip	Stage Efficiency Enhancement of Pipe over Vane Island Diffusers using a 'Corrected' Throat Size
110%	1.11	+2.75%
105%	1.07	+1.75%
100%	1.04	+0.50%
90%	0.95	-0.25%
80%	0.86	-0.75%
70%	0.81	-0.25%

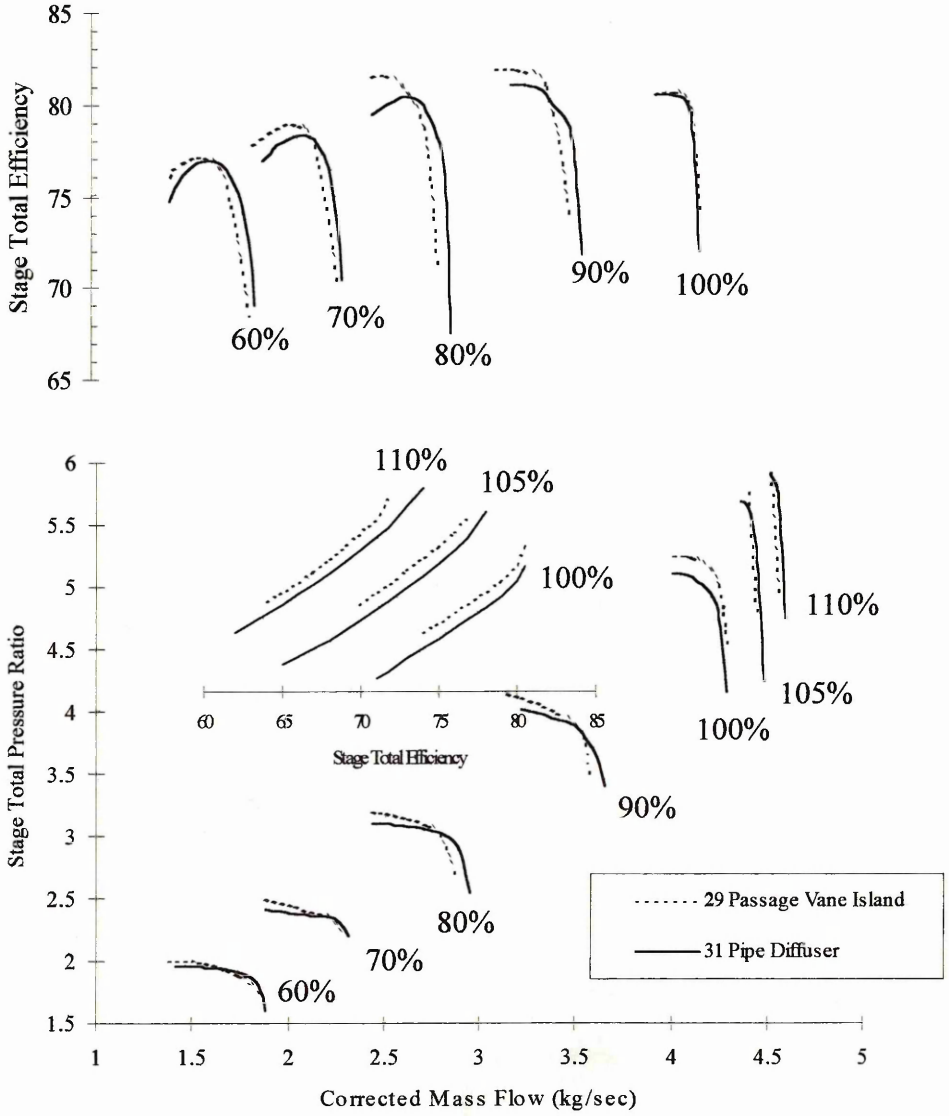


Figure 3.12 Rolls-Royce Tests with 35D Compressor: Comparison between a 31 Pipe and 29 Vane Island Diffuser

3.7. CLOSURE

A pipe diffuser has been designed, manufactured and experimentally analysed to investigate the effect of throat size on stage performance and range. The pertinent findings of this study are:

- The customisation of the Herbert (1980) centrifugal compressor design program using empirical blockage data from Kenny (1970) has resulted in a successful pipe diffuser design with acceptably sized throat.

- Pipe diffusers, as hypothesised in the introduction, have been shown to offer significant efficiency enhancements (up to 2-3%) over conventional vane island diffuser designs at pressure ratios above 5½ ($M_{tip} > 1.1$).
- Oversizing diffuser throats only results in approximately equal increments of throat blockage without desired additional pseudo- and semi- vaneless space diffusion.
- The throat size is a controlling parameter for pipe diffusers and incorrect prescription invariably leads to significant penalties in both range and efficiency. An outcome of this investigation is a pipe diffuser throat size that will allow comparative studies between diffuser designs. The so-called 'design' diffuser throat is to be used. This is a compromise throat size that straddles the UK and North American design philosophies.
- For design purposes, the experiments have suggested the following guidelines for throat sizing:

  96< (Design Mass Flow)/(Diffuser Choke Mass Flow) < 100%

CHAPTER 4
Pipe Diffuser Sidewall Expansion

In Chapter 3 a pipe diffuser design procedure was described. This utilised a general centrifugal compressor design program (Herbert, 1980), together with additional empirical input from the work of Kenny (1970), to specify a diffuser geometric throat area. Once completed, the number of pipes could be chosen. This was selected to minimise the meridional step, or sidewall expansion, between the impeller tip and the diffuser leading edge in order to avoid perceived step losses. Figure 4.1 shows the resulting relationship between the number of diffuser passages and the sidewall expansion using the current impeller as an example (repeated here from Chapter 3 for convenience). Consequently strict adherence to this design philosophy, would result in a 37 pipe arrangement.

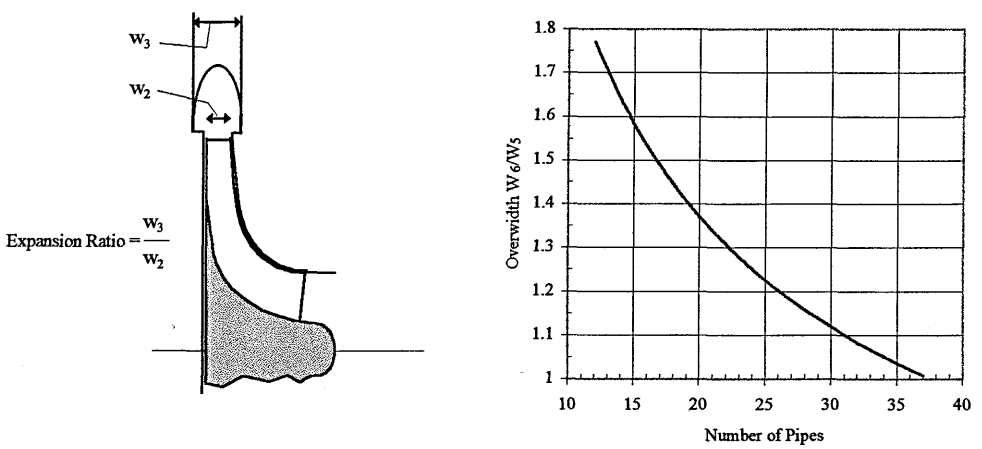


Figure 4.1 *Effect of Number of Pipes on Sidewall Expansion Ratio for 'Diffuser-Design' Throat Size*

Prior to this work, the author was aware of an investigation by Elder and Gill (1984) who showed significant range improvements for vaned diffusers with low numbers of passages. However, such improvements could only be replicated with pipe diffusers by increasing the sidewall expansion ratio. This was undertaken here and the advantages and disadvantages of this alternative design philosophy are reported in this chapter. In addition, a pipe diffuser with an oval rather than circular cross-section is considered. This had the advantage of a low number of blade passages for enhanced range but with minimal sidewall expansion to reduce step losses.

Outline of Chapter

In the opening section, geometric design considerations for pipe diffusers are discussed. It is shown that even with departures from the conventional pipe diffuser design philosophy, the incidence and leading edge radius remains relatively unchanged. This is highlighted by using the current impeller as a test case.

This is followed by a description of the 4 pipe diffusers examined, together with motivations for their inclusion in this current study. The influence of each pipe diffuser design on the compressor stage is then discussed. In particular the effect on range and throat blockage are examined as these form the bases of the stage performance.

In this chapter, the emphasis is on accumulating design-type information suitable for optimising the inlet geometry of pipe diffusers and all parameters that could be collated to form design rules from this work are presented Although to gather such information invariably required detailed measurements, these are only presented in summary form here (i.e. average planar values etc.). The actual detailed flow measurements and how they describe the flowfield are discussed later in Chapter 5.

4.1. Pipe Diffuser Geometric Design Considerations

In Chapter 3, a 'conventional' pipe diffuser design philosophy, based on Kenny's (1969,1970,1972) research was described. Using this philosophy, the impeller tip was utilised as the pipe tangency radius and the number of pipes was selected to minimise sidewall expansion. In order to improve this 'conventional' design, modifications were considered including: alternative tangency radii, enforcing sidewall expansion and also alternative 'pipe' cross-sections.

Given a diffuser throat size, there are two main geometric features that the literature suggests should be optimised: these are the diffuser leading edge radius and the leading edge incidence. Preliminary calculations indicated that potential designs using the impeller tip as the tangency radius would result in a leading edge radii range between $1.07 < R_{le}/ R_{tip} < 1.11$ (see Figure 4.2). This range is comparable to those for conventional

vane island diffusers and therefore there would seem little motivation to choose an alternative tangency radius unless some improvements in incidence could be achieved.

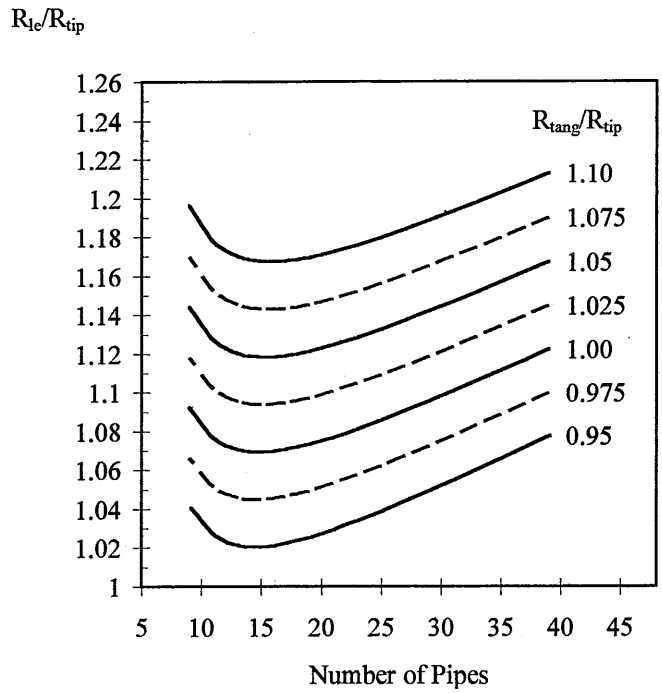


Figure 4.2 Effect of Tangency Radius on the Diffuser Leading Edge Radius (Non-dimensionalised by Impeller Tip Radius)

Reeves (1977) suggested that incidence was of paramount importance and recommended its optimisation by varying the pipe tangency radius and/or the diffuser cross-section. A preliminary study of this was carried out by the author using the current compressor as a test case. Figure 4.3 shows that bisector incidence (at diffuser choke) is fairly insensitive to the tangency radius. In addition, the freedom introduced by allowing non-circular cross sections gives the designer only a little extra control over incidence as seen in Figure 4.4. Reeves (1977) in his paper suggested far more control (particularly as he regarded incidence as a range indicator). It is possible that for pipe diffusers, Reeves neglected the flow angle change associated with the sidewall expansion (a backward facing meridional step would reduce the radial velocity component at the impeller tip making the flow more tangential). The author believes that neglecting this change is not justified as the path length from the impeller tip to the diffuser leading edge can be up to 2 to 3 impeller tip heights- a sufficient distance for the flow to assume a new direction.

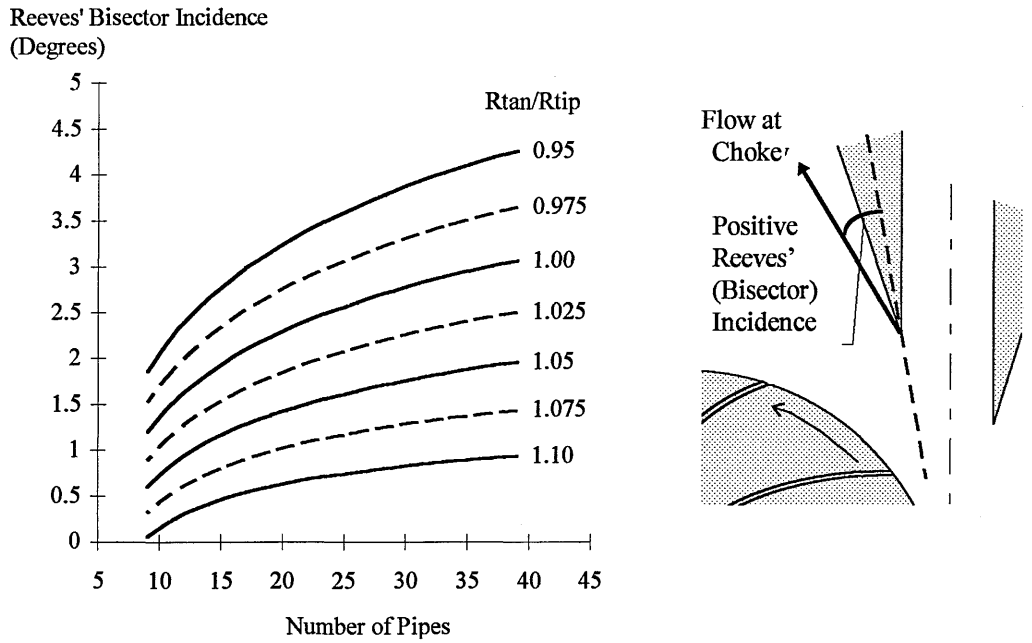


Figure 4.3 *Effect of Tangency Radius on the Diffuser Leading Edge Incidence (Non-dimensionalised by Impeller Tip Radius)*

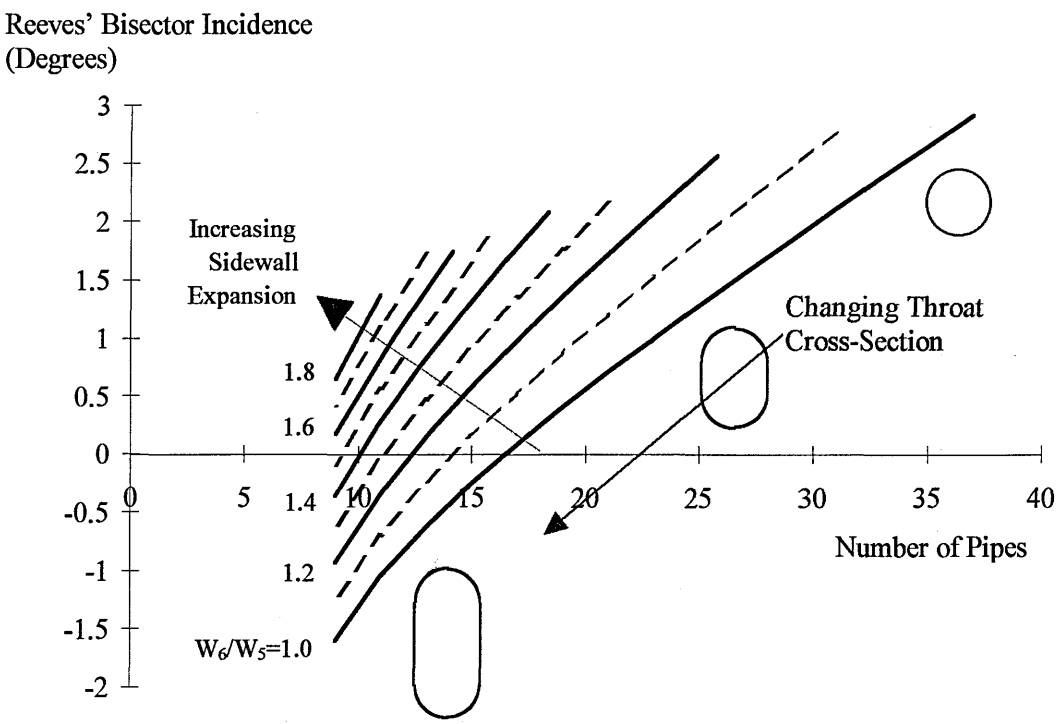


Figure 4.4 *Effect of Sidewall Expansion on Reeves' Incidence (Assumes Impeller Tip Used as Pipe Tangency Radius)*

To summarise, despite the restrictive nature of pipe diffuser geometry, the designs 'naturally' led to reasonable leading edge radii (i.e. similar to those found for vaned equivalents) when the pipe tangency radius was chosen to be the impeller tip radius. This is the Kenny (1970) philosophy and it would therefore merit adoption.
It has also been shown here that alternative diffuser cross-sections have little impact on diffuser leading edge geometry and the only possible benefit in their use would seem to be a reduction in perceived sidewall expansion step losses. In addition, little control over the leading edge incidence has been noted.

4.2. DESCRIPTION OF THE DIFFUSERS TESTED

The four diffusers examined are shown in Figure 4.5 and Table 4.1. The first and datum consisted of 31 pipes, representing the traditional design with minimal step (or sidewall expansion). This design was the subject of the area expansion investigation in Chapter 3. The second, the 22 pipe design, reflected the current limiting philosophy believed to be used by the US gas turbine industry for all diffusers, that of an overwidth ratio of 1.3. A further increase of sidewall expansion ratio to 1.7 with 13 pipes was completed following favourable experimental results from the aforementioned designs. This was somewhat larger than would have been originally selected and was carried out in order to avoid having the same number of vanes as impeller blades.

In order to assess the losses associated with the large sidewall expansion step for the 13 pipe diffuser, an oval equivalent design was conceived. This was chosen to fit with minimum sidewall expansion, thus fixing the radii required for throat construction. Working with a fixed throat area then allowed the prescription of the distance between the centres of these construction radii. In order to improve the comparison between the 13 circular and 13 oval pipe diffusers, the oval pipe diffuser was designed with the same leading edge radius. This involved using a tangency radius (measured normal to the pipe cross-section centriod- see APPENDIX G) slightly smaller than that of the impeller tip.

It should be noted that, as described in the earlier chapter, the conical portion of the pipe diffusers were not modelled. The pipe diffuser throat flow was abruptly dumped into a wide vaneless diffuser. It is considered that this influenced surge but upstream component performances were largely representative. In all cases the cylindrical throat was set to equal 1 hydraulic diameter long.

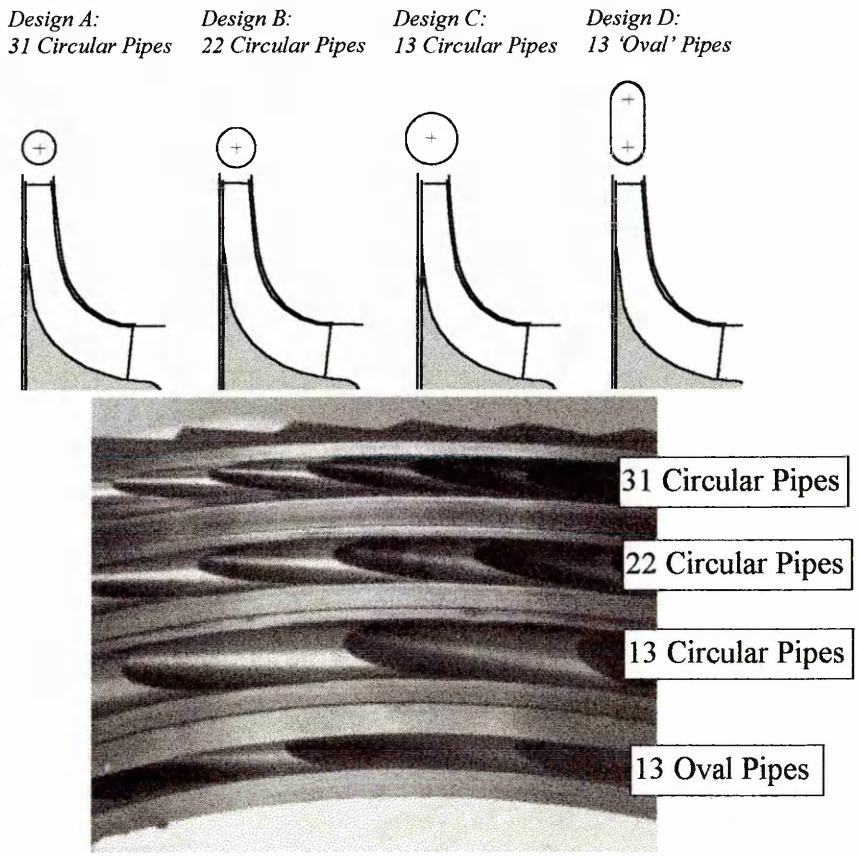


Figure 4.5 Sketch and Photograph of Tested Pipe Diffuser Configurations

Table 4.1 Geometric Details of Tested Pipe Diffusers

Pipe Design	Number of Pipes	Sidewall Expansion W_6/W_5	Leading Edge (Bisector) Angle*	Bisector Incidence**	R_{le}/R_{tip}	Total Throat Area (mm^2)
A	31	1.105	65.95°	2.80°	1.101	4290
B	22	1.311	69.46°	2.41°	1.078	4290
C	13	1.707	74.13°	1.73°	1.071	4290
D	13	1.05	67.35°	0.40°	1.071	4290

* defined in nomenclature

**assuming an impeller discharge flow angle corresponding to inducer choke

4.3. OPERATIONAL RANGE

Figure 4.6 shows the operating range of the centrifugal compressor with all of the examined pipe diffusers. The range improvements (surge to choke) are presented in Table 4.2 with the associated surge margins (surge to design point) at 100% speed presented in Table 4.3. The diffusers with lower numbers of pipes perform with the largest operational range. This is as shown in the literature, but the actual reason or reasons for this improvement are not clear. The literature suggests that the operational

ranges of diffusers are influenced by several factors and these are explored below in an attempt to explain the associated range improvements.

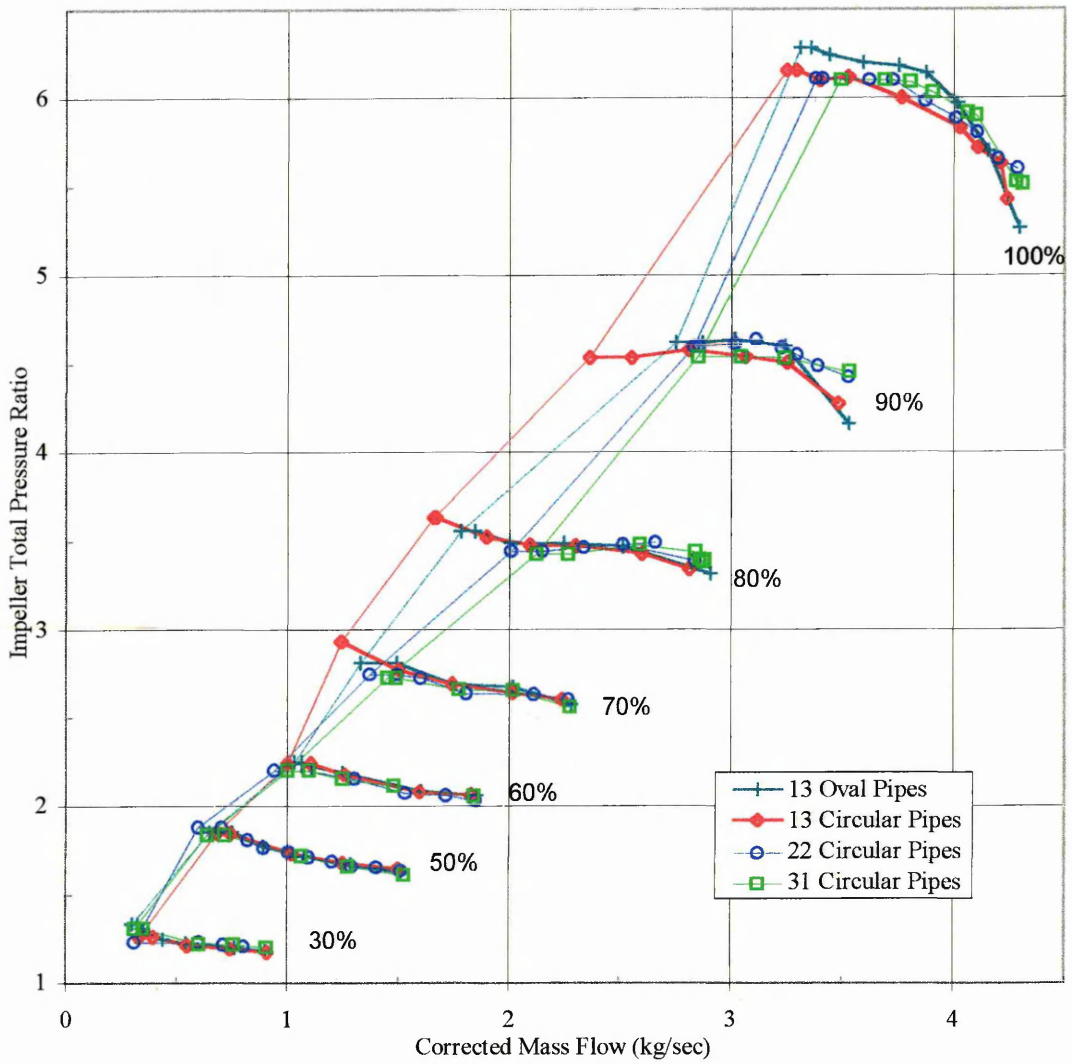


Figure 4.6 Effect on Range of Different 'Pipe' Diffuser Types

Table 4.2 Effect of Number of Pipes on Flow Range

% of Design Speed	% Range Improvement over 31 Pipe Diffuser		
	22 Pipes (Circular)	13 Pipes (Circular)	13 Pipes (Oval)
30%	0%	-3%	1%
50%	5%	-5%	0%
60%	7%	0%	-1%
70%	10%	27%	21%
80%	17%	67%	63%
90%	3%	78%	24%
100%	15%	32%	32%

Table 4.3 Effect of Number of Pipes on Surge Margin

% of Design Speed	% Surge Margin Improvement over 31 Pipe Diffuser		
	22 Pipes (Circular)	13 Pipes (Circular)	13 Pipes (Oval)
100%	18%	40%	30%

4.3.1 Effect of Operational Speed on Range

At low speeds, due to compressibility effects, the inducer section is ascribed to the degradation of flow that pre-empts stall. At higher pressure ratios, it is the downstream diffuser that is blamed. This phenomenon, due to compressibility effects, is described by Elder and Gill (1984) as synonymous with that seen for multistage axial compressors but with the inducer and diffuser representative of the initial and final stages of an axial multistage compressor. The trend of inducer incidence mismatch is shown in Figure 4.6 for the tested compressor at and below 60% of the design speed. Above this, it is the downstream diffuser that is believed instrumental in causing surge.

It is well documented in the literature that excessive diffusion within the semi-vaneless-space is one of the main causes of surge in a compressor stage. We can gain an approximation of this diffusion by examining the flow area ratio across the semi-vaneless space. The flow area ratio at surge is shown in Figure 4.7 and is seen to have some sensitivity to impeller tip speed (or alternatively Mach number). Figure 4.7 has been correlated using the Herbert (1980) compressor design program for the 35D compressor with 31 pipe diffuser. Each point denotes the onset of surge measured at Rolls-Royce by Pinot (1978) for each speed line. The Rolls-Royce data was used as the experiments carried out as part of this current work did not include the diffusing cone which is believed to influence surge. At impeller speeds of 60% and below, as mentioned above, surge is expected to be caused by inducer stall. At higher speeds, where surge is controlled by the diffuser conditions, a strong impeller rotational speed (or Mach number) influence is observed. This shows that at elevated tip speeds the diffusers are able to tolerate higher flow area ratios implying that larger amounts of pressure recovery are possible within the semi-vaneless space. This in fact does occur and is shown in Figure 4.8. Later in this chapter, however, it will be demonstrated that this benefit is at the cost of increased throat blockage.

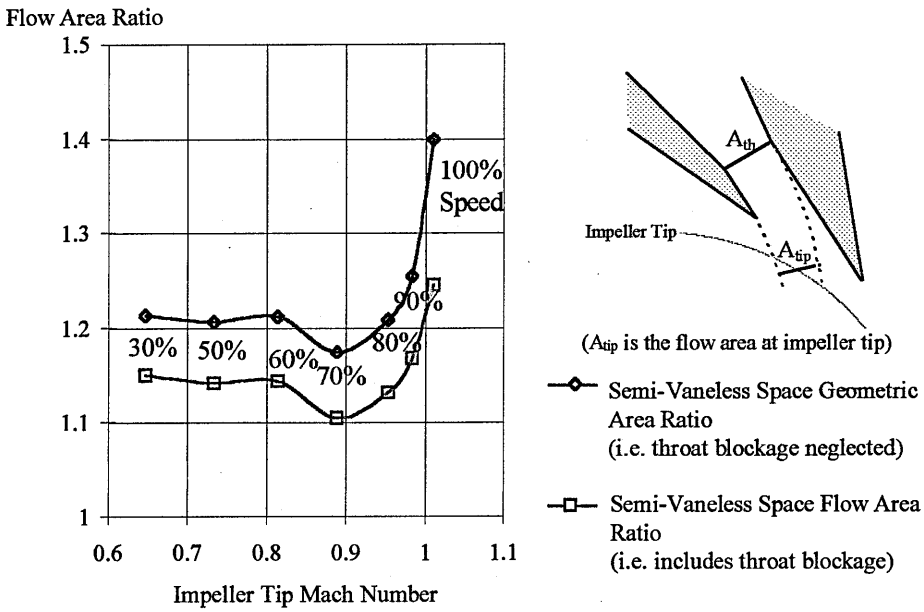


Figure 4.7 Geometric and Actual Semi-Vaneless-Space (SVS) Flow Area Ratios

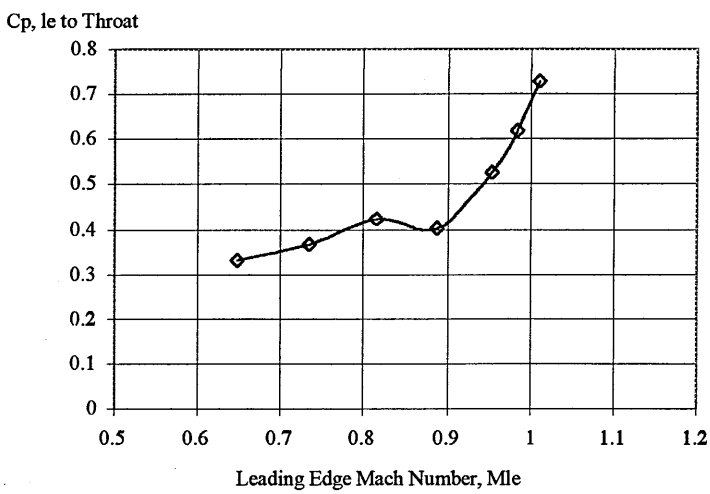


Figure 4.8 Static Pressure Recovery within Semi-Vaneless-Space

4.3.2 EFFECT OF WETTED DIFFUSER AREA ON RANGE

Came and Herbert (1980) describe the ratio of (wetted semi-vaneless-space)/(diffuser throat area) or A_w/A_g as a factor effecting surge. The A_w/A_g ratio was hypothesised to be a representative non-dimensional path length from diffuser leading edge to throat and therefore using this parameter, diffusers with large values of A_w/A_g would be expected to be less susceptible to the flow breakdown that is expected to precede stall. This area ratio correlation was enhanced by Elder and Gill (1984) by multiplying by the number of

impeller blades (N_I), see Figure 4.9. Even as admitted by the originators, this correlation included a great deal of scatter and was felt crude due to the omission of other relevant determinants (e.g. impeller backsweep, matching etc.). For the diffusers tested, the following (Aw/A_g). N_I values were calculated. See Table 4.4.

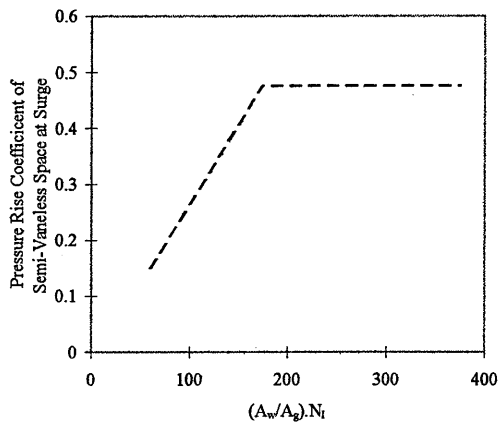


Figure 4.9 Semi-Vaneless-Space Pressure Recovery at Surge (Elder and Gill (1984))

Table 4.4 Semi-Vaneless Space Geometry for Pipe Diffusers Tested

Pipe Design	Number of Pipes	(Aw/A_g). N_I	X_{svs} (mm)	$X_{svs}.\sqrt{N_D}$
A	31 (Circular)	66	9	50
B	22 (Circular)	72	22	103
C	13 (Circular)	73	36	130
D	13 (Oval)	90	35	126

Clearly the range of (Aw/A_g). N_I tested is very limited and no conclusive evidence can be gained here from its examination. It is of interest, however, that the limiting pressure recovery for all of the pipe diffusers examined was approximately 0.5- corresponding to the plateau in Figure 4.9. In addition, it is somewhat surprising to see that the smallest wetted flow area is calculated for the high pipe number configuration (note that A_g and N_I are invariant). This unexpected result is explained by examination of the semi-vaneless-space centreline distant, X_{svs} , depicted in Figure 4.10 and quantified in Table 4.4.

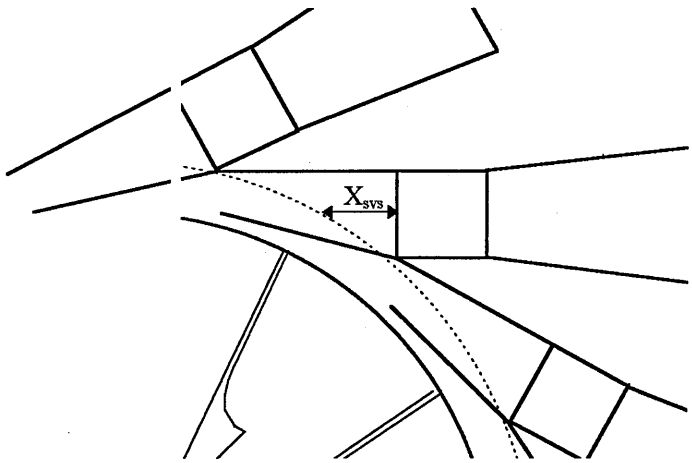


Figure 4.10 Definition of Centreline Flow Distance, X_{svs}

The dimension X_{svs} indicates the length of the semi-vaneless-space and is a reasonable approximation of the mean pathline for the examined diffusion process. We can now use this dimension and apply it to 2-D diffuser data, Figure 4.11. On the y-ordinate, the area ratio is known. However, for an x-ordinate point, we need to account for the number of passages. Here the dimension X_{svs}, is multiplied by the square root of the number of diffusing passages in order to gain a equivalent (diffuser length/ throat radius) ratio i.e.

We have $\frac{L_{Diffuser}}{D_{throat}} = \frac{X_{svs}\sqrt{\pi N_D}}{\sqrt{4A_{throat}}}$,

Hence, given a constant throat size we get , $\frac{L_{Diffuser}}{D_{throat}} \propto X_{svs}\sqrt{N_D}$

Although both the area and length ratios would be near unity and outside the scope of the data set shown, a cone internal angle may be calculated. For the 31 pipe diffuser this internal included angle (2θ) is approximately 16° near surge. A diffuser with this divergence would be expected to operate with significant regions of wall separated flow (Reneu et al 1994). To improve matters, larger values of $X_{svs}.\sqrt{N_I}$ would be required to relieve the diffusion process. Such improvements are seen for the diffusers with low numbers of pipes, and as these have the best range, the results here would tend to support a diffuser-cone-angle related correlation.

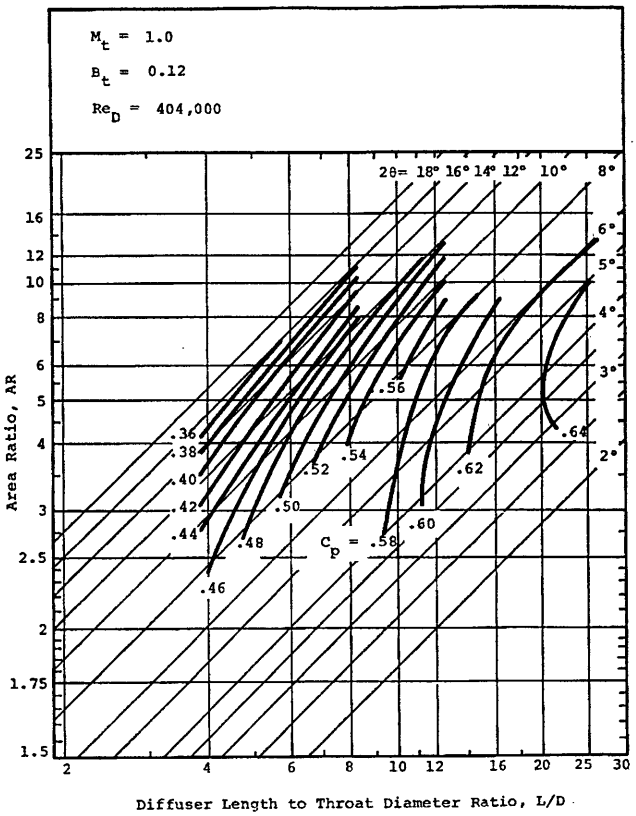


Figure 4.11 Sample 2 -D Diffuser Data (Dolan and Runstadler, 1973)

4.3.3 EFFECT OF DIFFUSER LEADING EDGE INCIDENCE ON RANGE

Poor correlation with the Reeves (1977) range data is seen (see Figure 4.12). This is particularly true for the 'oval' design which, disappointingly, did not achieve the expected range enhancement over its circular counterpart despite improved incidence. It should be noted, however, that the ranges plotted for the tested pipe diffusers have been scaled by using results from (Pinot 1978), who also tested a 31 pipe diffuser on the 35D compressor but *with* downstream diffusing cone and 'fishtail' bends. The ranges measured by Pinot (1978) were then divided by those of configuration 'A', a 31 pipe diffuser without cone. The operating range (surge to choke) without diffusing cone was 2.85 times greater than that with. Such a large divisor is clearly cause for concern and casts considerable doubt as to the accuracy of the resultant data. However, the trends are expected to be consistent irrespective of the configuration downstream of the diffuser throat and therefore the data strongly indicates that the Reeves' incidence should not be a prime consideration in pipe diffuser design. This follows earlier discussions with Rolls-Royce.

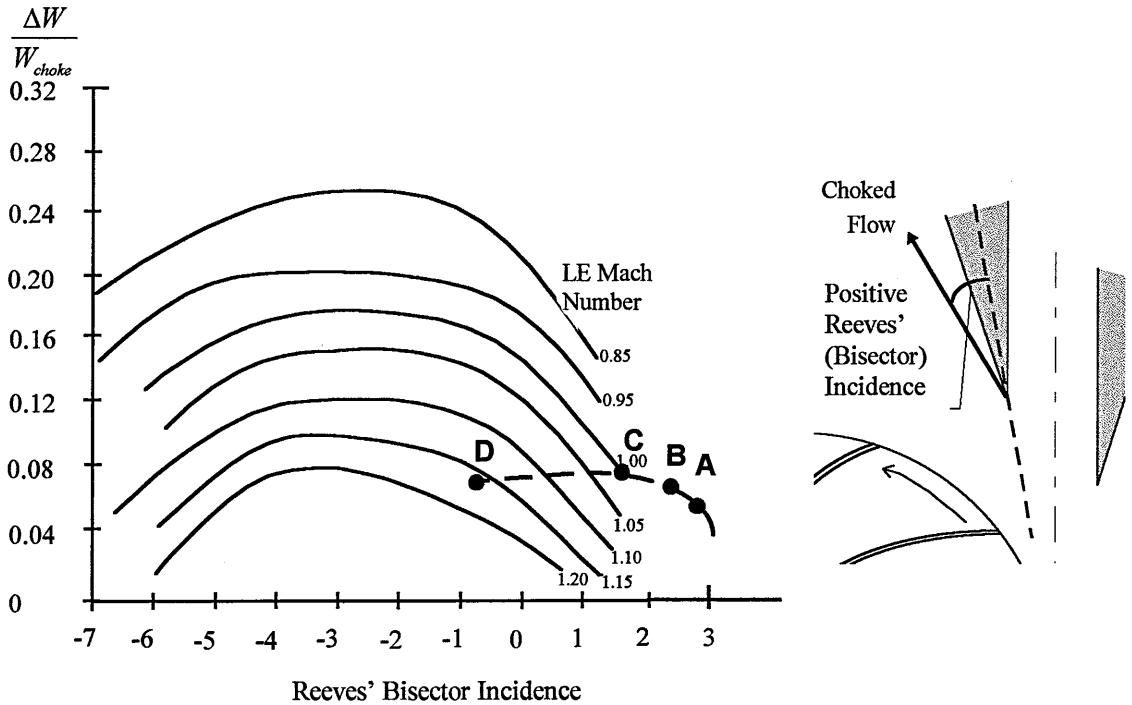


Figure 4.12 *Range-Incidence Correlation [Contours from Reeves (1977)]*
(Nominal leading edge Mach number of tested diffusers was 1.0)

An alternative incidence, commonly used for vaned diffuser design, is that between the flow and the *suction* surface. This surface in vaned diffuser calculations (e.g. Herbert (1980)) determines the flow expansion within the semi-vaneless-space flow (see Figure 4.13). The suction surface incidences, at choke, for the pipe diffuser configurations examined in this thesis are presented in Figure 4.14.

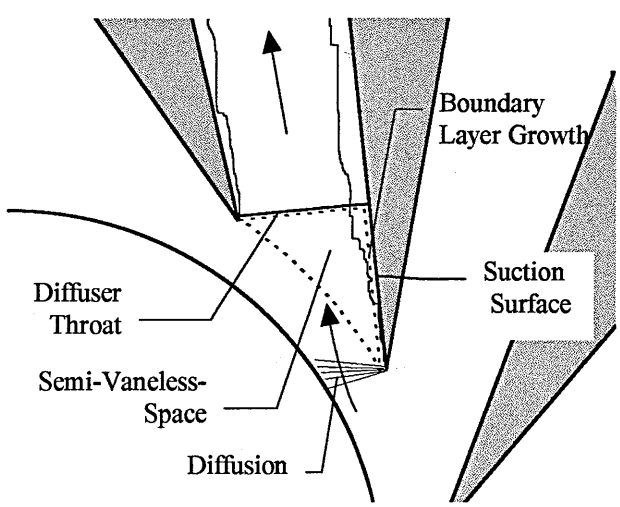


Figure 4.13 *Semi-Vaneless-Space Flow*

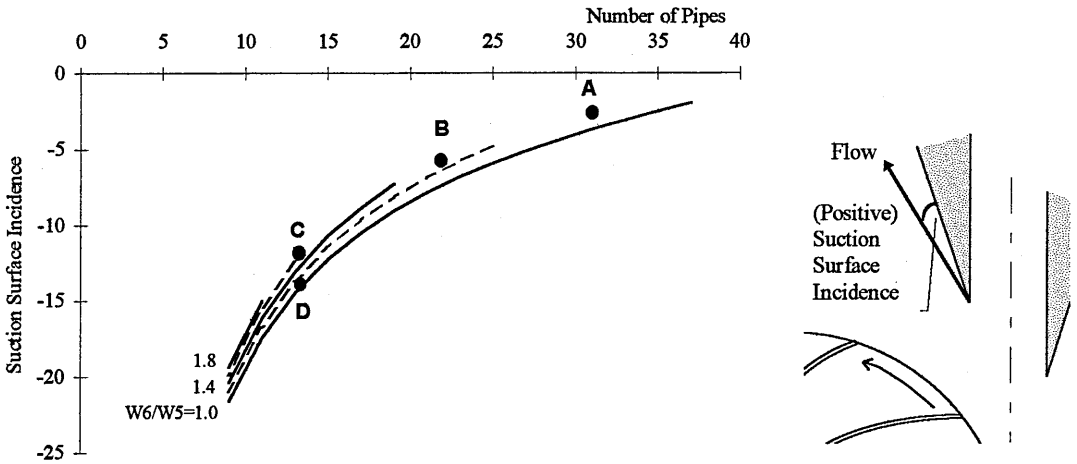


Figure 4.14 *Effect of Sidewall Expansion on Suction Surface Incidence (at Choke)*

In all cases, the suction surface incidence is seen to be negative. For the diffusers with lower numbers of pipes, this flow mismatch approaches 15°. This apparently large incidence is due to the wedge angle which is directly related to the number of passages (wedge angle = $360°/N_D$). The use of the bisector incidence would therefore seem to be a more sensible choice for pipe diffusers.

4.3.4 Effect of the Number of Diffuser Passages (or Pipes) on Range

It is most apparent from these tests that the number of diffuser passages strongly effects the range. Surprisingly, however, the 'oval' pipe diffuser operated with less range than its circular counterpart, indicating that other factors may be significant. One already highlighted here is the pathline within the semi-vaneless space. This dimension would seem to correlate well with the range measured.

4.3.5 Concluded Primary Range Enhancing Parameters

Incidence has been shown to be a poor range indicator. Although not fully understood, reducing the numbers of pipes has shown to give improved range. This has already been demonstrated for conventional vaned diffusers by Elder and Gill (1984) and to some extent for pipe diffusers by Groh (1969) and Japiske (1980), although it was only after completing all experimental work that the author became aware of the last two references.

Range, although important, is not the only consideration for diffuser design; as for example it is well known that a vaneless diffuser, out of all diffuser types, will generally

operate with the largest range but with a trade-off in peak efficiency. Throat blockage; losses within semi-vaneless-space; overall stage performance and flow unsteadiness are other factors that could influence the chosen diffuser design. These factors are now discussed for the examined pipe diffusers.

4.4. LOSSES WITHIN THE PSEUDO- AND SEMI- VANELESS SPACES

From detailed area traverses of the pipe diffuser throats and measurements at the impeller tip, the losses within the pseudo- and semi- vaneless spaces of each pipe diffuser build could be evaluated. The diffuser throat traverses, described in detail in the next chapter, were carried out using a pneumatic total pressure probe of minimal frontal area (0.9mmØ) to reduce its influence on the flow-field. The measured total pressures were then mass-weight-averaged to yield a planar value. The region's inlet total pressure, that of the impeller tip, was calculated from the static performance instrumentation where careful positioning of numerous tip static pressure tappings was undertaken to minimise the influence of static pressure field distortions due to the downstream diffusers. Generally, the impeller tip static pressure was calculated from the average of five tappings.

Figure 4.15 presents the losses across the 100% speed characteristic for each of the diffusers. The measured losses were surprisingly consistent with little variation between diffusers. In particular there was little distinction between the two 13 pipe configurations where a noticeable step loss variation was expected.

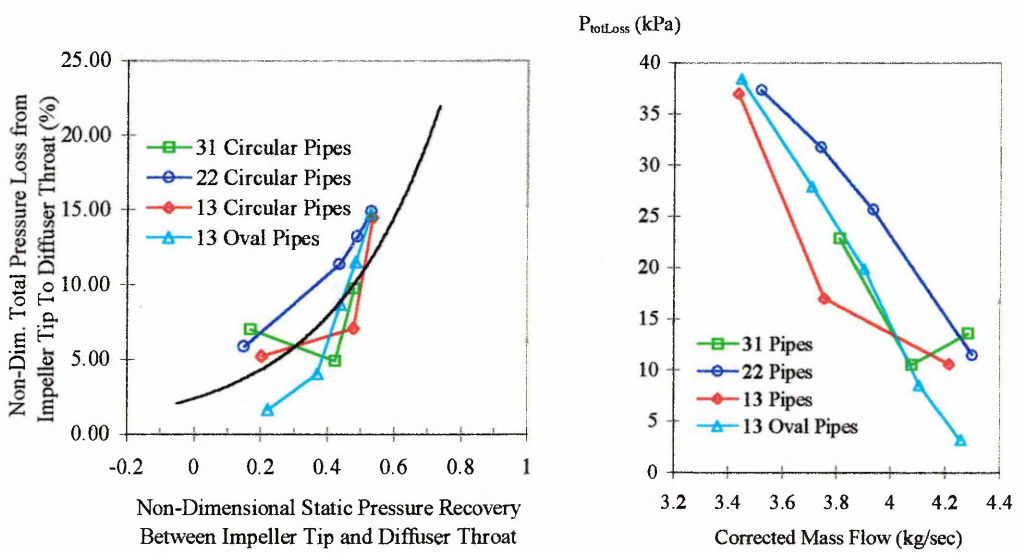


Figure 4.15 *Losses within Semi- and Pseudo- Vaneless Spaces (Left-Hand Graph is Non-Dim wrt Tip Dynamic Pressure)*

The step losses for the 13 and 22 circular pipes diffusers are estimated as 11.5 and 3.5 kPa respectively (based on ESDU 1981). These losses are sufficiently large to be detected in Figure 4.15, but paradoxically they are not. There is insufficient information onto which to base a reason for this but the author hypothesises that the sidewall step, in some manner, is improving the jet/wake mixing process at impeller exit.

4.5. THROAT BLOCKAGE

Throat blockage, as described in Chapter 1, is a controlling diffuser performance factor and is of primary importance to diffuser designers. It is for this reason that a great deal of measurements were taken at the diffuser throat. In this investigation, both total pressure and static pressure instrumentation were used. However, quite soon during the diffuser throat investigation, it became apparent that the two types of instrumentation gave different readings for the throat blockage. As the total pressure blockage measurements were taken *directly*, and consequently assumed correct by the author, this variation was of particular concern as up to now, previous investigators had relied upon static pressure measurements for their correlations. The discrepancies in the two sets of measured blockage data may be seen by comparing Figures 4.16 and 4.17. The first shows blockage calculated from (pneumatic) static pressure tappings; the second shows blockages measured by total pressure traverses. Reasons for the discrepancy between these results are discussed below.

4.5.1 DISCREPANCIES IN BLOCKAGE MEASUREMENTS

The method of blockage calculation and associated experimental measurements are given below in order to highlight possible sources of error

a) *Blockage Calculated from Static Tapping Measurements:* Given the impeller discharge total pressure and temperature, the throat static pressure and the mass flow through the impeller; the diffuser throat blockage may be calculated. Figure 4.16 shows the calculated values and compares them with those presented by Kenny (1970). Given that the flow Mach number at the leading edge of the pipe diffusers was nominally sonic and that the supersonic Kenny relation should be used, there is a large difference between the measurements. If losses (not directly measured by Kenny (1970,1972)) within the semi-vaneless space are included, the resulting correlations become even worse with some of the blockages even becoming negative near choke. Clearly this is impossible and the erroneous contribution has been identified as the static pressure tapping measurement. It will be shown in Chapter 5 that there is a great deal of swirl rotating in-plane of the diffuser throat area. This secondary flow elevates the detected static pressure, beyond that of the real mean planar value which as a consequence reduces the calculated throat blockage.

Blockage Calculated from Total Pressure Traverses: Total pressure traverses may be used to calculate the blockage using the definition:

$$Blockage = 1 - \frac{\sum_i \dot{m}_i}{\dot{m}_{peak}}$$

where the m_{peak} is the mass flow based on the peak value and the m_i terms are the elemental area contribution for each traverse point. The elemental contributions were summated to give a total mass flow (rather than using the bellmouth measured value) in order to provide a consistent mass flow comparison. These measurements yield blockages to ±4.1% and are shown in Figure 4.17.

It is hypothesised that as Kenny (1970,1972) completed tests with diffusing cones, it is possible that he was able to carry out some back-calculation using 2D diffuser data to gain improved blockage values. This hypothesis is supported here as blockage measurements, taken directly by total pressure traverses, correlate well with the Kenny (1972) data. All data shown after Figure 4.17 will refer to the measurements taken directly by the throat total pressure traverses. This significantly reduces the amount of presented data but will ensure consistency and accuracy.

The critical reader will have noted that the error introduced due to the flow swirl also affects the pressure recovery term on the x-axis of these plots. However, the static pressure variation to cause a 5% error in blockage nominally equates (near design mass flow) to 0.5 in Cp units. Therefore the expected 'errors' in the static pressure only have a minor effect on the predicted pressure recovery and hence the relationship shown in Figure 4.17 is of acceptable accuracy.

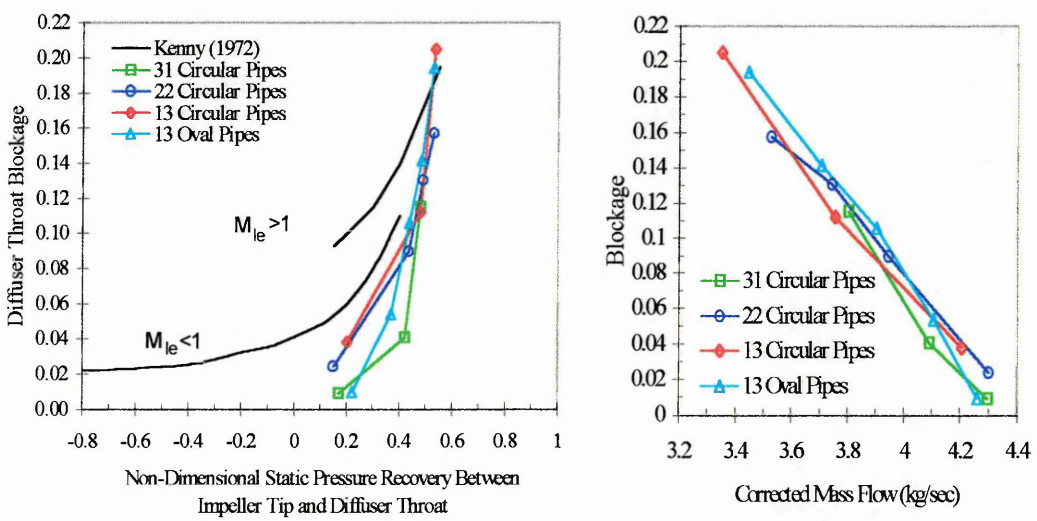


Figure 4.16 *Throat Blockage -v- Static Pressure Recovery within Semi- and Pseudo- Vaneless Spaces (Calculated from Statics)*

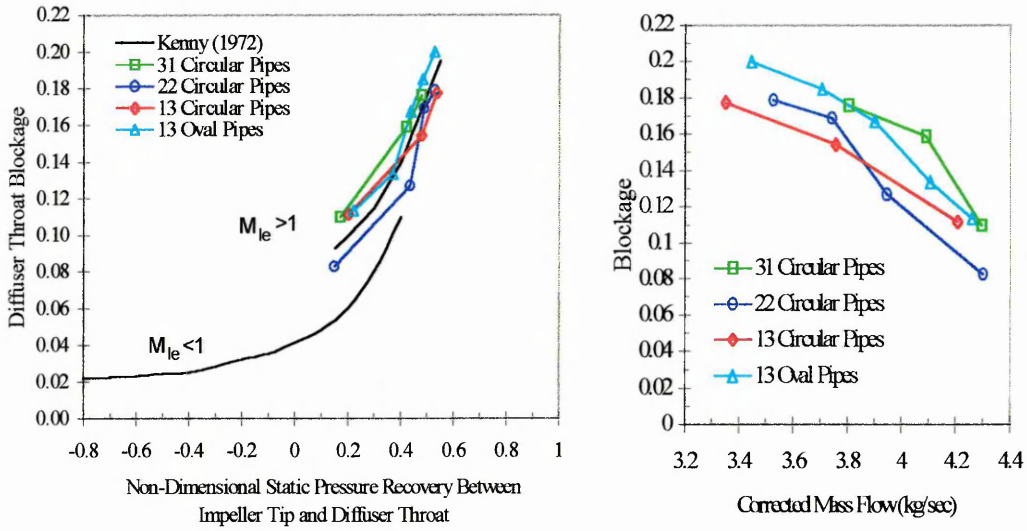


Figure 4.17 Throat Blockage -v- Static Pressure Recovery within Semi- and Pseudo- Vaneless Spaces (Measured using Traverse)

4.5.2 BLOCKAGE VARIATION WITH PIPE DIFFUSER DESIGN

The detailed total pressure traverses at the diffuser throat showed only minor variations in throat blockage between each of the designs (see Figure 4.17). This data varies only slightly from that of Kenny's (1970,1972) but represents, what the author believes, is the only throat-area-traverse derived data available for diffusers. A slight trend of reduced blockage for the diffusers with low numbers of pipes is visible although this variation is well within the expected accuracy of measurements. From the pipe diffuser experiments carried out here, some additional blockage information may also be gained from examination of the diffuser choked condition. Combining this 'choked' data with that found by traversing the throat, a curve that may be used for design can be constructed (see Figure 4.18). The blockage data is presented in the same form as that given by Dean (1974) i.e. the pressure recovery from the *impeller tip to the diffuser throat* is plotted on the x-ordinate, and no distinction is made between subsonic and supersonic flows. The merging of the sonic/subsonic data would seem an apt simplification for pipe diffusers due to the following:

- Analysis of the blockage data for the complete tested range of diffusers has not yielded separate subsonic and supersonic blockage/pressure-recovery trends.
- Removing the sonic/subsonic segregation will significantly simplify the design process: it is not a design-type calculation to evaluate the leading edge Mach number of a pipe diffuser due to the geometric complexity of the pseudo- and semi- vaneless spaces. Choosing the wrong curve could result in an incorrect throat size specification by as much as 4%.

In addition it should re-iterated from Chapter 3, that there is some uncertainty as to the measurement planes used by Kenny to define pressure recovery and therefore the data should be used with some caution. It would seem, however, as there is excellent agreement with the measurements taken here, that Kenny used the pressure recovery from the *impeller tip to the diffuser throat* rather than just across the *semi-vaneless-space*.

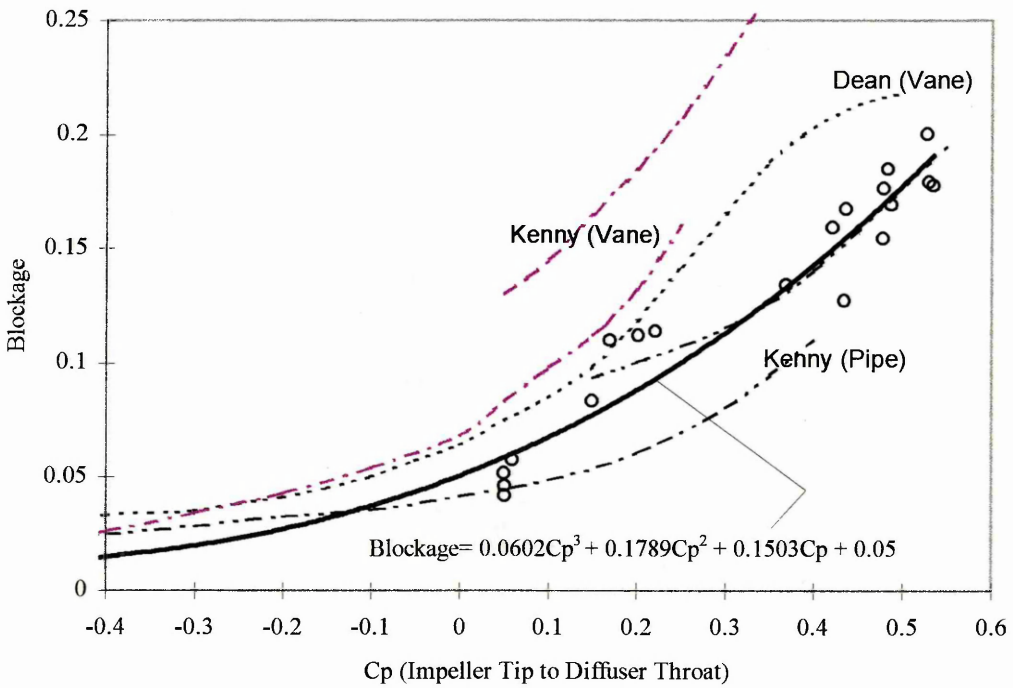


Figure 4.18 Blockage against Pressure Recovery between Impeller Tip and Diffuser throat

4.5.3 Effect of Incidence on Throat Blockage

Kenny (1984) presented an incidence/blockage best fit curve for pipe diffusers which showed very tight correlation with maximum deviations less than blockages of 0.5%. The best fit curve is reproduced in Figure 4.19 together with data from the current study. Quite clearly, the correlation of data from the current study is very poor, even for the near 'conventional' 31 pipe diffuser. However, the projected gradients of each pipe configuration show some conformity. It is possible that Kenny (1984) could have presented data accumulated from only one diffuser arrangement and this could be the reason for his apparently good correlation.

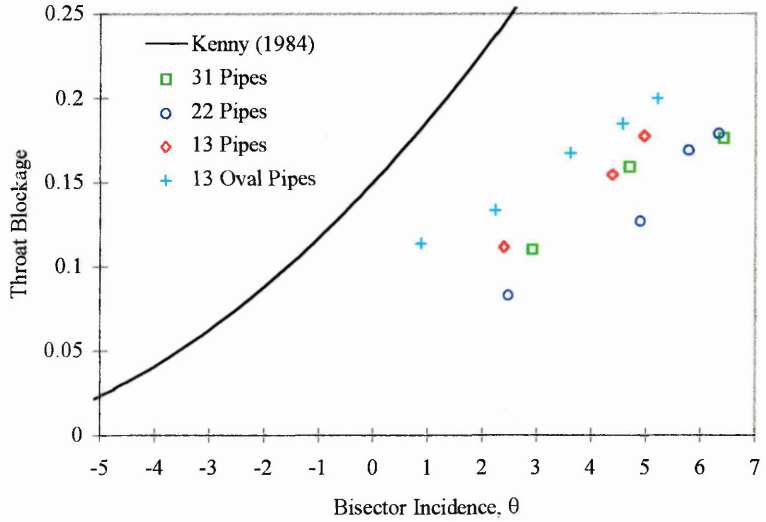


Figure 4.19 *Effect of Incidence on Throat Blockage*

4.6. STAGE PERFORMANCE

Using the detailed total pressure traverses across the diffuser throat an assumed stage performance was calculated. Again, as in Chapter 3, a diffuser with area ratio 4.82 and length/throat-diameter ratio of 13.9 was chosen, allowing a 'fair' comparison to be made between the current and previous Rolls-Royce designs (see Figure 4.20). There are discrepancies between the current and the Rolls-Royce tested 31 pipe diffusers. In terms of pressure ratio, the current 31 pipe diffuser shows some superiority. This difference is believed to be due to the inapplicability of the Dolan and Runstadler (1973) data that was used to evaluate a stage performance. Somewhat contradictory is a reduced stage total efficiency for the current 31 pipe design. This difference is attributed to the measurement and interpretation of work input to the stage. In both cases the work input was calculated from the total temperature rise across the stage. The measurement planes adopted, however, varied considerably and in addition there is the possibility that Rolls-Royce used a discretional radiated heat allowance in their calculation procedure.

Between each diffuser arrangement tested here there is little variation noticed either in terms of performance or efficiency. A major difference observed, however, is range and this is improved without penalty by the designs with low numbers pipes.

It should be noted that the optimistic curve fit for the 13 circular pipe diffuser was only carried out after considering the measured trends for the loss and blockage (Figures 4.15 and 4.18). In fact there is some justification to improve this implied performance further as the measured blockages for this pipe arrangement were generally lower than those for the other designs.

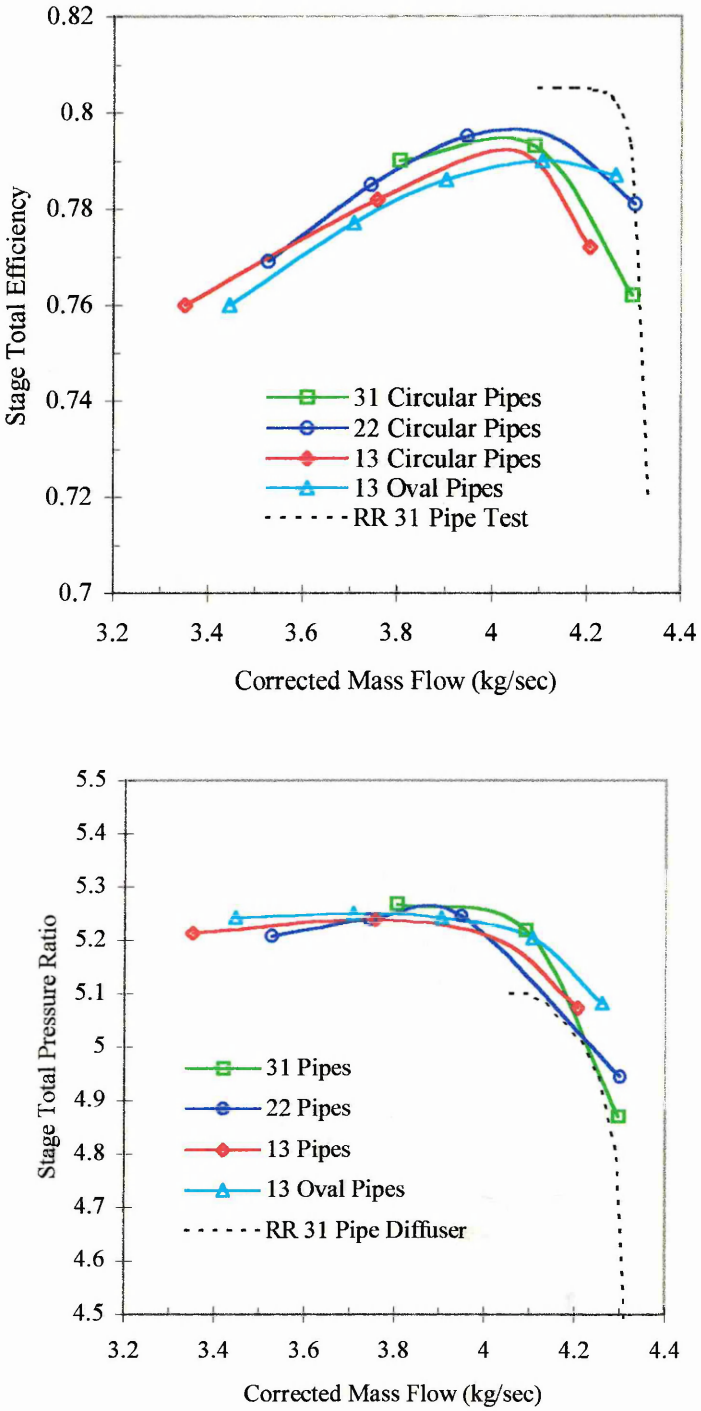


Figure 4.20 *Stage Performance of Each Diffuser Configuration*

4.7. FLOW DISTORTION AND UNSTEADINESS

The major disadvantage noted of the configurations with fewer pipes was the noticeable increase in flow unsteadiness. These are of concern to designers as excessively high unsteady aerodynamic loadings can cause high cycle fatigue even at normal operating conditions (examples of which are documented by Japiske (1980)).

At the impeller tip, circumferential distortions in static pressure are caused by the influence of the diffuser. Such distortions were measured using a series of circumferentially placed static pressure tappings at the impeller exit. The effect of each pipe diffuser design on the impeller tip static pressure distortion over each respective operational range, is shown in Figure 4.21. The vaneless diffuser values were included to give some idea of the accuracy of static tappings at the impeller tip as theoretically there should be no distortion in the vaneless configuration. Such distortions are 'seen' by the impeller tip as it rotates and may be regarded as a measure of the flow unsteadiness in the rotating frame. The large differences are expected to be caused by many effects including incidence, pipe diffuser leading edge radius, impeller tip Mach number and diffuser leading edge aerodynamic loading. However, the larger static pressure distortions were shown to be strongly influenced by leading edge shocks that penetrated the impeller periphery (these are discussed in Chapter 5). Shocks were particularly prevalent in configurations with few pipes and this is reflected in their elevated values of distortion in Figure 4.21. A similar investigation was also carried out by Japikse (1980) who also showed stronger shock structures for diffusers with lower numbers of pipes. He attributed two impeller failures to peripheral static pressure field distortion.

In the stationary frame, the flow unsteadiness was detected using high speed pressure transducers. These were located within the pseudo-vaneless-space at the same radius for each test ($1.04R_2$). This static pressure unsteadiness is presented in terms of range (i.e. max-min) in Figure 4.22. These measurements were averaged 500 times to remove non-synchronous data. The associated loadings on the leading edges of the pipe diffuser passages are seen to be significantly lower than those for the impeller. The strong relationship between number of pipe diffuser passages and unsteadiness seen at the impeller tip is not shown in the pseudo-vaneless space.

As well as static pressure, total pressure measurements were made of the flow unsteadiness using miniature Kulite probes at the diffuser throat. Distortions, similar to those measured using a pneumatic probe, were measured at the pipe throat using the unsteady total pressure probes. However, most unexpected were strong planar pulsations. Figure 4.23 presents the range of throat-plane averaged total pressure. Stronger pulsations are detected for the pipe diffusers with fewer numbers of pipes.

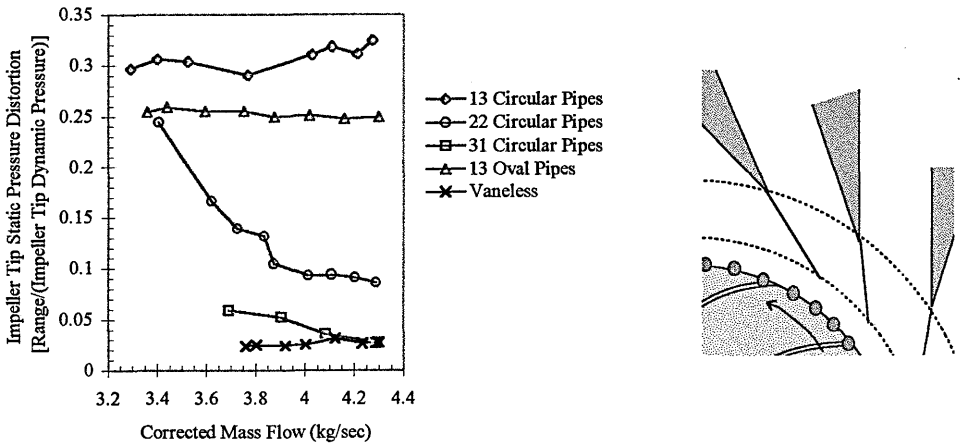


Figure 4.21 Impeller Tip Static Pressure Distortion

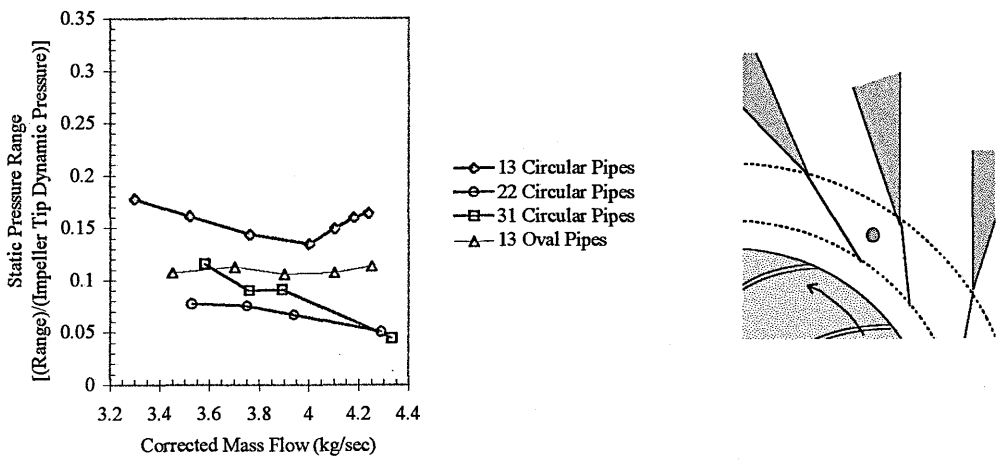


Figure 4.22 Static Pressure Unsteadiness within Pseudo-Vaneless-Space

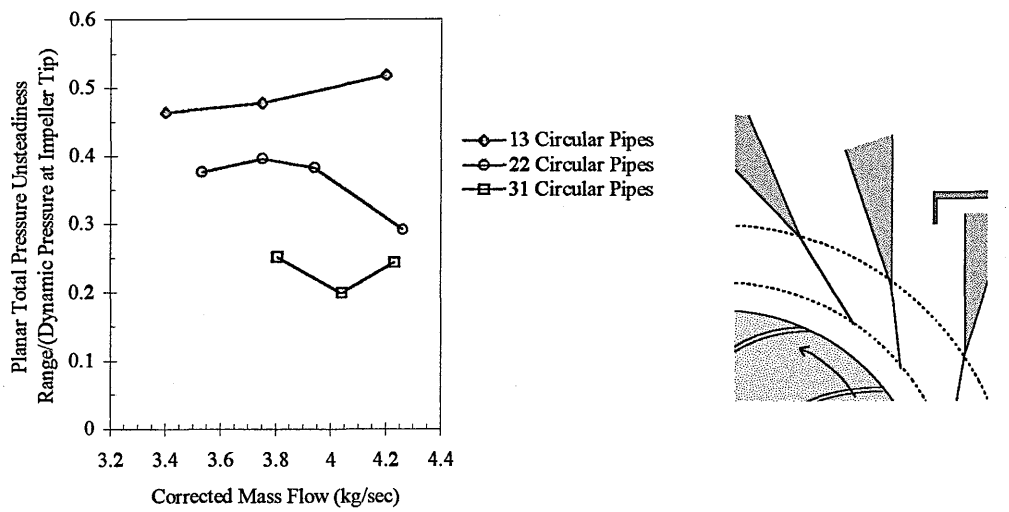


Figure 4.23 Planar Total Pressure Unsteadiness at Diffuser Throat

4.8. CLOSURE

Four pipe diffusers with varying sidewall expansion and numbers of pipes have been designed and experimentally investigated. Measurements taken have included overall performance and detailed area traverses using instrumentation specifically developed by the author for this investigation. Pertinent findings are as follows:

- It was shown that when the impeller tip is used as the impeller tip tangency radius, the generated pipe diffuser geometry naturally leads to reasonable diffuser inlet designs.
- By reducing the number of pipes (and generally increasing sidewall expansion) significant operating range benefit has been achieved without performance penalty. This improvement, however, may be at the cost of increased fatigue loading on the impeller tip.
- The effect of incidence on the performance and range has been shown to be minimal.
- A new design correlation for blockage has been uniquely compiled from direct throat traverses (See Figure 4.18). Unlike the Kenny (1970,1972) correlations, subsonic and supersonic blockage relations are combined to form one curve.
- Measurements of throat blockage have confirmed that pipe diffusers operate with significantly less throat blockage than vaned diffusers and therefore suffer from lower losses within the downstream conical channel. Comparison of blockage relations show that the pipe diffuser can operate with up to 5% less throat blockage.

CHAPTER 5
Detailed Flow within Pipe Diffusers

The flow exiting the impeller of a typical centrifugal compressor has been shown in Chapter 2 to include regions of high and low speed flow that in the stationary frame result in a highly unsteady incident flow to the downstream diffuser. The diffuser section must accept this flow and convert a pre-set amount of velocity head into useful static pressure by the most efficient means possible. Probably the most important, yet little understood part of this flow is that from the impeller tip to the diffuser throat. In this region there is generally strong diffusion which may result in excessive total pressure losses together with the possibility of introducing flow with large blockage into the downstream diffuser channel. The previous two chapters have concentrated on assessing both losses and blockage with a view to assembling design rules. The emphasis in these chapters has been to examine the consequences of controlled changes of geometry in order to isolate the influence of individual geometric features. In order to understand the trends and correlations found in these earlier chapters and to gain further insight into pipe diffuser flows, additional detailed flow measurements were undertaken within each of the tested pipe diffuser configurations. The complete measurement data set, including measurements taken as part of Chapters 2, 3 and 4, consisted of pneumatic and unsteady flow measurements in and around the pseudo- and semi- vaneless spaces with a concentration of measurements taken at the influential diffuser throat. These measurements are believed to be unique and provide the reader with new information about the flow 'seen' by the downstream conical portion of the pipe diffuser.

Through this work more appropriate boundary conditions for possible laboratory and/or computer simulations of the flow in the conical diffusing sections will become available. Up until now, designers have been ignorant of this inlet flow and have relied upon 2-D experimental data with steady uniform inlet conditions. Further 2-D laboratory experiments with more realistic boundaries would, in conjunction with current design procedures, be expected to yield improved channel performance predictions.

As well as the experimental investigations, attempts at using a commercial CFD code to model the diffuser flow are latterly presented. These are particularly interesting as it is

felt that the next design level beyond the empirical 1-D gas dynamic correlations derived in Chapters 3 and 4, is to use CFD.

Outline of Chapter

The experimental investigations are examined first. Each section is presented in the order 'seen' by the flow (i.e. from impeller tip to diffuser throat). In this way the reader is lead through the flow domain and introduced to the main flow features in a logical fashion. Some 'back-stepping', however, is inevitable due to the strong influence of the diffuser on the upstream flow-field. Finally, complementary computational studies are presented.

5.1. IMPELLER TIP

In Chapter 2 measurements of flow at the discharge of the 35D compressor were presented and were shown to be typical of centrifugal machines with a wake located on the shroud/blade-suction surface. In the stationary frame, the combination of this wake and the remaining 'clean' flow appears strongly pulsating. Total pressure ranges of 1 bar and flow angle variations of 30° were recorded.

Additional influence, due to the downstream diffuser leading edges, is felt in terms of static pressure distortion. This can be severe, as shown in Chapter 4, for arrangements incorporating diffusers with small number of pipes.

5.2. VANELESS, PSEUDO- AND SEMI-VANELESS SPACES

For examination of the flow entering the throat of the downstream diffuser, it is more convenient to lump the vaneless, pseudo- and semi- vaneless spaces together. For the pipe diffusers examined here the vaneless region is relatively very small and will be included with the pseudo-vaneless space. In the most unlikely situation that the reader finds himself with a significantly large vaneless space, the design rules and descriptions in the introductory review for vaneless diffusers could be utilised.

The flow into the pseudo-vaneless space is partially bounded with vanes that grow axially to bridge the passage width, the two sides meeting at the radius designated here as the diffuser leading edge (see Figure 5.1). Centrally the flow is unbounded and therefore, given incidence, twin vortices are expected to be formed as described in Chapter 1 and shown in Figure 5.1. Midway between the sideplates in the pseudo-vaneless space (and therefore away from the diffuser elliptic leading edges) radial diffusion is expected in a manner akin to that seen in a vaneless diffuser. Near the diffuser side-walls, the flow is locally turned by the, partially passage spanning, diffuser leading edge.

In this section it will be shown that the flow in this region is further complicated by the formation of shocks. The formation of these is shown to depend on the flow condition and, principally, on the number of pipes. The 'suction' and 'pressure' surfaces should be noted in Figure 5.1.

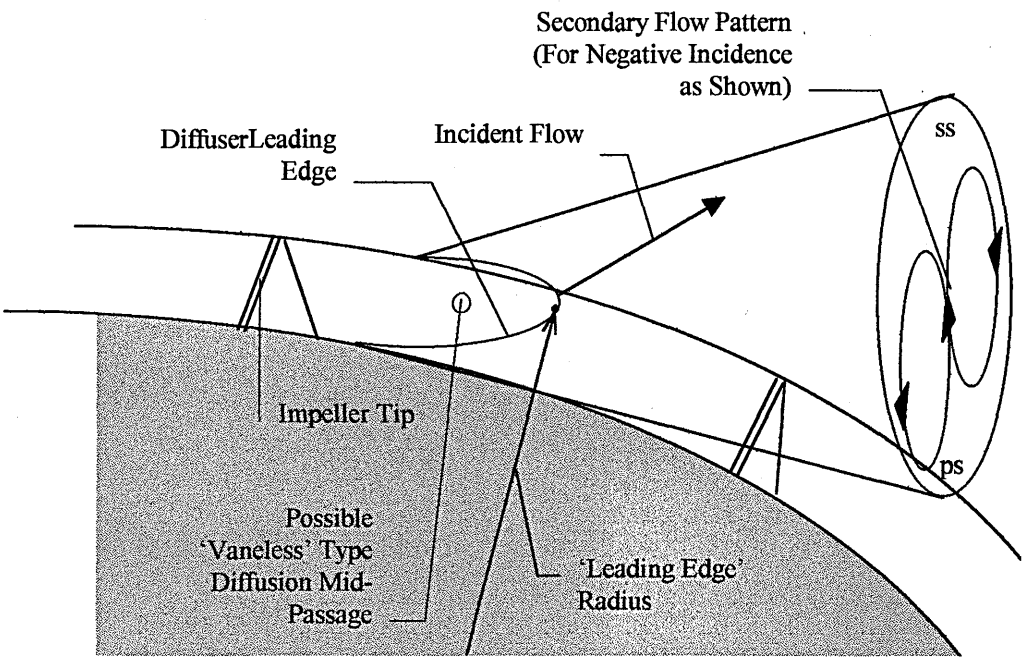


Figure 5.1 Pseudo- and Semi-Vaneless Space Flow

Figures 5.2 to 5.5 display the Mach number distribution within each of the vaneless-, pseudo- and semi- vaneless spaces of the 31, 22, 13 (circular) and 13 (oval) pipe diffusers. In all cases, the Mach number was calculated from the impeller tip total pressure and no account is made for losses. Each sketch is nominally to scale (1:1) and gives the reader a better perception of the size of the domain.

The most distinctive feature that differentiates the pipe diffusers with low numbers of pipes is the near-continual (apart possibly near choke) presence of a detached leading edge shock. For both diffusers with 13 pipes, a pseudo-vaneless space acceleration on the diffuser leading edge suction surface is seen and this occurs at all flow rates. Then, just prior to the leading edge, there is a rapid deceleration of the flow. This is characteristic of a shock and is particularly pronounced at lower mass flows. A similar region of elevated Mach number is also seen 'near surge' for the diffusers with 31 and 22 pipes. Although the resolution of measurement locations is quite coarse, the presence of a shock can similarly be argued.

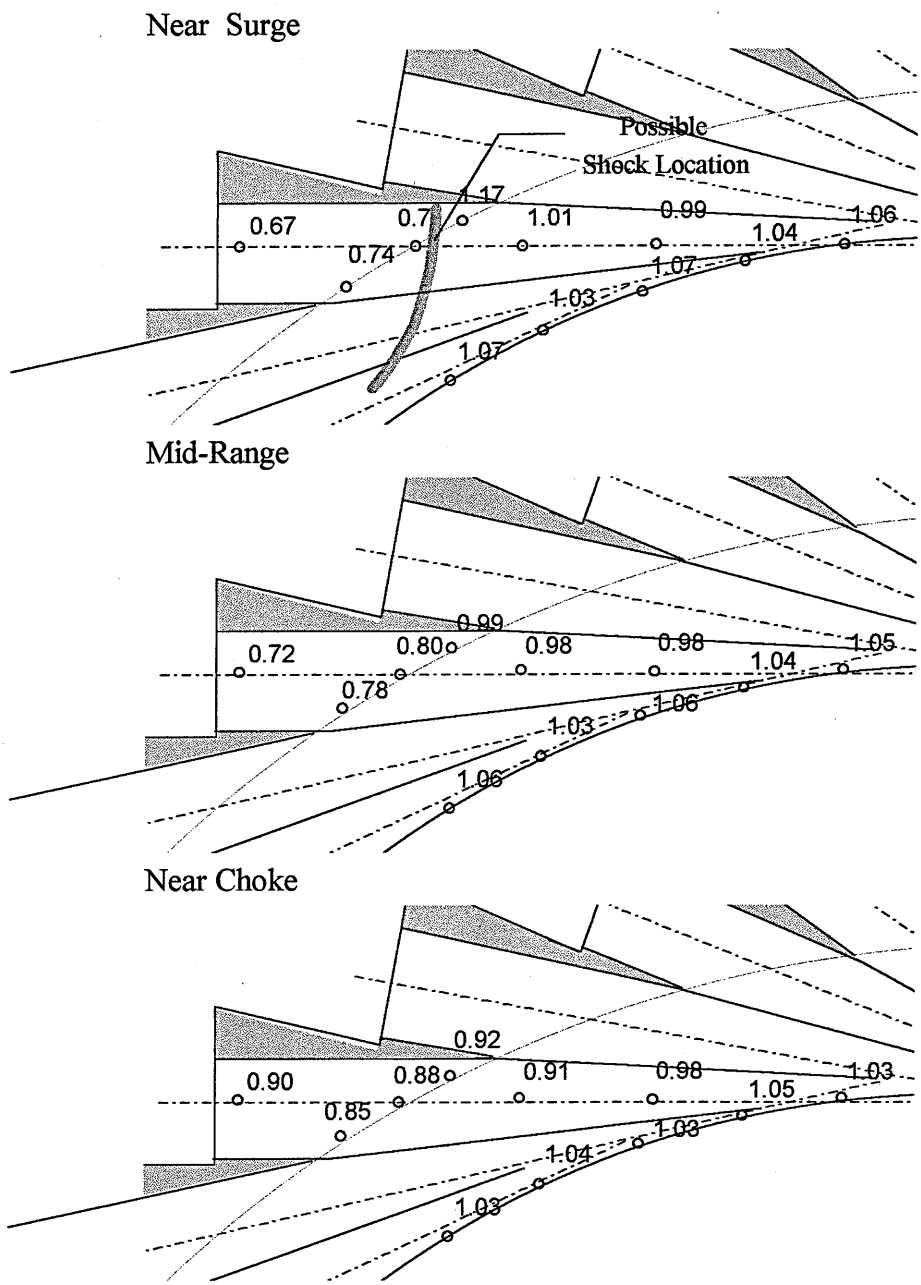


Figure 5.2 Mach Number Distribution within Pseudo- and Semi-Vaneless Spaces of 31 Pipe Diffuser

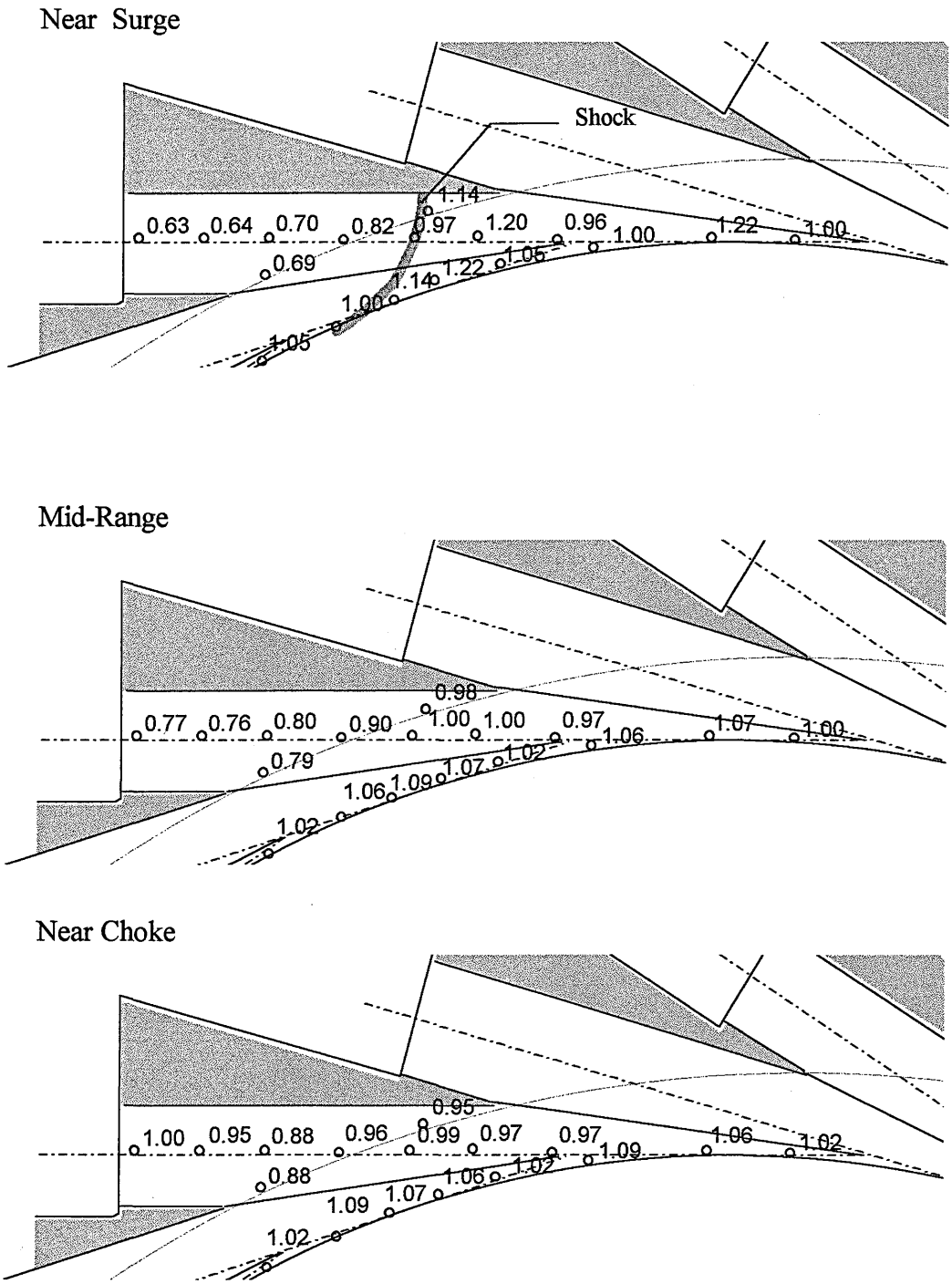


Figure 5.3 Mach Number Distribution within Pseudo- and Semi-Vaneless Spaces of 22 Pipe Diffuser

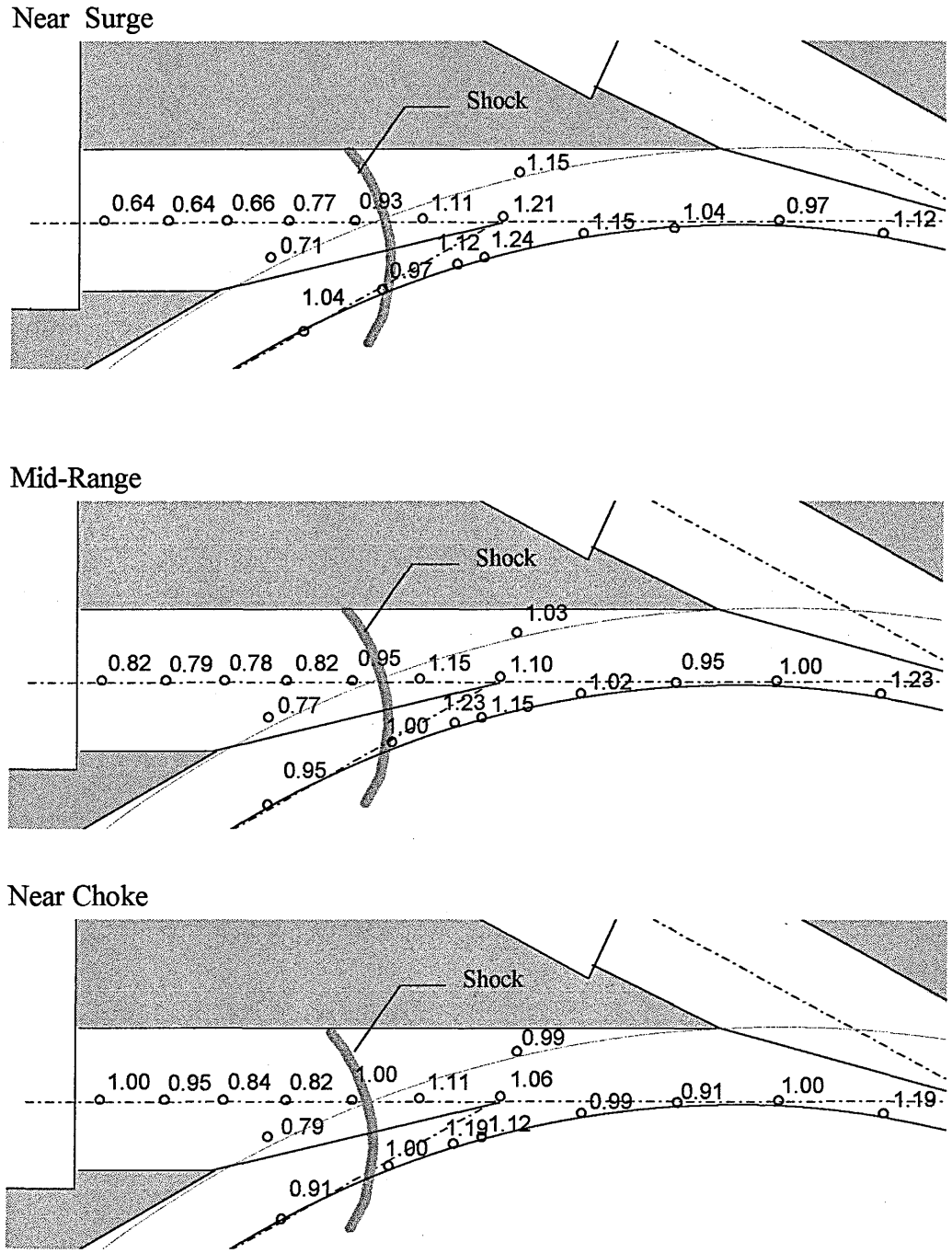


Figure 5.4 Mach Number Distribution within Pseudo- and Semi-Vaneless Spaces of 13 (Circular) Pipe Diffuser

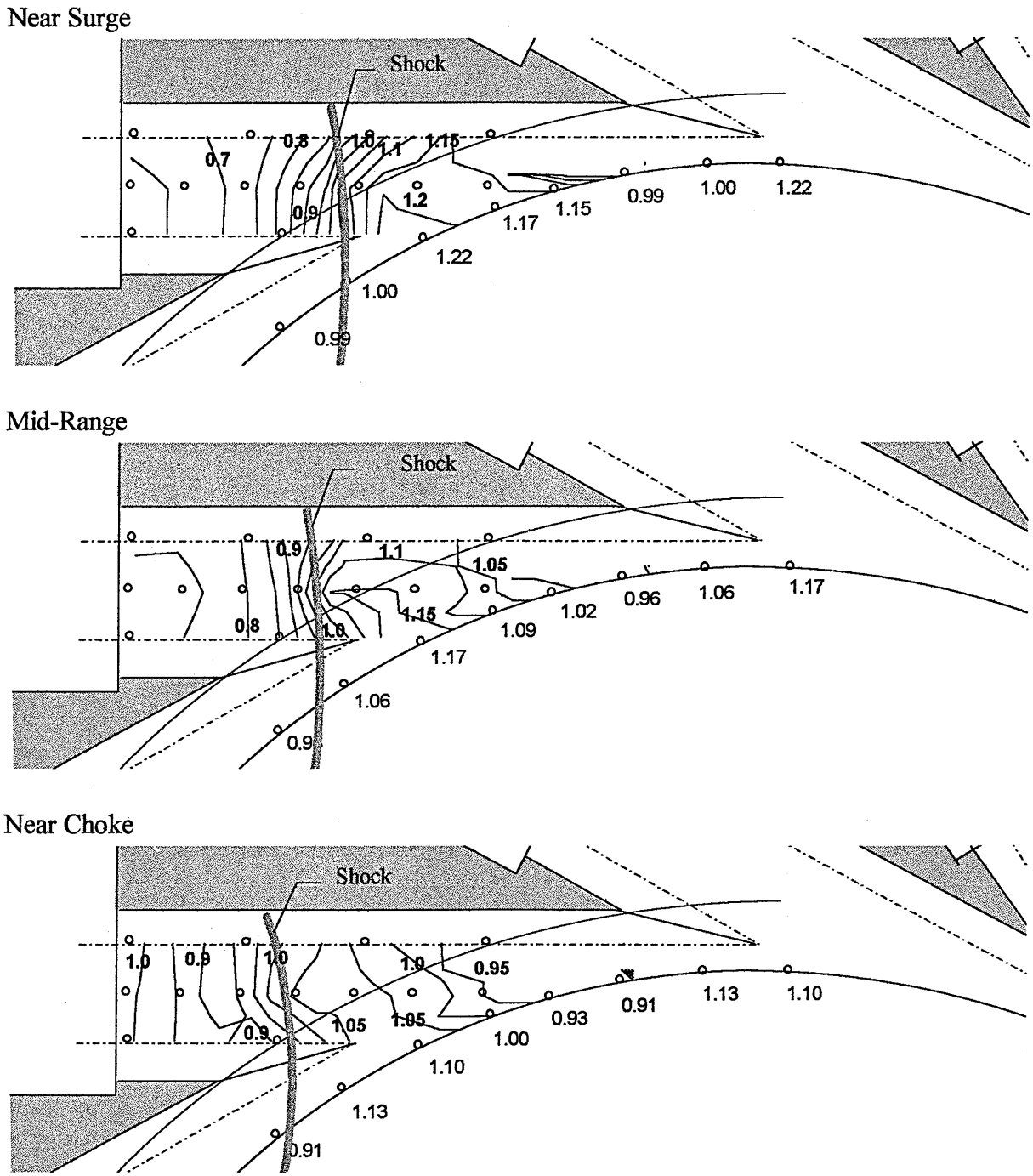


Figure 5.5 Mach Number Distribution within Pseudo- and Semi-Vaneless Spaces of 13 (Oval) Pipe Diffuser

5.2.1 LEADING EDGE WEDGE ANGLE

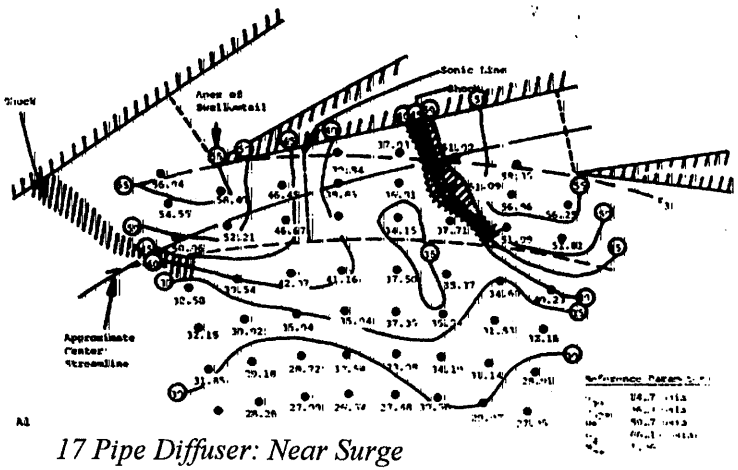
It is well known that a detached shock will form upstream of a wedge should excessive turning be asked of a supersonic incident flow (e.g. Kuethe and Chow, 1986). The limiting flow angle, up to which a shock will be attached, is related to the incident Mach number. The maximum Mach number detected here of M=1.24, limits flow turning to only 5°, and assuming zero bisector incidence this allows a maximum wedge angle of 10°. The wedge angle that forms the leading edge of the diffusers here is simply a function of the number of passages as shown in Table 5.1.

Table 5.1 Leading Edge Wedge Angles

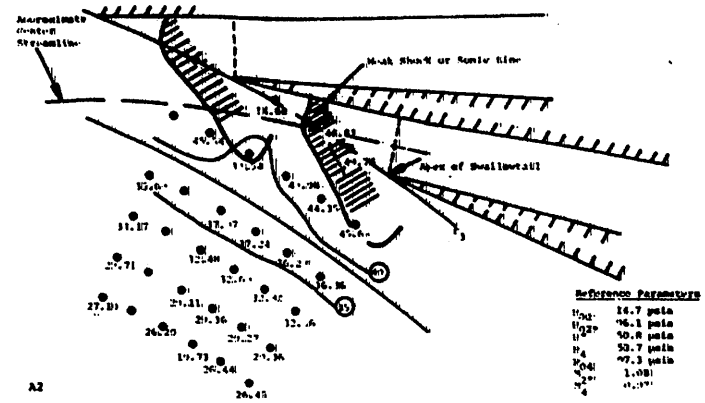
Number of Pipes	$\theta_{wedge} = \frac{360^o}{N_D}$
31 (Circular)	11.61°
22 (Circular)	16.36°
13 (Circular)	27.69°
13 (Oval)	27.69°

These angles confirm our initial interpretation of the static tappings; that all shocks are detached or bow in all of the pipe diffuser configurations. Japiske (1980) carried out a similar investigation on two pipe diffusers with extreme numbers of pipes (17 and 34) with a 6:1 pressure ratio compressor. Similar shocks patterns over the range of operations were noted: bow shocks over the complete 100% speed line for the 17 pipe diffuser and shock free operation near choke for the 34 pipe diffuser (see Figure 5.6).

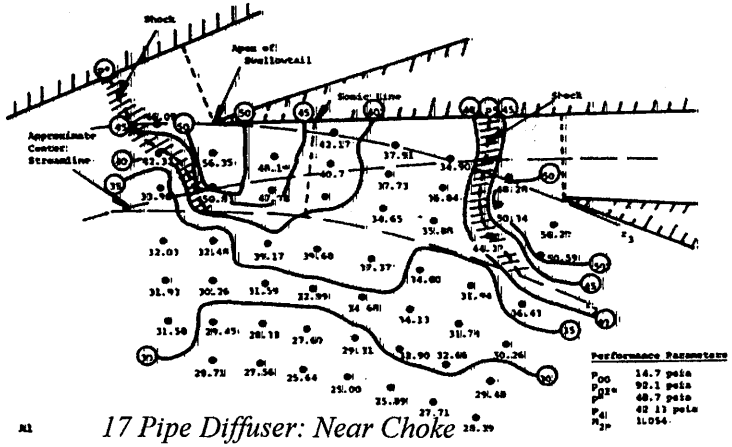
A design advantage of conventional vane-type diffusers would seem to be the 2-D geometry allowing the use of Mach wave and oblique shock theory. For pipe diffusers, however, the precise strength and location of the shocks discussed cannot be predicted using 2-D methods due to the pipe circular cross section and elliptic leading edges. CFD methods would seem to have the potential to overcome this difficulty.



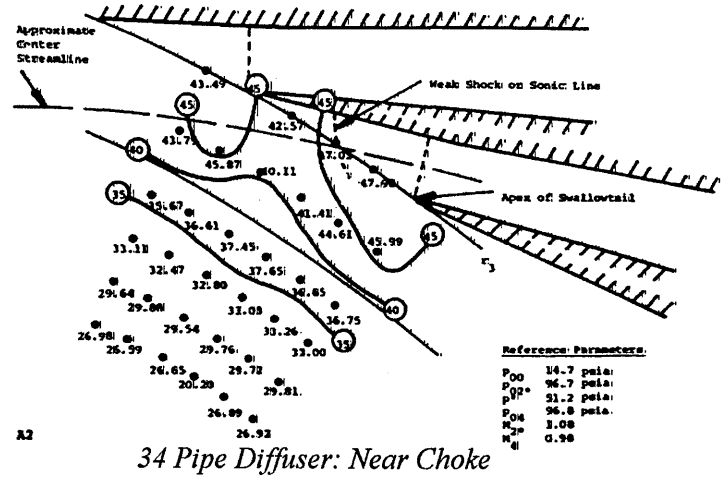
17 Pipe Diffuser: Near Surge



34 Pipe Diffuser: Near Surge



17 Pipe Diffuser: Near Choke



34 Pipe Diffuser: Near Choke

Figure 5.6 Comparison Between a 17 and 34 Pipe Diffuser (Japikse (1980) Pressure Ratio = 5)

5.2.2 IMPELLER TIP STATIC PRESSURE FIELD DISTORTION

The major disadvantage noted of the configurations with fewer pipes was the noticeable increase in flow distortion within the vaneless, pseudo-vaneless and semi-vaneless spaces. These are of concern to designers as excessively high unsteady aerodynamic loadings can be transmitted to rotating components leading to high cycle fatigue even at normal operating conditions (examples of which are documented by Japikse (1980)).

At the impeller tip, circumferential distortions in static pressure are caused by the downstream influence of the diffuser. Such distortions were measured using a series of circumferentially placed static pressure tappings at the impeller exit. The effect of each pipe diffuser design on the impeller static pressure distortion over each respective operational range , was shown in Figure 4.21. Increased static pressure distortion at the impeller tip (denoted by the inner radius in Figures 5.2 and 5.5), was detected for diffusers with low numbers of pipes. Intuitively, reducing the number of pipes would increase the pipe leading edge loading and, assuming a fixed leading edge radius, cause further distortion to the impeller tip pressure field. An important question is whether the leading edge bow shock strongly influences the magnitude of this distortion particularly as careful design could help alleviate the situation. The two 13 pipe diffusers offer an ideal basis for comparison. With less acceleration indicated in the pseudo-vaneless space and consequently a weaker bow shock, the 13 oval pipe diffuser consistently exhibits reduced leading edge static pressure distortion when compared against its circular equivalent. It would seem from this observation that the leading edge bow shock strength has a direct influence over tip static pressure distortion. A similar but more decisive indication is shown in the 22 pipe diffuser which from Figure 5.3 is seen to operate shock free near choke but when throttled back to near surge develops a bow shock. The tip static pressure distortion (Figure 4.21) for the 22 pipe diffuser reflects this, demonstrating that the formation of the bow shock more than doubles the flow distortion. The 31 pipe diffuser arrangement, however, shows little distortion with a minor rise towards surge expected to be triggered only by increased diffuser loading despite indications of a bow shock formed near surge. As will be discussed later, the presence of this shock is somewhat debatable. However, it is hypothesised that should such a shock exist, it might not penetrate the impeller wheel due to the (slightly) increased leading edge radius of this design. In either scenario, the 31 pipe diffuser has shown that in some instances it is possible with careful design to alleviate or even totally remove diffuser leading edge shocks.

Similar differences in static pressure distortion were also recorded by Japiske (1980). He showed an increase of 260% in distortion between a 17 and 34 pipe diffuser configuration. The magnitude of this variation is similar to the experiences recorded here.

As the impeller blades sweep through this distorted static pressure field they subjected to a cyclic loading. It is this that is expected to give a measure of the fatigue loading on the impeller blade. As mentioned earlier, such a loading failure is documented by Japikse (1980).

5.2.3 Unsteady Static-Pressure Measurements within The Pseudo- and Semi- Vaneless Spaces

Pressure transducers were mounted within the pseudo-vaneless space (at 1.04% R_{tip}) of each pipe diffuser build in order to measure the unsteady aerodynamic forces acting on the diffuser leading edges. The amplitude of static pressure measurement for each diffuser arrangement and over each respective operational range, was shown in Chapter 4 not to be strongly dependant on the number of diffuser pipes (Figure 4.22). In addition, further readings were taken along the diffuser centreline for the 13 oval pipe diffuser and are shown below in Figure 5.7

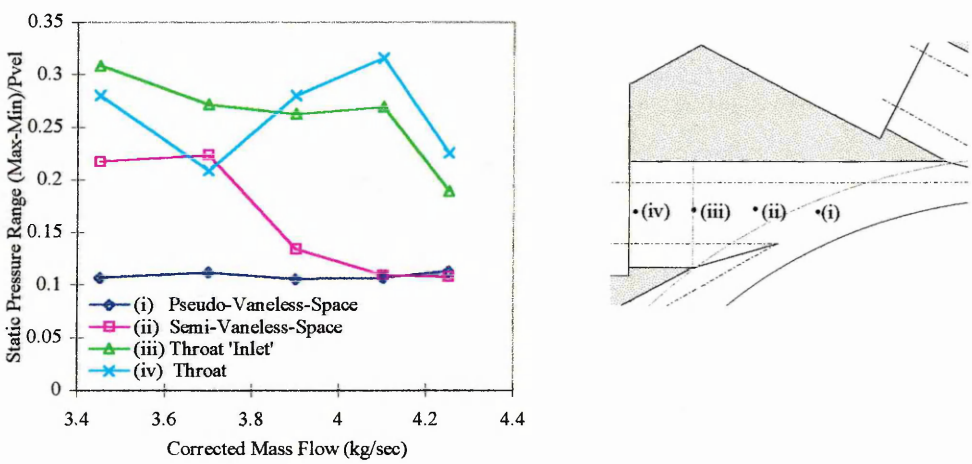


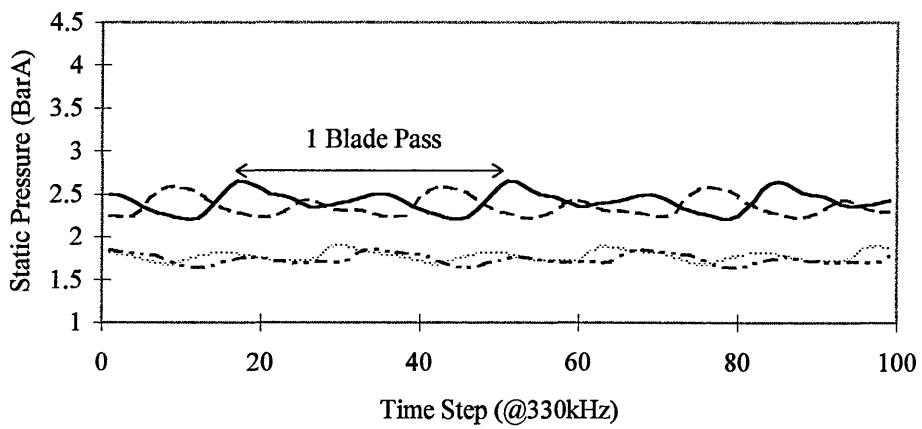
Figure 5.7 Amplitude of Static Pressure within Pseudo-and Semi- Vaneless Spaces (Non-Dim. wrt Impeller Tip Velocity Head)

Near choke the level of unsteadiness increases as the flow progress through the pseudo- an semi-vaneless spaces. This increase in unsteadiness is expected following the trends of Abdel-Hamid et al (1987) with the static pressure fluctuation amplified by the diffusion process. As the flow rate is decreased to 3.7kg/sec, the pseudo-vaneless space unsteadiness rises steeply (location (ii)). The unsteadiness in the throat-inlet region also increases steadily after a sharp rise near choke whereas that at the throat outlet, remains high, but somewhat inconsistent with flow rate. This apparent 'ceiling' of throat unsteadiness has been predicted by Japikse (1980), from a discussion with Dean R.C Jnr,

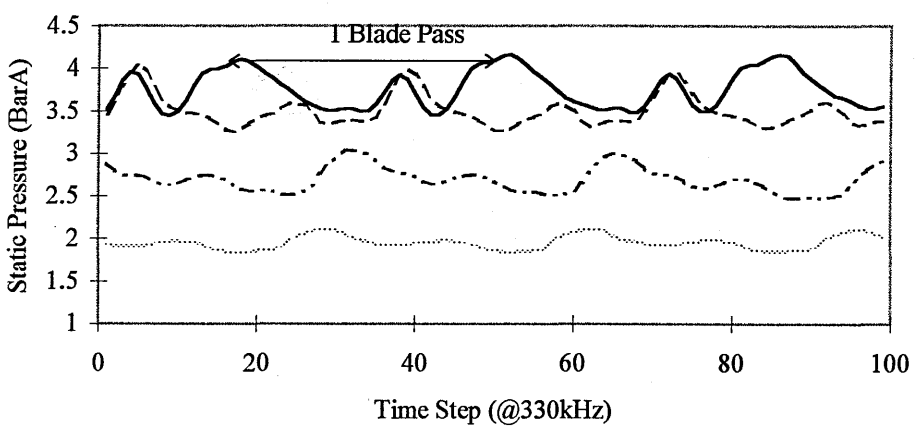
and supported by an unsteady shock phenomenon presented by Kantrowitz (1958). Japikse (1980) hypothesised that the pipe diffuser bow shock once developed would attenuate any further unsteadiness. The detailed measurements made here tend to support this idea although the evidence is somewhat limited.

Figure 5.8 compares the measurements within the 13 oval pipe diffuser plotted against time. Near choke, the mean levels and amplitude of fluctuation of static pressure are

Corrected Mass Flow =4.25kg/sec (Near Choke)



Corrected mass Flow =3.45kg/sec (Near Surge)



Key:

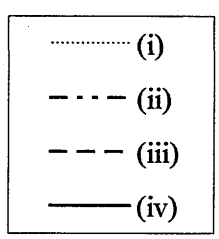


Figure 5.8 Static Pressure Measurements within Pseudo-and Semi- Vaneless Spaces

similar. Near surge, however, the mean levels diverge due to diffusion between the impeller tip and diffuser throat. As the data acquisition was triggered at the same impeller location in each example, the flow features may be followed through the domain. Two peaks of elevated static pressure per blade pass are seen throughout, particularly when operating near surge (see Figure 5.8). These would seem to correspond to those measured at impeller discharge (see Figure 2.13) . It is interesting to note the large magnitude of the diffusion within the pseudo and semi-vaneless spaces and this highlights the importance of the correct design of this region.

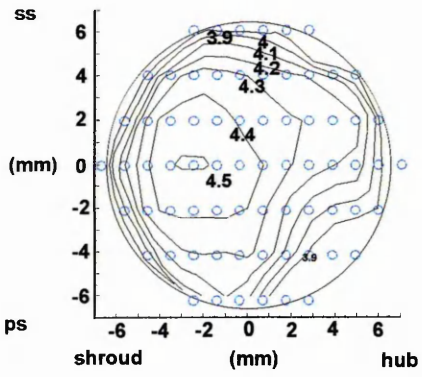
5.3. DIFFUSER THROAT

The diffuser throat is of primary interest to compressor aerodynamicists as the flow in this region has a controlling influence over the downsteam cone effectiveness. In Chapter 1, the controlling influence of diffuser throat blockage was introduced: unnecessary increases in throat blockage directly implied excessive diffuser cone losses. In Chapters 3 and 4 this parameter was extensively investigated, as together with throat Mach number and channel geometry the diffuser effectiveness could be read from experimental performance charts. The more popular of these data sets (i.e. Runstadler and Dolan (1973) for conical diffusers; Runstadler and Dean (1970) for channel diffusers) were assembled under laboratory conditions with steady, fully developed, inlet conditions. For pipe diffusers however, as will be shown here, the inlet (or diffuser throat) conditions are far from this ideal with severe flow distortion and unsteadiness. Such conditions are well known to significantly influence the channel effectiveness (e.g. Japiske (1984)) and it is this therefore for this reason that this area is examined in detail here. The author is unaware of any other such detailed experimental investigation into diffuser throat flows, either for a pipe diffuser or any other diffuser type.

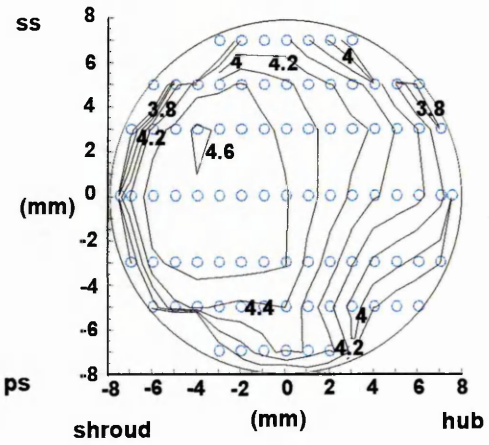
The throat of each of the four diffusers were traversed using both a pneumatic total pressure probe and an ultraminiature pressure transducer (details of these devices are given in APPENDIX B). In order to maintain reader continuity, some of the detailed results are presented in APPENDIX I. Despite this, these results should not be undervalued as they are of primary importance in determining diffuser effectiveness and are believed unique.

Figure 5.9 presents the total pressure measured at the throat of each pipe diffuser when operating at 3.8kg/sec (i.e. approximately mid-range)(see Figure 5.1 for the definition of suction surface, ss, and pressure surface, ps). These measurements were taken using a pneumatic (slow response) pressure probe with a 0.9mm diameter face. For each circular diffuser there is one distinct total pressure peak located near the shroud with, diametrically opposite, a low pressure region. The shape and location of the total pressure fields remained virtually unchanged despite variations in cross-section.

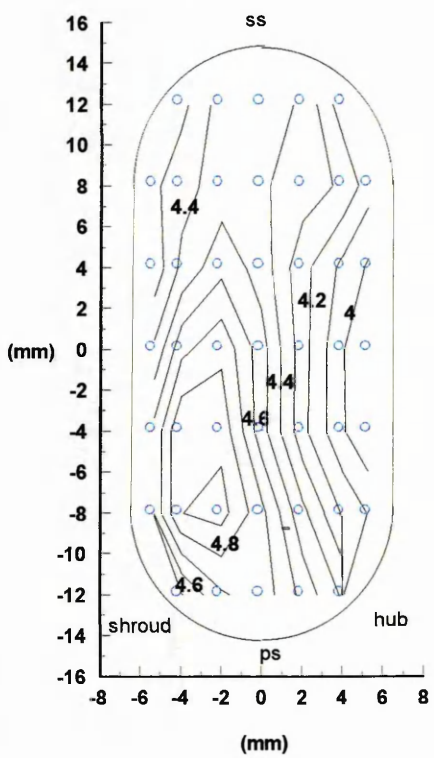
31 Circular Pipe Diffuser



22 Circular Pipe Diffuser



13 Oval Pipe Diffuser



13 Circular Pipe Diffuser

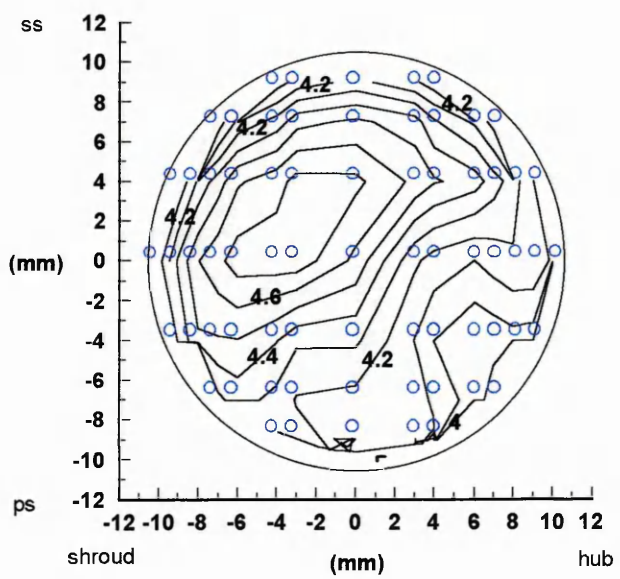


Figure 5.9 Total Pressure at Diffuser Throats (BarA)

Interestingly, the position of the total pressure peak for the oval configuration is, whilst still close to the shroud, much closer to the pressure surface than the other configurations. An examination of incidence, in an attempt to understand the flow mechanism, did not yield any consistent correlation. The oval configuration also provides some evidence of the lower pressure region but in this case it spans much of the hub-side surface.

Figure 5.10 compares the measurements taken with the pneumatic (slow response) and pressure transducer (fast response) instruments at the throat of the 13 circular-throat diffuser. These measurements were taken with both high spatial (see Figure 5.11) and temporal (333kHz) resolution. The unsteady measurements shown in Figure 5.10 were time averaged.

Both measurement instruments yield similar results both quantitatively and qualitatively. From choke to surge a general trend of increasing discharge total pressure, following the impeller characteristic, may be seen. For each mass flow the distinct total pressure peak located mid-height near the shroud is seen to rotate clockwise toward the passage suction surface as the mass flow is reduced. Interestingly the vertical shift of this peak is seen opposite to that expected from impeller discharge flow angle considerations. This implies that the position is dependant on some rotational effects. A trough is seen at all flow rates at four o'clock. It is suggested that this region of flow is a wake formed by incidence mismatch at the diffuser leading edge. Such a pattern in not seen near the shroud side of the diffuser due to improved incidence matching (the shroud flow is near tangential as is the near-shroud pipe leading edge). Similar flow patterns over the complete operating range were seen for both the 31 and 22 pipe diffusers and are documented in APPENDIX I. However, slightly different trends were seen at the throat of the 13 oval pipe diffuser (see Figure 5.11). Again, the flow pattern changes little over the compressor operating range but in this case, as already mentioned, the total pressure peak is located near the channel pressure surface. Near the suction surface, at high flow rates, a small elevated region of total pressure is seen to grow. As the mass flow is increased there is a trend for the high total pressure core region to migrate towards the suction surface. Therefore unlike the circular equivalent, the 13 oval pipe diffuser throat flow reflects changes in the impeller exit flow angle. No axial movement (i.e. from shroud to hub), indicative of flow swirl, is detected. The elongated section would seem to have surpressed such swirl.

Unsteady flow measurements at the throat of the 13 pipe diffuser (mid-range: m_{corr}=3.75kg/sec) are shown in Figure 5.13. These are typical of all the diffusers examined here (details of others are given in APPENDIX J). The throat flow displays a dominate longitudinal pulsation, and most remarkably, the flow structure remains virtually consistent in time apart from some 'flattening' of the peak near longitudinal

troughs at choke. In all cases a peak total pressure is visible near the shroud side mid-height. The magnitude of these longitudinal pulsations have been presented in Chapter 4, but what remains undiscussed is the time-based picture presented by these pulsations. The planar averages are plotted against time in Figure 5.14. These confirm the strong pulsations which are a major finding of this work. The amplitude of these pulsations are independent of flow rate and show two total pressure peaks per blade pass as also measured at the discharge of the impeller (see Chapter 2). Clearly assuming fully mixing out uniform flow at the diffuser throat, as is assumed in many design calculations, is grossly incorrect. As the measurements were triggered at the same location (once per revolution), it is interesting to note the slight phase lag in Figure 5.14. This lag is attributed to the decreased flow velocities at lower flow rates and the time taken for the flow to travel from the impeller tip to the diffuser throat.

Figure 5.15 shows the throat total pressure at the longitudinal maxima and minima of the traces presented in Figure 5.14. As shown in Figure 5.13, generally the flow patterns at extremes remained constant despite the dominate longitudinal oscillation. This fact may be of use in later laboratory simulations of pipe diffuser flows as the distortion is typical of that seen in pipe bend flows. Suitably bent ductwork may therefore provide representative conditions for enhanced 2D pipe channel tests. Air flow could be provided by a reciprocating compressor, preferably without a reservoir so that it could provide some of the longitudinal unsteadiness highlighted in this study.

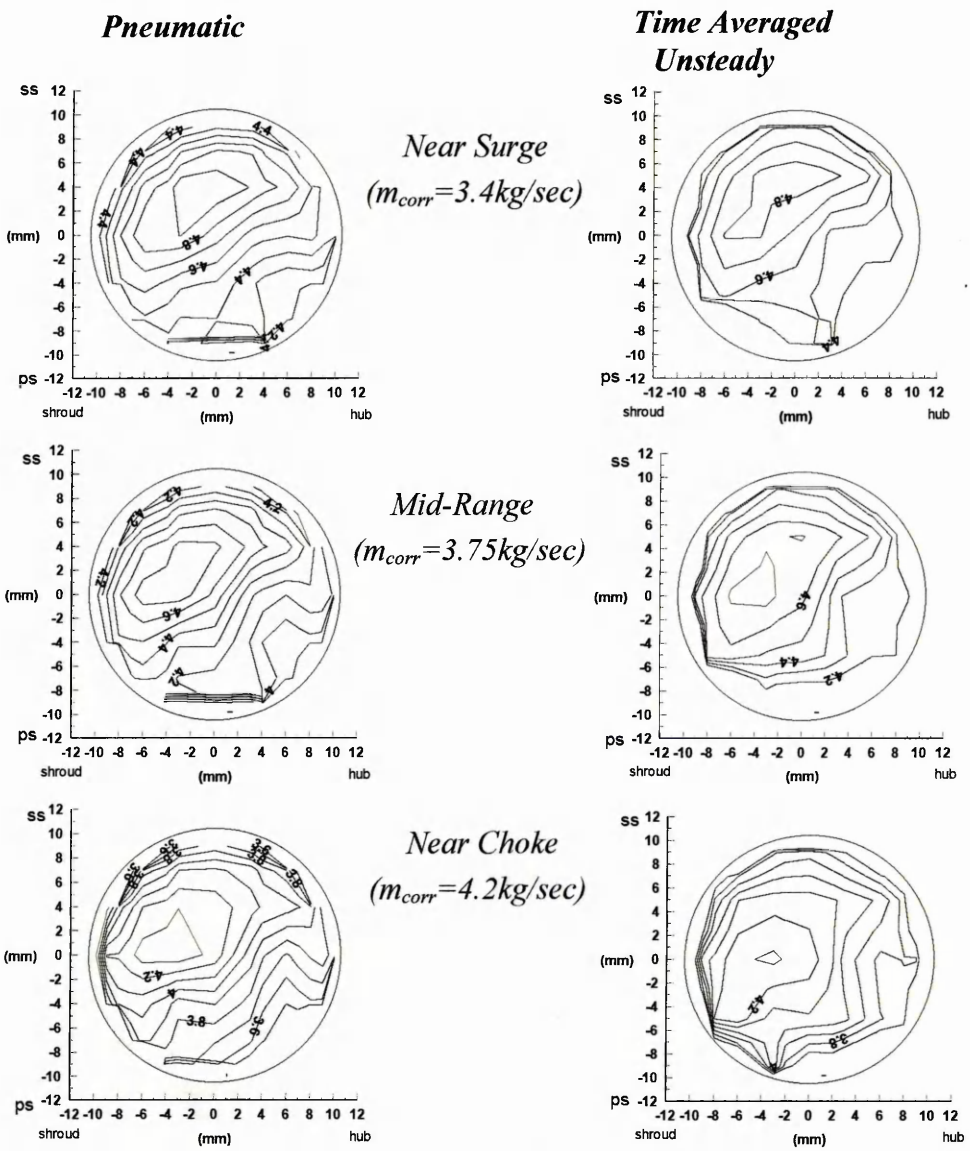


Figure 5.10 *Total Pressure (BarA) at 13 Circular Pipe Diffuser Throat Exit*

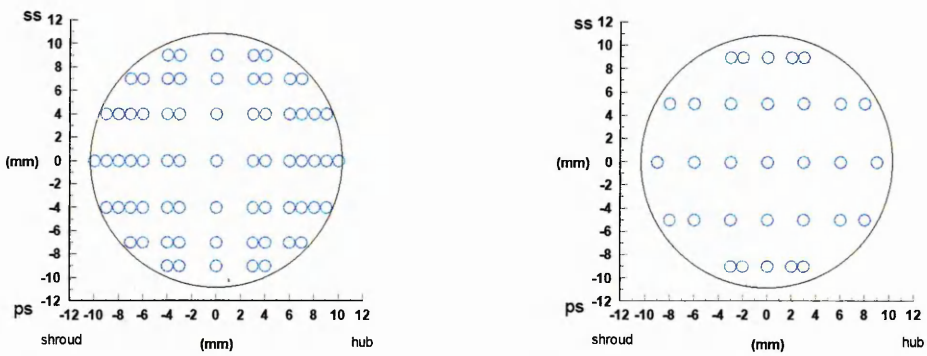
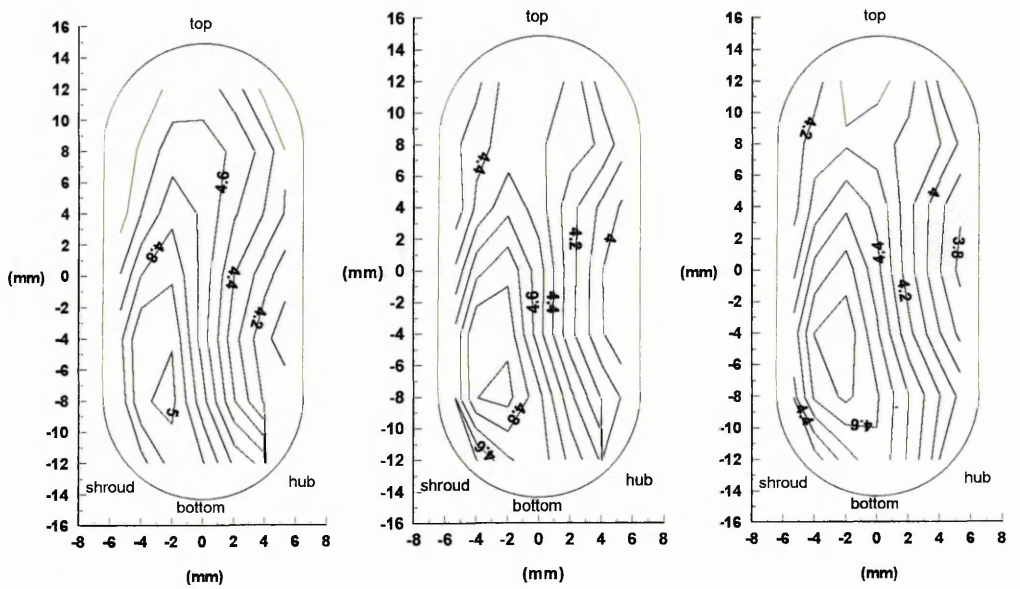
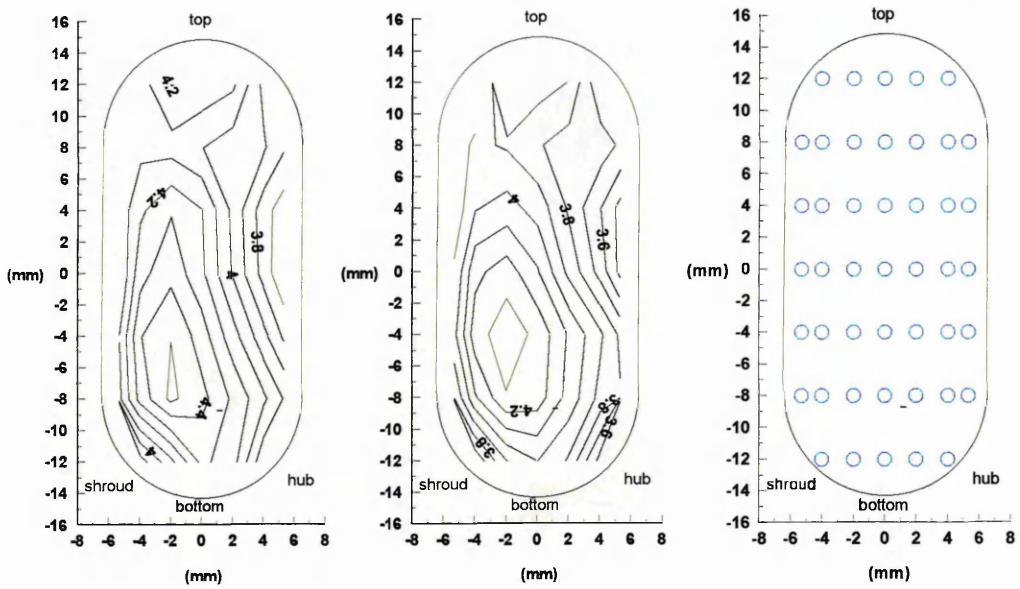


Figure 5.11 *Measurement Location at 13 Circular Pipe Diffuser Throat Exit*



m_{corr} = 3.45 kg/sec m_{corr} = 3.7 kg/sec m_{corr} = 3.9 kg/sec



m_{corr} = 4.1 kg/sec m_{corr} = 4.25 kg/sec Measurement Locations

Figure 5.12 Total Pressure Measurements at the Throat of the 13 (Oval) Pipe Diffuser

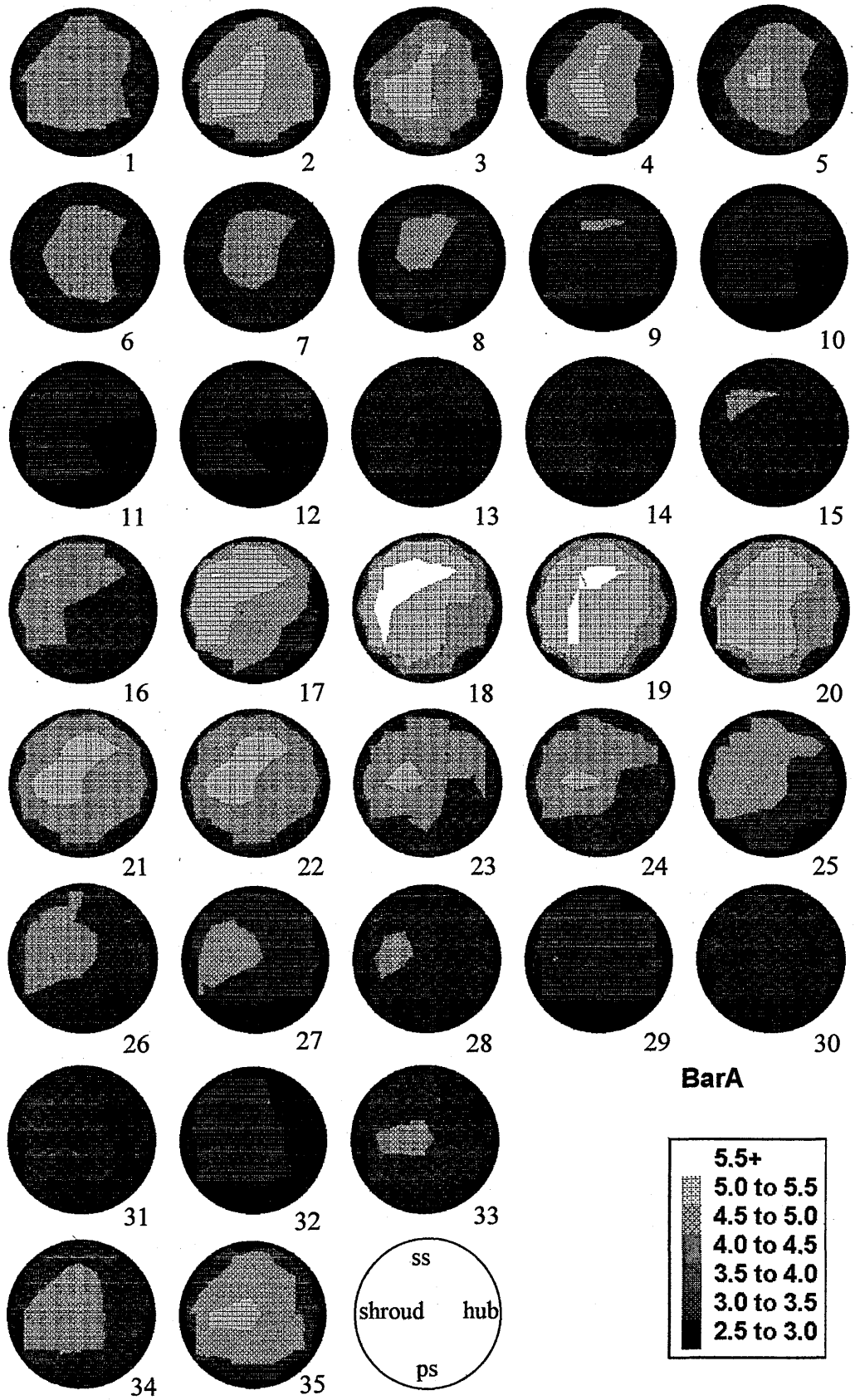


Figure 5.14 Unsteady Total Pressure at 13 (Circular) Pipe Throat (BarA)

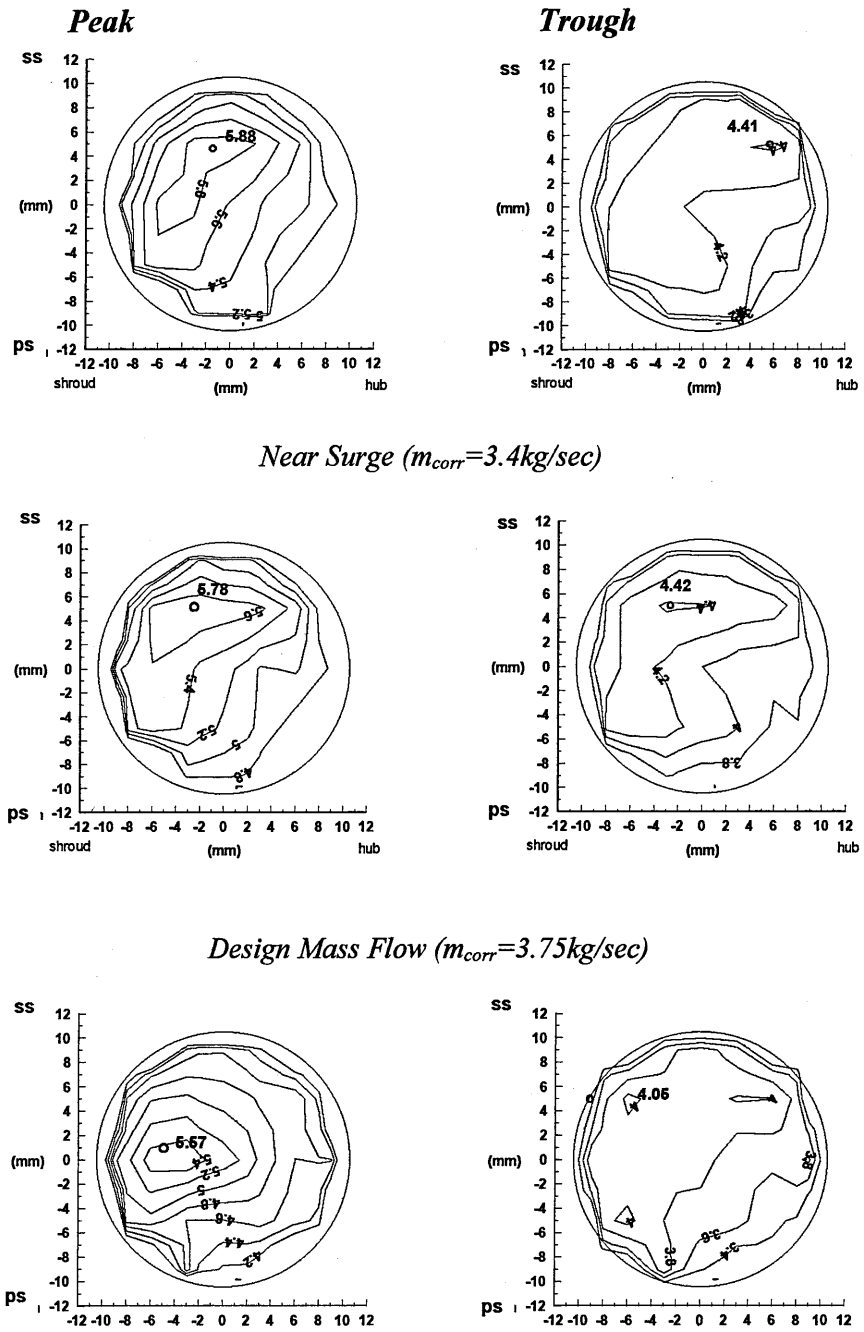


Figure 5.15 *Range of Total Pressure (BarA) Measured at 13 Pipe Diffuser Throat Exit*

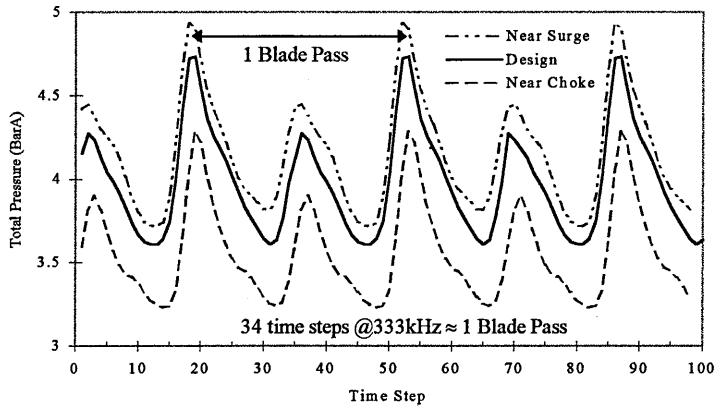


Figure 5.14 Plane-Average Total Pressure Pulsations Measured within Diffuser Throat

5.4. COMPUTATIONAL MODELS

In order to gain further insight of the flow within the pseudo- and semi- vaneless space regions, RAMPANT, the commercial code found suitable for modelling the 35D impeller flow, was again utilised. A numerical model of the 31 pipe diffuser, regarded here as the most 'conventional' diffuser design (i.e. followed Kenny's (1970,1972) design philosophy) was constructed. The computational mesh (Figure 5.16) took advantage of the unstructured capability of the code and comprised of 30,605 tetrahedra. Boundary conditions included inlet total pressure and flow angle profiles (from the pneumatic traverses) and uniform static pressure at the throat which acted as the domain discharge. As only 1 pipe channel was modelled, periodic boundary conditions were used to 'join' matching regions of pseudo-vaneless space.

Computations were carried out on a DEC Alpha workstation and each solution required approximately 15 hours to converge (assuming single user). Further runs (3 or 4) were required at each examined operating condition in order to fine tune the boundary conditions and ensure the correct mass flow. An option to prescribe the mass flow, and therefore reducing solution times, was not used as the inlet profiles of total pressure and flow angle could not be simultaneously prescribed. It was the intent of the author to use the most authentic boundary conditions available in order to gain the most representative solution.

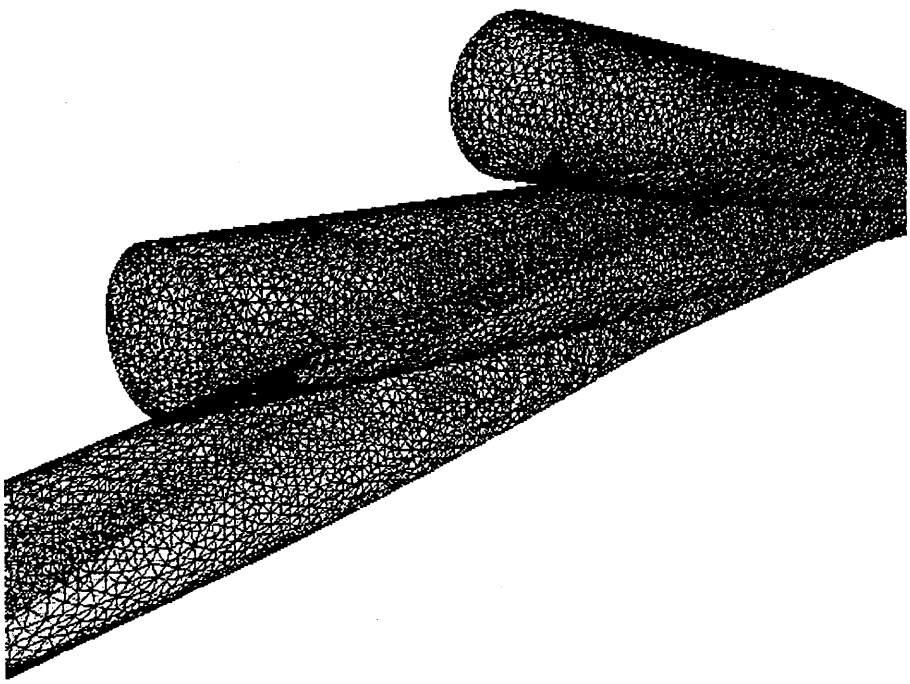


Figure 5.16 *Pipe Diffuser Computational Mesh*

5.4.1 Discussion of Predicted Flows within the Pseudo- and Semi-Vaneless Spaces

Figures 5.17 and 5.18 shown the static pressure and Mach number distributions within the 31 pipe diffuser at the extremes of operation. Near choke the flow is seen to gradually decelerate within the pseudo-vaneless space prior to entry into the throat. Near surge, much stronger diffusion is seen but without any shock as suggested by measurement. Close examination of Figure 5.2 shows that the only evidence for a shock is a single static tapping on the leading edge radius on the suction side of the blade. This measurement location is subject strong localised pressure gradients as seen in Figure 5.18. Together with the evidence that very little static pressure distortion was measured at the impeller tip, it is more likely that no shock is present in this diffuser configuration.

Evidence of the strong swirl within the diffuser is shown for both of these two flow conditions in Figure 5.19. There are two sources of vorticity hypothesised. The first is due to the flow angle gradient from shroud to hub with near reverse flow measured near the shroud. This combination, when channelled, naturally induces rotation in the sense shown at the 'near surge' condition. The second is formed by the leading edge diffuser

scallop: at choke, the flow is at its most radial and given positive incidence to the elliptic leading edge would form the twin vortex pattern as shown for the 'near-choke' case. The asymmetry of the choke flow is thought due to be caused by a combination of both effects.

CFD predictions of throat total pressure (Figure 5.20) show none of the asymmetry shown in the experimental traverses. Experiment measurements showed a weighting toward the shroud. This would suggest a flaw in the model and it is expected that further enhancement could only be achieved by improving the inlet and discharge boundaries by placing them further away from the diffuser. This might even involve modelling the impeller itself particularly for the diffusers with low numbers of pipes where significant flow distortion has been detected due to the influence of the diffuser.

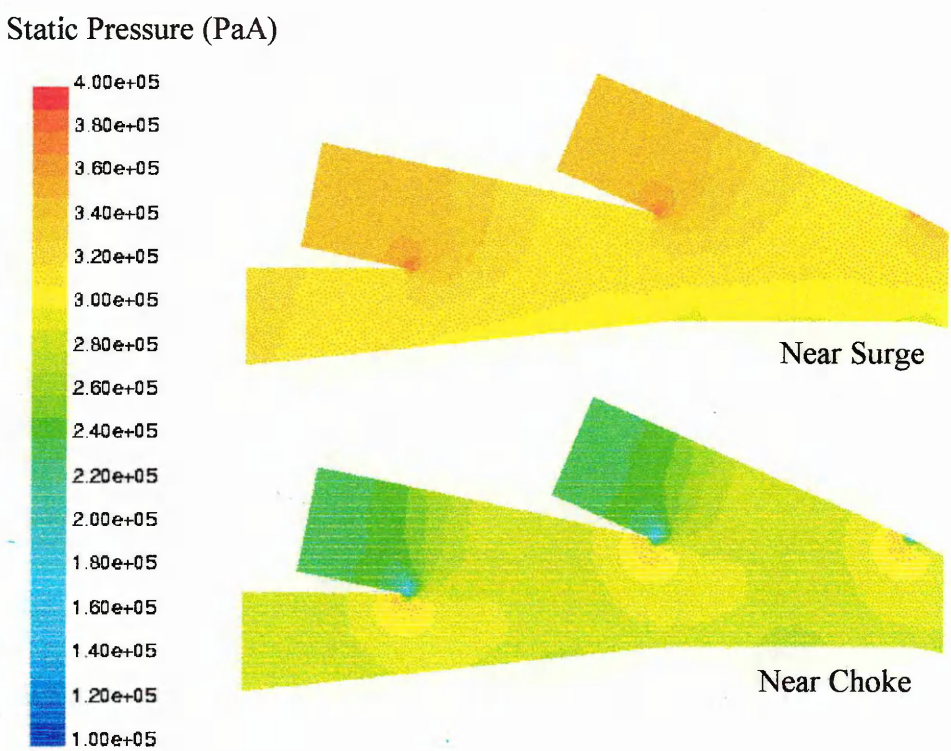


Figure 5.17 Static Pressure within 31 Pipe Diffuser (CFD)

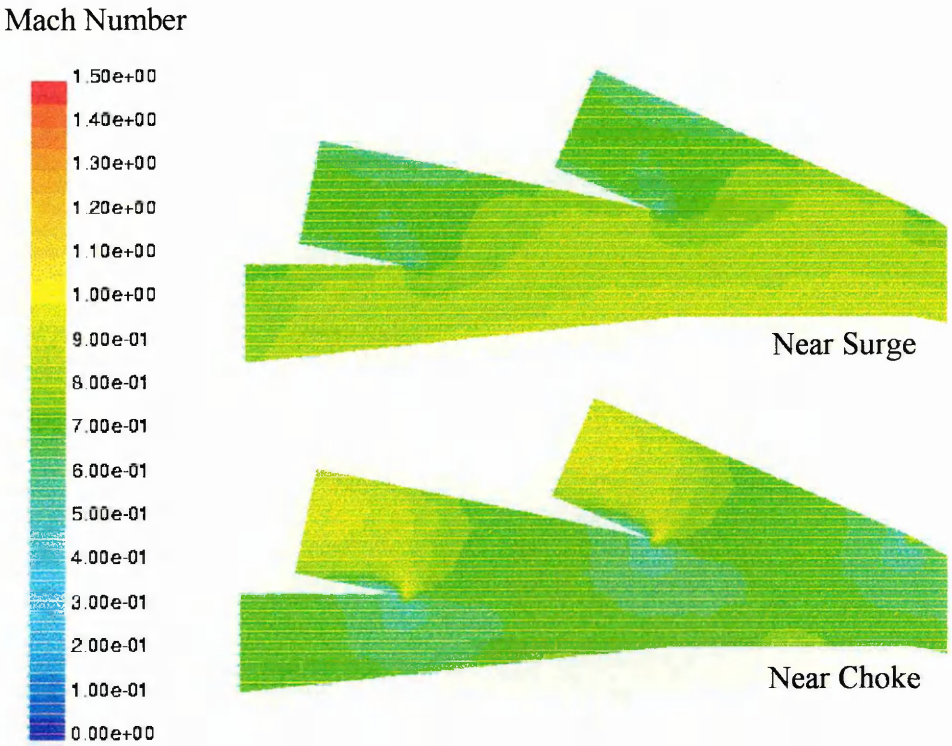


Figure 5.18 Mach Number within 31 Pipe Diffuser (CFD)

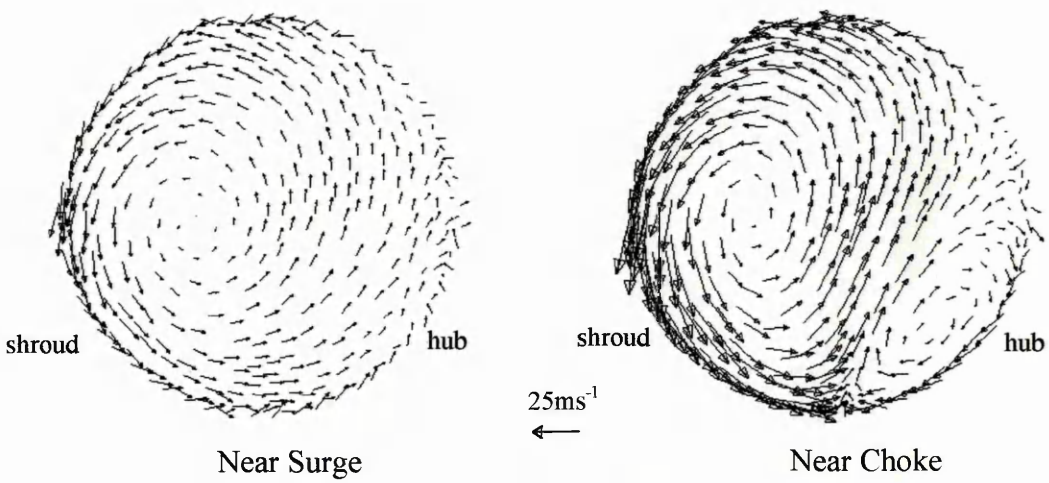


Figure 5.19 Secondary Flow at 31 Pipe Diffuser Throat (CFD)

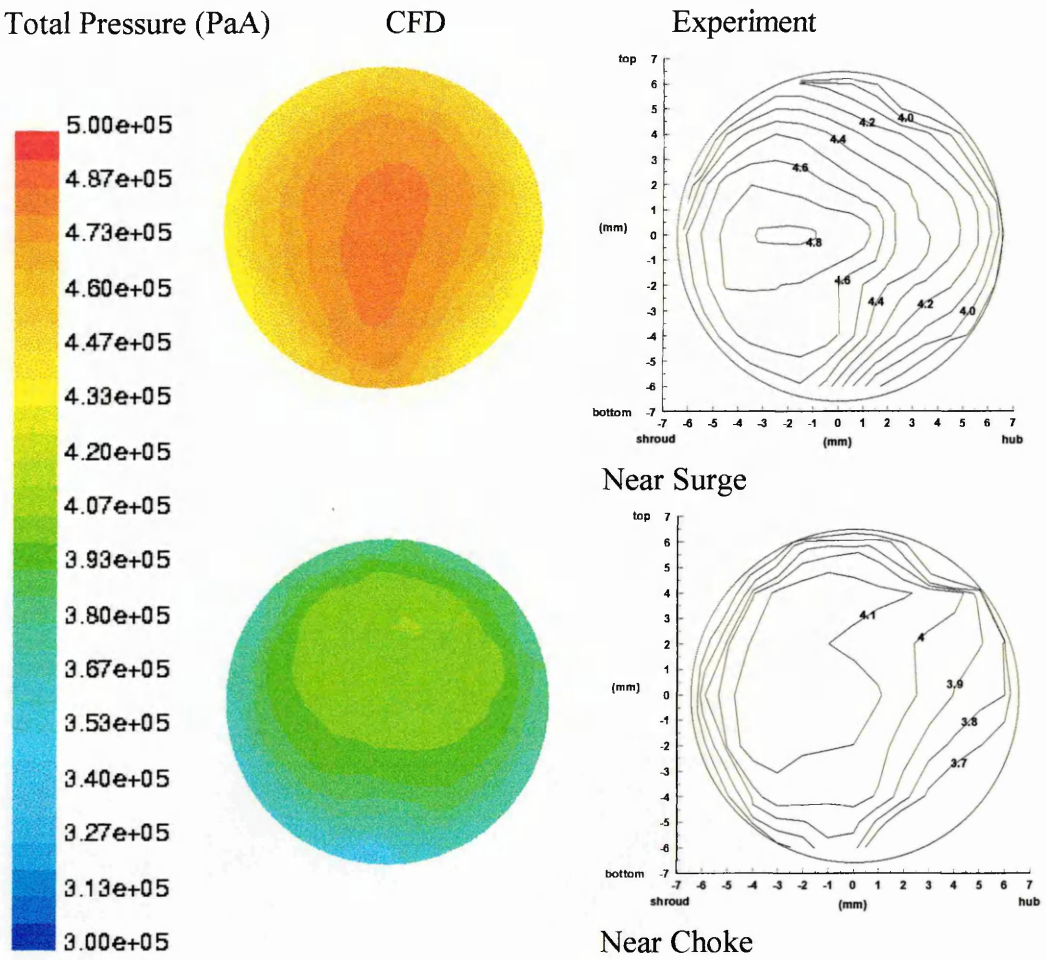


Figure 5.20 Total Pressure at 31 Pipe Diffuser Throat (CFD)

5.4.2 USING RAMPANT AS A DIFFUSER DESIGN TOOL

At first glance, CFD would seem a readily available design tool due to its ability to representatively model both the pipe diffuser complex geometry and the governing equations of motion. The limited measurements along the axis of the 31 pipe diffuser have shown reasonable agreement with CFD (see Figure 5.21) and the throat area traverse measurements have correlated well (apart from some axial displacement of the core flow).

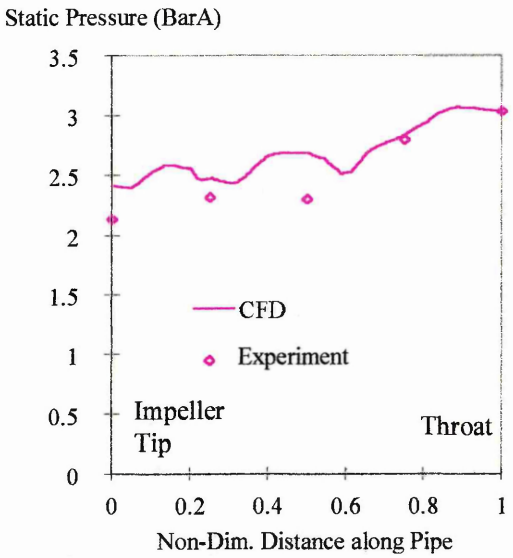


Figure 5.21 Static Pressure Distribution along Pipe Centreline

However, of importance to designers are the losses in this region, and more significantly, the throat blockage. Losses are not correctly predicted by RAMPANT, in fact one solution showed a slight rise in total pressure. Disappointingly, the throat blockage is also not well predicted and neither is the actual pressure rise across the pseudo- and semi- vaneless spaces at extreme duties. If predictions are superimposed on the experimental blockage curve derived earlier (Figure 5.22), the blockage calculated would seem incorrectly insensitive to the pressure recovery.

In its present form the computational model would seem inadequate as a diffuser design tool. In addition, should the designer decided to use CFD, he would most likely

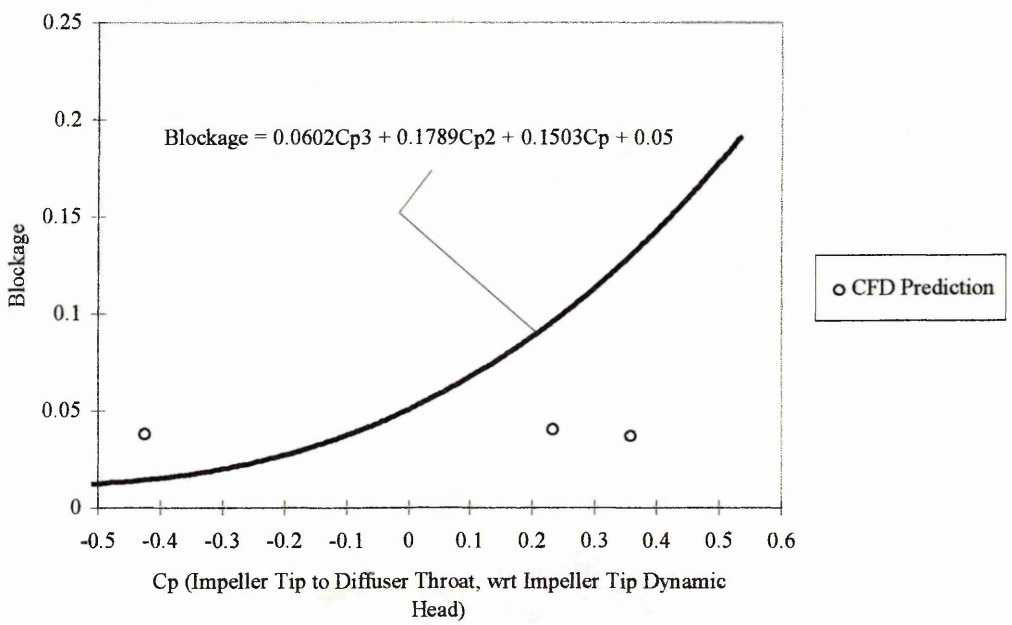


Figure 5.22 Predicted Blockage versus Static Pressure Recovery

include the downstream diffuser channel. Up to the diffuser throat, serious deficiencies have already been highlighted. It is hypothesised that these inaccuracies would be amplified in the downstream diffusion process and would render predications useless. Possible enhancements to the existing model could include mesh refinements, significantly more cells (by an order of magnitude) and alternative turbulence models. To achieve confidence would require a large number of test cases which are certainly outwith the scope of this present work.

5.5. CLOSURE

Detailed flow measurements taken within the pseudo- and semi-vaneless spaces of 4 different pipe diffusers have been presented and discussed.

- In terms of fatigue, strong static and unsteady pressure fields have been detected at the impeller tip and at the diffuser leading edge. There is evidence from Japikse (1980) that the amplitude of these distortions for diffusers with small numbers of pipes could be detrimental to the impeller fatigue life.
- Static pressure measurements have suggested that the distorted pressure field at the impeller tip is significantly influenced by diffuser leading edge bow shocks that penetrate the impeller periphery. Some careful design of this region may help alleviate this potential problem. The structural integrity of the current 13 pipe configurations (and impeller) should be carefully examined prior to commercial adoption.
- It has been shown that the unsteady flow from the impeller is amplified by the strong diffusion within the pseudo- and semi- vaneless spaces.
- At the diffuser throat, all diffusers have shown strong unsteadiness with a dominating longitudinal pulsation. Surprisingly, the general form of the throat total pressure field remains largely unchanged in time.
- Strong swirl patterns have been predicted at the diffuser throat. Such swirl is indicted by the experimental data in Chapter 4 and, as for the unsteady data, will provide additional input for diffuser channel performance predictions. The swirl significantly effects the blockage calculated from statics and casts some doubt on the Kenny (1970) blockage data.
- The application of CFD to design pipe diffusers would currently seem impractical due to long runs times (2-3 days) plus the time to build new computational meshes (1 day). Crucially however, poor results have been recorded here. A considerable amount of further development work will be necessary to improve and gain confidence in the pipe diffuser CFD performance predictions.

CHAPTER 6
Conclusions and Further Work

Probably the most complex flow region within a centrifugal compressor is that between the impeller tip and diffuser throat where a normally distorted impeller flow interacts with the diffuser inlet. The pipe diffuser was particularly little understood in this area which had not previously received any detailed study in the UK. In addition, due to commercial sensitivity, very little published information was available on pipe diffusers. The objective of this current research was to alleviate these deficiencies.

This thesis described a series of tests and accompanying computational analysis undertaken for the above study. The experiments focused on the flow exhausting from a 292.5mm diameter impeller rotating at 34,825 rpm (tip speed 533ms^{-1}) with a backsweep angle of 24°. The pipe-diffuser parametric changes undertaken closely follow the author's and supervisor's thoughts on design but were influenced by privileged information acquired by the team somewhat prior to the start of this project.

The experimental work involved a study of:

a) The impeller flows whilst in a vaneless configuration - detailed traverses were carried out to ascertain the flow entering the diffuser.
b) The influence of area expansion between impeller tip and diffuser throat - this parameter was expected to alter impeller/diffuser matching.
c) The influence of sidewall expansion between the impeller and pipe diffuser - this permitted throat pipe diameters other than the diameter of the impeller tip width to be used. Previous UK studies had minimised this expansion leading to excessive numbers of pipes and, the author felt, a much compromised design.

6.1. CONCLUSIONS

The pertinent findings of this study are:

a) An examination of Rolls-Royce test data, together with some empirical data created from this work to correct for non-optimum throat size, suggests that pipe diffusers may offer significant efficiency enhancements (up to 2-3%) over vaned diffuser designs at pressure ratios above 5½ ($M_{tip} > 1.1$).
b) A new measurement system has been developed based on a singularly mounted ultra-miniature pressure transducer. At each measurement location, the flow angle and total pressure were determined by curve fitting a series of 7 measurements taken at steps of 10°. The sensor arrangement was sufficiently small not to excessively influence the very small domain of interest and had the advantage of not requiring extensive high speed wind tunnel calibration.
c) The throat size is a controlling parameter for pipe diffusers and incorrect prescription invariably yields significant penalties in both range and efficiency. Vane island data should be used with caution for pipe diffuser design. The importance cannot be overstressed, particularly at high pressure ratios where the throat blockage variation can be as much as 5%.
d) Over-sizing the geometric throat area would only seem to introduce additional increments in blockage without changing the pseudo- and semi- vaneless space diffusion.
e) A new throat blockage relation, based (uniquely) on direct measurements within the diffuser throat, has been compiled for future throat designs. This combines subsonic and supersonic flow data to simplify the design process.
f) Significant range enhancement, without performance penalty, is possible by reducing the number of pipes and thereby incurring 'sidewall expansion' up to 1.7 times the impeller tip width. The losses, introduced by the expansion, appear to be offset by other influences. This benefit, however, has been at the cost of increased unsteadiness and flow distortion. In particular, at the impeller tip, pipe diffusers with low numbers of pipes are shown to cause significantly larger impeller tip static pressure distortions. These have previously been blamed for impeller failure.
g) Unique throat flow traverses have demonstrated that the flow entering the downstream conical diffuser is highly distorted and pulsates strongly. Experimentally derived diffuser performance maps, that invariably fix steady inlet conditions, should therefore be used with great caution. Surprisingly, the general form of the throat total pressure field remains unchanged in time: it would seem as if an unsteady longitudinal component had been superimposed onto a steady throat total pressure field.

h) The largest throat total pressure amplitudes measured have been for the diffusers with lower numbers of passages. These pulsations are shown to originate from the impeller, suggesting very little mixing to the jet/wake impeller flow structure prior to the diffuser throat.

i) As well as a great deal of 'academic' information about the detailed flow field between impeller and diffuser, a major contribution from this work is the large amount of design data which has been generated. This will not only allow designers to create successful pipe diffusers, but will also allow optimisation (together with quantitative trade-offs) of efficiency, range, flow unsteadiness and distortion.

6.2. FURTHER WORK

a) These flow studies have been limited to the flow between the impeller tip and the diffuser throat: the so-called pseudo- and semi-vaneless spaces. Now that the flow into the diffuser cone has been traversed, it would be interesting to add a diffuser channel, and perhaps downstream fish-tail diffusers, to assess the diffuser channel effectiveness to this highly skewed rotational and pulsating incident flow.

b) These experiments have been limited to a single impeller and it would be useful to carry out some additional work on another. It would be particularly interesting if this was a higher pressure ratio compressor- perhaps of the order PR = 8 to 10. It is for such machines that the benefits of pipe diffusers become large.

c) As CFD becomes more useful via improved solution algorithms and more powerful computers, the data compiled in this thesis could provide a series of test cases. The pipe diffuser pseudo- and semi-vaneless space data would provide a stern test for any code due to the strong diffusion, unsteadiness and possible shock wave formation. All data necessary for such simulations are compiled in this thesis to assist such an investigation.

References

Abdel-Hamid, A.N., Haupt. U. and Rautenberg, M. *"Unsteady Flow Characteristics in a Centrifugal Compressor with Vaned Diffuser"* ASME 87-GT-142, Presented at the International Gas Turbine Conference, Anaheim, California, 1987.

Adkins, R.A. *"The Effects of Compressibility on Diffuser Performance"* Lecture Notes, School of Mechanical Engineering, Cranfield University, 1994.

Bennett, I., Tourlidakis, A. and Elder, R.L. *"The Design and Analysis of Pipe Diffusers for Centrifugal Compressors"* EPSRC Research Grant Report No: GR/J 11706, 25 June 1997.

Bosman, C. and Ahrabian, D. *"Calculation of Stalled Flow in a Centrifugal Impeller"* IMechE Conference: Computational Methods for Turbomachinery, Paper No C67/84 pp173-182, 1984.

Brown, W.B. *"Friction Coefficients in a Vaneless Diffuser"* NACA 1311, 1947. [(Cited by Senoo (1984)].

Came, P.M. *"The Current State of Research and Design in High Pressure Ratio Centrifugal Compressors"* Procurement Executive, Ministry of Defence, Aeronautical Research Council Current Paper No. 1363, Her Majesty's Stationary Office, London, 1977.

Came, P.M. *"The Development, Application and Experimental Evaluation of a Design Procedure for Centrifugal Compressors"* Proc. Instn Mech Engrs Vol 192, pp49-67, March 1978.

Came, P.M. and Herbert, M.V *"Design and Experimental Performance of some High Pressure Ratio Centrifugal Compressors"* AGARD Conference Proceedings No. 282, Paper 15, 1980.

Cherrett, M.A. *"Temperature Error Compensation Applied to Pressure Measurements Taken with Miniature Semiconductor Pressure Transducers in a High-Speed Research Compressor"* Technical Memo P1192, Royal Aircraft Establishment, Oct 1990.

Cherrett, M.A., Bryce, J.D. and Ginder, R.B. *"Unsteady 3D Flow in a Single-Stage Transonic Fan. Part 1: Unsteady Rotor Exit Flow Field"* ASME 94-GT-223, 1994.

Clements, W.W. and Artt, D.W. *"Performance Prediction and Impeller Diffuser Matching for Vaned Diffuser Centrifugal Compressors"* IMechE Conference Paper No. C256/87, pp 183-198,1987.

Clements, W.W. and Artt, D.W. *"The Influence of Diffuser Vane Leading Edge Geometry on the Performance of a Centrifugal Compressor"* ASME Paper 89-GT-163, Presented at the Gas Turbine and Aeroengine Congress and Exposition, June 4-8, Toronto, Ontario, Canada.

Cohen, H., Rogers, G.F.C and Saravanamuttoo, H.I.H. *"Gas Turbine Theory"* Longman Scientific & Technical, 3rd Edition, 1987.

Crandall, N.C., Dahl, T.J. and Lardner, T.J. *"An Introduction to Mechanics"* Longman Scientific & Technical, 3rd Edition, 1987.

Dawes, J Work contracted by I.Bennett to J.Dawes, School of Mechanical Engineering, Cranfield University, to test a filter circuit, June 1995.

Dawes, W.N. *"A Simulation of the Unsteady Interaction of a Centrifugal Impeller with its Vaned Diffuser: Flow Analysis"* ASME International Gas Turbine and Aeroengine Congress and Exposition, The Hague, Netherlands, 94-GT-105, 13-16 June 1994.

Dean (Jr), R.C. and Senoo, Y. *" Rotating Wakes in Vaneless Diffusers"* Journal of Basic Engineering, pp 563-574, Sept. 1960.

Dean (Jr), R.C. *" The Fluid Dynamic Design of Advanced Centrifugal Compressors"* Creare Technical Report, TN-185, p.76, July 1974.

Dean (Jr), R.C. and Young, L.R. *" The Fluid Dynamic Design of Advanced Centrifugal Compressors"* Creare Technical Report, TN-244, July 1976. [Cited in Japikse and Baines (1994)]

Dimmock, N.A. *"A Compressor Routine Test Code"* NGTE Report, R.246, Jan 1961.

Dolan, X.F. and Runstadler, P.W. *"Pressure Recovery Performance of Conical Diffusers at High Subsonic Mach Numbers"* NASA Contractor Report, NASA CR-2299, August 1973.

Dou, H. *"A Method of Predicting the Energy Losses in Vaneless Diffusers of Centrifugal Compressors"* ASME Paper 89-GT-158, Presented at the Gas Turbine and Aeroengine Congress and Exposition, June 4-8, 1989, Toronto, Canada.

Eckert, D. *"Detailed Flow Investigation within a High Speed Centrifugal Compressor Impeller"* ASME Journal of Fluid Engineering, 1976.

Elder, R.L. *"Centrifugal Compressors"* Short Course Lecture Notes, Cranfield University, 1994.

Elder, R.L. and Gill, M.E. *"A Discussion of the Factors Affecting Surge in Centrifugal Compressors"* ASME 84-GT-194, Presented at the 29th International Gas Turbine Conference, Amsterdam, Netherlands, June 1984.

Elder, R.L. *Private Discussion* Cranfield University, 1995.

Elektor *"Infocard No 110, Active RC Filters 2"* Source Unknown.

Fletcher C.A.J. *"Computational Techniques for Fluid Mechanics Vol. 1: Fundamentals and General Techniques "* Springer Verlag, 1988.

Fluent *"Fluent Users Guide"* Version 4.3, Fluent Inc. 10 Cavendish Court, Lebanon, NH 03766, Jan 1995.

Fox, R.W. and McDonald, A.T. *"Introduction to Fluid Mechanics"* John Wiley and Sons, New York, 1985.

Frigne, P. and van den Braembussche, R. *"One Dimensional Design of Centrifugal Compressors Taking into Account Flow Separation in the Impeller"* VKI Technical Note 129, June 1978.

Groh, F.G., Wood, G.M., Kulp, R.S. and Kenny, D.P. *"Evaluation of a High Hub/Tip Ratio Centrifugal Compressor"* ASME Paper No. 69-WA/FE-28, Journal of Basic Engineering, 1969.

Herbert, M.V. *"A Method of Performance Prediction for Centrifugal Compressors, Part I- Analysis, Part II - Comparison with Experiment"* National Gas Turbine Establishment, Reports and Memoranda No. 3843, February 1980.

Hirsch. C. *"Numerical Computation of Internal and External Flows, Vol. 1: Fundamentals of Numerical Discretization"* John Wiley and Sons, 1991.

Hirsch. C., Kang, S. and Pointel, G. *"A Numerically Supported Investigation of 3D Flow in Centrifugal Impellers, Part 2: Secondary Flow Structure"* ASME 96-GT-152, Presented at the ASME IGT Congress, Birmingham (UK), June 10-13, 1996.

Inoue, M. and Cumpsty, N.A. *"Experimental Study of Centrifugal Impeller Discharge Flow in Vaneless and Vaned Diffusers"* Journal of Engineering for Gas Turbines and Power, Vol. 106, April 1984.

Japikse, D. *"Review- Progress in Numerical Turbomachinery Analysis"* ASME Journal of Fluids Engineering, 1976 pp. 592-606, Dec. 1976.

Japikse, D. *"The Influence of Diffuser Inlet Pressure Fields on the Range and Durability of Centrifugal Compressor Stages"* AGARD Conference Proceedings: "Centrifugal Compressors, Flow Phenomena and Performance" AGARD-CP-282, 1980.

Japikse, D. *"Turbomachinery Diffuser Design Technology"* Concepts ETI, Inc., Norwich, Vermont, USA 05055, 1984.

Japikse, D. and Baines, N.C. *"Introduction to Turbomachinery"* Concepts ETI, Inc., Norwich, Vermont, USA 05055, 1984.

Johnson, M.W. and Moore, J. *"Secondary Flow Mixing in a Centrifugal Impeller"* Journal of Engineering for Power, ASME, January 1983.

Johnson, M.W. and Moore, J. *"The Influence of Flow Rate on the Wake in a Centrifugal Impeller"* Journal of Engineering for Power, ASME, January 1983.

Kantrowitz, A. *"One Dimensional Treatment of Non-Steady Gas Dynamics"* Section C of *Fundamentals of Gas Dynamics, Princeton*, New Jersey, Princeton University Press, 1958.

Kenny, D.P. *"A Novel Low-Cost Diffuser for High-Performance Centrifugal Compressors"* ASME Journal of Engineering for Power, pp37-47, Jan 1969.

Kenny, D.P. *"Supersonic Radial Diffusers"* AGARD Lecture Series #39, Advanced Compressors, VKI, Brussels, Belgium, June 1-4, 1970.

Kenny, D.P. *"A Comparison of the Predicted and Measured Performance of High Pressure Ratio Centrifugal Compressor Duties"* VKI Lecture Series No. 50, Advanced Radial Compressors, May 15-19, 1972.

Kenny, D.P. *"A Novel Correlation of Centrifugal Compressor Performance for Off-Design Prediction"* AIAA 79-1159, 1979.

Kenny D.P. *"The History and Future of the Centrifugal Compressor in Aviation Gas Turbines"* Society of Automotive Engineers. SAE SP-602, October 1984

Klassen, H.A. *"Performance of a Low Pressure-Ratio Centrifugal Compressor with Four Diffuser Designs"* NASA TN D-7237, March 1973.

Krain, H. *"Experimental and Theoretical Investigations on the Internal Flow in a Centrifugal Compressor"* AGARD Conference Proceedings: "Centrifugal Compressors, Flow Phenomena and Performance" AGARD-CP-282, 1980.

Krain, H. *"A Study on Centrifugal Impeller and Diffuser Flow"* Transactions of ASME, Journal of Engineering for Power, 81-GT-9, 1981.

Krain, H. *"Swirling Impeller Flow"* ASME Journal of Turbomachinery, Vol 110, 1988.

Kuethe, A.M. and Chow, C-Y. *"Foundations of Aerodynamics: Basis of Aerodynamic Design"* 4th Ed. John Wiley and Sons, 1986.

Lakshminarayana, B. *"An Assessment of Computational Fluid Dynamic Techniques in the Analysis and Design of Turbomachinery- The 1990 Freeman Scholar Lecture"* Journal of Fluids Engineering, Vol 113 1991.

Liepmann, H.W. and Puckett, A.E. *"Introduction to Aerodynamics of a Compressible Fluid"* John Wiley, New York, 1947. [Cited by Keuthe and Chow (1986)]

McKenzie, A.B. *"Passive Stall Control for Fans and Compressors"* Turbo Compressor and Fan Stability Seminar, IMechE, April 1993.

McNally, W.D. and Sockal, P.M. *"Review- Computational Methods for Internal Flow with Emphasis on Turbomachinery"* ASME Journal of Fluids Engineering, Vol. 107 pp 6-22, March 1985.

Moses, H.L. *"The Behaviour of Turbulent Boundary Layers in Adverse Pressure Gradients"* MIT Gas Turbine Lab. Report #73, Jan 1964 [Cited in Kenny (1972)].

Pampreen, R.C. *"Compressor Surge and Stall"* Concepts ETI, Inc., Norwich, Vermont, USA, 1993.

Pinot, P. *"Test of Pipe Diffuser on 35D Research Compressor"* Rolls-Royce Report, No: LCP 00218, Aero Division, Leavesden, Watford, November 1978.

Pratt, C. M. *"Results of Further Experiments on 5:1 Centrifugal (CF1) of Impeller Optimisation"* Rolls-Royce Report, No: LCP 00098, Aero Division, Leavesden, Watford, December 1973.

Press, W.H. et al. *"Numerical Recipes: the Art of Scientific Computing (FORTRAN version)"* Cambridge University Press, 1989.

RAMPANT *"Rampant Users Guide"* Version 3.1, Fluent Inc. 10 Cavendish Court, Lebanon, NH 03766, July 1994.

Rees, B. *Presentation* Given at a Turbomachinery Group Meeting, School of Mechanical Engineering, Cranfield University 1994.

Reeves, G.B. *"Design and Performance of Selected Pipe-Type Diffusers"* ASME Paper 77-GT-104, 1977.

Renau, L.R., Johnston, J.P. and Kline, S.J. *"Performance and Design of Straight Two Dimensional Diffusers"* ASME Paper 66-FE-10, Trans. ASME Journal of Basic Engineering, Vol 89, pp141-150, 1967. [(Cited in Japikse and Baines (1994)]

Roark, R. J. and Young, W.C. *"Formulas for Stress and Strain"* 5th Edition, McGraw-Hill, New York, 1975.

Rodgers, C. *"The Performance of Centrifugal Compressor Channel Diffusers"* ASME Paper No. 82-GT-10,1982.

Runstadler, P.W. and Dean, R.C. *"Straight Channel Diffuser Performance at High Inlet Mach Numbers"* ASME Paper No. 63-WA/FE-19. [Cited in Kenny (1970)].

Runstadler, P.W. and Dolan, F.X. *"Further Data on the Pressure Recovery Performance of Straight-Channel, Plane-Divergence Diffusers at High Subsonic Mach Numbers"* Journal of Fluids Engineering, pp 373-383, September 1973.

Senoo, Y. and Kyushu, U. *"Vaneless Diffusers"* von Karman Institute for Fluid Mechanics, Lecture Series 1984-07, 1984.

Senoo, Y., Kinishita, Y. and Ishida, M. *"Asymmetric Flow in Vaneless Diffusers of Centrifugal Blowers"* ASME Journal of Fluids Engineering, pp 104-113, March 1977.

Skoch, G.J., Prahst, P.S., Wernet, M.P., Wood, A.J. and Strazisar, A.J. *" Laser Measurements of the Flow Field in a 4:1 Pressure Ratio Centrifugal Impeller"* ASME 97-GT-342, June 1997.

Smout, P.D. *"The Measurement of Near-Wall Flows Using Pneumatic Wedge Probes"* PhD Thesis, Cranfield University, Jan 1995.

Stickney, T.M. *"Recovery and Time Response Characteristics of Six Thermocouple Probes in Subsonic and Supersonic Flow"* NACA TN 3455, July 1955.

Schlichting, H. *"Boundary Layer Theory"* 4th Ed., McGraw Hill, New York, pp572-576., 1960.

Tourlidakis, A.T. *"Numerical Modelling of Viscous Turbomachinery Flows with a Pressure Correction Method"* Ph.D Thesis, Cranfield University, March 1992.

Tourlidakis, A.T. *Unpublished work carried out at Cranfield University* 1996.

Tourlidakis, A.T. Private Discussion, 1997.

Verdonk, G. *"Theoretical and Experimental Investigation of the Flow at the Inlet of the Vaned Diffuser for a High Pressure Ratio Centrifugal Compressor"* von Karman Institute, Technical Note 125, March 1978.

Whitfield, A., and Baines, N.C. *"Design of Radial Turbomachines"* Longman Scientific and Technical, England, 1990.

APPENDIX A

Overall Performance Instrumentation

The instrumentation necessary for impeller performance measurement is presented here together with the calculation procedure adopted. In addition, static pressure tapping locations are given. These were placed on the impeller shroud and on the diffusers.

A.1. PRIMARY PERFORMANCE INSTRUMENTATION

The primary instrumentation is shown in Figure A.1. and is accompanied afterwards by detailed descriptions of the individual measurement systems. These are presented in the order seen by the flow i.e. from bellmouth inlet to impeller discharge.

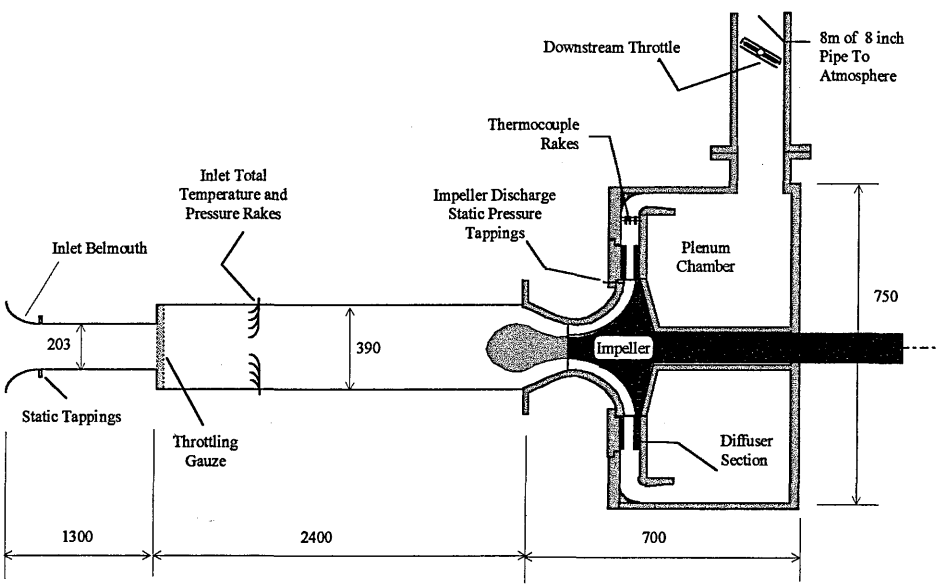


Figure A.1 Primary Instrumentation of the Compressor Rig (Dimensions in mm)

A.1.1 AMBIENT CONDITIONS

A laboratory standard mercury-in-glass thermometer was used to measure the inlet ambient temperature (± 0.25 °C). The atmospheric pressure was taken from the University's test site facility comprising of a Druck Micromanometer Type: DPI 140 (Accuracy: ±0.15mbar). No corrections were made for humidity.

A.1.2 MASS FLOW MEASUREMENT

Measurement was made upstream of the compressor using a calibrated inlet bellmouth. The pressure at the vena-contracta was measured via four equi-spaced static tappings using a calibrated micromanometer, Type: Furness Model FCO 510 with an accuracy of ±0.08% of reading.

A.1.3 INLET THROTTLING GAUZE

Due to limitations in the drive turbine power/speed characteristic when the compressor operated at 100% of design speed, a coarse gauze mesh was inserted to throttle the inlet flow and lower the inlet air density, thus reducing the power required to drive the compressor.

Care was taken to ensure that there was no significant reduction in the operating Reynolds number.

A.1.4 INLET TOTAL TEMPERATURE RAKES

Four temperature rakes were placed, within the inlet ducting, downstream of the bellmouth entry and throttling gauze. Each of these consisted of five 'K'-type thermocouples, radially positioned for equi-flow-area weighting.

A semi-circular enclosure was used (see Figure A.2 below) and the readings required no 'recovery' correction primarily due to the low local Mach numbers [Stickney (1955)].

'K'-type thermocouples have an uncalibrated accuracy of ±0.5°C over an operating temperature of approximately 800°C. To check the measurement system, a sample batch were check calibrated against an in-house Platinum-Resistance Thermometer (±0.05°C).

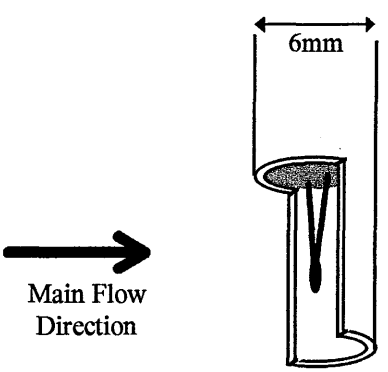


Figure A.2 Sample Thermocouple Sensor

A.1.5 INLET TOTAL PRESSURE PROBES

The total pressure was measured within the same plane as the inlet temperature rakes. Likewise, they were positioned for equi-flow-area weighting and consisted of five probes per rake. The probes themselves were of plain tube construction, radially inserted and bent at a right angles to point into the flow (See Figure A.3 below). Kiel probes were not used in this region as no appreciable flow swirl was expected. The 45° internal chamfer allowed a skew flow incidence of ±10° [Dimnock (1961)] without significant loss of accuracy.

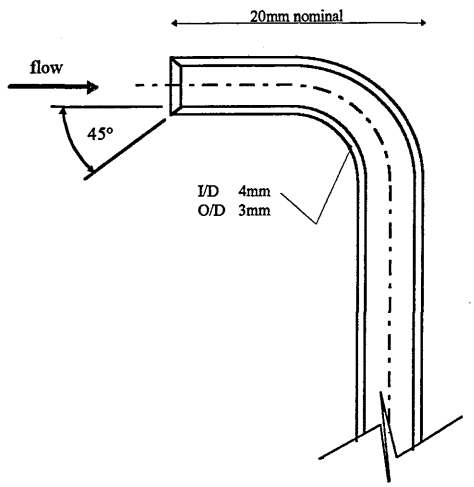


Figure A.3 Sample Total Pressure Probe

Measurements from these probes were taken using Pressure transducers (Type: Druck PDCR 22), the accuracy of which is given in Table A.1.

Table A.1 Accuracy of Scani-Valve Pressure Transducer

Full Scale Deflection (FSD)	50 psig
Maximum deviation	± 0.015% FSD
Span Drift (%FSD/°C)	± 0.0015% FSD

During the compressor tests when a full instrumentation scan was taken, the transducer readings were 'offset' using a channel open to atmosphere. This was used to help correct for minor temperature drifting.

All pressure transducers were calibrated using a Druck digital pressure indicator Model DPI 601 with Namas Calibration. The specifications of which are given below:

Table A.2 Accuracy of Reference Calibration Instrument

Full Scale Deflection (FSD)	300 psig
Maximum deviation	± 0.007% FSD
Span Drift (%FSD/°C)	± 0.006% FSD

A.1.6 IMPELLER EXIT STATIC PRESSURE PROBES

Of primary importance was to use a consistent method of performance evaluation irrespective of diffuser configuration and it was decided that instead of measuring the discharge total pressure directly, it would be evaluated from the static pressure at the impeller tip. Five equally spaced static tappings were located on the shroud and were of plain cylindrical type without internal chamfer. Measurements were recorded routinely via the scani-valve system.

A.1.7 DISCHARGE THERMOCOUPLES

At discharge, due to the reduced flow depth, instead of 5 as for the inlet, only 3 thermocouples were used to span the vaneless space. Four rakes of 'K' type thermocouples were again utilised.

A.1.8 CONTROL OF MASS FLOW

The system mass flow was controlled using a flap valve downstream of the discharge plenum.

A.1.9 ROTATIONAL SPEED

The impeller speed was detected near the rotor front bearing with the use of a magnetic pick-up. An independent secondary system measured the drive turbine speed using an optical arrangement.

Close to source, both systems were interpreted and a then encoded as 5V TTL (square wave) pulses. A pulse was transmitted every revolution.

A.1.10 TIP CLEARANCE MEASUREMENT

Tip clearances were monitored during compressor testing using capacitance probes manufactured by Rotor-Data. (Type: ES 1291 processor with MS 0901-100 type probes). Three probes were used and located at different meridional locations representing, inlet, mid-impeller and discharge (see Figure A.4).

The probes were calibrated by mounting the impeller in a lathe and taking measurements at varying clearances at the three different meridional shroud locations. Calibration in this manner was necessary due to the sensitivity of the probes to the rotor blade material and thickness.

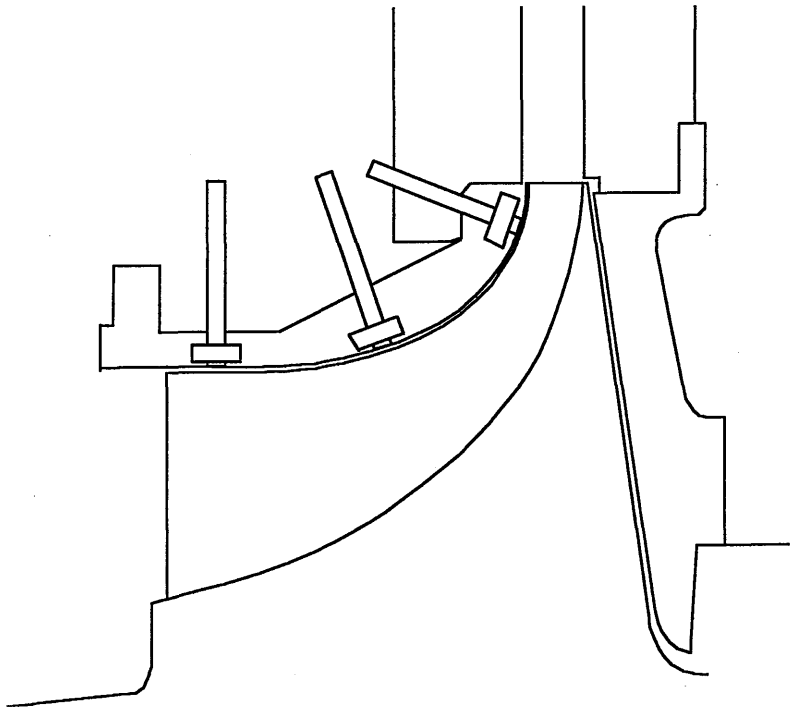


Figure A.4 Location of Capacitance Probes

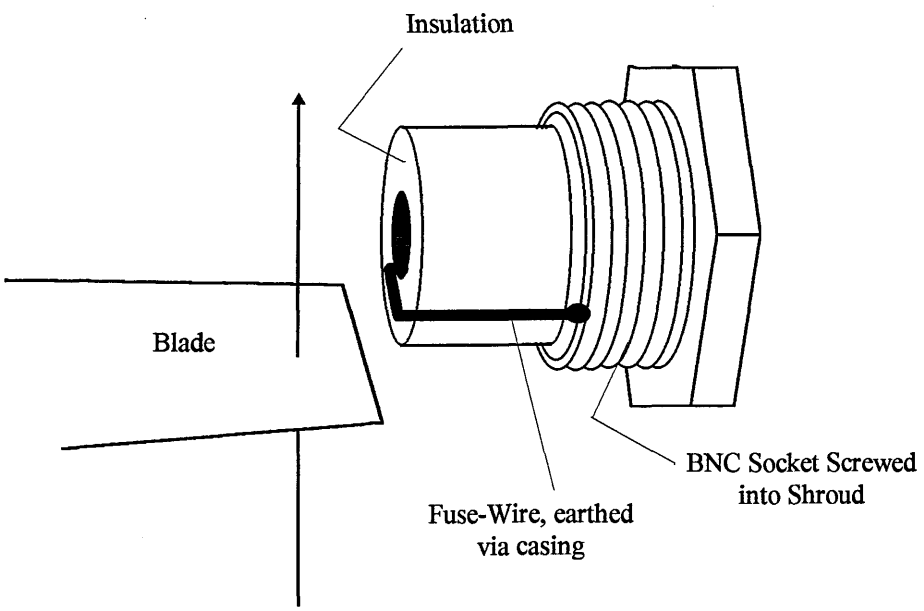


Figure A.5 Cut-Wire Probe Detail

A.1.11 TIP CLEARANCE SAFETY MONITORING

In order to ensure that the impeller did not move in a plane not monitored by the Rota-Data system, a cut-wire probe scheme was manufactured and used to safeguard against shroud contact.

Each 'sensor' was constructed from a panel mounted BNC socket. The central core was insulated and contained an electrical positive feed. This was attached to thin fuse wire, looped such that it would be cut if the impeller came too close to the shroud. The end of this wire was soldered onto the BNC casing and was thus normally earthed.

Eight channels were used, and all were connected to a logic NOR gate as shown below:

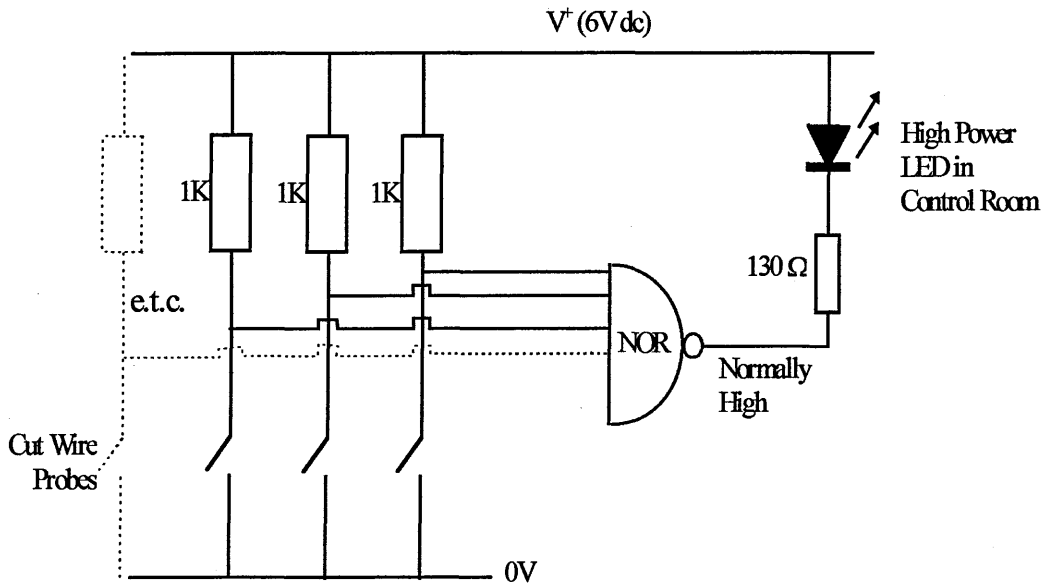


Figure A.6 Cut -Wire Probe Logic Electronics

A.2. PERFORMANCE DATA ACQUISITION AND ANALYSIS

A dedicated PC was used to drive the performance measurement systems. This was located within an adjacent armoured control room. This level of protection was necessary due to the dangerous nature the high speed facility.

A.2.1 HARDWARE

From the control room, the PC communicated with a 'Di-An DMS' modular data acquisition system via an RS232 port. The 'Di-An' system consisted of a core controller with

digital I/O (Input/Output) that communicated with a 13 bit (1 bit for ± and 12 bits for magnitude) Analogue-to-Digital-Converter (ADC) and a multiplexer arrangement that allowed switching between acquisition modules, each designed for a specific transducer input. See Figure A.7. Specific module types utilised are given in Table A.3.

Table A.3 Performance Acquisition Hardware

Module Function	Di-An Designation
Controller	DMS 561
Speed	DMS 251
Thermocouple	DMS 235
ADC	DMS 230
Digital Input/Output	DMS 221
Analogue Input	DMS 234

A.2.1.1 Temperature

For this particular study four thermocouple modules (designated 1 to 4) and one pressure module (designated 5) were utilised.

Each of the thermocouple modules had 8 channels, designated 0 to 7. On each of these modules, channel 7 was used as an offset datum, with the connecting thermocouple submerged within a reference ice cell.

A.2.1.2 Rotor Speed

For the impeller speed, the once-per-revolution TTL type pulses sent from the rig were counted (using another specialised 'Di-An' Module) over a pre-set sample interval, thus allowing the rotor rotational speed to be evaluated.

A.2.1.3 Pressure

Instead of one transducer per pressure tapping, a 'scanivalve' switching system was used. This allowed one pressure transducer to switch between 48 pressure tappings or channels. Communication between the scanivalve system and the PC was achieved via a dedicated digital output module. The pressure transducer outputs, in terms of a voltage, were fed into Di-An module 5, then through the 'Di-An' ADC to the PC. In all, two scani-valve systems were used. These systems proved very reliable, and due to their switching mechanism, reduced the number of pressure transducers required. However, their operation was very slow: a full scan of all 48 channels would take approximately 3 minutes.

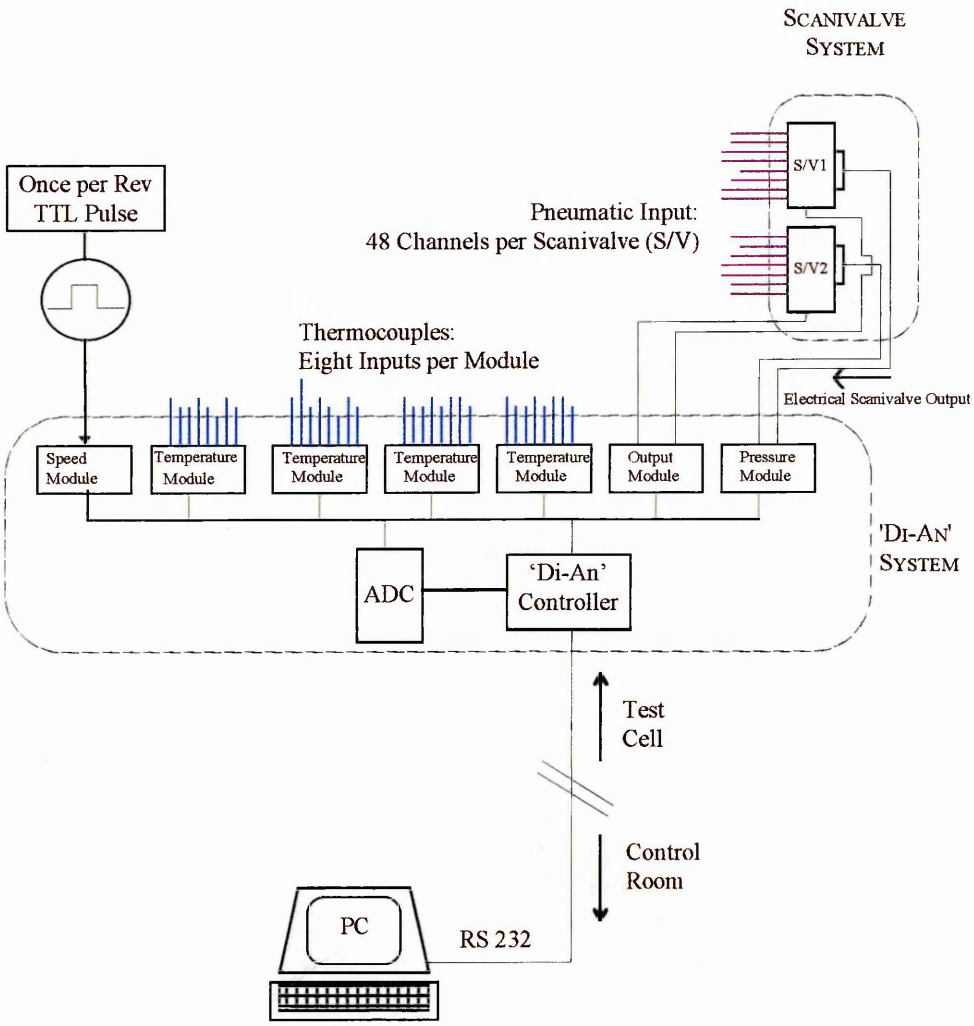


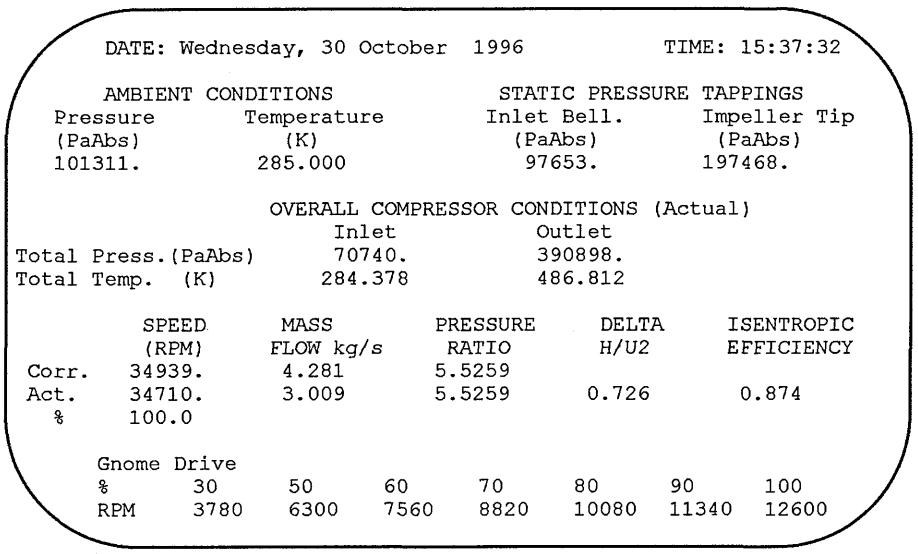
Figure A.7 Overall View of Performance Data Acquisition

A.2.2 PERFORMANCE PROGRAM SOFTWARE

The Driving software for the performance data acquisition was written in FORTRAN '77 and compiled using SALFORD FORTRAN 386. The program had two main modes of operation as described below:

A.2.2.1 Monitor Mode

This continually completed a limited scan of the instrumentation and presented salient operating conditions on-screen. Update frequency was optimised to approximately every 2-3 seconds. A sample output screen is shown in Figure A.8.



DATE: Wednesday, 30 October 1996 TIME: 15:37:32

AMBIENT CONDITIONS		STATIC PRESSURE TAPPINGS	
Pressure (PaAbs)	Temperature (K)	Inlet Bell. (PaAbs)	Impeller Tip (PaAbs)
101311.	285.000	97653.	197468.

OVERALL COMPRESSOR CONDITIONS (Actual)

	Inlet	Outlet
Total Press.(PaAbs)	70740.	390898.
Total Temp. (K)	284.378	486.812

	SPEED (RPM)	MASS FLOW kg/s	PRESSURE RATIO	DELTA H/U2	ISENTROPIC EFFICIENCY
Corr.	34939.	4.281	5.5259		
Act.	34710.	3.009	5.5259	0.726	0.874
%	100.0				

Gnome Drive							
%	30	50	60	70	80	90	100
RPM	3780	6300	7560	8820	10080	11340	12600

Figure A.8 Sample Monitor Performance Screen During Experimental Testing

All designations are as clearly stated apart from the 'Gnome Drive' heading at the lower portion of the screen. This gave the speed of the drive turbine necessary to set a particular corrected compressor speed. The drive turbine speed itself was updated using a fast independent system (updated approximately 10 times more frequently than the Di-An screen output), and thus it was useful for fine tuning the operating condition.

A.2.2.2 **Complete Scan Mode**

In this mode a complete instrumentation scan of all pressures and temperatures were made. All performance measurements plotted within this thesis were carried out in this mode. After each complete scan all data was written to file. The general format is shown in Figure A.9 and is similar to the screen-shot shown earlier in Figure A.8, apart from the lower columns of data. The first three columns refer to the measurements taken using the scani-valve system and the latter two record the thermocouple measurements. The array TT(*,*) has designations (Module Number, Channel Number). It may be noted that all TT(*,7) channels read near 0 (°C) because, as described earlier, they were connected to an ice cell for zero offset. All remaining temperatures are displayed in Kelvin. Section A.4 contains listings of all measurement locations and computer array addresses.

FILE:vda118.DAT
TITLE: 35D COMPRESSOR RIG TESTS
Program DAP20f.for

DATE: Wednesday, 22 May 1996 TIME: 16:03:41

AMBIENT CONDITIONS		STATIC PRESSURE TAPPINGS	
Pressure (PaAbs)	Temperature (K)	Inlet Bell. (PaAbs)	Impeller Tip (PaAbs)
100030.	286.000	96816.	201173.

OVERALL COMPRESSOR CONDITIONS (Actual)

	Inlet	Outlet
Total Press. (PaAbs)	69426.	401379.
Total Temp. (K)	283.879	489.782

	SPEED (RPM)	MASS FLOW kg/s	PRESSURE RATIO	DELTA H/U2	ISENTROPIC EFFICIENCY
Corr.	34819.	4.072	5.7814		
Act.	34560.	2.811	5.7814	0.745	0.887

SV Port	Valve1 (PaAbs)	Valve2 (PaAbs)	Location	Temp (K)
0	69358.	201660.	TT(0,0)	272.200
1	100030.	100030.	TT(0,1)	489.967
2	69448.	200579.	TT(0,2)	283.961
3	69537.	204903.	TT(0,3)	283.781
4	69448.	198146.	TT(0,4)	283.961
5	69448.	200579.	TT(0,5)	283.541
6	69537.	61919.	TT(0,6)	283.661
7	69537.	59216.	TT(0,7)	0.900
8	69448.	64081.	TT(1,0)	283.721
9	69537.	70838.	TT(1,1)	283.961
10	69448.	75433.	TT(1,2)	284.021
11	69358.	88678.	TT(1,3)	283.781
12	69448.	95705.	TT(1,4)	283.901
13	69358.	107868.	TT(1,5)	284.141
14	69358.	112734.	TT(1,6)	283.661
15	69180.	114085.	TT(1,7)	-0.480
16	69358.	124627.	TT(2,0)	283.841
17	172193.	132735.	TT(2,1)	283.721
18	100030.	143277.	TT(2,2)	284.201
19	100119.	160575.	TT(2,3)	284.201
20	100119.	100030.	TT(2,4)	490.987
21	100119.	167333.	TT(2,5)	490.027
22	100119.	182739.	TT(2,6)	489.307
23	100119.	194632.	TT(2,7)	0.000
24	100209.	216526.	TT(3,0)	489.787
25	307130.	226797.	TT(3,1)	490.627
26	100209.	241122.	TT(3,2)	489.067
27	100119.	252475.	TT(3,3)	489.067
28	100119.	258151.	TT(3,4)	489.907
29	100030.	270044.	TT(3,5)	488.947
30	100119.	289234.	TT(3,6)	489.427
31	100119.	288423.	TT(3,7)	0.480
32	100119.	288694.	TT(4,0)	490.267
33	102623.	102733.	TT(4,1)	-219.502
34	102623.	102733.	TT(4,2)	-219.502
35	102623.	102733.	TT(4,3)	-219.502
36	102623.	102733.	TT(4,4)	-219.502
37	102623.	102733.	TT(4,5)	-219.502
38	102623.	102733.	TT(4,6)	-219.502
39	102623.	102733.	TT(4,7)	1.080
40	102623.	102733.	TT(5,0)	489.967

DATE: Wednesday, 22 May 1996 TIME: 16:03:41

Figure A.9 Sample Full Performance Instrumentation Scan Data File

A.2.2.3 Performance Calculation Method

A.2.2.3.i General Definitions

The performance of the rotor was evaluated using the following definitions:

Corrected Mass flow Rate $$m_{corr} = \frac{m\sqrt{\theta}}{\delta} \quad \text{(A.1)}$$

Corrected Speed $$N_{corr} = \frac{N}{\sqrt{\theta}} \quad \text{(A.2)}$$

Where the two correction coefficients are defined as

$$\theta = \frac{T_{01}}{T_{ref}} \quad \text{(A.3)}$$

and $$\delta = \frac{p_{01}}{p_{ref}} \quad \text{(A.4)}$$

The following reference conditions were used:

$T_{ref} = 288.15\ ^{o}K$ and $p_{ref} = 1.01325 \times 10^{5}\ Pa$

Overall performance parameters were calculated as:

Pressure Ratio $$P_R = \frac{p_{02}}{p_{01}} \quad \text{(A.5)}$$

Impeller Isentropic Efficiency $$\eta_{is} = \frac{P_R^{\frac{(\gamma-1)}{\gamma}} - 1}{\frac{T_{02}}{T_{01}} - 1} \quad \text{(A.6)}$$

where γ was evaluated for the mean total temperature using the polynomial fit given by Dimnock (1961). Mass flow was calculated from

$$m = C_d A_{duct} \sqrt{\frac{\gamma}{R}} \frac{p_{01}}{\sqrt{T_{01}}} \sqrt{\frac{2}{\gamma - 1}} \left[\left(\frac{p_{belmouth}}{p_{01}} \right)^{\frac{2}{\gamma}} - \left(\frac{p_{belmouth}}{p_{01}} \right)^{\frac{(\gamma+1)}{\gamma}} \right]^{1/2} \quad \text{(A.7)}$$

A.2.2.3.ii Calculation of Discharge Total Pressure

As there were no discharge kiel probe rakes, the rotor discharge total pressure was calculated from static tappings and the discharge temperature thermocouple rakes.

As the author is aware of at least two methods of doing this, the calculation is given verbatim below. The approach begins by an examination of the flow at impeller discharge.

The radial velocity at impeller tip is calculated from continuity:

$$V_{r_2} = \frac{m}{\rho_2 A_2} \tag{A.8}$$

For a perfect gas we therefore get

$$V_{r_2} = \frac{m.R.T_2}{A_2 p_2} \tag{A.9}$$

We also have that $T_2 = T_{02} - \frac{V_2^2}{2.C_p}$ (A.10)

Together with $V_2 = \left(V_{t_2}^2 + V_{r_2}^2\right)^{1/2}$ (A.11)

this yields

$$\left(\frac{m^2 R^2}{2C_p A_2^2 p_2^2}\right) T_2^2 + T_2 - \left[T_{02} - \frac{V_t^2}{2C_p}\right] = 0 \tag{A.12}$$

where V_t is calculated from the Euler Turbine Equation for no prewhirl i.e.

$$V_{t_2} = \frac{(T_{02} - T_{01})C_p}{u} \tag{A.13}$$

One should note that the expression in the square brackets in A.12 is always positive. This implies that there is one positive and one negative solution to the above quadratic in T. As the temperatures are all measured absolute, our solution is clearly the positive of these.

We may now solve for the total discharge total pressure i.e.

$$M_2 = \left\{ \left[\frac{T_{02}}{T_2} - 1 \right] \frac{2}{\gamma - 1} \right\}^{\frac{1}{2}} \tag{A.14}$$

$$p_{02} = p_2 \left(1 + \frac{\gamma - 1}{2} M^2 \right)^{\frac{\gamma}{\gamma - 1}} \tag{A.15}$$

Pressure ratio and isentropic efficiency may then be calculated directly from equations (A.5) and (A.6) respectively.

A.2.2.3.iii Discussion of Method for Discharge Total Pressure Evaluation

The main assumption required for the above method is the prescription of the flow area at discharge. Here an estimate of blockage is required. Very little information was readily available for this impeller but the value was not expected to exceed 10% (based on the Herbert (1980) design program) and most likely to be approximately 5%.

If we therefore assume this value we should now attempt to assess the incurred error. This may be illustrated by examination of the impeller discharge velocity triangle. See Figure A.10.

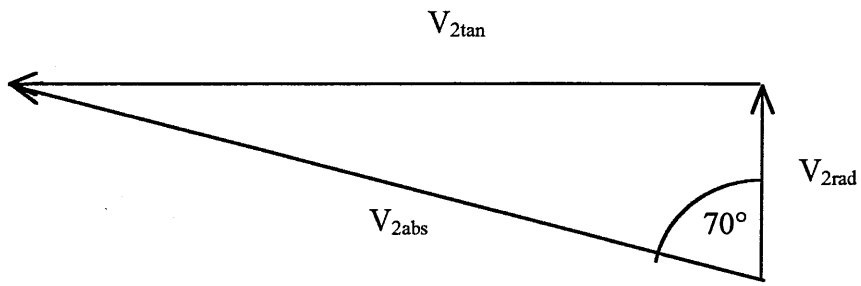


Figure A.10 Velocity Triangle at Impeller Discharge

For the design flow angle of approximately 70°, the ratio of the radial to tangential Mach numbers is:

$$M_{2tan}/M_{2rad} \approx 2.75$$

The Euler turbine equation gives us the tangential term and this is independent of the tip blockage. Therefore any errors in blockage prescription would manifest themselves only as a perturbation in radial Mach number.

From Figure A.10 we have

$$M_2 = \sqrt{M_{2\tan}^2\left(1+\frac{M_{2rad}^2}{M_{2\tan}^2}\right)}$$

Assuming a 5% error in blockage this results in approximately an error of 0.033% in absolute discharge Mach number equating to 0.04% in total pressure.

A.3. ACCURACY AND ERROR ESTIMATES

In sections A.1 and A.2 the instrumentation required to evaluate the compressor performance was described together with associated errors. Assuming operation at the 100% speed design point and judiciously selecting the possible extreme values for each measurement, the overall errors could be estimated. These were as follows:

Table A.4 Errors in Overall Performance

Mass Flow	± 0.02 kg/sec(±0.5%)
Total Pressure Ratio	± 0.050
Isentropic Efficiency	± 0.62%

A.4. LOCATION OF DETAILED STATIC PRESSURE TAPPINGS

For the vaned diffuser arrangement, static tappings were placed on the impeller shroud (15 equi-spaced on meridional profile) and on the shroud side of the vaned diffuser (10 radially equi-spaced extending from impeller tip to 130% of the impeller radius). See Figure A.11. The location of static pressure tappings for the pipe diffusers is given in Figure A12 to A15. All of these values of pressure were recorded using the scanivalve system at each operating point. Section A.5 tabulates the computer storage details for these points.

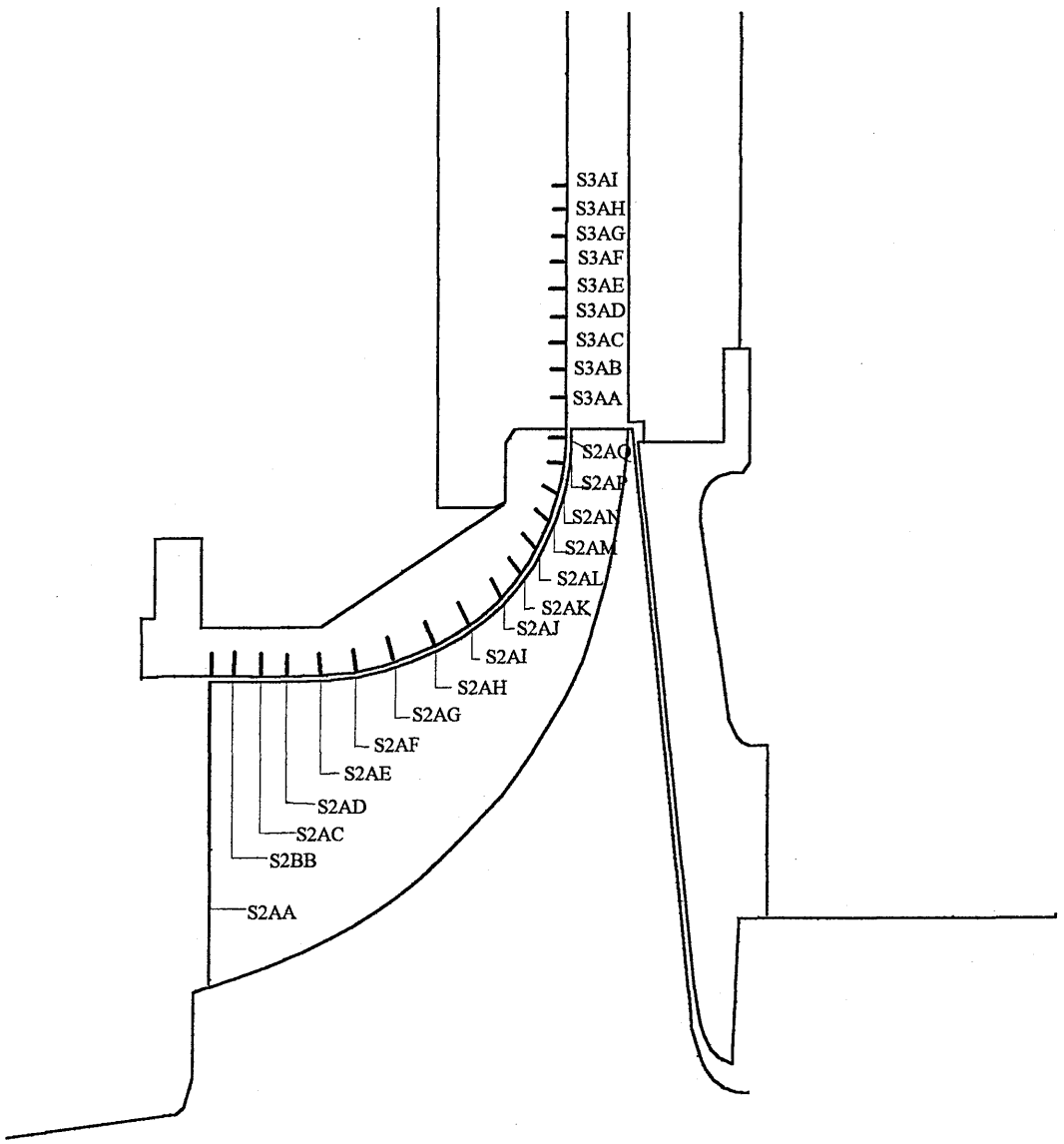


Figure A.11 Shroud Static Tapping Locations

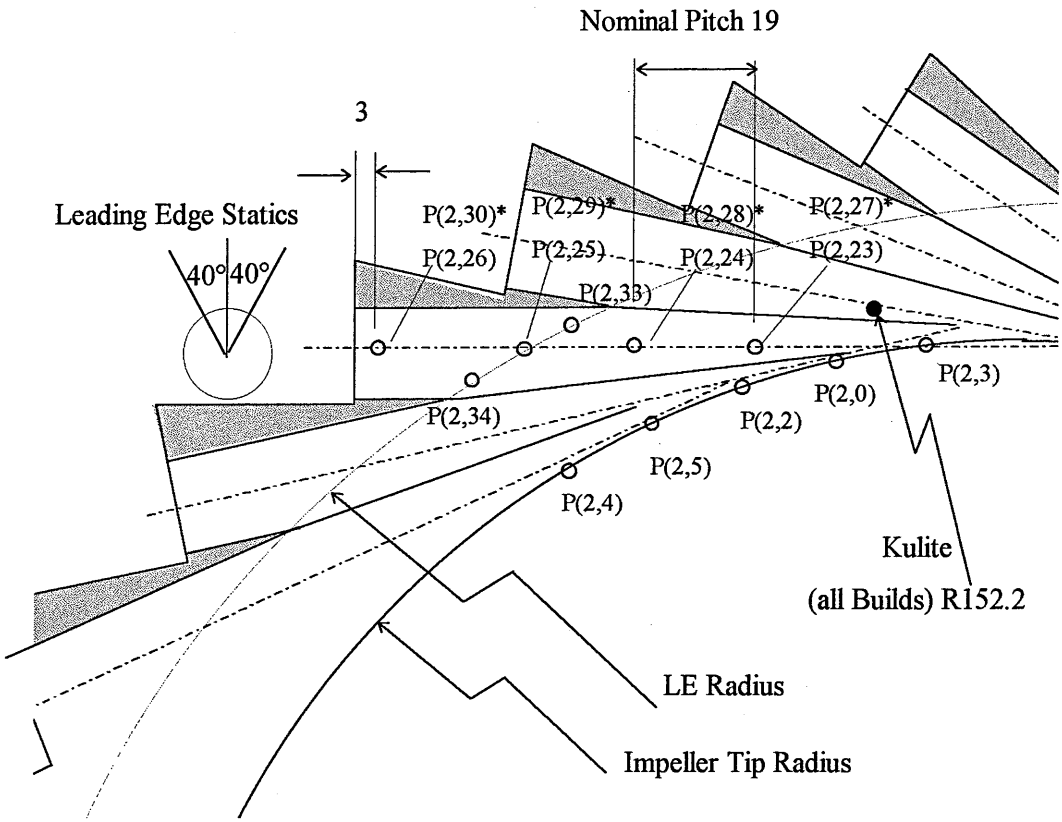


Figure A.12 31 (Circular) Pipe Diffuser Measurement Locations

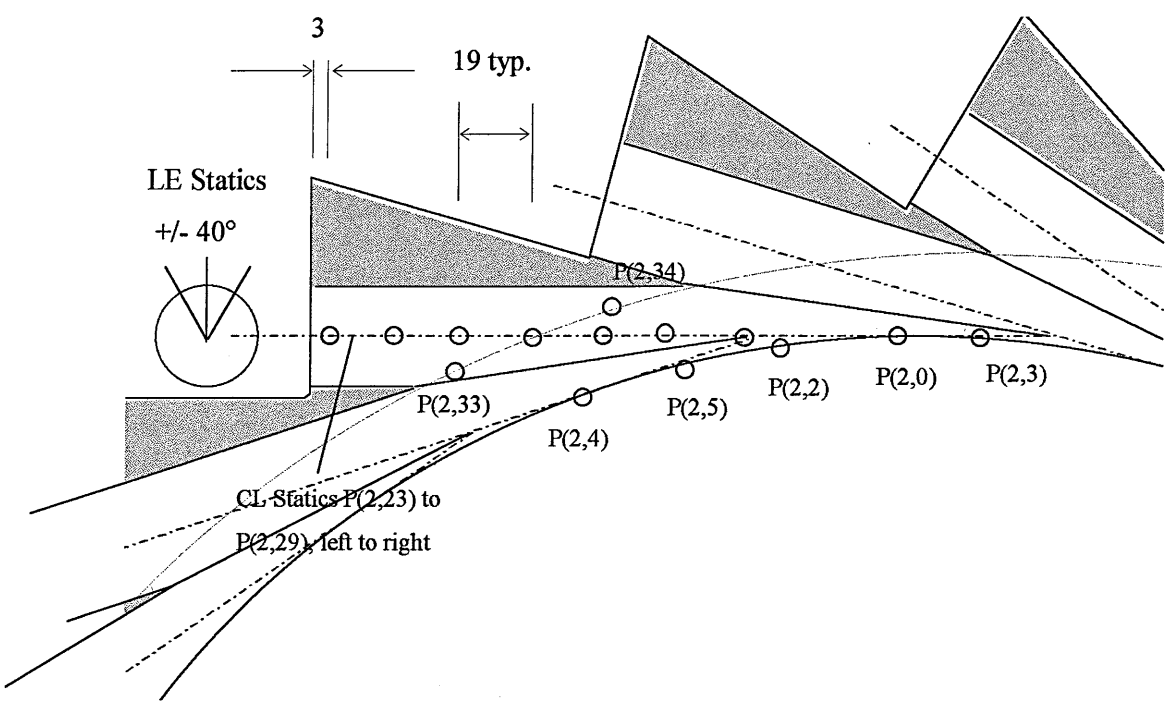


Figure A.13 22 (Circular) Pipe Diffuser Measurement Locations

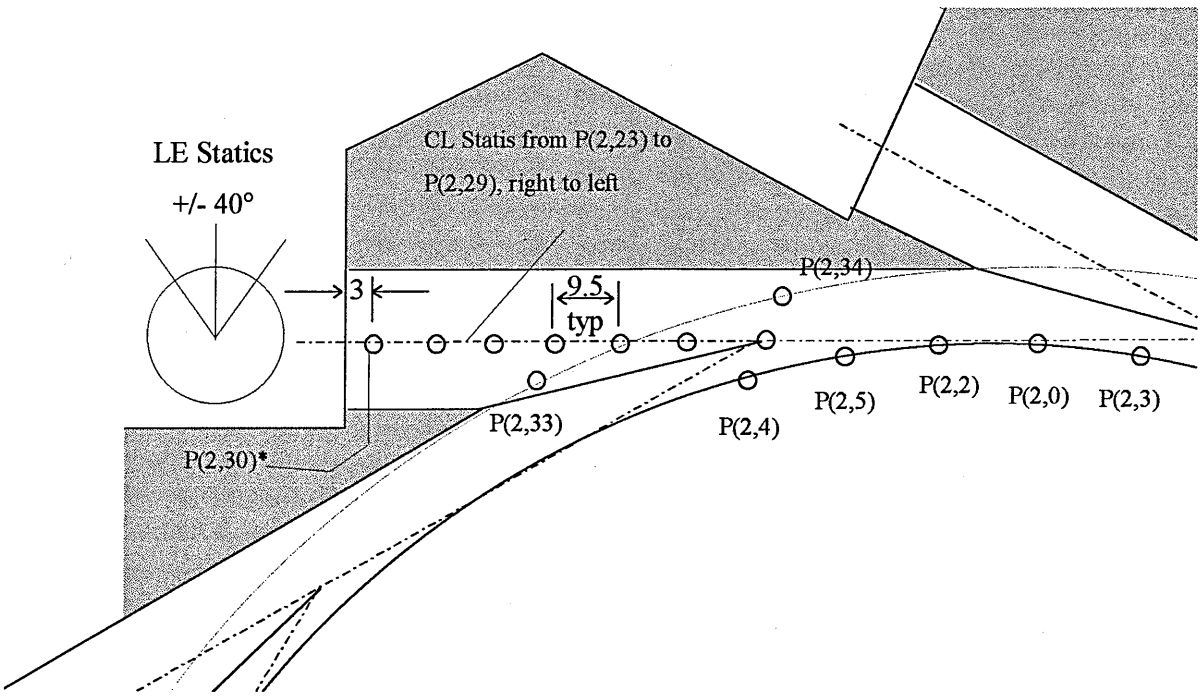


Figure A.14 13 (Circular) Pipe Diffuser Measurement Locations

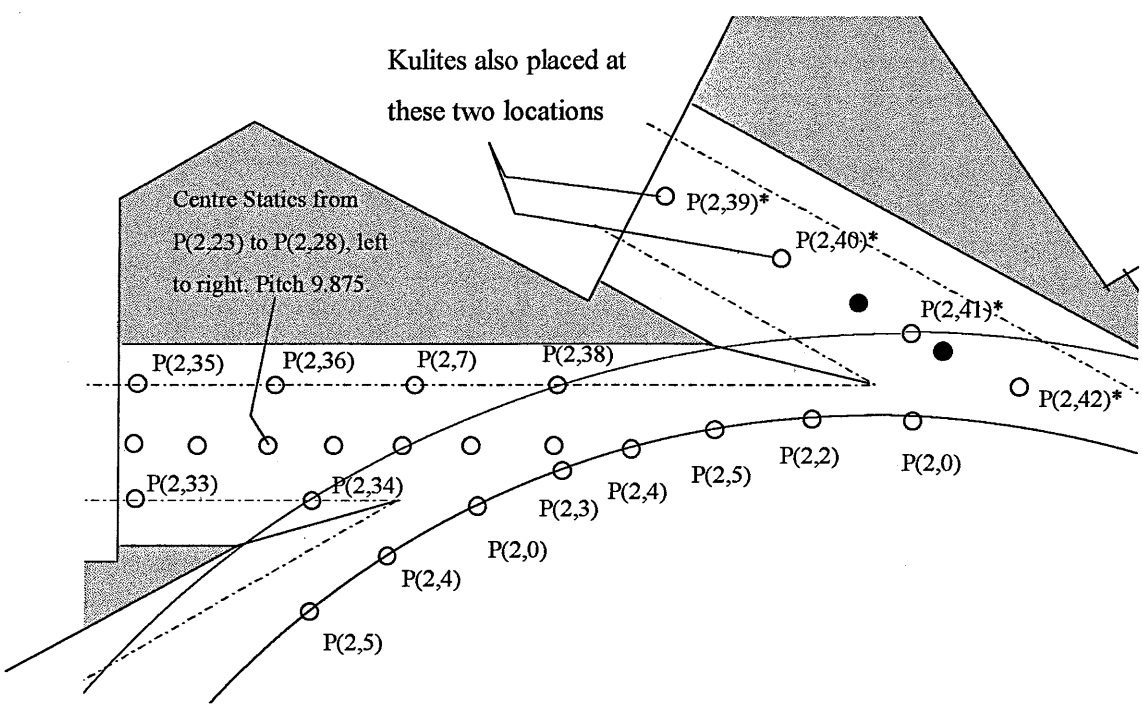


Figure A.15 13 (Oval) Pipe Diffuser Measurement Locations

A.5. MEASUREMENT LOCATIONS

Table A.5 Pressure Instrumentation Schedule

ITEM	DESCRIPTION	RANGE	S/V CHAN.	PORT No.	COMP. ADDR.	REMARKS
1	Inlet bellmouth static pressure	0-1 Bar	-	-	Pin	Separate Serial Port Connection
2	Scanivalve 1 Offset	± 3.4 BarG	s/v 1	1	P(1,1)	
3	Scanivalve 2 Offset	± 3.4 BarG	s/v 2	1	P(2,1)	
4	Inlet Stagnation pressure rake 1	± 3.4 BarG	s/v 1	2	P(1,2)	Probe nearest to centerline
5	Inlet Stagnation pressure rake 1	± 3.4 BarG	s/v 1	0	P(1,0)	Position used in monitor scan
6	Inlet Stagnation pressure rake 1	± 3.4 BarG	s/v 1	3	P(1,3)	
7	Inlet Stagnation pressure rake 1	± 3.4 BarG	s/v 1	4	P(1,4)	Probe nearest to wall
8	Inlet Stagnation pressure rake 2	± 3.4 BarG	s/v 1	5	P(1,5)	Probe nearest to centerline
9	Inlet Stagnation pressure rake 2	± 3.4 BarG	s/v 1	6	P(1,6)	
10	Inlet Stagnation pressure rake 2	± 3.4 BarG	s/v 1	7	P(1,7)	
11	Inlet Stagnation pressure rake 2	± 3.4 BarG	s/v 1	8	P(1,8)	Probe nearest to wall
12	Inlet Stagnation pressure rake 3	± 3.4 BarG	s/v 1	9	P(1,9)	Probe nearest to centerline
13	Inlet Stagnation pressure rake 3	± 3.4 BarG	s/v 1	10	P(1,10)	
14	Inlet Stagnation pressure rake 3	± 3.4 BarG	s/v 1	11	P(1,11)	
15	Inlet Stagnation pressure rake 3	± 3.4 BarG	s/v 1	12	P(1,12)	Probe nearest to wall

16	Inlet Stagnation pressure rake 4	± 3.4 BarG	s/v 1	13	P(1,13)	Probe nearest to centerline
17	Inlet Stagnation pressure rake 4	± 3.4 BarG	s/v 1	14	P(1,14)	
18	Inlet Stagnation pressure rake 4	± 3.4 BarG	s/v 1	15	P(1,15)	
19	Inlet Stagnation pressure rake 4	± 3.4 BarG	s/v 1	16	P(1,16)	Probe nearest to wall
20	Exit Static Pressure 1	± 3.4 BarG	s/v 2	2	P(2,2)	
21	Exit Static Pressure 2	± 3.4 BarG	s/v 2	3	P(2,3)	
22	Exit Static Pressure 3	± 3.4 BarG	s/v 2	0	P(2,0)	Used in monitor scan
23	Exit Static Pressure 4	± 3.4 BarG	s/v 2	4	P(2,4)	
24	Exit Static Pressure 5	± 3.4 BarG	s/v 2	5	P(2,5)	
25	Shroud Static Pressure S2AA	± 3.4 BarG	s/v 2	6	P(2,6)	
26	Shroud Static Pressure S2AB	± 3.4 BarG	s/v 2	7	P(2,7)	
27	Shroud Static Pressure S2AC	± 3.4 BarG	s/v 2	8	P(2,8)	
28	Shroud Static Pressure S2AD	± 3.4 BarG	s/v 2	9	P(2,9)	
29	Shroud Static Pressure S2AE	± 3.4 BarG	s/v 2	10	P(2,10)	
30	Shroud Static Pressure S2AF	± 3.4 BarG	s/v 2	11	P(2,11)	
31	Shroud Static Pressure S2AG	± 3.4 BarG	s/v 2	12	P(2,12)	
32	Shroud Static Pressure S2AH	± 3.4 BarG	s/v 2	13	P(2,13)	
33	Shroud Static Pressure S2AI	± 3.4 BarG	s/v 2	14	P(2,14)	
34	Shroud Static Pressure S2AJ	± 3.4 BarG	s/v 2	15	P(2,15)	

35	Shroud Static Pressure S2AK	± 3.4 BarG	s/v 2	16	P(2,16)	
36	Shroud Static Pressure S2AL	± 3.4 BarG	s/v 2	17	P(2,17)	
37	Shroud Static Pressure S2AM	± 3.4 BarG	s/v 2	18	P(2,18)	
38	Shroud Static Pressure S2AN	± 3.4 BarG	s/v 2	19	P(2,19)	
39	Shroud Static Pressure S2AO	± 3.4 BarG	s/v 2	20	P(2,20)	
40	Shroud Static Pressure S2AP	± 3.4 BarG	s/v 2	21	P(2,21)	
41	Shroud Static Pressure S2AQ	± 3.4 BarG	s/v 2	22	P(2,22)	
42	Vaneless Diffuser Static Pressure S3AA	± 3.4 BarG	s/v 2	23	P(2,23)	
43	Vaneless Diffuser Static Pressure S3AB	± 3.4 BarG	s/v 2	24	P(2,24)	
44	Vaneless Diffuser Static Pressure S3AC	± 3.4 BarG	s/v 2	25	P(2,25)	
45	Vaneless Diffuser Static Pressure S3AD	± 3.4 BarG	s/v 2	26	P(2,26)	
46	Vaneless Diffuser Static Pressure S3AE	± 3.4 BarG	s/v 2	7	P(2,27)	
47	Vaneless Diffuser Static Pressure S3AF	± 3.4 BarG	s/v 2	8	P(2,28)	
41	Vaneless Diffuser Static Pressure S3AG	± 3.4 BarG	s/v 2	9	P(2,29)	
42	Vaneless Diffuser Static Pressure S3AH	± 3.4 BarG	s/v 2	0	P(2,30)	
43	Vaneless Diffuser Static Pressure S3AI	± 3.4 BarG	s/v 2	1	P(2,31)	
44	Vaneless Diffuser Static Pressure S3AJ	± 3.4 BarG	s/v 2	2	P(2,32)	

APPENDIX B
Detailed Instrumentation

Traverses were carried out using a both a pneumatic total-pressure probe and a pressure transducer arranged to measure total pressure. These are described in turn.

B.1. PNEUMATIC PRESSURE PROBE

For simplicity, a plain tube arrangement was chosen (see Figure B.1), which had the added advantage of being relatively cheap to manufacture and of minimal frontal blockage. As it was envisaged to use this probe to get flow direction as well as total pressure, the entrance plane of the probe was filed square in order to increase the angular sensitivity.

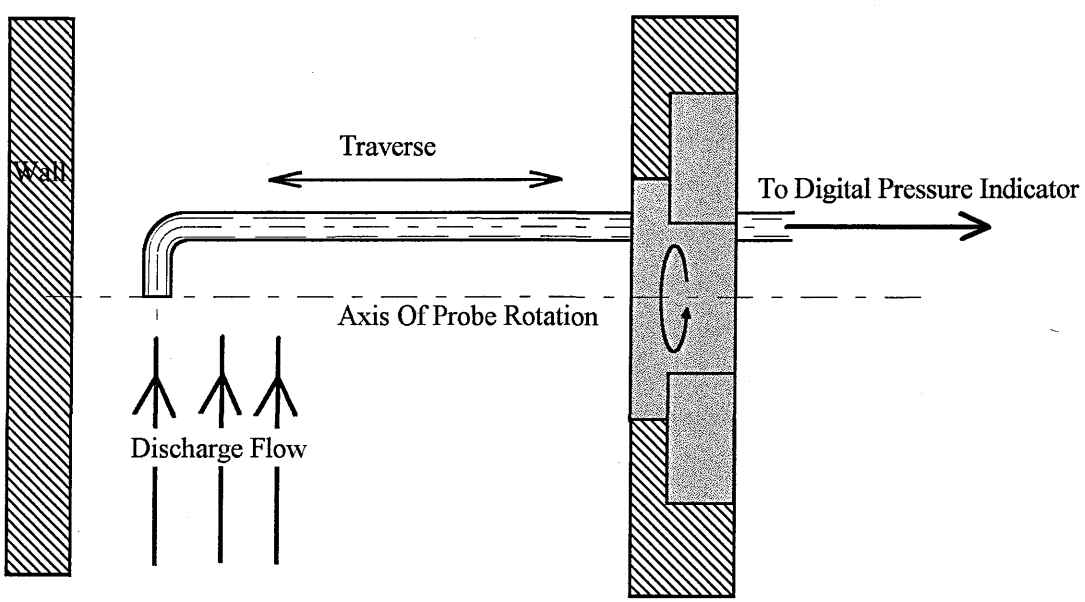


Figure B.1 Plain Tube Traverse Arrangement

The final design was effected by the following factors:

B.1.1 SIZE

In order to measure within the pipe diffuser throats without disturbing the flow, it was necessary to use a probe with minimum exposed cross-section. The nearly sonic Mach numbers within the pipes meant that even a relatively small blockage could cause the targeted pipe passage to choke prematurely. This was of particular concern as the pipe

cross-sectional-area to be traversed was itself small, sized to nominally match the impeller tip width of 12.3mm. Figure B.2 shows the effect of probe diameter on the effective blockage if placed within the throat of a 12.3mm diameter pipe.

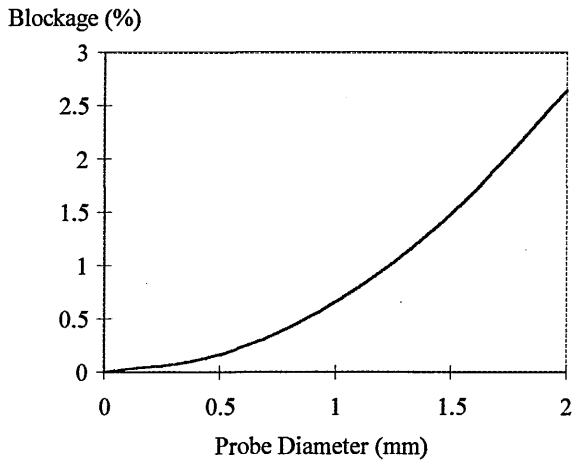


Figure B.2 Pipe Flow Area Blockage as a function of Probe Diameter

From previous published work on diffusers, aerodynamic throat blockages from approximately 5% to 15% were expected, but more commonly around the mean value of 10%. Using Figure B.2, it is clear that even small measurement probe diameters would have significant contribution to the blockage. As a compromise it was decided to set a maximum probe diameter of 1.5mm equating to a contribution of 1.5%.

Finally, it should be noted that the offset head design removed the possible of additional blockage due to the probe support tube.

B.1.2 MECHANICAL INTEGRITY, STATIC AND DYNAMIC ANALYSIS

The probe was to be subjected to large fluctuating aerodynamic loads and should a failure occur, the debris could impinge on the impeller tip causing unrecoverable damage. As a precaution, an analysis was completed to assess the structural integrity of the potential design and to size the diameter of the probe.

B.1.2.1 MECHANICAL LOADINGS

Body forces are assumed negligible and the worst loading scenario is prescribed as that when the flow is normal to the probe sensing face area, measuring at impeller discharge at 100% of design speed.

In addition, is assumed that the largest traverse is 22mm (this is the 'bare' passage width downstream of the diffuser modules)

The complete probe assembly load model is shown below in Figure B.3.

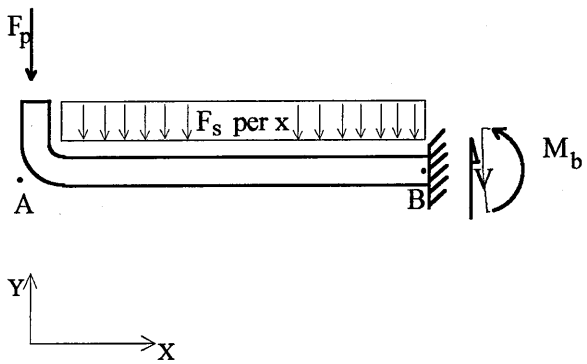


Figure B.3 Aerodynamic Loading on Probe

B.1.2.2 AERODYNAMIC FORCES ACTING:

Force per unit length along support tube = $F_{A_1} = \frac{1}{2}\rho_a v^2 2r_s C_{D_s}$

Force due to flow normal to head = $F_{A_2} = \frac{1}{2}\rho_a v^2 A_p C_{D_p}$

For the two different shapes, Fox and McDonald (1985) give the following empirical drag constants

$C_{D_s} = 1.2$ and $C_{D_p} = 1.17$

The former is based on a Reynolds number of 1×10^5, using predicted impeller discharge conditions and a shaft diameter of 3mm.

Assuming an encastré boundary condition at the support, the maximum normal stress may then be evaluated from:

$$\sigma_{max} = -\frac{r_2 M_B}{I} \qquad \text{-(B.1)}$$

where the 2nd moment of area for the tube cross section is given by:

$$I = \frac{\pi}{4}\left(r_2^4 - r_1^4\right)$$

and the moment at the support is simply:

$$-M_B = \frac{1}{2}x^2.F_s + x.F_p \qquad \text{-(B.2)}$$

For small deflections this gives

$$-E.I\frac{d^2v}{dx^2} = \frac{x^2}{2}F_s + x.F_p$$

$$-E.I\frac{dv}{dx} = \frac{x^3}{6}F_s + \frac{x^2}{2}.F_p + c_1$$

$$-E.I.v = \frac{x^4}{24}F_s + \frac{x^3}{6}.F_p + c_1.x + c_2$$

solving together with the following encastré boundary conditions:

$$x = l,\ \frac{dv}{dx} = 0 \qquad \Rightarrow \qquad c_1 = -\frac{l^3}{6}F_s - \frac{l^2}{2}F_p$$

$$x = l,\ v = 0 \qquad \Rightarrow \qquad c_2 = -\frac{l^4}{8}F_s - \frac{l^3}{3}F_p$$

Substituting back into the above we get

Maximum vertical displacement, $v_{\max} = -\frac{1}{E.I}\left(F_s\frac{l^4}{8} + F_p\frac{l^3}{3}\right)$ -(B.3)

and the maximum slope, $\varphi_{(radians)} = \left.\frac{dv}{dx}\right|_{x=0} = \frac{1}{EI}\left(F_s\frac{l^3}{6} + F_p\frac{l^2}{2}\right)$ -(B.4)

The above relations were checked using superposition theory against standard load cases given in Crandall et al (1984).

B.1.2.3 STRUCTURAL DYNAMICS

Approximate beam models were used (see Roark (1975))

For the first planar mode $f_p = \frac{1.732}{2\pi}\sqrt{\frac{E.I.g}{Wl^3 + 0.236wl^4}}$ -(B.5)

where the first term in the denominator is the support tube distributed loading (per unit length) and the second is for an end load. Here this is the aerodynamic force acting on the right angle portion of the probe.

For the torsional mode $f_t = \frac{1.57}{2\pi}\sqrt{\frac{GK}{J_s l}}$ -(B.6)

where the total distributed inertia, $J_s = \frac{1}{2}m\left(r_2^{\,2} - r_1^{\,2}\right)$

and the torsional stiffness constant, $K = \frac{1}{2}\pi\left(r_2^4 - r_1^4\right)$

B.1.2.4 DESIGN STRESS

Stainless steel type AISI 304 was used due to its corrosion resistant qualities and pre-formed availability. The following physical properties available are shown in Table B.1

Table B.1 Properties of AISI 304 Stainless Steel

Temperature °C	UTS (MPa)
17	515- 2240
175	448- 1949

In order to gain properties at the maximum flow temperature of 235°C, linear interpolation was used. From a comparison with similar stainless materials, this was

thought conservative. An additional factor of safety was introduced by using the lower bound values of the tabulated stress ranges.

To protect the probe against fatigue, the design stress was set at the endurance limit, prescribed at 40% of UTS, i.e. 169 MPa.

B.1.2.5 Analysis of Preliminary Design Sizing Exercise

Using the design equations detailed above, a table of results for a variety of potential stainless-steel tubes are given in Table 2.

Table B.2 Design Criteria for Probe

Standard Gauge No	Outside Diameter (mm)	Inside Diameter (mm)	$f_{torsional}$ (Hz)	f_{planar} (Hz)	Curvature (°)	Displacement (mm)	Max Stress σ_{max} (MPa)
16	1.65	1.2	29.1K	321	1.22	0.35	393
14	2.05	1.55	28.1K	439	0.66	0.19	267
13	2.34	1.77	28.1K	539	.44	0.12	203
12	2.65	2.0	28.2K	657	.30	0.085	157
125	2.65	2.1	26.7K	622	0.33	0.095	175
11	2.95	2.3	27.2K	750	0.23	0.065	135
10	3.3	2.5	28.0K	921	0.15	0.044	101
8	4.04	3.28	28.5K	1459	0.061	0.017	54
6	4.98	4.07	25.5K	1579	0.052	0.0052	53

Taking each column in turn:

The first three denote cross-sectional dimensions. Our earlier stipulation implied that we should not exceed 1.5mm in diameter.

The fourth examining torsional vibration, shows much higher frequencies than those of the blade passing tone of 9.9kHz for the impeller. However, the opposite is true for the fundamental plane-wise mode. In this shape the probe vibrates at much lower frequencies. Normally we would expect frequencies of twice or, to be very safe, three times the natural to be unable to excite to destruction. At approximately 50 times less than the blade passing frequency the probe is considered 'safe' and unaffected by the forcing excitement.

The displacements due to loading (both curvature and linear) are also tabulated. For all tube diameters examined, these displacements are considered acceptable as we would only expect to measure approximately 3.6mm (≈2.5% tip radius) from the impeller discharge.

The final column imposes the greatest restriction. This is the bending stress evaluated at the encastré support end of the probe. In order to use AISI 304 stainless steel the

probe support must be at least 12 gauge. This however imposes a large blockage at the measurement plane. To overcome this difficulty, the probe was constructed from two diameters. The main support portion consisted of 12 Gauge tubing, into which an inner portion 0.9mm diameter was inserted (See Figure B.4). The arrangement therefore has the structural rigidity and strength required together with the advantage of a small measurement head cross-section.

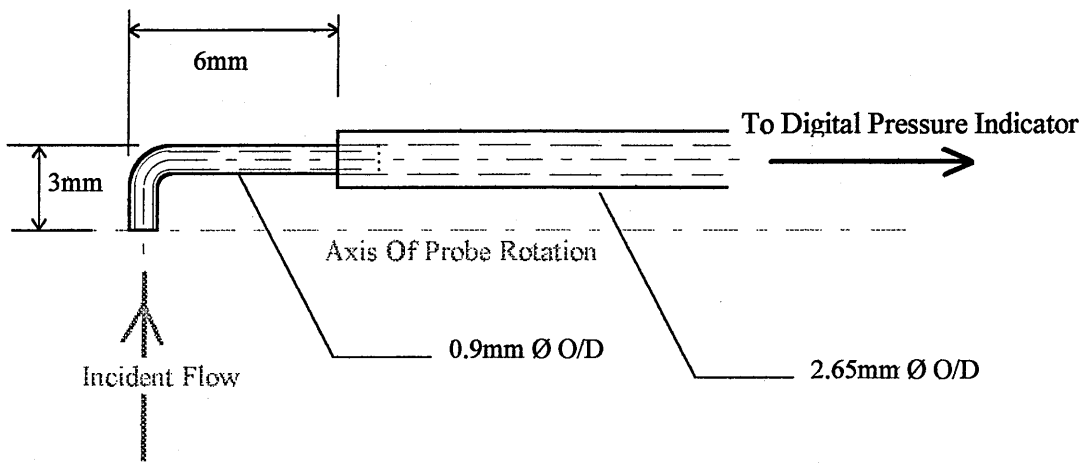


Figure B.4 Sketch of Pneumatic Probe used in Pipe Throat and Impeller Discharge Traverses

B.1.3 CALIBRATION OF THE PNEUMATIC PROBES

B.1.3.1 PRESSURE MEASUREMENT

Pressure, both during calibration and testing, was measured via a long flexible tube (>3m long) connected to a Druck Digital Pressure Indicator (See Table B.3).

Table B.3 Pneumatic Instrumentation Accuracy

Type	Druck DPI 101
Deviation	0.033% FSD
Zero Drift	0.0035 %FSD/°C
Range	700 kPa Gauge

The instrument was connected via an RS232 serial type connector to an ADC card located within a PC. This allowed automated data acquisition during the experimental phase of testing. A large LCD display on the DPI gave an additional reassuring readout.

B.1.3.2 ANGULAR CALIBRATION

All pneumatic total pressure probe angular calibrations were carried out within a wind tunnel operating at up to a Mach number of 0.8 (Figure B.5).

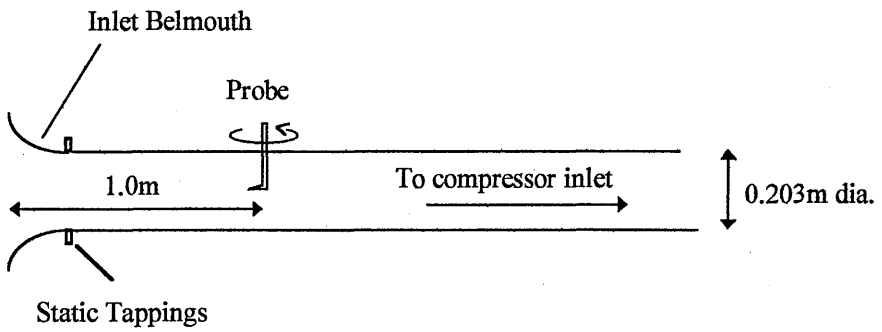


Figure B.5 Wind Tunnel Angular Calibration

The 'calibration' itself was only required to set a datum reference angle to compensate for any misalignment incurred during traverse assembly. The probe was mounted on a plane perpendicular to the flow and rotated at 10 deg increments about the axis shown in Figure B.5. A sample distribution is shown in polar form below (Figure B.6). The mean flow direction may be seen at a nominal 90 degrees.

The calibration was carried out every time the traversing gear was stripped to ensure consistent alignment. Offsets of up to 5 degrees were sometimes noted, justifying the time spent on this exercise.

B.1.3.3 DETERMINATION OF THE MEAN FLOW DIRECTION

A 2nd order polynomial curve fit was used to determine the flow direction for both the wind tunnel angular calibration and during experiment. i.e.

$$p = \sum_{i=1}^{3} a_i \theta^{(i-1)} \qquad \text{-(B.7)}$$

where θ is the indicated measurement angle, p is the total pressure and the a_i's are the unknown constants, solved using Singular Value Decomposition (SVD) (Press (1989)). During compressor testing the author only found the confidence to use this expression by incorporating a graphical interface into his curve fitting program that allowed the scrutiny and possible manual override of each curve fit. This precaution was well justified as during testing there were occasional spurious curve fits. Despite this, the robust SVD algorithm never caused the data acquisition program to 'crash'. A sample curve fit (for the distribution shown in Figure B.6) is given in Figure B.7.

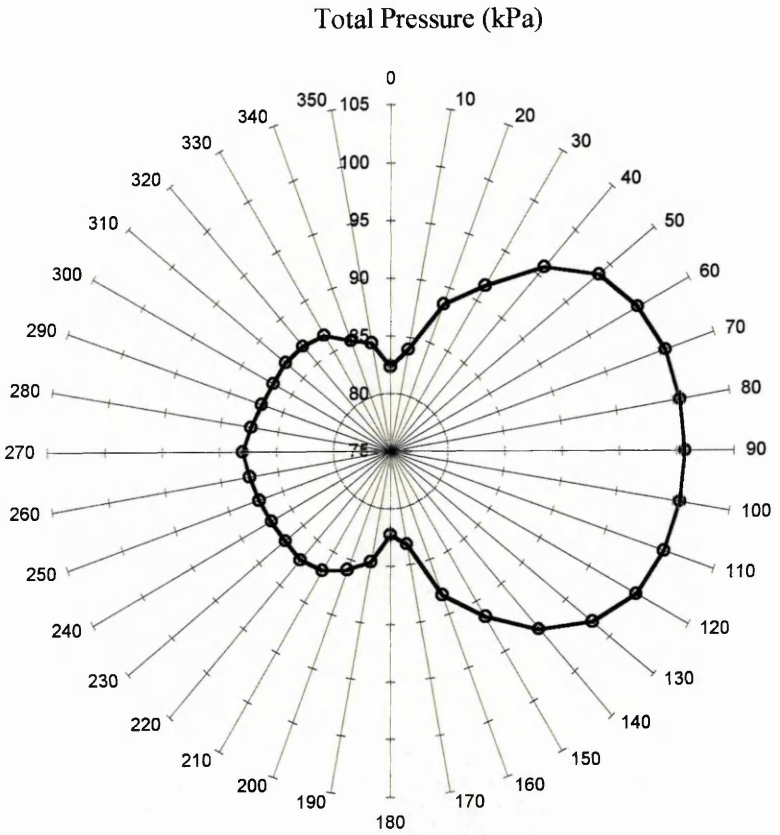


Figure B.6 A Sample Total Pressure Pneumatic Probe Polar Plot

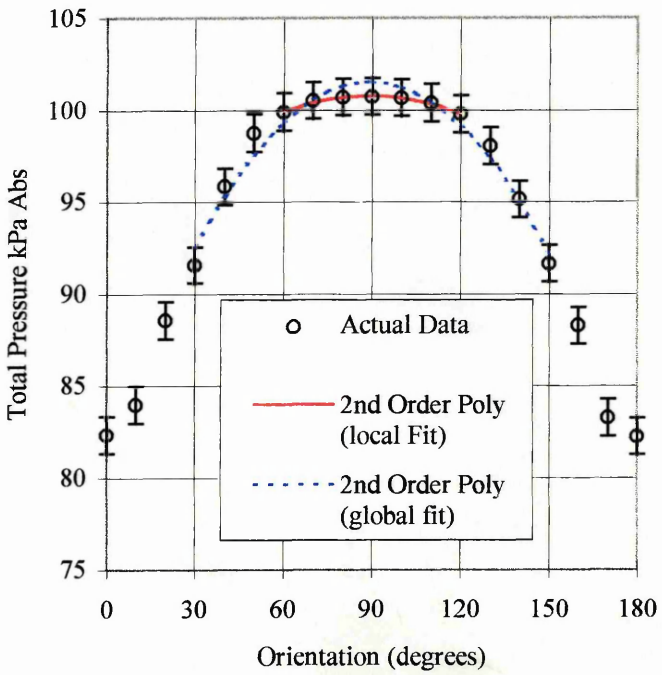


Figure B.7 Angular Calibration of Pneumatic Probe

Note that two curve fits are plotted. Although both are 2nd order polynomial equation curve fits, each was correlated from different ranges. The 'Local Fit' is the range that the data acquisition program would use to find the flow angle during testing. The second, designated 'Global Fit', was fitted over a wider range (from 30 to 150°) and was used for angular calibration. The latter shows a slight over-shoot at the peak but was considered to yield a more accurate datum angle due to the probe's increased angular sensitivity at larger incidences. This factor is described further in the next section

B.1.3.4 IMPORTANCE OF ANGULAR RANGE IN CALIBRATION AND TESTING

If we introduce an angular sensitivity parameter, dp/d(theta), and plot this against theta for our sample data we can see that, as may be intuitively expected, that the probe has little angular sensitivity near the mean flow direction (Figure B.8). This is one of the main criticisms of this type of probe. Other types (e.g. wedge, pyramid, claw, cobra) are far superior in this insensitive region. However, as long as large angle perturbations (around 20 to 40 degrees) are present then this major deficiency is overcome. Therefore, for both calibration and experimental operation, measurements were always recorded over wide angular ranges. For calibration, normally the range extended ±90° of the mean flow direction; during experiment this was reduced to ±30°. In both cases, pressures were recorded in steps of 10°.

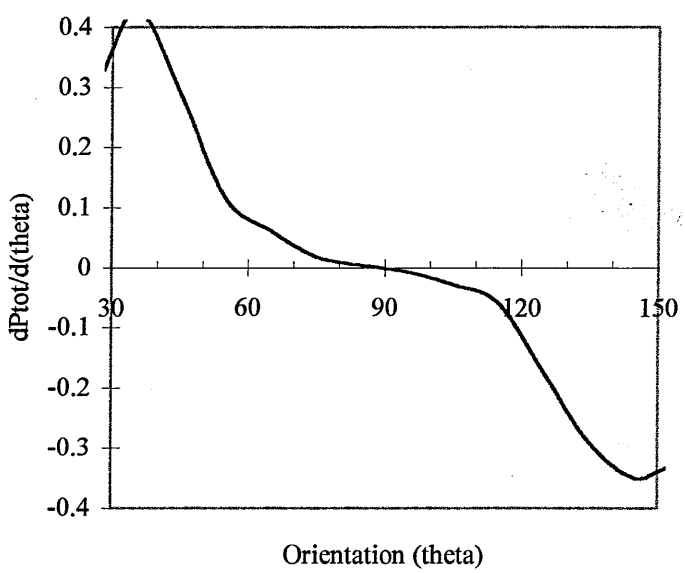


Figure B.8 Pneumatic Probe Sensitivity and Different Yaw Angles

B.1.3.5 ACCURACY OF THE CURVE FIT

A manual over-ride was always used during testing and this makes the estimation of errors difficult. However, from a great deal of experience in examining the data and the excellent correlation that has been found with other instrumentation it is estimated that the flow angle is accurate to ±2° and that the pressure error introduced by the incorrect angular specification is less than 2% of the velocity head. This pressure variation is more than 20 times more than that associated with the Druck DPI 101 and therefore the accuracy of the measurement system is estimated as 2% of the velocity head.

B.2. HIGH SPEED TOTAL PRESSURE TRANSDUCERS PROBES

In order to gain transient flow measurements at the compressor discharge, several Kulite XCE-062 High temperature Ultra-miniature pressure transducers were utilised. Specification of these is given in Table B.4.

Table B.4 Specification of Kulite Sensors

Type:	XCE-062
Pressure Range:	0-17 BarA ±0.02Bar
Max. Operating Temp.:	273°C
Natural Frequency:	900 kHz
Excitation Volts:	10V
Max Output:	100mV

These allowed measurements to be made at 100% design compressor speeds, and had a natural frequency of approximately 90 times higher than that of the impeller blade passing frequency.

B.2.1 MOUNTING OF SENSORS

There were several options available for mounting these transducers, the final choice was influenced by the following factors:

B.2.1.1 SENSITIVITY TO UNSTEADY FLOWS

It was necessary to simplify the arrangement to reduce the potential deleterious influence of unsteady flows. It is well documented and accepted in the literature that wedge type probes suffer from inaccuracies within unsteady flow fields due to unsteady aerodynamic effects. To compensate for these would require either an unsteady calibration or to ensure the 'natural frequency' of the combined probe arrangement was sufficiently higher than the expected excitation frequencies. Such a programme would be difficult and introduce an unacceptable time burden on this current programme.

B.2.1.2 ANGULAR SENSITIVITY

In order to measure the flow direction, it is necessary that the probe arrangement has sufficient angular sensitivity This was discussed earlier in section B.1.3.2.i for the pneumatic arrangement, but is equally applicable here. The conclusions were that a single total pressure sensor arrangement would only be suitable if readings were taken over a sufficiently large range.

B.2.1.3 SENSITIVITY TO WALL EFFECTS

Near-wall measurements are well known (e.g. Rees(1994)) to significantly effect the readings on claw and wedge type probe arrangements due to the complex interaction between the static and total tappings on the probe heads. Such effects are absent for a single sensor probe.

B.2.1.4 THERMAL AND VELOCITY GRADIENTS

Wedge, or pyramid probes with several sensor locations, whether of pneumatic or transducer type, are susceptible to errors induced by flow gradients. These probes are calibrated within uniform flow regimes and any deviation from these conditions introduces inaccuracies into the measurements.

B.2.1.5 CHOSEN CONFIGURATION

As the smallest transducer available was of 1.5mm diameter, it was felt that any additional fairing e.g. to form a cylindrical arrangement (minimum diameter possible approximately 3.5mm) or with additional transducers form a wedge type probe, would in both cases impose too much blockage on the flow.

Two single transducer configurations were tried and are shown below in Figure B.9. The upper featured a Kulite located within a hole drilled into the probe support stainless steel tube (12 Gauge). This design was not particularly successful - the strong unsteady flows at the discharge of the impeller were able to loosen the RTV (Room Temperature Vulcanising) rubber and through fatigue break the electrical connections.

The lower, and more successful design, featured some difficult pipe bending to ensure that at least half of the transducer was fully enclosed within the tubing. Again, RTV was used to fix the probe in place but in this instance the wires were safely placed within the tubing itself. This design has proven the most robust and to date has remained operational despite approximately 40 hours of run-time..

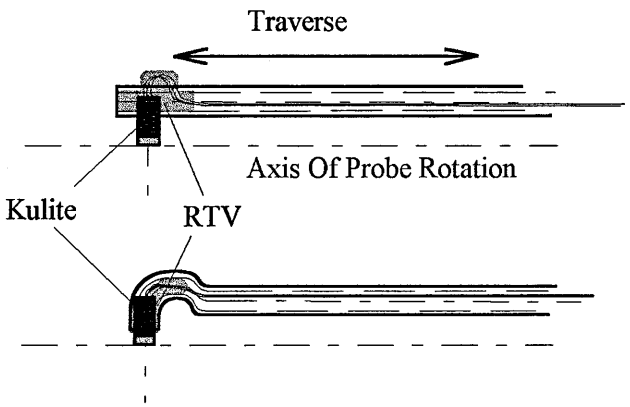


Figure B.9 Mounting Arrangements used for Kulite Probes

B.2.2 CALIBRATION

Ultra-miniature pressure transducers are notorious for temperature drifting. With operating temperatures ranging up to 250°C it was therefore necessary that a full calibration encompassing variation in both pressure and temperature was carried out for each probe.

B.2.2.1 APPARATUS

It was necessary to manufacture a pressure vessel that would allow heating to 250°C in a stable and controllable manner.

A large rectangular block of steel (200 × 100 × 75 mm) was used into which the mounted pressure transducer and a calibrated thermocouple were inserted. See Figure B.10. Together with insulation on top, and a variable power supply for the heater element, the above apparatus met all the design requirements. During calibration, particular attention was made to ensure that an equilibrium condition was reached prior to recording values.

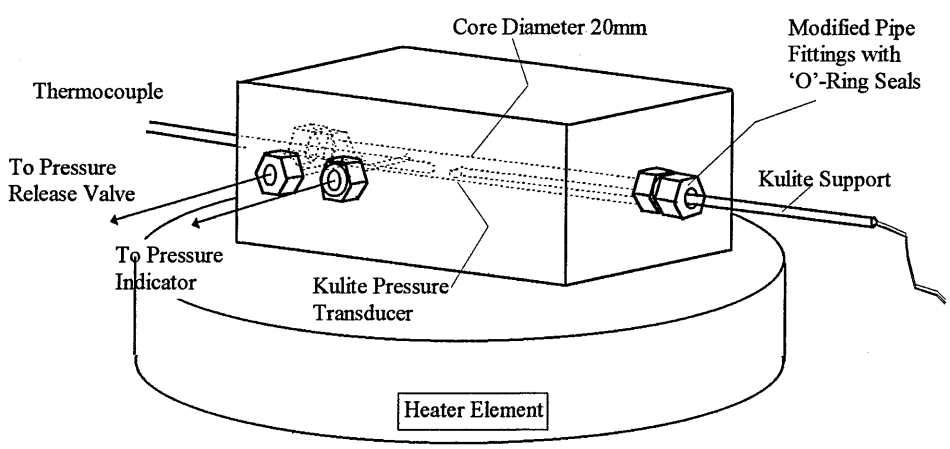


Figure B.10 Temperature/Pressure Calibration Apparatus

B.2.2.2 TEMPERATURE/PRESSURE

The Kulite sensor may be shown diagramatically as a whetstone bridge, and much like a strain gauge arrangement, it is on of these arms that are deflected on the application of an external pressure. In order to compensate for temperature, not one but two voltage measurements were required for each Kulite pressure transducer (See Figure B.11).

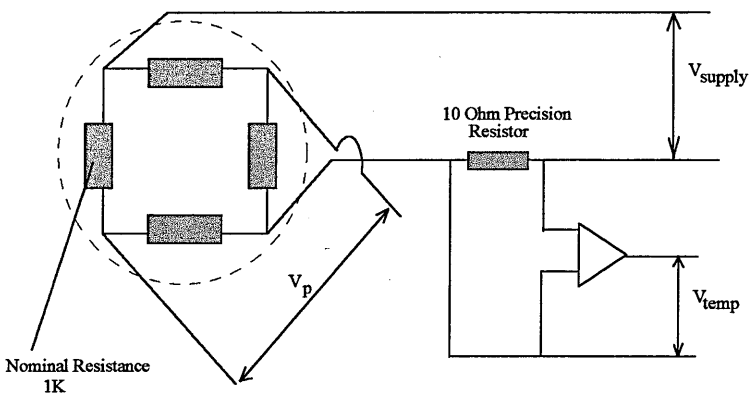


Figure B.11 Kulite Sensor Bridge Voltages

The first measured the potential across a 10 Ohm precision resistor, inserted in series with the bridge supply. This was a crude but effective method of measuring the bridge current accurately and it was shown experimentally that V_{temp} was only sensitive to temperature. Figure B.12 shows a sample calibration. These readings of V_{temp} and temperature were taken over a pressure range of 1-8 BarA, with very little scatter visible. The second channel detected the voltage across the bridge (V_p) which, after temperature correction, gave a unique total pressure. See Figure B.13

B.2.2.3 ANGULAR CALIBRATION OF KULITE PRESSURE TRANSDUCERS

The same angular calibration wind tunnel experiment used for the pneumatic probes was repeated here for the Kulite pressure transducers. However, some changes were needed to the curve-fit routines used for the pneumatic data due to some erroneous 'under-shoot' situations found when post-processing (see Figure B.14). Such results were only very occasionally detected (approximately in 2% of measurements) at the extremes of the angular measurement range. For the pneumatic data these errors could be corrected interactively using a computer program, however, this would be impractical for the unsteady Kulite work because of the large amount of data. As a consequence, further numerical studies were undertaken to find an accurate and robust method of

curve-fitting the unsteady data that would give reliable curve fits without the need for visual confirmation.

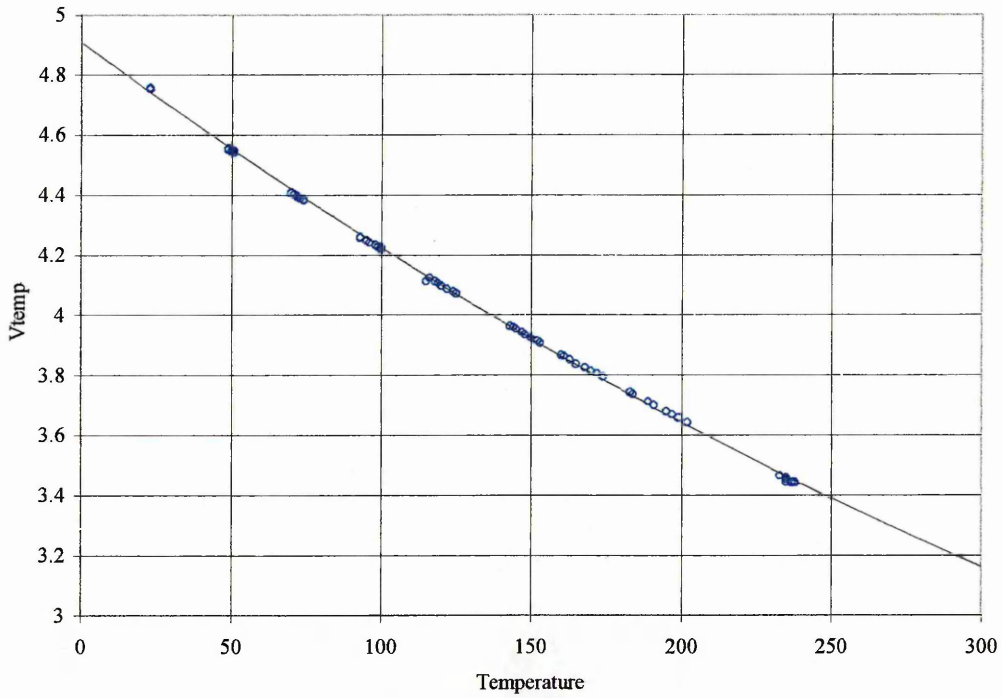


Figure B.12 Sample Temperature/Bridge 'Current' Relationship

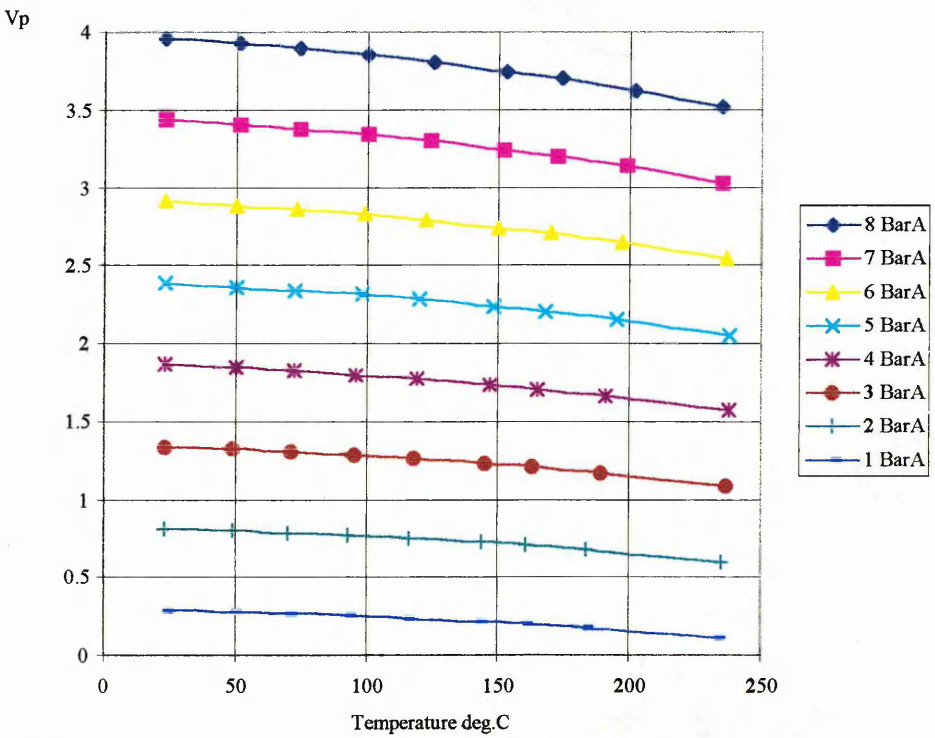


Figure B.13 Sample Corrected Pressure v Temperature Plot

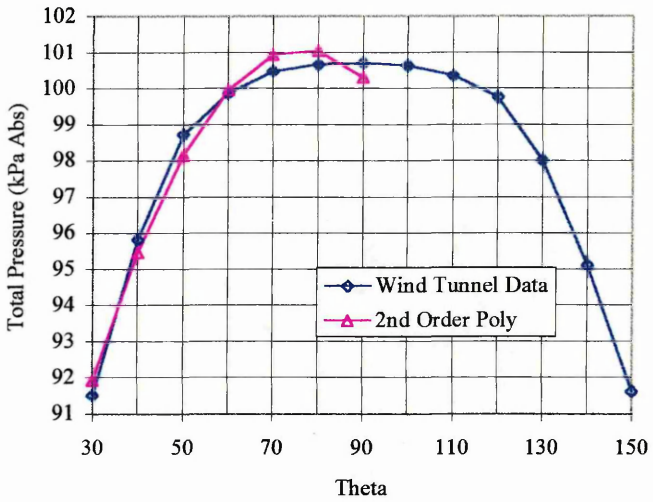


Figure B.14 *Pneumatic 'Overshoot' Example: Mean direction is 90° but curve fit gives 77°*

Using wind tunnel angular calibration data for the Kulite pressure transducers probes, curve fits of groups of seven data points spaced at 10° intervals were completed. These fits at the extreme angles showed similar trends as shown for the pneumatic arrangements (e.g. see Figure B.14 showing curve fit from 30° to 90°) and it was clear that an alternative trial function was necessary. Initially higher order polynomial schemes were considered but these could possibly introduce additional difficulties; as for example the mathematics of peak pressure detection and the possibility of further erroneous fits in alternative circumstances. Finally it was decided to use, what is essentially a polynomial of infinite order, a cosine function. This followed the shape of the experimental curve naturally over the ±60° range and had a template that had the 'stiffness' of having only a few unknown variables, such as found in the second order polynomial approximation.

The curve fit unknowns were found, again, using Singular Value Decomposition (SVD), primarily due to its robustness and resilience to unsuitable data. However, incorporation of the cosine trial function was only possible after some trigonometric manipulation as follows:

The SVD algorithm requires that the curve fit equation be expressed as a *linear* combination of trial functions i.e. of the form

$$y = \sum_i a_i f_i(x) \qquad \text{-(B.8)}$$

or in terms of pressure, P, and flow angle, θ we have

$$P = \sum_i a_i f_i(\theta) \qquad \text{-(B.9)}$$

where the a_i's are the unknown constants, $f_i(\theta)$ are the pre-defined functions. It is important to note that these functions themselves need *not* be linear.

The formulation was straightforward for the 2nd order polynomial case where the trial functions were $f_1(\theta)=1$, $f_2(\theta)=\theta$, $f_1(\theta)=\theta^2$ with the unknown a_i's, solved by SVD, giving the 2nd order polynomial required.

To introduce a cosine form, we can start with: $P=b_1+b_2\cos(\theta+b_3)$ -(B.10)

Expanding this we get

$P=b_1+b_2(\cos\theta\cos b_3-\sin\theta\sin b_3)$

This may be also written as

$P=a_1+a_2\cos\theta+a_3\sin\theta$ -(B.11)

where

$b_3=\tan^{-1}\left(\frac{a_3}{a_2}\right)$ -(B.12)

$b_2=\frac{a_2}{\cos b_3}$ -(B.13)

$b_1=a_1$ -(B.14)

The a_i's are the sought values, evaluated by the SVD algorithm. From these the b_i's may be found. The coefficient b_3 gives the flow angle at which the total pressure is a maximum (the zero datum) and (b_1+b_2) is the peak magnitude. The author did consider the possibility of using the value b_1 to evaluate the local static pressure (i.e. by interpolating for pressure at right angles to the flow). Unfortunately, this did not work and to continue would have most likely required calibration at a variety of Mach numbers for which facilities were not readily available.

Many millions of data points were to be taken using the Kulite probes and therefore it was necessary to ensure that the curve-fit algorithm used for flow direction evaluation did not require any visual interactive confirmation by the author. A series of checks were undertaken and are described below.

B.2.2.4 CURVE FITTING THE WIND TUNNEL DATA

Using wind tunnel angular calibration data as before, curve fits of groups of seven data point of 10° intervals were completed. The resulting curve fits were very pleasing and showed excellent prediction even when the flow was outside the angular range. Eight curve fits are shown in Figure B.15 with the mean of the scanned range varying from -30° to +30° of the actual mean.

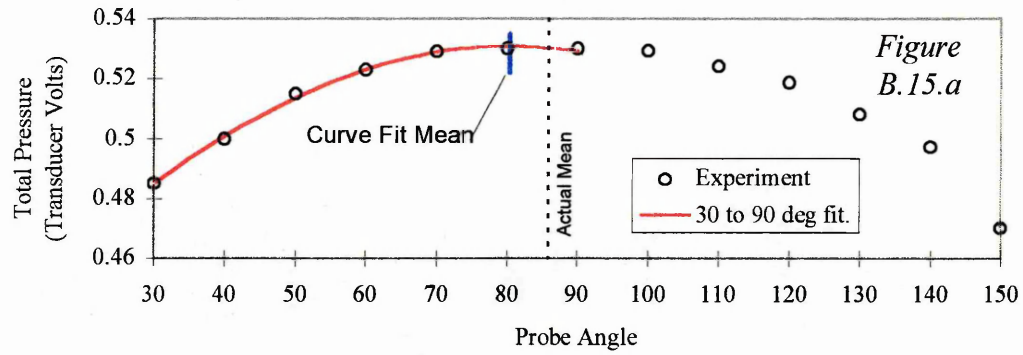


Figure B.15.a

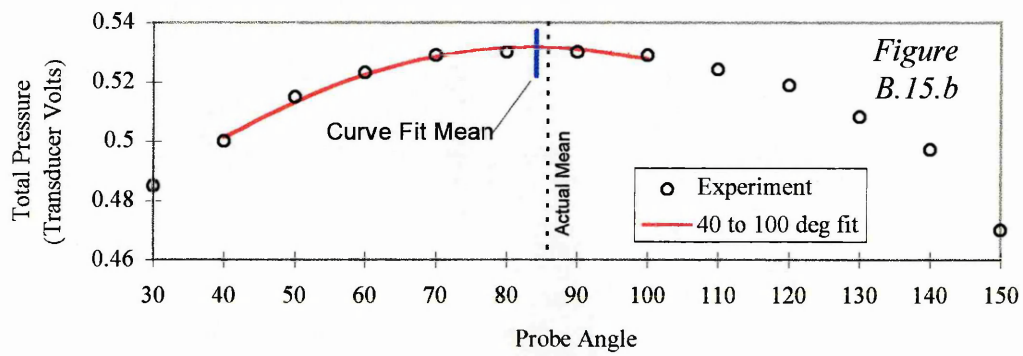


Figure B.15.b

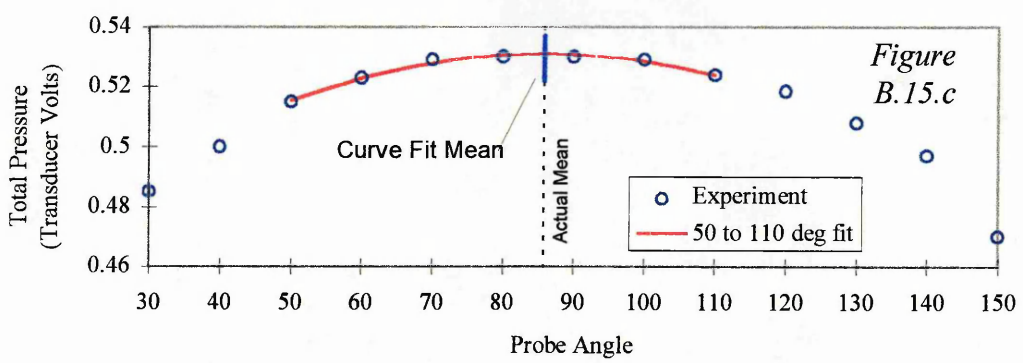


Figure B.15.c

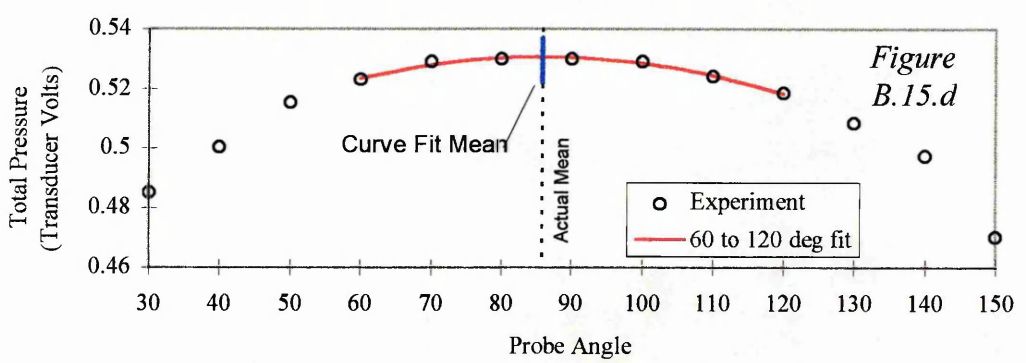


Figure B.15.d

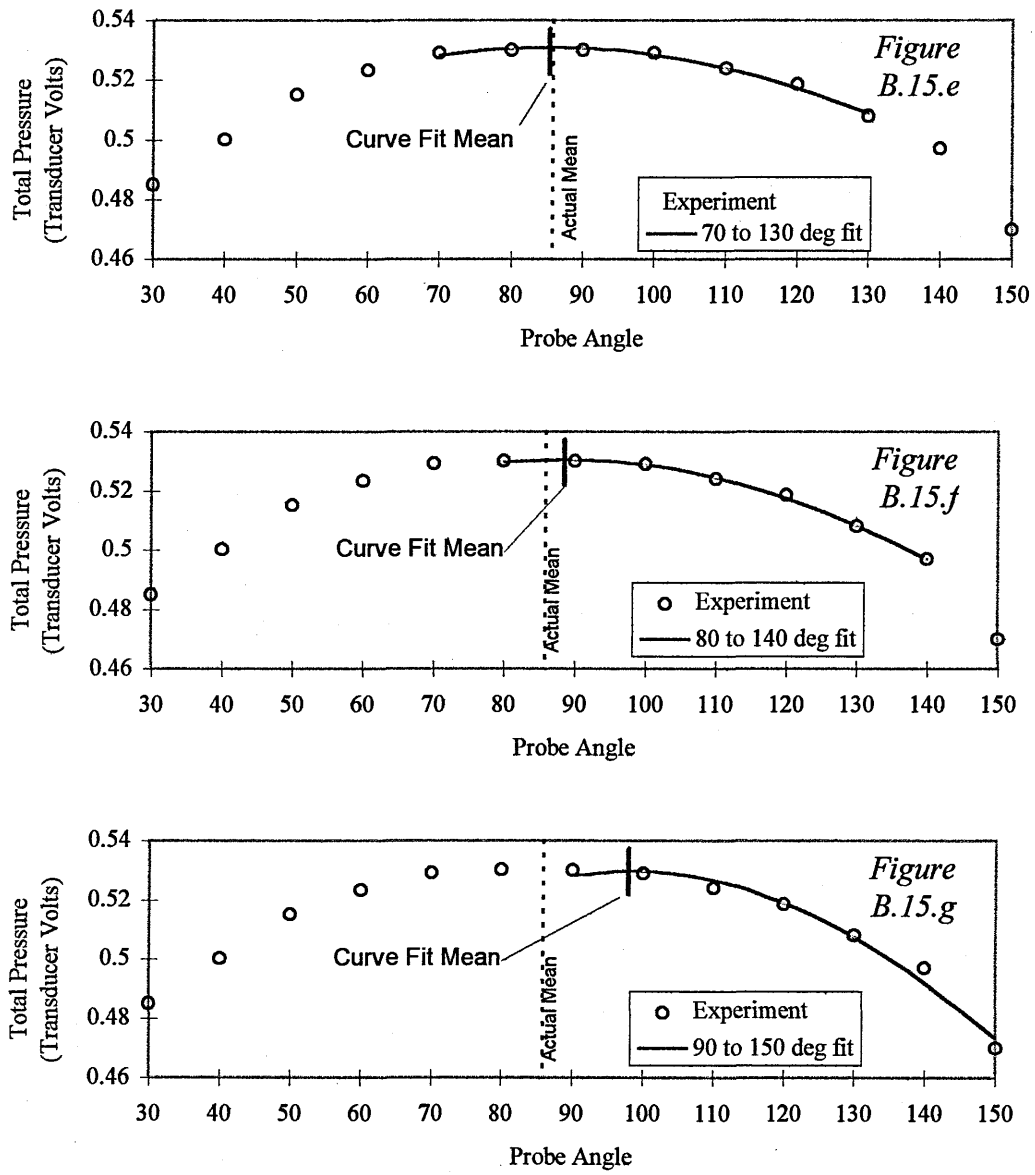


Figure B.15 Curve Fitting Kulite Wind Tunnel Angular Data

The calculated flow angles may be collectively plotted as shown in Figure B.16 and B.17.

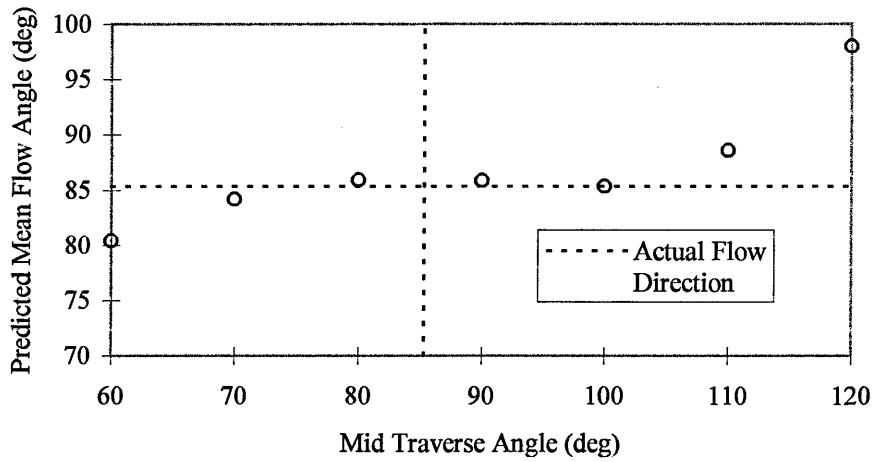


Figure B.16 Flow Angle Error

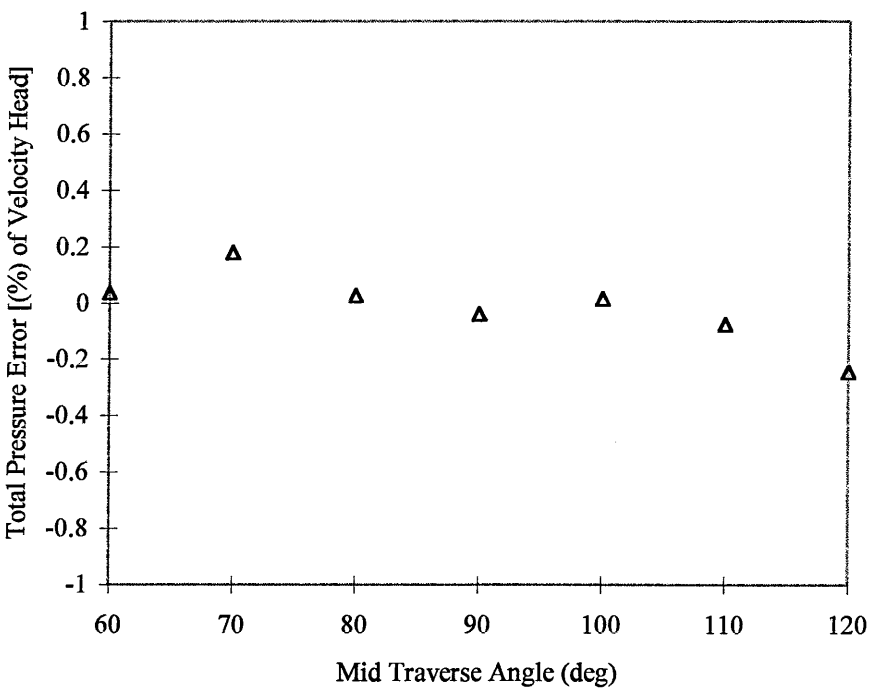


Figure B.17 Total Pressure Error

The angular error noted at the expected extreme flow angles (±30°) has been reduced from 13° to 7° using the cosine interpolation curve fit. The pressure error (as a percentage of velocity head) has also been reduced from 1.1% to 0.25%.

B.2.2.5 ERRORS IN CURVE FITTING

On traversing the complete impeller discharge over the whole 80% and 100% flow range, the maximum flow variation was only ±18½°, giving an estimated error of ±3° for all values recorded and post-processed. The total pressure error introduced by the curve fit is much lower than that for the probe itself and its contribution is neglected. Using the cosine curve-fit a small correction could be made to the predicted flow angle using Figures B.16 and B.17.

B.3. TRAVERSE GEAR

B.3.1 MECHANICAL DESIGN

In order to traverse the flow at the impeller discharge a mechanism was required that would allow both axial and rotational degrees of freedom, the latter for detecting the flow direction. See Figure B.18 below.

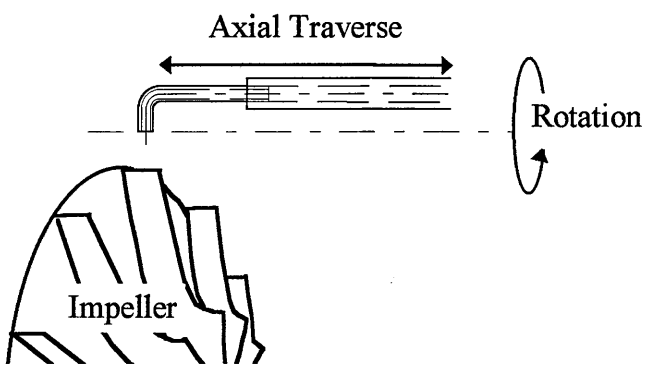


Figure B.18 Axial and Rotational Degrees of Freedom Required by Traverse

In addition the traverse unit was required to

- withstand and seal against the 5 Bar impeller discharge pressure
- operate at 250°C
- be a maximum of 300mm axial length to locate between existing scantlings
- be suitable for mounting both pneumatic and Kulite probes
- allow operation on different shroud wall thickness
- traverse 22mm in the axial direction with an accuracy of 0.1 mm
- rotate at least 60° to an accuracy of 0.25°

All of the specifications were attained and the design is shown in Figure B.19.

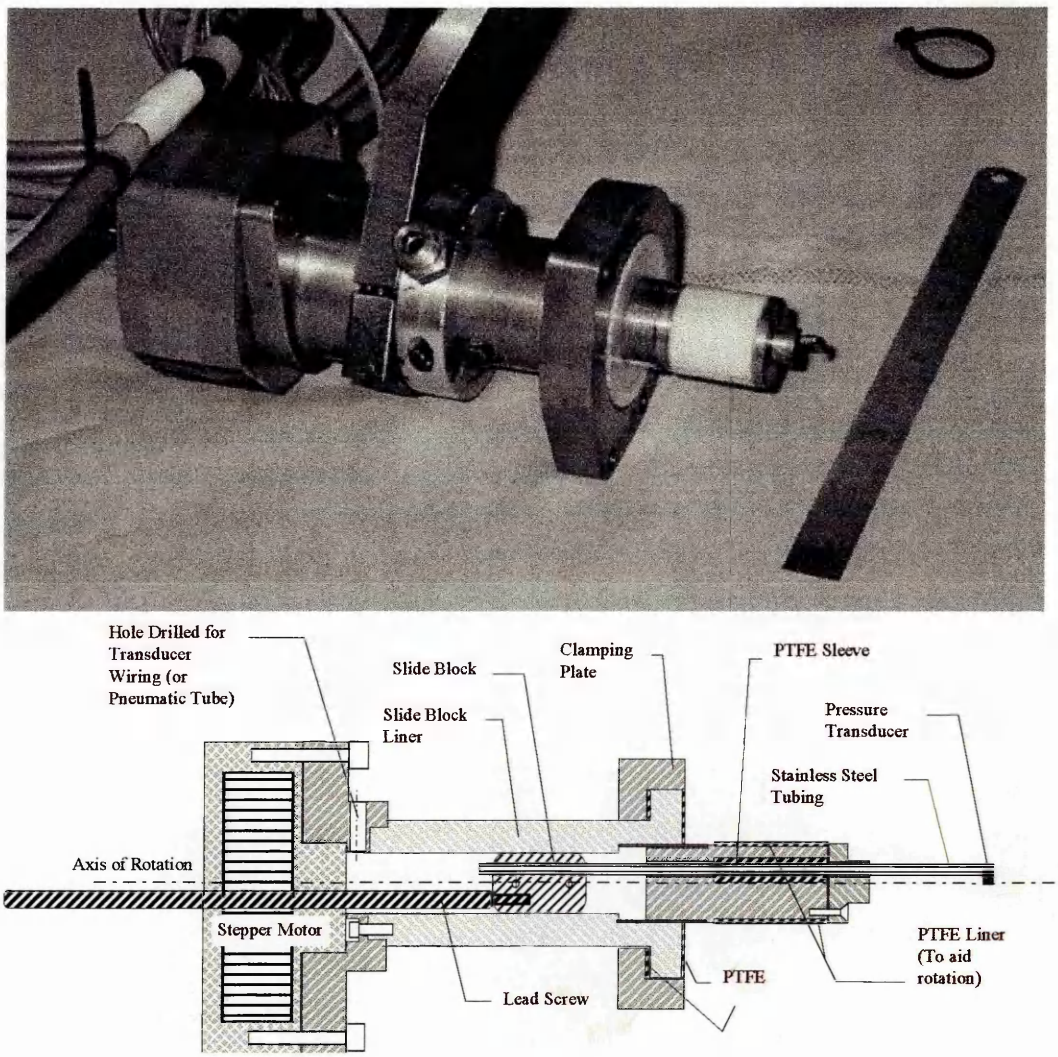


Figure B.19 Photograph of, and Cross-Section through, Traverse Gear

Complete engineering drawings, designed and drawn by the author specifically for this research, are filed within the School of Mechanical Engineering, Cranfield University (Drawings No:PA26952-PB26959, PB27571, PB27578-PC27582, PB27587; Full designations are available in APPENDIX C).

B.3.2 ELECTRO-MECHANICAL CONTROL HARDWARE

Two stepper motors were required for remote operation, one for each degree of freedom. Both were air cooled to prevent overheating and arranged for linear movement. Rotation of the probe was achieved through a level arm that allowed 70° of movement. The general arrangement is shown in Figure B.20.

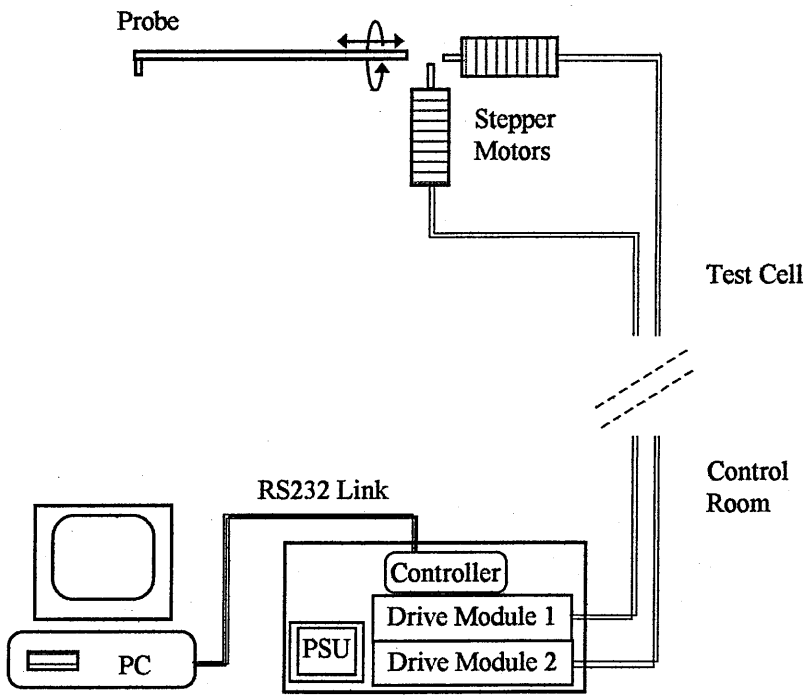


Figure B.20 Electro-Mechanical Control of Traverse Gear

The specification of individual components is given below

Table B.5 Stepper Motor Control Hardware

Component	Specification
Controller	2 Axis Type: RS Components 440-098
Drive Module 1	3.5A Type: RS Components 440-051
Drive Module 2	6A Type: RS Components 440-240
Stepper 1	Type: RS Components 318-705 Maximum Force 125N Accuracy ±0.01mm
Stepper 2	Type: Unimatics Linear Actuator Model ETS 32-A08PZZ0-CC150-A Maximum Force 1000N Accuracy ±0.04mm
PC	'486 DX2 66Mhz, 16MB RAM, VGA Graphics

B.3.3 ELECTRO-MECHANICAL CONTROL SOFTWARE

Although the stepper control card may itself be programmed to run independently of the PC, it was decided to control 'interactively', with the PC supplying simple single line commands only such as 'Axis 1, Move X number of Steps'. In this way all of the control itself was dictated by the PC, and through the use of computer routines, automated traverses of limitless complexity were possible.

No previous investigators within the department had used this type of stepper control board before and therefore the author had the opportunity to choose the programming language. VISUAL BASIC (Version 3.0) was selected, particularly due to its graphical interface. This was thought of particular importance for operation within a noisy and somewhat stressful experimental environment.

The VISUAL BASIC program main windows are shown below in Figure B.14, consisting of the header menu, the traverse window and the data acquisition window.



Figure B.21(a) Header Window

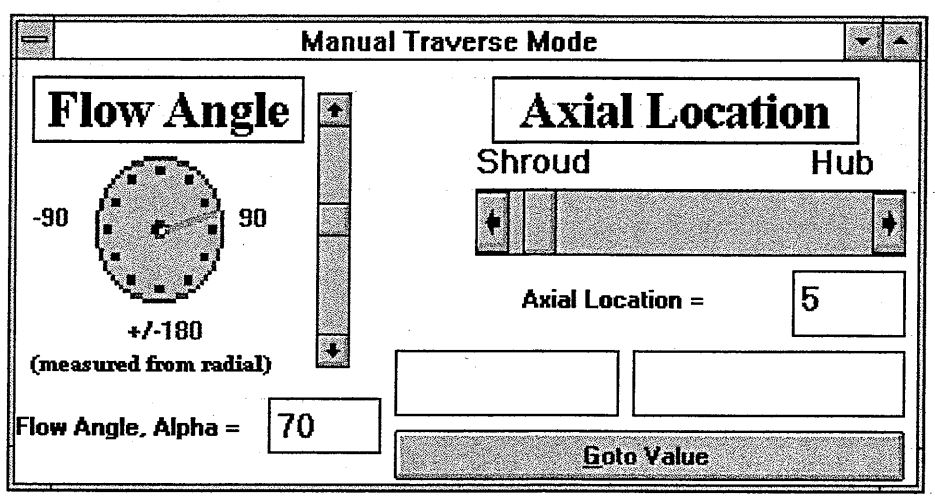


Figure B.21(b) Traverse Window

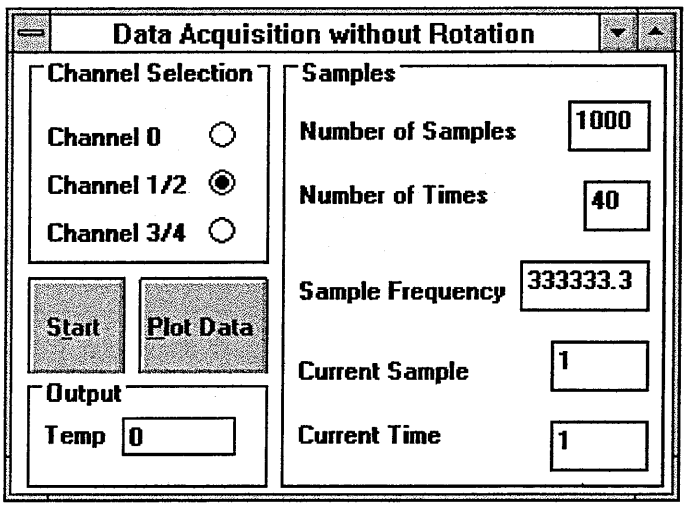


Figure B.21(c) Data Acquisition Window

In the traverse window, the horizontal and vertical scroll bars, or the input boxes could be used to invoke a traverse. Generally, the program was set-up with 0.1° angular and 0.1 mm axial resolutions.

Also included within the program framework was a traverse 'Datum/Zero' window function.

B.3.4 DATA ACQUISITION

B.3.4.1 HARDWARE

The general arrangement is shown below in figure B.22. Two configurations are indicated, differentiated by pressure measure probe type.

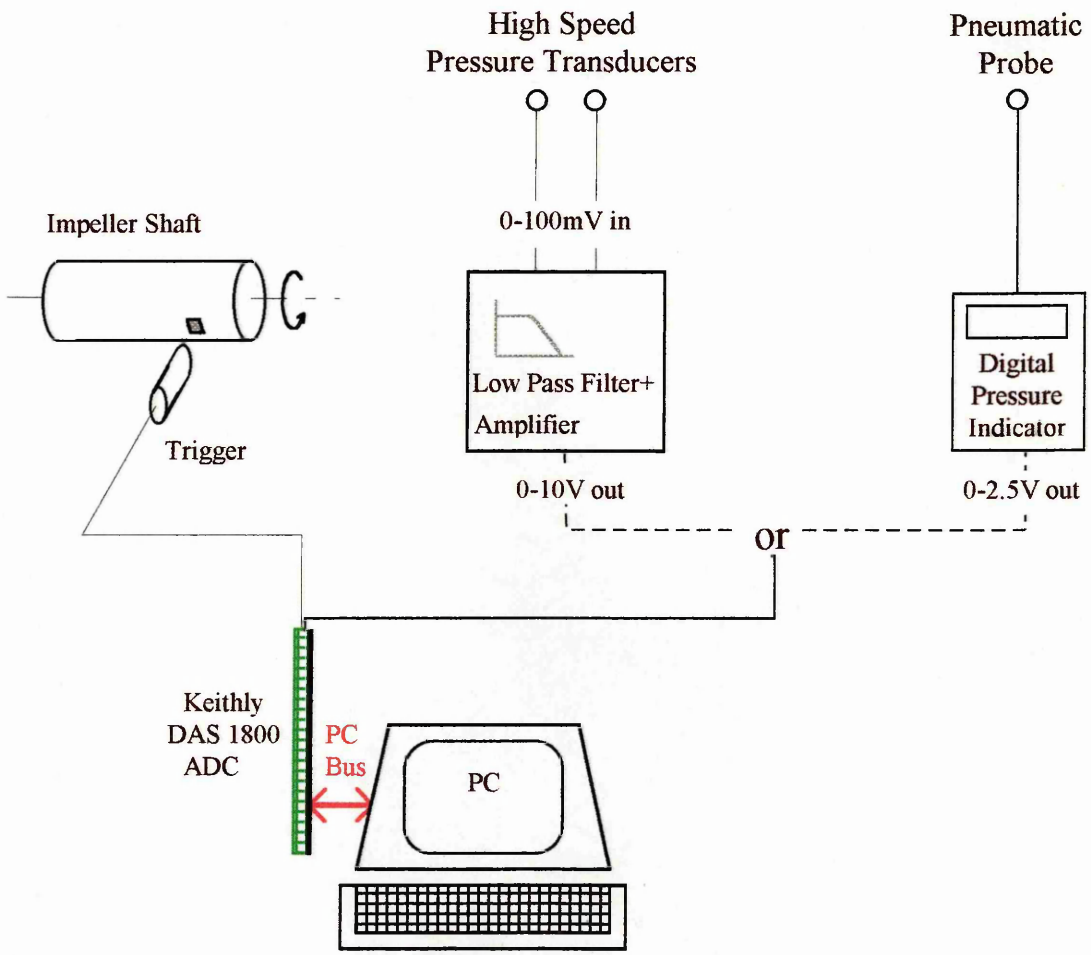
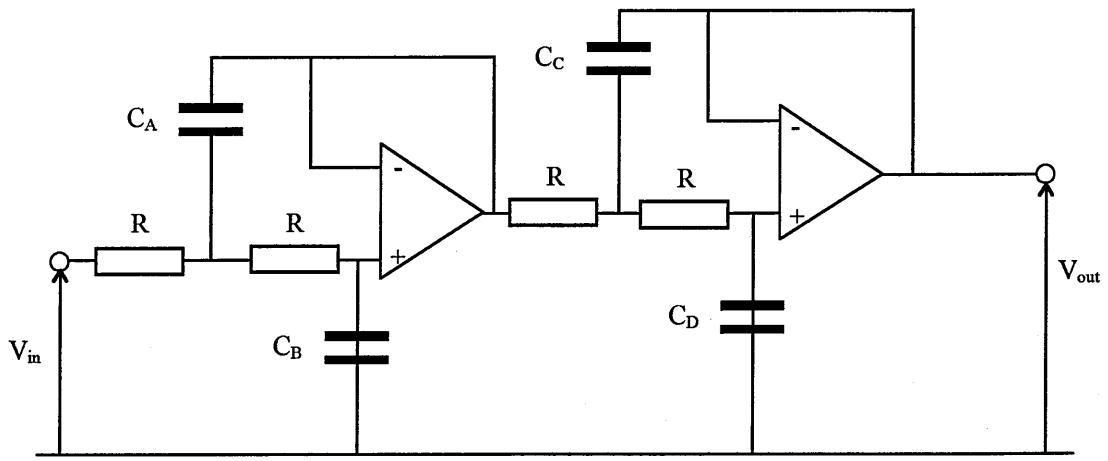


Figure B.22 Pressure Data Acquisition

B.3.4.2 KULITE PRESSURE TRANSDUCER SIGNAL CONDITIONING

The signals from the Kulite were amplified by 100 and passed through a fourth order anti-aliasing filter with a design low pass cut-off 100 kHz. The circuit built is shown below in Figure B.23.



Component	Equation	Value Used
R	4.7 to 10kMΩ	732Ω
C_A	$=\frac{1.0824}{2\pi f.R}$	2.139nF
C_B	$=\frac{0.9239}{2\pi f.R}$	1.826nF
C_C	$=\frac{2.6130}{2\pi f.R}$	5.165nF
C_D	$=\frac{0.3827}{2\pi f.R}$	756pF

Figure B.23 *Pressure Transducer Amplifier/Filter Circuit (Butterworth low-pass 24db/decade (Elektor))*

This circuit was built and tested (Dawes,J (1995)) and gave a characteristic as shown below in Figure B.24.

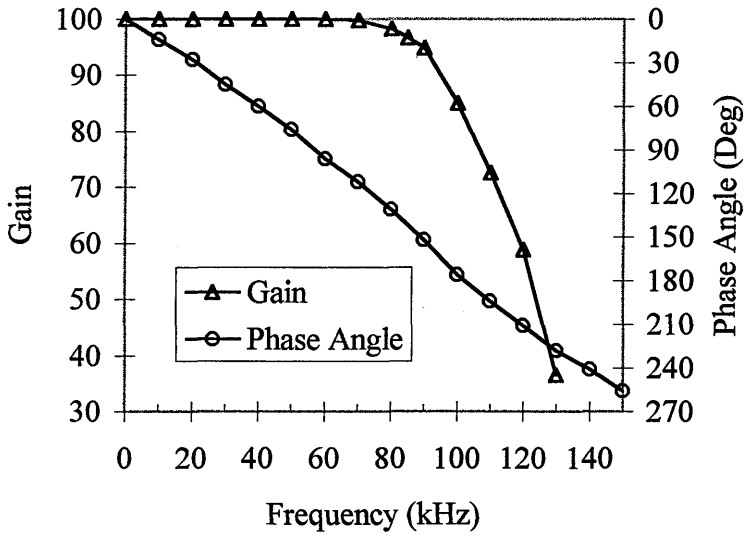


Figure B.24 Bode Plot of Amplifier/Filter Circuit

The equations noted in Figure B.23 are only approximate and together with some minor mismatch of components, the design cut-off of 100kHz crept up to 125kHz (for -3dB). This was not of any particular concern as this was still much less than half of the sampling frequency (333kHz) theoretically required to prevent aliasing. The phase angle variation with frequency was virtually linear over the interested frequency range, implying a constant lag of all signals.

The checking of the above did alleviate some of the fears of using a *Butterworth* circuit. One of the alternatives was to use a *Bessel* type arrangement. This circuit is identical to that of the *Butterworth* with the exception that all the resistors are swapped with capacitors and vice- versa. It is well documented that the Bessel type yields a more linear phase/frequency relationship, but this is at the expense of a constant negative gain slope throughout the range. Calibration demonstrated, however, that the choice of circuit built was suitable for the application chosen despite a possible degradation in achievable phase angle linearity.

A Keithly DAS-1800 high speed ADC card sampled the outputs at 333kHz. (Note: Blade passing frequency at design = 9.9kHz). This card was fitted into an expansion slot of the PC used for traversing. This allowed one program to both control the traversing and data acquisition, thus forming a unitary measurement system.

A once per revolution digital trigger was used. This was connected directly to the ADC card, ensuring a 'next clock pulse' sample (i.e. sample initiated within 1/33mhz, for the computer used) and was PC software/operating-system independent. Samples were

saved directly into memory (necessary to avoid hard disc access time limitations) using a proprietary DMA (Direct Memory Access) utility, thus avoiding hardware bottlenecks. Partial post processing of the data was carried out during acquisition and although this was limited, it was of sufficient quality to ensure that the system was functioning correctly and that the probes were undamaged. The latter scenario was quite frequent due to the extreme operational conditions. The average life of a Kulite probe was of the order 15 hours although this was very variable.

B.3.4.3 PNEUMATIC PRESSURE SIGNAL CONDITIONING

In this case, the signal from the Digital Pressure Indicator (DPI) was read directly into the Keithly DAS-1800 ADC card used for the Kulites. The trigger was not required and the input signals were sampled at much lower frequencies (≈1kHz). As the ADC card and software written featured programmable input ranges, very little work was necessary when switching between the two probe types.

B.3.4.4 ADC BOARD CALIBRATION AND ACCURACY

The board was calibrated against a Fluke Digital Voltmeter (Type 70 Series II Multimeter) with NAMAS calibration.

The 12 bit range of the card implies the range accuracies shown in Table B.6.

Table B.6 ADC Board Accuracy

Range	Accuracy
0-10V	+/- 0.00244 V
0-2.5V	+/- 0.00061 V

B.4. WEDGE PROBE

The compressor inlet was traversed using a wedge probe in order to determine if there was any flow distortion. The probe was of conventional pneumatic type as shown below:

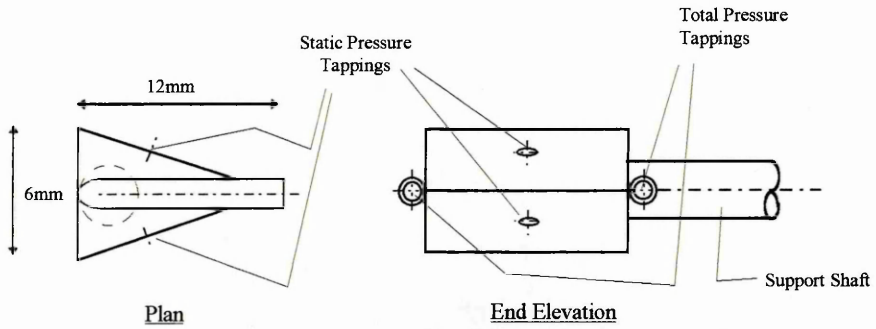


Figure B.25 Sketch of Pneumatic Wedge Probe

B.4.1 CALIBRATION

Calibration was carried out within the same wind tunnel used for the total pressure probes at Mach numbers of 0.2, 0.4 and 0.6. The collective yaw coefficient curves are shown in Figure B.26.

The yaw coefficient showed little sensitivity to Mach number over the range tested and therefore a single polynomial fit was used to represent all data. Initially a fit covering the complete calibration range of ±25° was used (denoted '...fit over complete range' in Figure B.26). However, during the initial post processing of experimental results, such a large range was found unnecessary, and in order to improve the fit over the range of interest, a new fit over ±10° was used. This improved the accuracy of the angular measurements.

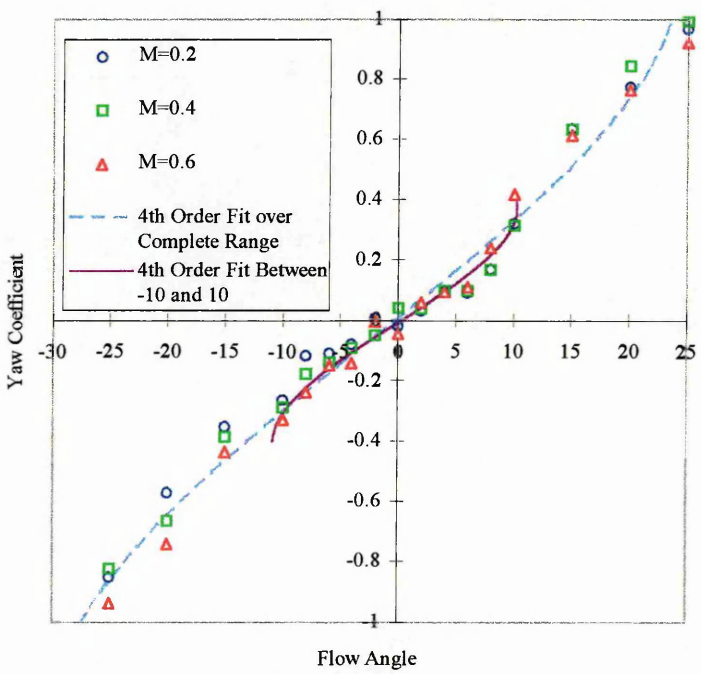


Figure B.26 Calibration of Wedge Probe

APPENDIX C
Engineering Drawings

Substantial engineering modifications were required to the existing rig prior to diffuser testing. Relevant engineering drawings are listed below, together with the drawings for instrumentation traverse.

Drawing Number	Issue	Description	Drawn by
PA26950	A	Pipe Diffuser Perspex Model	I.Bennett
PD26951	A	Outlet Thermocouple Rake	I.Bennett
PA26952	A	GA of Linear Trav. Assembly	I.Bennett
PB26953	A	Traverse Gear Plug	I.Bennett
PB26954	A	Holding Plate	I.Bennett
PA26955	A	Slide Cylinder Liner	I.Bennett
PB26956	A	Slide Block	I.Bennett
PB26957	A	End Plate	I.Bennett
PB26958	A	PTFE Washer	I.Bennett
PB26959	A	PTFE Gasket	I.Bennett
PB26960	A	Modification to Existing 35D Shroud	I.Bennett
PB26961	A	Outer Shroud Spacer Ring	I.Bennett
PB26962	A	Outer Shroud Cover Plate	I.Bennett
PA26963	A	Inner Ring Assembly (3 Drawings)	I.Bennett
PA26964	A	Impeller Shroud Machining	I.Bennett
PB27565	A	Diffuser Backplate	I.Bennett
PB27566	A	Shroud Spacer Ring	I.Bennett
PC27567	A	Hubside Diffuser Spacer Ring	I.Bennett
PB27568	A	Vaneless Diffuser Shroud-Side Parts	I.Bennett
PB27569	A	Vaneless Diffuser Hub-side Parts	I.Bennett
PC27570	A	Vaneless Diffuser Support Tube	I.Bennett
PB27571	A	Traverse Gear Blanking Plate	I.Bennett
PB27572	A	Impeller Discharge Laser Window	I.Bennett

PB27573	A	Laser Window Full Blanking Plate	I.Bennett
PB27574	A	LHS Inner Shroud Laser Hole Detail	I.Bennett
PC27575	A	Rotadata Tip Clearance Probe 1	I.Bennett
PC27576	A	Static Tapping Instrumentation	I.Bennett
PC27577	A	Rotadata Probe No. 2	I.Bennett
PB27578	A	35D Traverse Support Bracket	I.Bennett
PC27579	A	35D Gear Spacers	I.Bennett
PB27580	A	Traverse Gear Spacers	I.Bennett
PA27581	A	Traverse Gear Lever Arm	I.Bennett
PC27582	A	Traverse Gear Clamp	I.Bennett
PC27583	A	Laser Window Bracket	I.Bennett
PB27584	A	Laser Window Lower Spacer	I.Bennett
PB27585	A	Laser Window Upper Spacer	I.Bennett
PC27586	A	Rota Data Probe No. 3	I.Bennett
PB27587	A	Linear Traverse Gear Holding Plate	I.Bennett
PB27588	A	Inner Space Support	I.Bennett
A2/27675	A	Pin for Pneumatic Connector	I.Bennett
A1/27676	A	Static Tapping Connector (Female)	I.Bennett
A1/27677	A	Static Tapping Connector (Male)	I.Bennett
A0/27678	A	Offset Discharge Laser Window	I.Bennett
A1/27679	A	31 Pipe Diffuser	I.Bennett
A1/27680	A	22 Pipe Diffuser	I.Bennett
A0/27681	A	Second Inner Shroud Design	I.Bennett
A1/27682	A	13 Pipe Diffuser	I.Bennett
A1/27683	A	13 (Oval) Pipe Diffuser	I.Bennett

APPENDIX D
Impeller Measurements at 80% of Design Speed

This appendix is a compilation of the detailed flow measurements taken at 80% of design speed. Traverses at inlet and at the impeller discharge ($1.05R_{tip}$) were undertaken. At compressor inlet, a wedge-type pneumatic probe was used to map the flow angle and total pressure distribution. At impeller discharge, a traverse gear initially incorporating a pneumatic probe and then a pressure transducer were used. Again, both local flow angle and total pressure were recorded. Actual operating duties are complied in APPENDIX E, the contents of which may be suitable for specifying boundary conditions for CFD modelling. These reduced speed measurements are, in the opinion of the author, more consistent than those measured at full speed. Despite this they have been removed from the core work. This omission is due to the emphasis of this current study on pipe diffusers and that performance enhancement is expected for these at elevated impeller tip discharge Mach numbers. Therefore the majority of the work presented in the main text has concentrated on measurements taken at full operating speed.

D.1. Inlet Pneumatic Probe Traverses

These were taken 39 mm upstream of the impeller using a wedge probe and are shown in Figures D.1 and D.2.

D.2. Impeller Tip Total Pressure Traverse

Measurements taken using high speed pressure transducers are presented in Figures D.3 to D.8. As for the 100% measurements presented within the core of this thesis, the time interval on the x-ordinate axis is 1/3 of a milli-second and the blade position is omitted in all plots due to possible distortion of the flow from the impeller tip to the measurements plane.

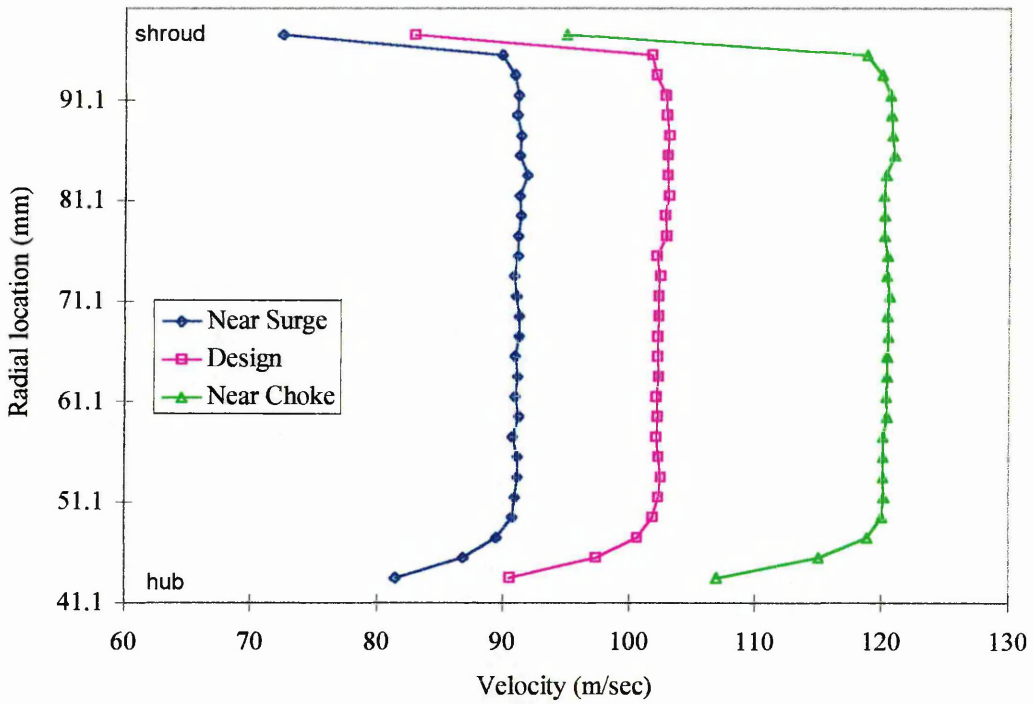


Figure D.1 Impeller Inlet Velocity Profile

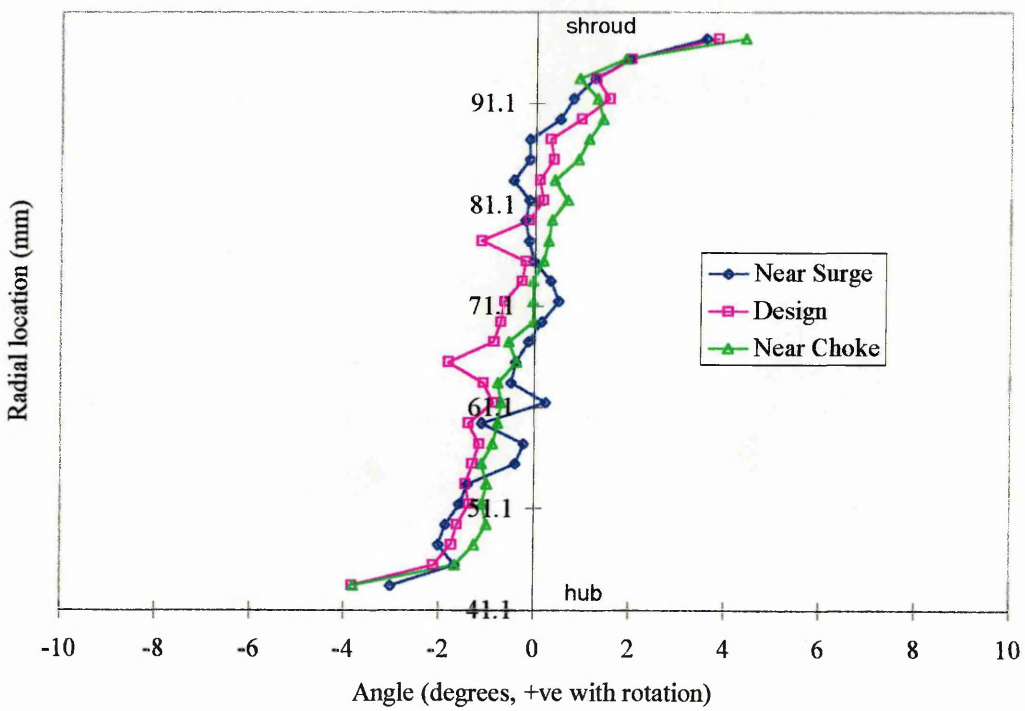
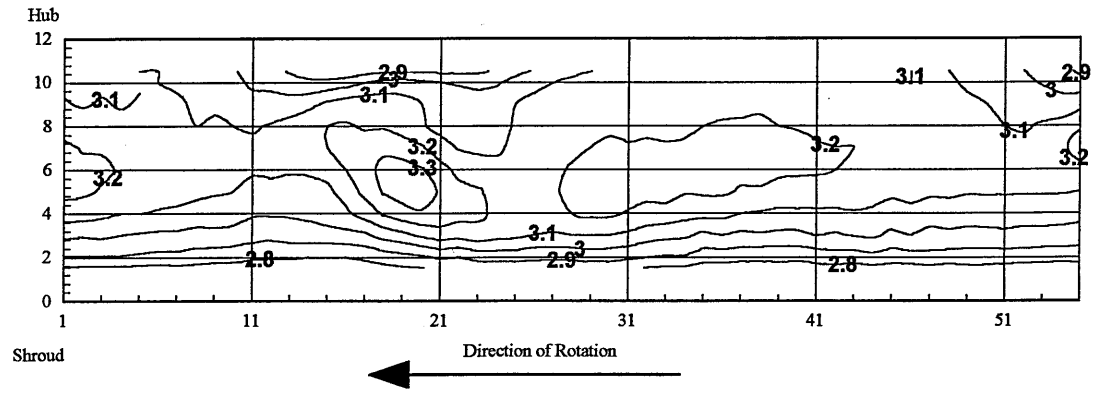
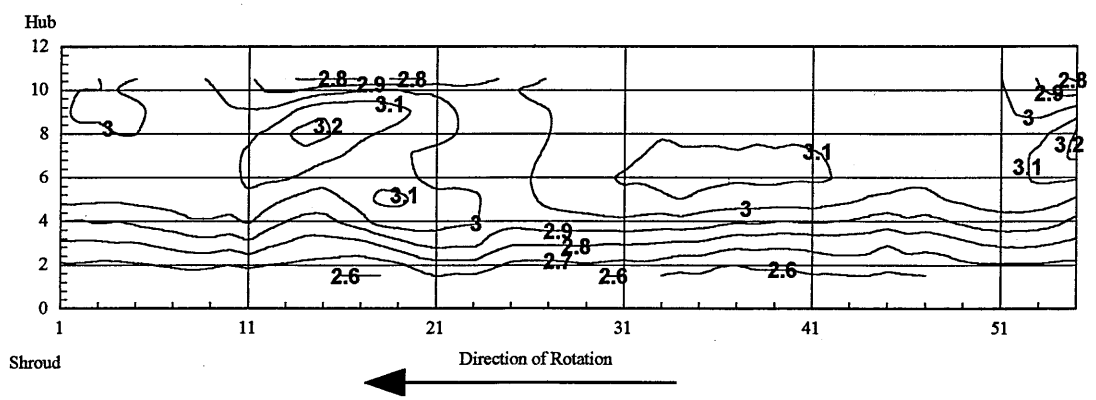


Figure D.2 Impeller Inlet Absolute Flow Angle Profile

80% Surge (VDA142/9V)



80% Design (VDA147/10V)



80% Choke (VDA150/11V)

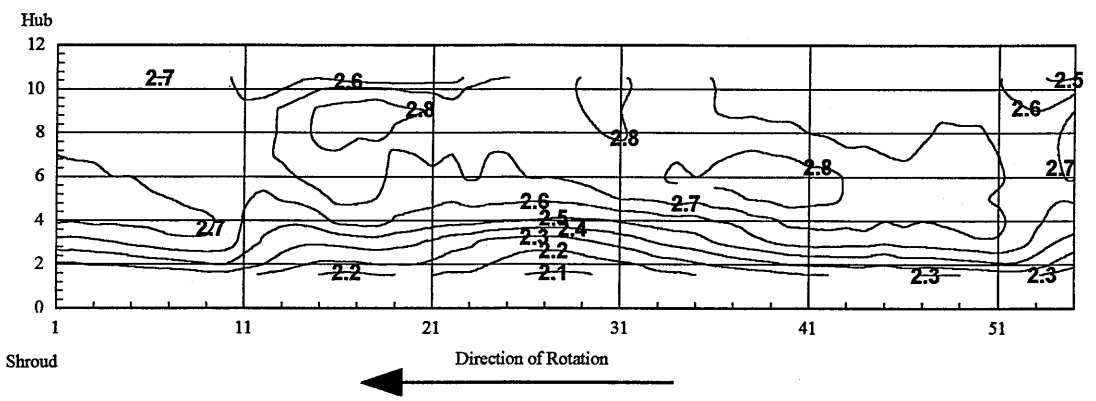
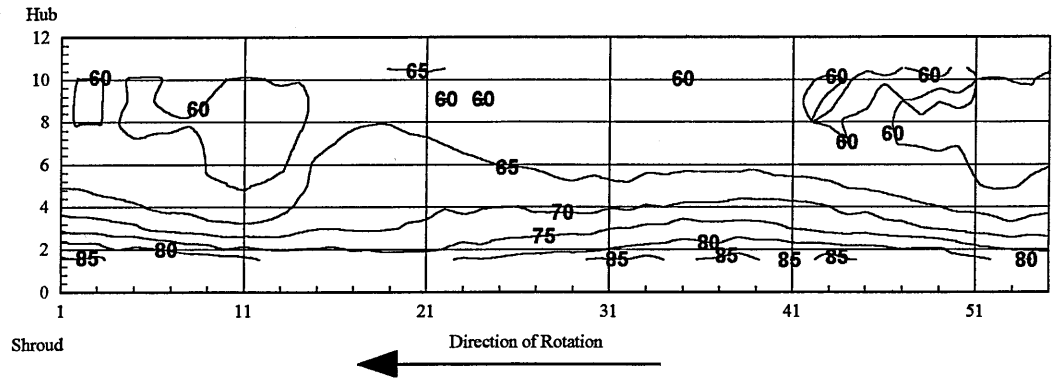
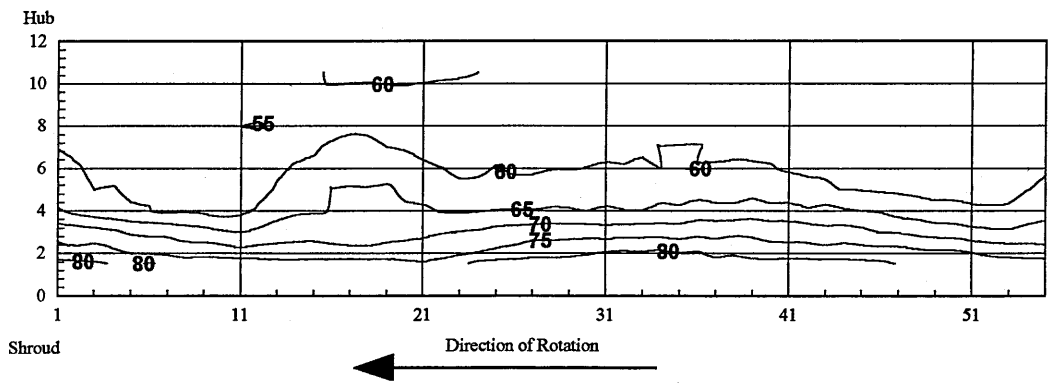


Figure D.3 Total Pressure at Impeller Discharge (BarA)

80% Near Surge (VDA142/9V)



80% Design (VDA142/10V)



80% Near Choke (VDA150/11V)

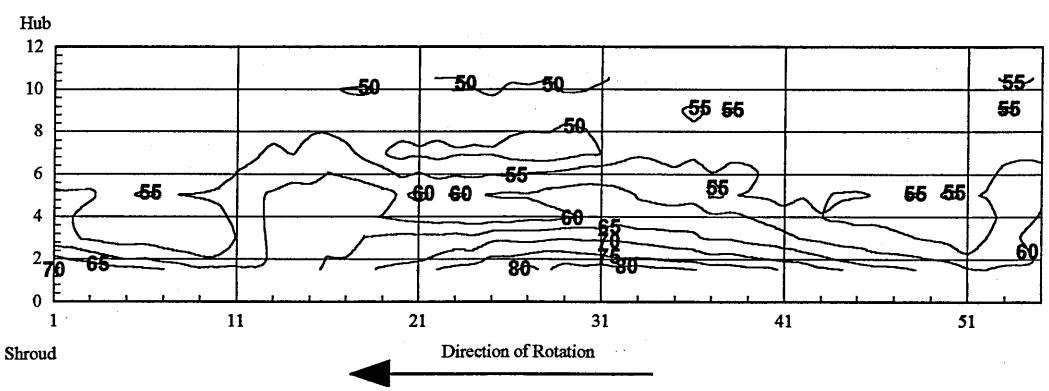
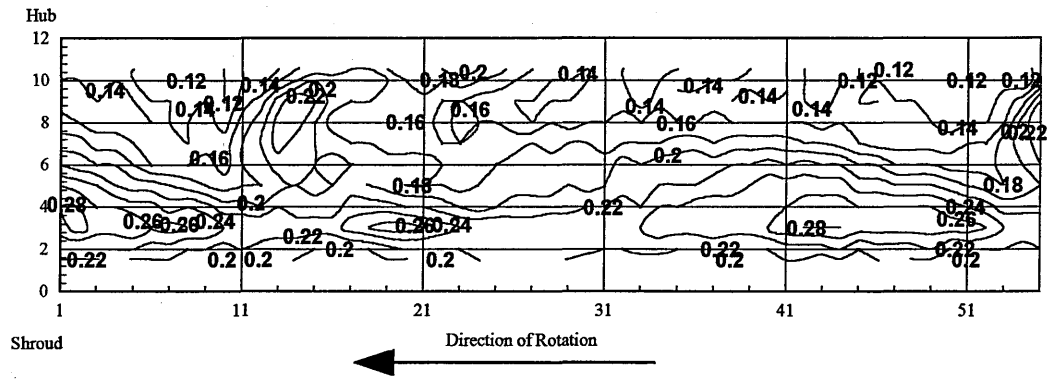
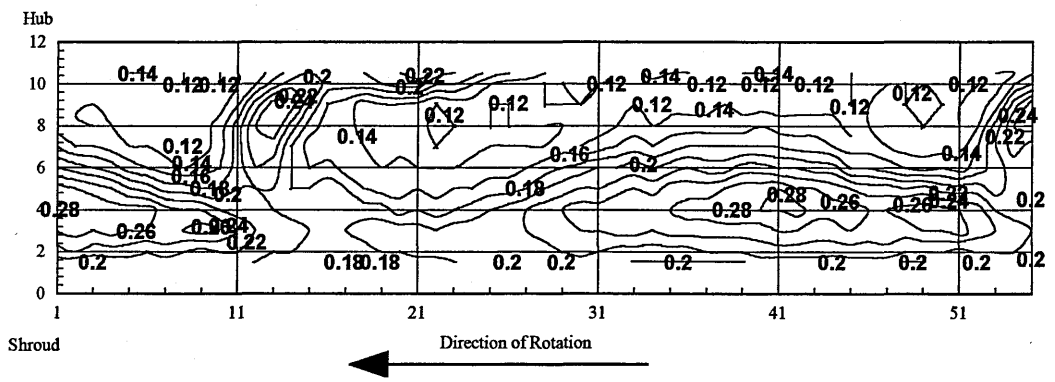


Figure D.4 Absolute Impeller Discharge Angle (Degrees from Radial)

Near Surge (VDA142/9V)



80% Design (VDA147/10V)



80% Near Choke (VDA150/11V)

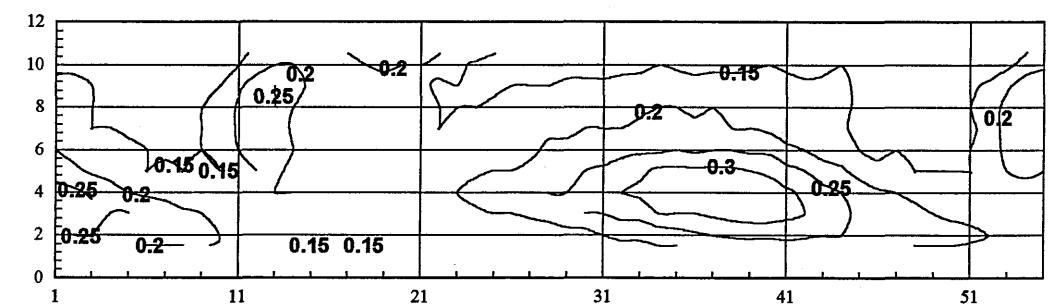
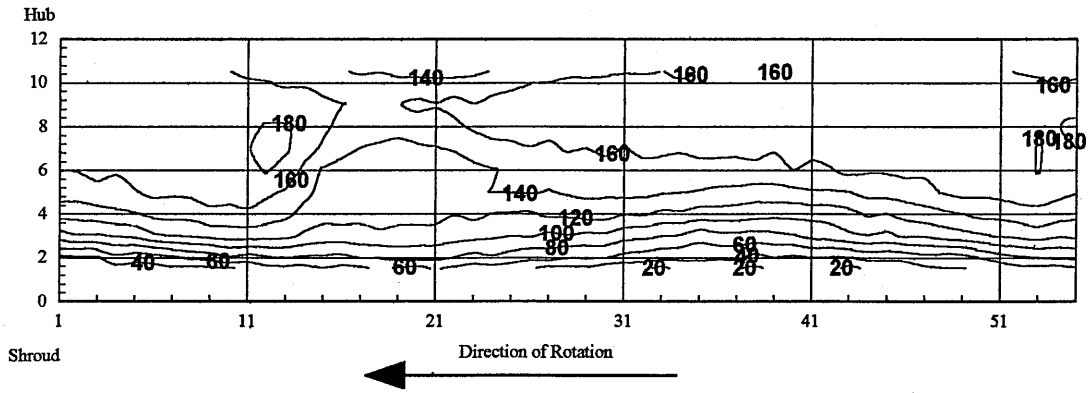
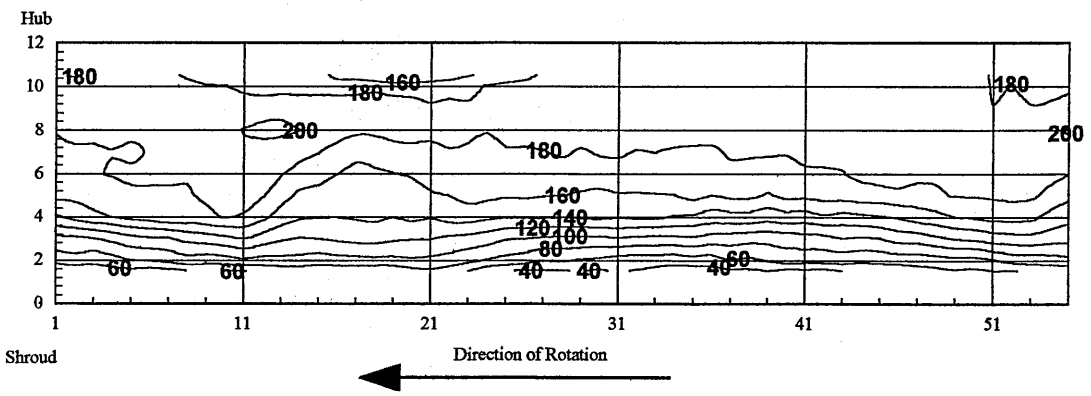


Figure D.5 Standard Deviation of Total Pressure (80% of Design Speed)

80 % Near Surge (VDA142/9V)



80% Design (VDA147/10V)



80% Near Choke (VDA150/11V)

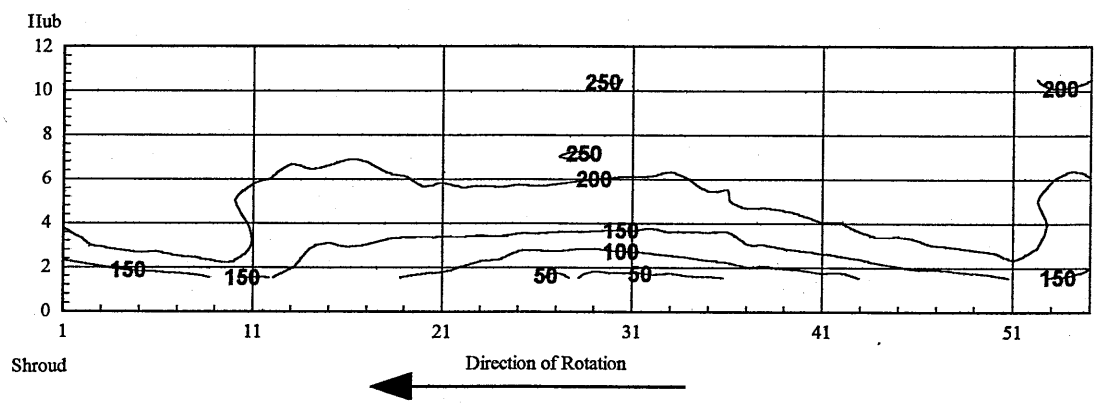
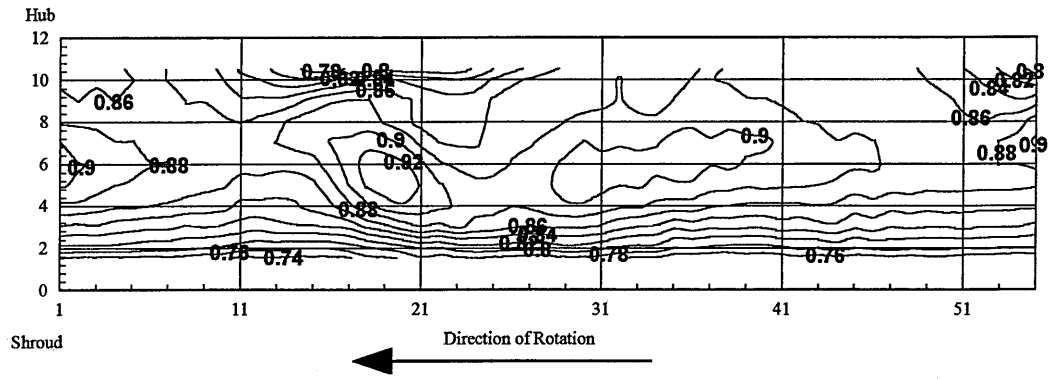
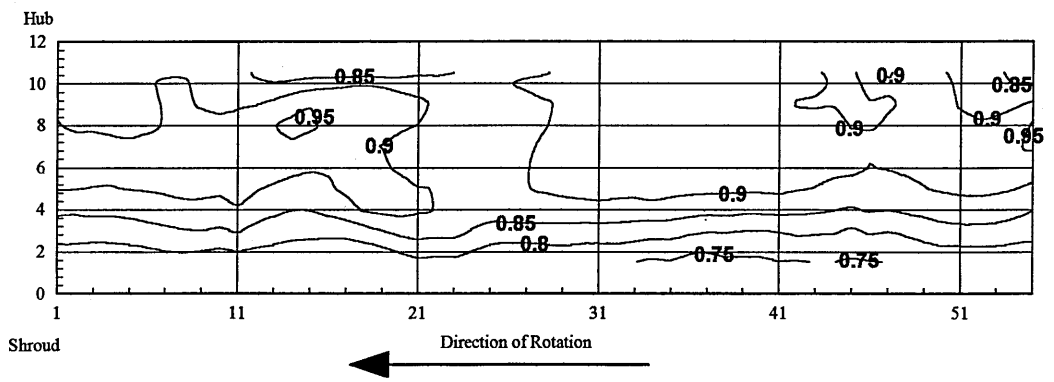


Figure D.6 Radial Velocity (m/sec)

80% Near Surge (VDA142/9V)



80% Design (VDA147/10V)



80% Near Choke (VDA150/11V)

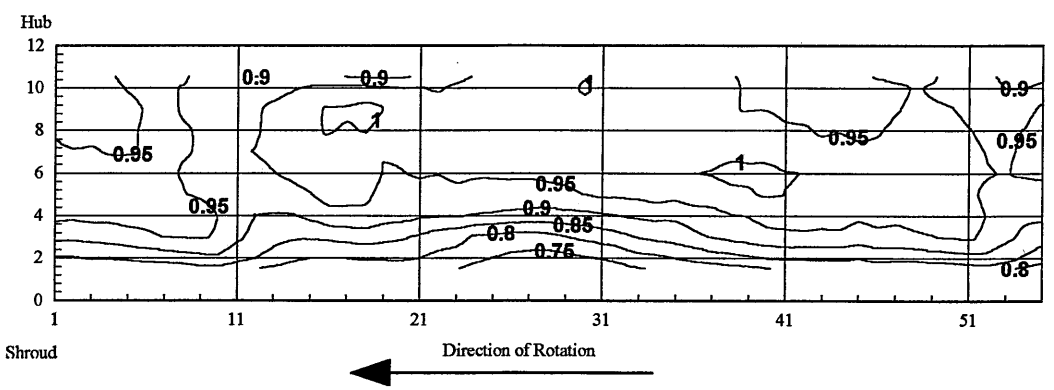


Figure D.7 Absolute Mach Number at Impeller Discharge

APPENDIX E
Overall Performance Data for Traverses

The tables below show the overall performance measurements of the 35D compressor with vaneless diffuser. The performance was evaluated using both conventional 'static' instrumentation (described in Appendix A) and detailed traverse instrumentation (described in Appendix B). The recorded total pressure and flow angle data from the detailed instrumentation was mass and area weighted respectively. Tables E.1 and E.2 record measurements taken using the pneumatic traverse and that taken simultaneously using the static instrumentation respectively; Tables E.3 and E.4 presents the same data but for the unsteady traverse.

Table E.1 Pneumatic Total Pressure (Averaged Traverse) Measurements

Pdischarge (BarA)	Mass Average (P_{pneu})	4.31	4.07	3.74	2.88	2.61	2.19
	Mean	4.24	4.02	3.84	2.90	2.63	2.21
	Max	4.66	4.37	4.08	3.09	2.79	2.34
	Min	2.80	2.82	3.30	2.62	2.28	1.82
	delta (P_{pneu}-P_{dap})*	-0.08	0.06	0.04	0.01	0.01	0.04
	delta (P_{pneu}-P_{dap})/ P_{dap}%	1.8%	1.5%	1.1%	0.4%	0.4%	1.9%
Absolute Disch. Angle (Degrees)	Mass Average	71.0	70.2	69.5	66.30	64.27	60.25
	Mean	71.7	70.7	69.7	65.63	63.76	60.13
	Max	90.3	83.7	86.2	81.83	78.27	66.27
	Min	66.8	67.5	64.8	61.45	60.27	56.82
	delta Theta	1.12	1.85	2.66	-1.49	0.67	5.13

* P_{pneu} - mass weighted pneumatic probe measurement
P_{dap} - static instrumentation measurement

Table E.2 Pneumatic Total Pressure Static Instrumentation Measurements

% Speed		100%	100%	100%	80%	80%	80%
Flow Condition		surge	design	choke	surge	design	choke
Performance Data File(s)		vda122	vda118	vda124	vda132	vda138	vda140
Traverse Name		dvda144-155	dvda132-143	dvda158-166	6v	7v	8v
Corrected Mass Flow (kg/sec)		3.81	4.07	4.29	2.90	3.25	3.80
Actual Conditions	Speed (rpm)	34,800	34,560	34,890	28200	28110	28110
Mass Flow (kg/sec)		2.74	2.81	2.82	2.37	2.55	2.73
Impeller Total Pressure Ratio		6.03	5.78	5.57	3.40	3.25	2.93
Isentropic Eff		89.0	88.7	87.0	89.10	88.10	83.90
Inlet Total Temperature (K)		287.5	283.9	287.3	292.3	291.9	291.9
Discharge Total Pressure (Pa) (P_{dap})		4.39	4.01	3.70	2.87	2.60	2.15
Discharge Total Temperature (K)		501.4	489.8	493.8	428.5	423.7	416.2
Discharge Static Pressure (BarA)		2.17	2.01	1.85	1.71	1.53	1.21
Tip Speed (m/sec)		532.1	528.4	533.4	431.2	429.8	429.8
Mach Number		1.05	1.04	1.05	0.89	0.90	0.94
Disch Tstatic (K)		410.1	402.1	404.9	369.4	364.3	353.5
Absolute Discharge Velocity (m/sec)		428.3	419.9	422.6	344.7	345.6	354.9
Absolute Tangential Velocity (m/sec)		403.9	391.6	389.0	317.6	308.2	290.7
Absolute Flow Angle (wrt radial)		70.6	68.9	67.0	67.1	63.1	60.0
Discharge Density (kg/m3)		1.85	1.74	1.59	1.61	1.47	1.20
Power (kW)		588	582	584	325	338	341
Number of Samples per blade		33.81	34.04	33.72	41.72	41.85	41.85
Absolute Radial Velocity (m/sec)		142.4	151.5	165.1	134.0	156.4	203.6

Table E.3 Unsteady (Kulite) Total pressure Measurements

Percentage of Design Speed		100%	100%	100%	80%	80%	80%
Flow Condition		surge	design	choke	surge	design	choke
Unsteady Data File Name		3v	2v	4v	9v	10v	11v
Corrected Mass Flow (kg/sec)		3.81	4.07	4.29	2.90	3.25	3.80
Pdischarge (BarA)	Mean	4.27	3.94	3.69	3.05	2.92	2.58
	Mass Average	4.28	3.95	3.70	3.07	2.94	2.60
	Max	5.21	4.64	4.38	3.35	3.23	2.88
	Min	3.66	3.54	3.31	2.73	2.55	2.09
Absolute Discharge Angle (Degrees)	Mean	69.48	68.36	67.48	67.43	64.44	58.10
	Mass Average	68.47	67.45	66.42	66.95	63.90	57.74
	Max	87.46	92.48	92.41	87.49	84.53	83.83
	Min	61.38	59.90	54.70	55.94	54.67	46.12
Standard Deviation of Total Pressure (BarA)	Mass Average	0.44	0.33	0.43	0.19	0.18	0.19
	Max	0.59	0.54	0.62	0.29	0.29	0.34
	Min	0.32	0.18	0.29	0.12	0.11	0.12
Total Temperature (K)	Mean	499.60	491.00	497.00	430.71	420.90	414.90
	Mass Average	498.70	491.60	497.00	426.90	417.20	411.30
	Max	523.91	511.80	518.86	438.85	427.80	422.50
	Min	486.50	480.20	483.60	418.62	413.80	407.70
Mach Number (Absolute)	Mean	1.02	1.02	1.04	0.84	0.86	0.91
	Mass Average	1.02	1.02	1.04	0.85	0.87	0.92
	Max	1.19	1.16	1.18	0.93	0.96	1.01
	Min	0.90	0.94	0.95	0.73	0.73	0.71
Radial Velocity (m/sec)	Mean	132.40	138.80	146.60	126.48	144.54	184.40
	Mass Average	137.55	143.10	152.13	130.15	148.45	187.60
	Max	204.50	216.40	243.70	192.73	205.23	254.18
	Min	19.63	-17.63	-17.50	12.98	27.96	30.44
Absolute Tangential Velocity (m/sec)	Mean	390.90	381.70	382.52	300.32	296.46	290.20
	Mass Average	390.00	380.90	381.91	292.19	288.64	281.40
	Max	456.40	435.30	442.50	335.29	323.38	325.50
	Min	349.40	348.70	335.30	267.10	273.90	263.70
Rel. Tangential Vel. (m/sec)	Max	65.50	53.60	59.94	35.00	26.70	35.40
	Min	-41.40	-33.00	-47.25	-33.30	-22.60	-26.50

Table E.4 Static Performance Instrumentation Measurements for Unsteady Traverse

Percentage of Design Speed	100%	100%	100%	80%	80%	80%
Flow Condition	surge	design	choke	surge	design	choke
Performance Data File	vda122	vda118	vda124	vda142	vda147	vda150
Unsteady Data File Name	3v	2v	4v	9v	10v	11v
Corrected Mass Flow (kg/sec)	3.81	4.07	4.29	2.90	3.25	3.80
Speed (rpm)	34,800	34,560	34,890	28,230	28,110	28,230
Mass Flow (kg/sec)	2.74	2.81	2.82	2.69	2.96	3.35
Impeller Total Pressure Ratio	6.03	5.78	5.57	3.37	3.26	2.93
Isentropic Eff	89.0	88.7	87.0	89.2	88.6	84.0
Inlet Total Temperature (K)	287.5	283.9	287.3	296.2	293.9	296.0
Discharge Total Pressure (Pa)	4.39	4.01	3.70	3.21	3.03	2.65
Discharge Total Temperature (K)	501.4	489.8	493.8	432.7	426.1	421.6
Discharge Static Pressure (BarA)	2.17	2.01	1.85	1.91	1.79	1.50
Tip Speed (m/sec)	532.1	528.4	533.4	431.6	429.8	431.6
Mach Number	1.05	1.04	1.05	0.89	0.90	0.94
Discharge Total Temperature (K)	410.1	402.1	404.9	373.0	366.3	358.1
Absolute Discharge Velocity (m/sec)	428.3	419.9	422.6	346.3	346.6	357.3
Absolute Tangential Velocity (m/sec)	403.9	391.6	389.0	317.9	309.1	292.5
Absolute Flow Angle (wrt radial)	70.6	68.9	67.0	66.6	63.1	54.9
Discharge Density (kg/m3)	1.85	1.74	1.59	1.78	1.70	1.46
Power (kW)	588	582	584	369	393	423
Number of Samples per blade	33.81	34.04	33.72	41.67	41.85	41.67
Absolute Radial Velocity (m/sec)	142.4	151.5	165.1	137.3	156.8	205.2

APPENDIX F

Details of CFD Solver and Equations Solved

The CFD programs used in this thesis solved the compressible Navier Stokes equations together with a standard k-ε turbulence model. As such, the following equations were solved (e.g. Rampant (1994),Hirsh (1990))

Mass

$$\frac{\partial}{\partial t}\int_{\Omega}\rho d\Omega + \oint_{S}\rho\overline{w}.d\overline{S} = 0 \qquad \text{-(F.1)}$$

where $\overline{w}$ is the velocity in the rotating frame of reference

Momentum

$$\frac{\partial}{\partial t}\int_{\Omega}\rho\overline{w}d\Omega + \oint_{S}\left(\rho\overline{w}\otimes\overline{w} + p\bar{I} - \bar{\bar{\tau}}\right).d\overline{S} = \int_{\Omega}\rho\left[-2\overline{\omega}\times\overline{w} - \overline{\omega}\times(\overline{\omega}\times\bar{r})\right]d\Omega \qquad \text{-(F.2)}$$

where $\overline{\omega}$ is the angular velocity of the rotating frame

and viscous stress tensor, $\tau_{ij} = \mu_{eff}\left(\delta_i w_j + \delta_j w_i\right) - \frac{2}{3}(\nabla.\overline{\omega})\partial_{ij}$ -(F.3)

Energy

$$\frac{\partial}{\partial t}\int_{\Omega}\rho E^{*}d\Omega+\oint_{S}\left(\rho\overline{w}I_{r}-K_{eff}\nabla T-\overline{\overline{\tau}}.\overline{w}\right).d\overline{S}=0 \qquad \text{-(F.4)}$$

where the relative total energy, $E^{*}=e+\frac{\overline{w}^{2}}{2}-\frac{\overline{u}^{2}}{2}$ -(F.5)

Rothalpy, $I_{r}=h+\frac{\overline{w}^{2}}{2}-\frac{\overline{u}^{2}}{2}$ -(F.6)

Tangential velocity of reference frame, $\overline{u}=\overline{\omega}\times\overline{r}$ -(F.7)

Turbulent Kinetic Energy

$$\frac{\partial}{\partial t}\int_{\Omega}\rho k d\Omega+\oint_{S}\rho k\overline{w}.d\overline{S}-\oint_{S}\frac{\mu_{e}}{\sigma_{k}}\nabla k.d\overline{S}=\int_{\Omega}\left(P-\rho\widetilde{\varepsilon}\right)d\Omega \qquad \text{-(F.8)}$$

Turbulent Dissipation

$$\frac{\partial}{\partial t}\int_{\Omega}\rho\varepsilon d\Omega+\oint_{S}\rho\varepsilon\overline{w}.d\overline{S}-\oint_{S}\frac{\mu_{e}}{\sigma_{\varepsilon}}\nabla\varepsilon.d\overline{S}=\int_{\Omega}\left[\frac{\varepsilon}{k}\left(C_{1}P-C_{2}\rho\varepsilon\right)\right]d\Omega \qquad \text{-(F.9)}$$

where the production term, $P=-\frac{2}{3}\rho k\nabla.\overline{w}+\mu_{t}\Phi$ -(F.10)

and $\Phi=\nabla\overline{w}_{ji}\left(\nabla\overline{w}_{ji}-\nabla\overline{w}_{ij}\right)-\frac{2}{3}\left(\nabla.\overline{w}\right)^{2}$ -(F.11)

and the dissipation term compressibility correction,

$$\widetilde{\varepsilon}=\frac{C_{\mu}k^{2}}{\mu_{t}/\left(1+2k/c^{2}\right)+\mu_{laminar}} \qquad \text{-(F.12)}$$

together with the standard k-ε model constants and algebraic equations i.e.

$$\mu_{eff} = \mu_{laminar} + \mu_t \qquad \text{-(F.13)}$$

$$\mu_t = \frac{C_\mu \rho k^2}{\varepsilon} \qquad \text{-(F.14)}$$

$$k_e = k_{laminar} + \frac{\mu_e c_p}{\mathrm{Pr}_t} \qquad \text{-(F.15)}$$

$$C_\mu = 0.09$$

$$\mathrm{Pr}_t = 0.7$$

$$\sigma_k = 1.0$$

$$\sigma_\varepsilon = 1.3$$

$$C_1 = 1.44$$

$$C_2 = 1.92$$

and the logarithmic 'Law of the Wall' for cells adjacent to wall surfaces

$$u^+ = 5.0 + 0.41(\ln y^+) \qquad \text{-(F.16)}$$

where $u^+ = \frac{u}{u_\tau}$, $y^+ = \frac{u_\tau y}{\nu}$, $u_\tau = \left(\frac{\tau_w}{\rho}\right)^{\frac{1}{2}}$ and $\tau_{wall} = \mu\left(\frac{\partial u}{\partial y}\right)_{wall}$

APPENDIX G
Pipe Diffuser Geometry

For consistency, a generalised pipe diffuser arrangement is assumed and is shown in Figure G.1.

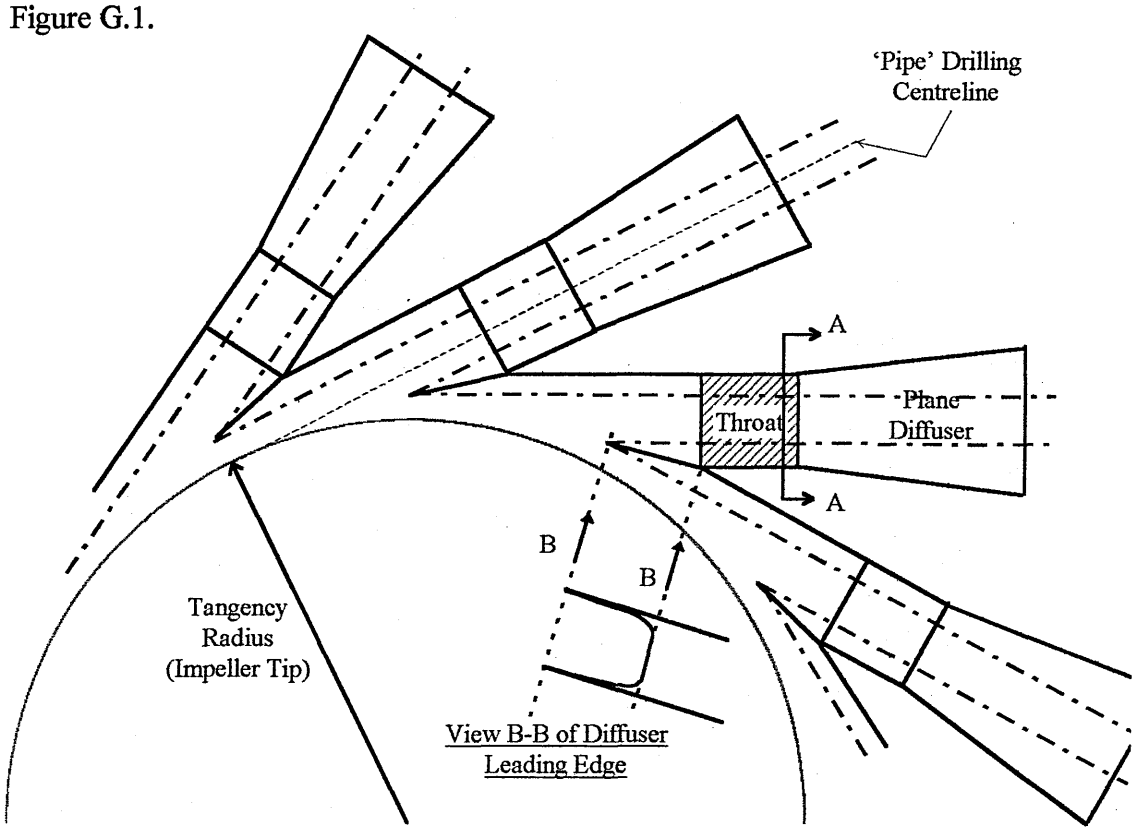


Figure G.1 Generalised Pipe Diffuser Geometry

This generalisation allows distortion of the cylindrical drilling to allow portions of straight wall as shown in Figure G.2. The dimension, b, is in the same direction as the impeller axis of rotation.
The cross-sectional area of a 'pipe', A_{th} is therefore:

$$A_{th} = \pi r_t^2 + 2r_t h + 2r_t b + hb \qquad \text{-(G.1)}$$

To simplify the derivation of the governing trigonometry, a Cartesian frame of reference is superimposed onto the geometry. The impeller axis of rotation is the assumed origin with one of the pipe centrelines running parallel to the x-axis (See Figure G.3).

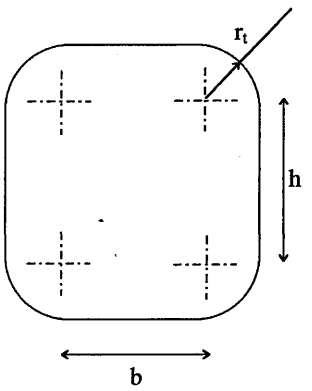


Figure G.2 Section A-A: Generalised Pipe Diffuser Cross Section Throat

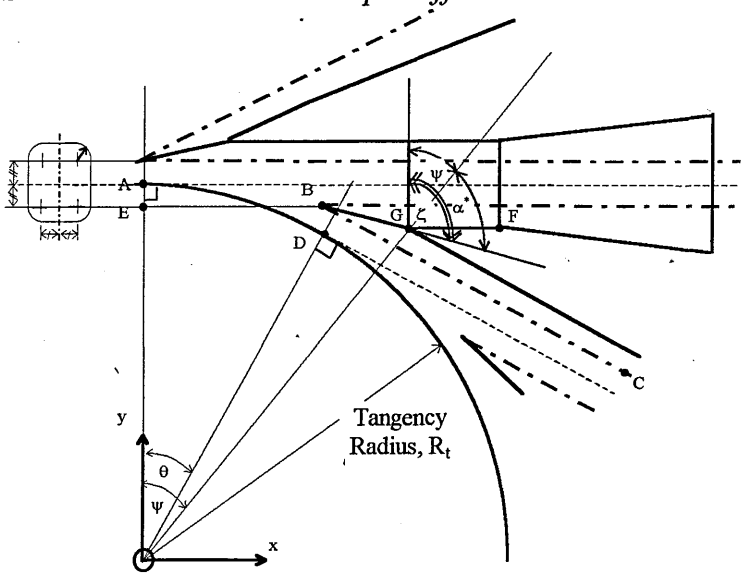


Figure G.3 Generalised Pipe Diffuser Geometry Nomenclature

Assuming the tangency radius is based on a line passing through the centre of this cross-section, the following trigonometric relations may be derived:

Consider line AB $\quad y_B = R_t - \frac{h}{2}$ -(G.2)

and equation of line BC

$$y_B - \left(R_t + \frac{h}{2}\right)\cos\theta = -\tan\theta\left[x_B - \left(R_t + \frac{h}{2}\right)\sin\theta\right]$$

$$\therefore \quad x_B = \frac{y_B - \left(R_t + \frac{h}{2}\right)\cos\theta}{-\tan\theta} + \left(R_t + \frac{h}{2}\right)\sin\theta \qquad \text{-(G.3)}$$

from these we get the co-ordinates of point B in a pipe 'scallop' i.e.

$$B = \left(\left(\frac{\left(R_t - \frac{h}{2}\right) - \left(R_t + \frac{h}{2}\right)\cos\theta}{-\tan\theta} + \left(R_t + \frac{h}{2}\right)\sin\theta\right), \left(R_t - \frac{h}{2}\right)\right)$$

Similarly, for line GF

$$y_G = R_t - \frac{h}{2} - r_t \qquad \text{-(G.4)}$$

and GD

$$y_G - \left(R_t + \frac{h}{2} + r_t\right)\cos\theta = -\tan\theta\left[x_G - \left(R_t + \frac{h}{2} + r_t\right)\sin\theta\right]$$

$$\therefore \quad x_G = \frac{y_G - \left(R_t + \frac{h}{2} + r_t\right)\cos\theta}{-\tan\theta} + \left(R_t + \frac{h}{2} + r_t\right)\sin\theta \qquad \text{-(G.5)}$$

and we get the co-ordinates of point G i.e.

$$G = \left(\left(\frac{\left(R_t - \frac{h}{2} - r_t\right) - \left(R_t + \frac{h}{2} + r_t\right)\cos\theta}{-\tan\theta} + \left(R_t + \frac{h}{2} + r_t\right)\sin\theta\right), \left(R_t - \frac{h}{2} - r_t\right)\right)$$

where the point G lies on a pipe leading edge.

Examining the angles we get

$$\zeta = \frac{\theta^o}{2} + 90^o \qquad \text{-(G.6)}$$

$$\theta = \frac{360^0}{number\ of\ pipes} \qquad \text{-(G.7)}$$

$$\psi = \tan^{-1}\left(\frac{x_G}{R_t - \frac{h}{2} - r_t}\right) \qquad \text{-(G.8)}$$

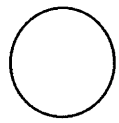
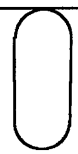
The bisector leading edge angle is given by: $\alpha^* = \zeta - \psi$ -(G.9)

and the leading edge radius, R_{le}, by $|OG| = \sqrt{\left(y_G^2 + x_G^2\right)}$ -(G.10)

together with the scallop radius, R_{sc}, $|OB| = \sqrt{\left(y_B^2 + x_B^2\right)}$ -(G.11)

Given a design throat area, number of pipes and sidewall expansion ratio, equations G.1 to G.11 may be iteratively solved for a unique solution, yielding a pipe geometry.

Table G.1 Geometric Details of all Pipe Diffusers Tested

Dimension	Pipe A -10% Throat	Pipe A -5% Throat	Pipe A 'Design Throat	Pipe A +5% Throat	Pipe B	Pipe C	Pipe D
Cross-Section							
Number of Pipes	31	31	31	31	22	13	13
Sidewall Expansion (W_3/W_2)	1.0511	1.077	1.105	1.132	1.312	1.706	1.05
Pipe Diameter (mm)	12.626	12.938	13.274	13.602	15.757	20.498	12.612
b (mm)	0	0	0	0	0	0	0
h (mm)	0	0	0	0	0	0	16.26
Tang. Radius, R_t (mm)	146.265	146.265	146.265	146.265	146.265	146.265	140.033
Bisector Angle* (deg)	67.00	66.49	65.95	65.43	69.46	74.13	67.35
Suction Surface Angle* (deg)	72.81	72.30	71.76	71.23	77.64	87.98	81.19
Leading Edge Radius, R_{le} (mm)	159.71	160.322	160.99	161.66	157.80	156.61	156.61
Scallop Radius, R_{sc} (mm)	147.02	147.02	147.02	147.02	147.66	150.64	148.47
R_{le}/ R_t (%)	1.092	1.096	1.101	1.105	1.079	1.071	1.0707
R_{sc}/ R_t (%)	1.005	1.005	1.005	1.005	1.010	1.030	1.015
Total Throat Area (mm^2)	3881.4	4075.5	4290.0	4504.5	4290.0	4290.0	4290.0
θ (deg)	11.61	11.61	11.61	11.61	16.36	27.69	27.69
x_b (mm)	14.87	14.87	14.87	14.87	21.03	36.05	67.57
y_b (mm)	146.26	146.26	146.26	146.26	146.26	146.26	132.2
x_g (mm)	76.95	78.49	80.14	81.75	75.83	77.63	93.16
y_g (mm)	139.95	139.80	139.63	139.46	138.39	136.02	125.89
ζ (mm)	95.81	95.81	95.81	95.81	98.18	103.85	103.85
ψ (mm)	28.80	29.31	29.85	30.38	28.72	29.72	36.50

*wrt radial direction

APPENDIX H

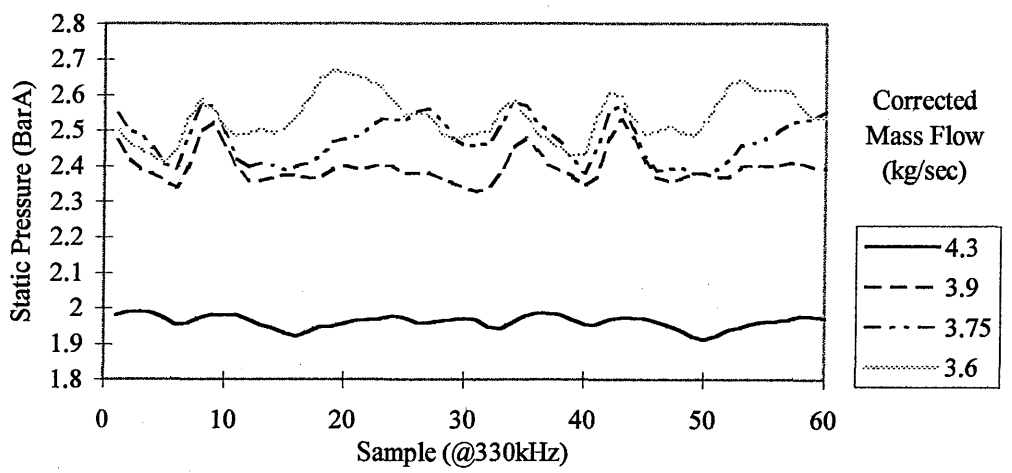
Unsteady Static-Pressure Measurements within the Pseudo- and Semi- Vaneless Spaces

Unsteady static pressure measurements were taken within each pipe diffuser using Kulite XCE-062 pressure transducers that were temperature compensated as described in Appendix B. To allow direct comparison, measurements were made at $1.04R_{tip}$ over the complete operating range of each pipe diffuser arrangement.

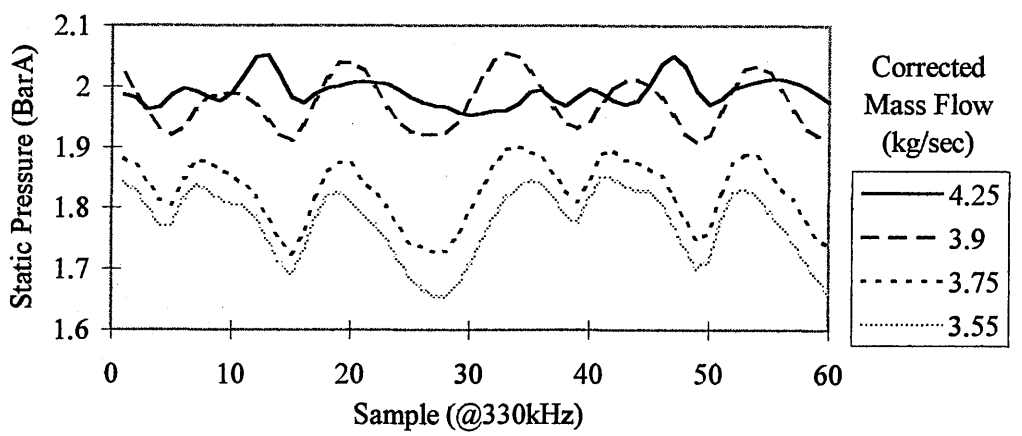
Further measurements were made at four locations along the complete pseudo- and semi-vaneless space passage for the 13 'oval' section pipe diffuser (i.e. pipe diffuser D).

All displayed data is the result of 500 ensemble averages, triggered once per revolution.

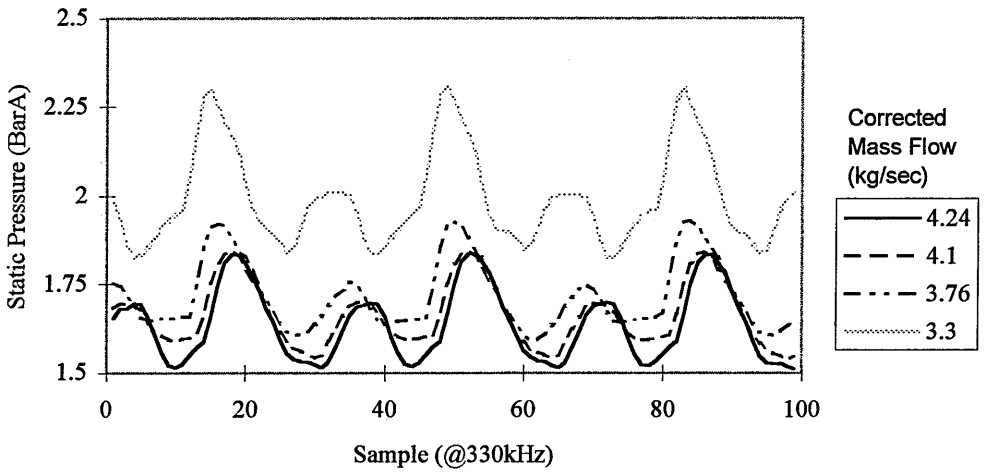
31 Circular Pipe Diffuser (Pipe Diffuser A)



22 Circular Pipe Diffuser (Pipe Diffuser B)

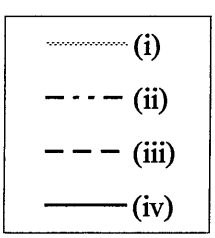


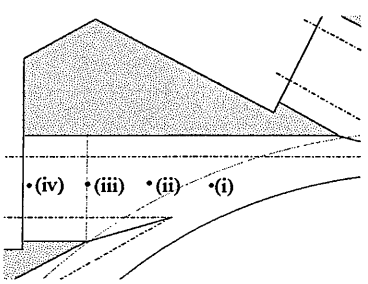
13 Circular Pipe Diffuser (Pipe Diffuser C)



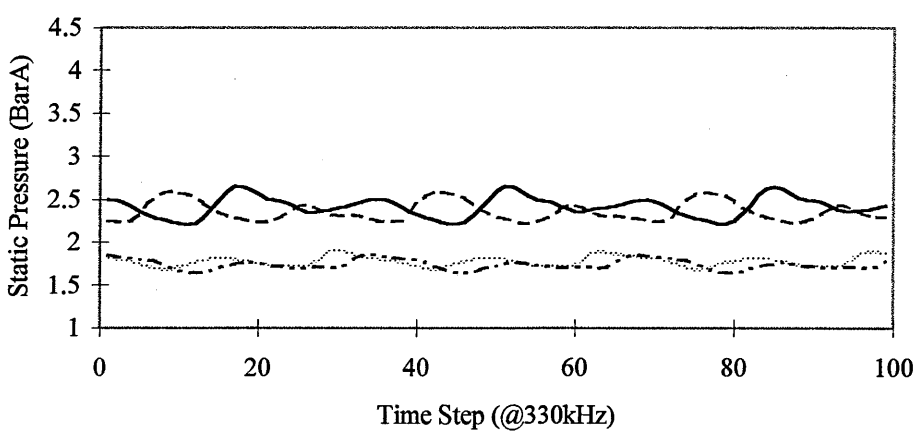
13 Oval Pipe Diffuser (Pipe Diffuser D)

Key:

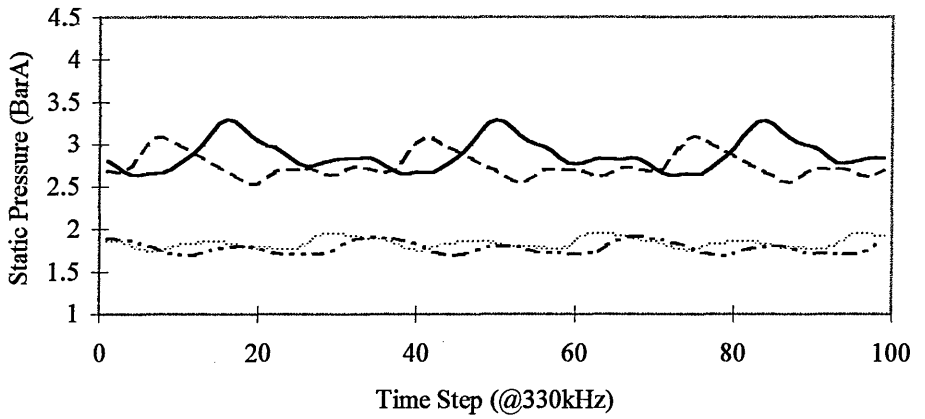




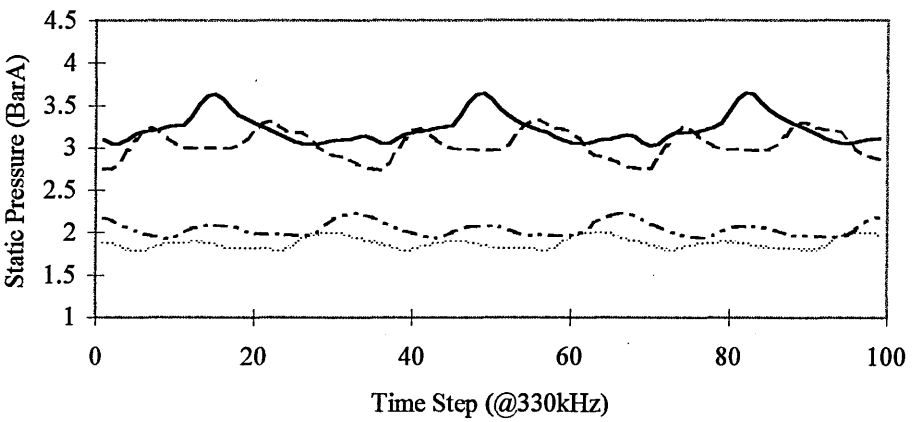
13 Oval Pipe Diffuser (Pipe Diffuser D): Corrected Mass Flow =4.25kg/sec



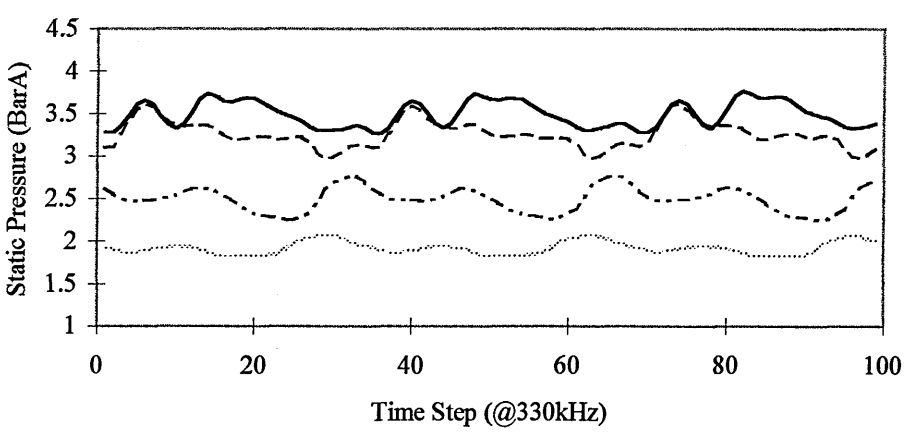
13 Oval Pipe Diffuser (Pipe Diffuser D): Corrected Mass Flow =4.1kg/sec



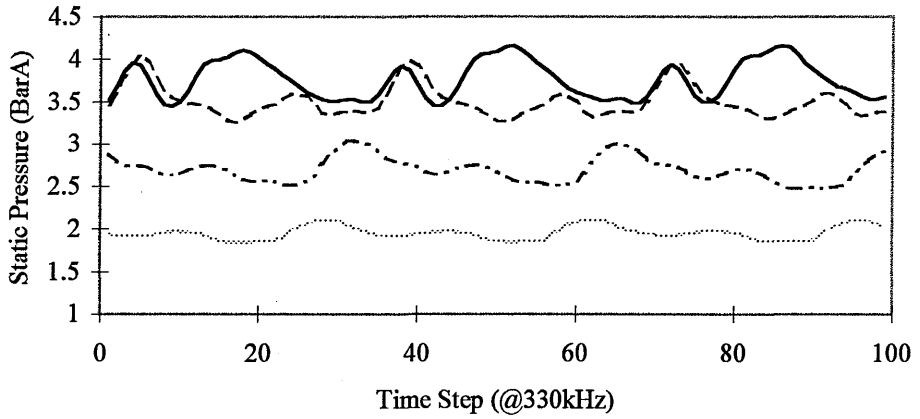
13 Oval Pipe Diffuser (Pipe Diffuser D): Corrected Mass Flow =3.9kg/sec



13 Oval Pipe Diffuser (Pipe Diffuser D): Corrected Mass Flow =3.7kg/sec



13 Oval Pipe Diffuser (Pipe Diffuser D): Corrected Mass Flow =3.45kg/sec



APPENDIX I
Pneumatic Diffuser Throat Traverses

I.1. Operating Points

The following tabulated operating duties were recorded using static instrumentation whilst traversing with the pneumatic total pressure instrumentation. The traversed measurements are presented in the accompanying section.

Table I.1 Operating Conditions for 31 Pipe Diffuser Traverses

Flow Condition	m_{corr} (kg/sec)	Corr. Speed (rpm)	$P_{tot\ out}$ (Pa)*	$P_{tot\ in}$ (Pa)	$T_{tot\ out}$ (K)	$T_{tot\ in}$ (K)
Near Surge	3.805	35002	464840	75883	498.0	284.6
Design	4.10	34918	424875	72324	491.6	284.2
Near Choke	4.30	34847	386650	70021	486.2	284.6

* At impeller discharge

Table I.2 Operating Conditions for 22 Pipe Diffuser Traverses

Flow Condition	m_{corr} (kg/sec)	Corr. Speed (rpm)	$P_{tot\ out}$ (Pa)*	$P_{tot\ in}$ (Pa)	$T_{tot\ out}$ (K)	$T_{tot\ in}$ (K)
At Surge	3.526	34951	483516	78728	494.31	279.05
Near Surge	3.743	34909	468871	76232	490.89	279.32
Near Design	3.949	34926	447006	73905	487.12	279.52
Near Choke	4.300	34961	393617	69819	480.64	279.46

* At impeller discharge

Table I.3 Operating Conditions for 13 Circular Pipe Diffuser Traverses

Flow Condition	m_{corr} (kg/sec)	Corr. Speed (rpm)	$P_{tot\ out}$ (Pa)*	$P_{tot\ in}$ (Pa)	$T_{tot\ out}$ (K)	$T_{tot\ in}$ (K)
Near Surge	3.349	34935	497214	80038	512.21	285.93
Mid-Range	3.756	34915	453097	75510	503.90	285.76
Near Choke	4.093	34930	409149	71517	496.86	285.64

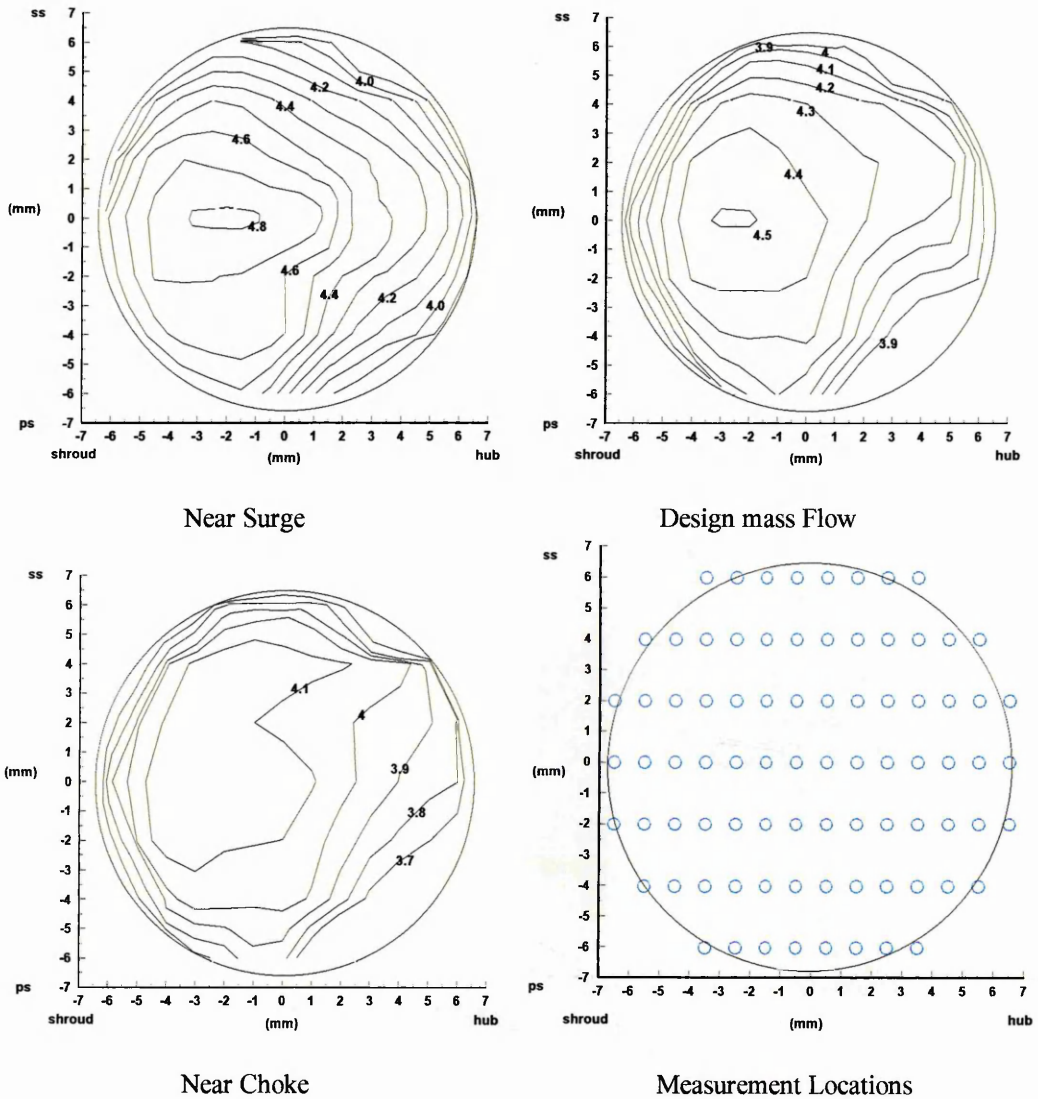
* At impeller discharge

Table I.4 Operating Conditions for 13 Oval Pipe Diffuser Traverses

Flow Condition	m_{corr} (kg/sec)	Corr. Speed (rpm)	$P_{tot\ out}$ (Pa)*	$P_{tot\ in}$ (Pa)	$T_{tot\ out}$ (K)	$T_{tot\ in}$ (K)
Near Surge	3.444	34935	495945	79035	512.26	287.09
	3.706	34907	470464	76104	505.84	286.87
Mid-Range	3.901	34912	449381	73835	502.85	287.29
	4.104	34917	418790	71471	499.20	287.46
Near Choke	4.260	34918	385914	69666	493.12	287.37

* At impeller discharge

I.2. MEASUREMENTS TAKEN AT DIFFUSER THROATS (BARA)



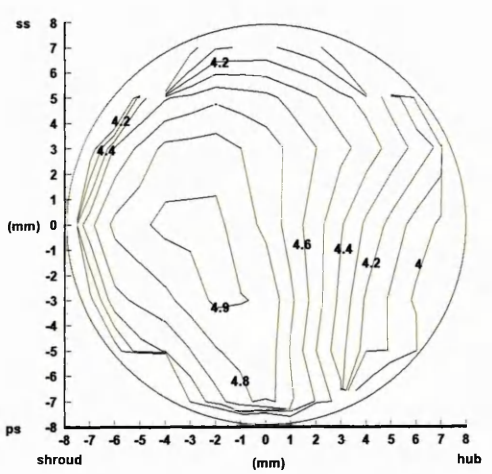
Near Surge

Design mass Flow

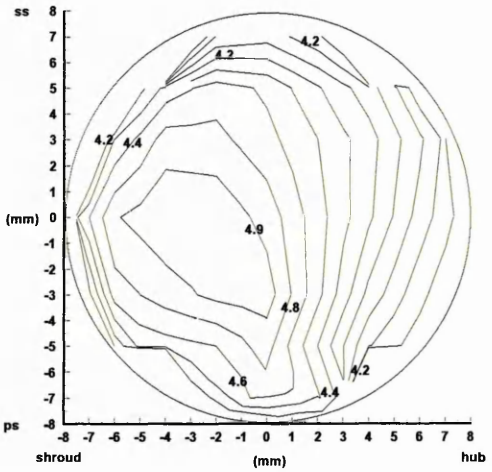
Near Choke

Measurement Locations

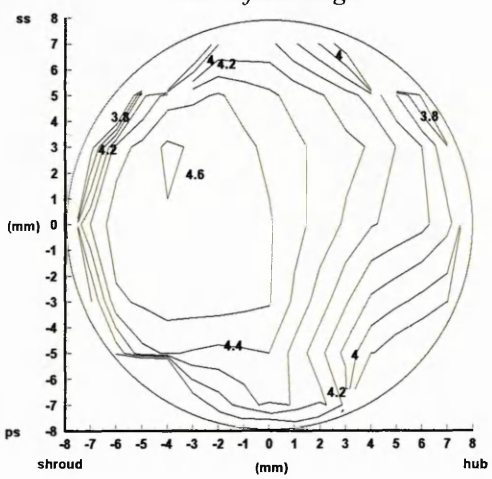
Figure I.1 31 Circular Pipe Diffuser Total Pressure (Bar A) at Diffuser Throat



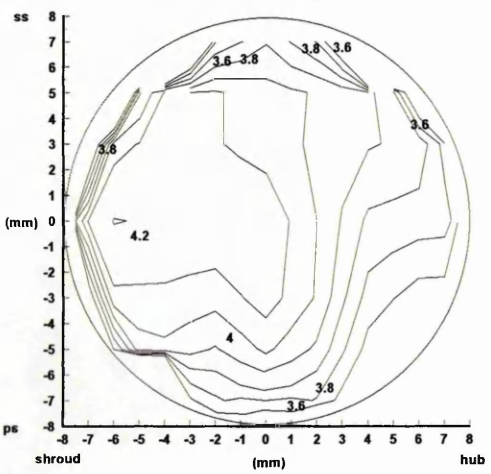
Just before Surge



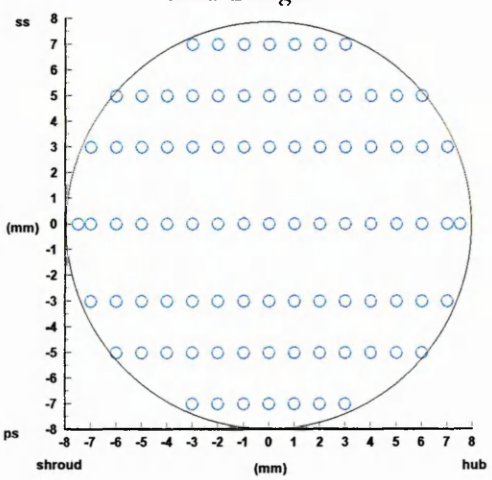
Near Surge



Near Design



Near Choke



Measurement Locations

Figure I.2 22 Pipe Diffuser Total Pressure at Diffuser Throat (Bar A)

APPENDIX J
Unsteady Diffuser Throat Traverses

The unsteady total pressure measurements taken within the diffuser throat of the pipe diffusers are presented here. As it is envisaged that comparison with computation predictions will involve computer 'movie' type presentations, the post-processed data (compensated for temperature) is given numerically. This will allow future investigators to import the data and manipulate it into the format of their choice.
Each data point represents an average of 500 (triggered once per revolution) samples. For brevity the data is presented as blocks of data with the x- and y-axis labels removed. The format for reading (or electronically scanning) the data precedes each data set.

J.1. 31 Circular Pipe Diffuser

Table J.1 Operating Conditions for 31 Pipe Diffuser Traverses

Flow Condition	m_{corr} (kg/sec)	Corr. Speed (rpm)	$P_{tot\ out}$ (Pa)*	$P_{tot\ in}$ (Pa)	$T_{tot\ out}$ (K)	$T_{tot\ in}$ (K)
Near Surge	3.803	34954	461020	75962	501.91	287.59
Design	4.055	34872	426036	72981	496.52	287.46
Near Choke	4.306	34951	378877	70217	489.05	287.65

* At impeller discharge

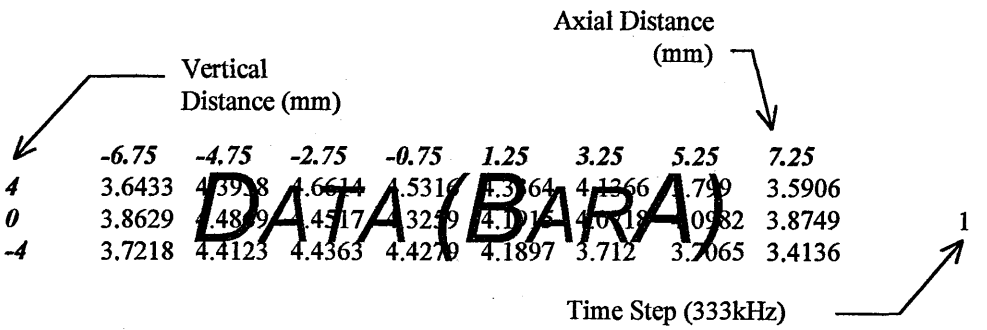


Figure J.1 Designations for 31 Circular Pipe Diffuser Data

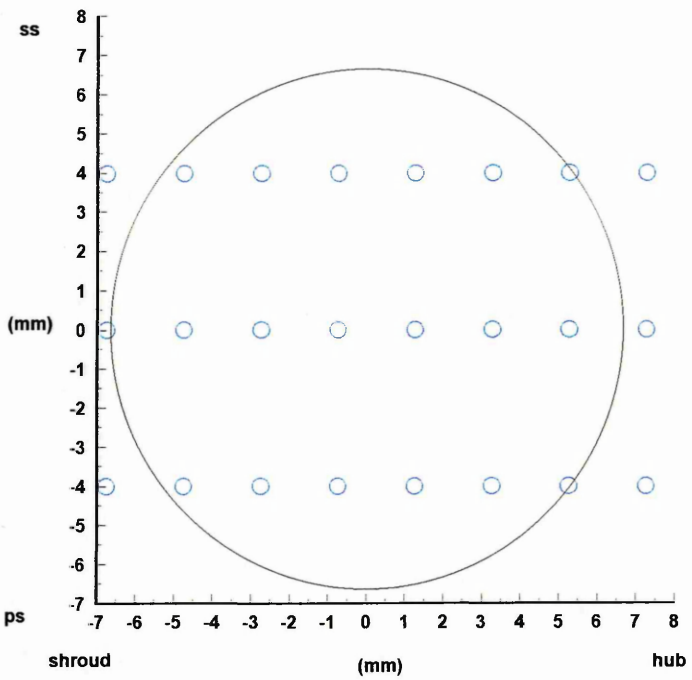


Figure J.2 Measurement Locations for 31 Circular Pipe Diffuser Unsteady Total Pressure Traverses

J.1.1 31 CIRCULAR PIPE DIFFUSER, 100% SPEED NEAR SURGE

3.643	4.394	4.661	4.532	4.336	4.137	3.799	3.591	
3.863	4.487	4.452	4.326	4.192	4.072	4.098	3.875	1
3.722	4.412	4.436	4.428	4.190	3.712	3.707	3.414	
3.742	4.564	4.856	4.737	4.553	4.325	3.899	3.651	
4.011	4.711	4.676	4.577	4.460	4.328	4.348	4.070	2
3.725	4.538	4.572	4.609	4.374	3.806	3.806	3.456	
3.767	4.627	4.886	4.748	4.538	4.305	3.916	3.724	
4.118	4.834	4.833	4.732	4.607	4.408	4.427	4.098	3
3.723	4.631	4.599	4.631	4.394	3.811	3.812	3.492	
3.677	4.555	4.735	4.612	4.351	4.134	3.842	3.738	
4.121	4.680	4.740	4.666	4.520	4.232	4.247	3.933	4
3.695	4.617	4.511	4.480	4.236	3.751	3.751	3.481	
3.510	4.423	4.518	4.482	4.274	4.074	3.793	3.674	
4.063	4.387	4.455	4.434	4.297	4.042	4.049	3.803	5
3.613	4.575	4.432	4.317	4.070	3.720	3.723	3.435	
3.416	4.421	4.458	4.446	4.320	4.157	3.830	3.620	
4.071	4.332	4.312	4.280	4.178	4.044	4.041	3.829	6
3.558	4.630	4.518	4.344	4.095	3.730	3.732	3.401	

3.495	4.545	4.641	4.622	4.529	4.355	3.937	3.661	
4.114	4.487	4.387	4.320	4.340	4.294	4.288	4.039	7
3.604	4.745	4.696	4.517	4.316	3.839	3.836	3.424	
3.649	4.695	4.883	4.915	4.853	4.629	4.082	3.780	
4.162	4.666	4.580	4.532	4.675	4.671	4.654	4.347	8
3.707	4.881	4.895	4.719	4.569	3.998	3.995	3.509	
3.747	4.762	4.970	5.018	4.959	4.690	4.149	3.885	
4.224	4.805	4.792	4.790	4.883	4.883	4.855	4.496	9
3.773	5.035	5.072	4.852	4.663	4.078	4.079	3.589	
3.734	4.747	4.832	4.794	4.716	4.492	4.088	3.888	
4.262	4.857	4.854	4.815	4.736	4.678	4.652	4.315	10
3.759	5.086	5.123	4.858	4.573	4.035	4.036	3.573	
3.638	4.612	4.655	4.584	4.495	4.324	3.996	3.765	
4.194	4.653	4.642	4.573	4.404	4.296	4.287	4.064	11
3.660	4.970	5.006	4.759	4.416	3.973	3.970	3.472	
3.519	4.415	4.487	4.524	4.519	4.362	3.991	3.604	
4.082	4.415	4.450	4.384	4.214	4.136	4.139	4.014	12
3.563	4.857	4.963	4.748	4.312	3.902	3.894	3.407	
3.467	4.376	4.452	4.527	4.610	4.440	4.019	3.538	
4.072	4.468	4.476	4.383	4.227	4.229	4.241	4.113	13
3.590	4.871	5.090	4.891	4.360	3.880	3.871	3.426	
3.559	4.448	4.571	4.589	4.616	4.412	4.007	3.582	
4.052	4.568	4.611	4.489	4.388	4.390	4.406	4.232	14
3.683	4.871	5.168	5.079	4.558	3.961	3.959	3.504	
3.659	4.382	4.542	4.616	4.674	4.496	4.037	3.631	
3.966	4.475	4.646	4.618	4.611	4.557	4.574	4.379	15
3.697	4.794	5.073	5.129	4.713	4.046	4.049	3.583	
3.639	4.285	4.449	4.666	4.840	4.684	4.114	3.652	
3.903	4.351	4.598	4.699	4.697	4.581	4.603	4.410	16
3.613	4.709	4.906	4.988	4.664	4.019	4.023	3.590	
3.545	4.372	4.548	4.686	4.817	4.658	4.130	3.691	
3.920	4.424	4.622	4.741	4.621	4.472	4.490	4.328	17
3.510	4.643	4.792	4.802	4.498	3.952	3.962	3.503	
3.515	4.408	4.580	4.550	4.508	4.374	4.017	3.719	
3.934	4.564	4.739	4.796	4.610	4.352	4.362	4.150	18
3.469	4.619	4.763	4.740	4.458	3.930	3.939	3.417	
3.524	4.307	4.483	4.405	4.326	4.225	3.930	3.661	
3.915	4.611	4.818	4.772	4.572	4.281	4.286	4.050	19
3.505	4.590	4.803	4.807	4.509	3.894	3.894	3.401	
3.501	4.229	4.460	4.474	4.422	4.264	3.925	3.559	
3.877	4.579	4.774	4.619	4.403	4.201	4.203	4.025	20
3.548	4.561	4.840	4.868	4.502	3.833	3.825	3.426	

3.453	4.246	4.537	4.593	4.519	4.324	3.941	3.548	
3.858	4.531	4.620	4.431	4.226	4.128	4.135	4.030	21
3.561	4.517	4.761	4.776	4.372	3.784	3.776	3.469	
3.442	4.245	4.523	4.521	4.400	4.251	3.915	3.626	
3.826	4.459	4.471	4.310	4.187	4.091	4.108	4.001	22
3.531	4.417	4.575	4.569	4.212	3.764	3.751	3.502	
3.485	4.197	4.431	4.290	4.154	4.098	3.866	3.688	
3.752	4.342	4.386	4.297	4.225	4.109	4.121	3.987	23
3.477	4.259	4.387	4.378	4.050	3.750	3.737	3.507	
3.543	4.109	4.334	4.204	4.035	4.023	3.843	3.687	
3.671	4.221	4.305	4.302	4.227	4.148	4.147	3.994	24
3.443	4.159	4.271	4.244	3.927	3.731	3.717	3.481	
3.544	4.084	4.328	4.270	4.094	4.073	3.846	3.689	
3.634	4.187	4.212	4.239	4.133	4.090	4.078	3.914	25
3.480	4.153	4.232	4.162	3.871	3.681	3.668	3.443	
3.501	4.133	4.415	4.387	4.241	4.130	3.841	3.709	
3.632	4.233	4.202	4.159	4.038	3.960	3.941	3.770	26
3.563	4.188	4.235	4.157	3.891	3.622	3.606	3.387	
3.475	4.209	4.543	4.491	4.361	4.172	3.849	3.695	
3.674	4.334	4.280	4.175	4.064	3.941	3.912	3.743	27
3.625	4.210	4.265	4.219	3.951	3.581	3.564	3.327	
3.514	4.283	4.671	4.599	4.398	4.222	3.890	3.651	
3.733	4.438	4.402	4.295	4.158	4.050	4.016	3.867	28
3.625	4.219	4.290	4.281	4.021	3.586	3.566	3.312	
3.580	4.314	4.673	4.565	4.331	4.225	3.908	3.677	
3.758	4.458	4.472	4.392	4.233	4.151	4.116	3.975	29
3.574	4.213	4.293	4.314	4.074	3.616	3.602	3.366	
3.610	4.238	4.479	4.351	4.153	4.089	3.861	3.760	
3.736	4.336	4.368	4.344	4.261	4.155	4.121	3.929	30
3.524	4.199	4.270	4.280	4.072	3.652	3.638	3.426	
3.567	4.112	4.266	4.163	4.016	3.958	3.812	3.785	
3.698	4.149	4.143	4.188	4.224	4.098	4.066	3.818	31
3.513	4.168	4.219	4.209	4.058	3.683	3.673	3.444	
3.503	4.057	4.199	4.128	4.008	3.926	3.782	3.706	
3.673	4.052	4.026	4.080	4.107	4.019	3.997	3.750	32
3.554	4.160	4.175	4.174	4.051	3.685	3.674	3.437	
3.492	4.123	4.288	4.206	4.055	3.955	3.758	3.614	
3.697	4.140	4.125	4.080	4.006	3.941	3.922	3.721	33
3.641	4.234	4.219	4.209	4.058	3.661	3.649	3.428	
3.570	4.275	4.502	4.399	4.166	4.020	3.757	3.582	
3.782	4.336	4.326	4.206	4.068	3.968	3.950	3.770	34
3.723	4.367	4.355	4.323	4.123	3.683	3.666	3.427	

3.677	4.456	4.733	4.644	4.395	4.219	3.845	3.611	
3.924	4.576	4.550	4.438	4.302	4.177	4.162	3.956	35
3.749	4.512	4.522	4.502	4.286	3.787	3.769	3.443	
3.757	4.610	4.913	4.802	4.560	4.350	3.926	3.686	
4.068	4.796	4.767	4.676	4.544	4.400	4.386	4.112	36
3.737	4.644	4.637	4.650	4.443	3.851	3.837	3.481	
3.752	4.642	4.922	4.753	4.483	4.257	3.908	3.752	
4.154	4.854	4.852	4.752	4.602	4.389	4.372	4.053	37
3.719	4.702	4.624	4.608	4.390	3.818	3.804	3.506	
3.639	4.538	4.750	4.608	4.315	4.084	3.821	3.733	
4.130	4.620	4.676	4.612	4.449	4.181	4.161	3.870	38
3.668	4.640	4.496	4.410	4.176	3.754	3.741	3.477	
3.481	4.413	4.533	4.476	4.278	4.070	3.801	3.647	
4.097	4.374	4.419	4.392	4.239	4.042	4.026	3.802	39
3.589	4.622	4.468	4.287	4.043	3.756	3.740	3.435	
3.425	4.450	4.534	4.483	4.347	4.176	3.855	3.609	
4.118	4.402	4.364	4.302	4.209	4.116	4.113	3.892	40
3.576	4.710	4.625	4.396	4.162	3.800	3.787	3.420	
3.530	4.581	4.752	4.718	4.611	4.433	3.985	3.680	
4.156	4.556	4.475	4.390	4.447	4.419	4.425	4.160	41
3.645	4.837	4.836	4.624	4.433	3.943	3.931	3.455	
3.671	4.709	4.978	4.997	4.901	4.677	4.122	3.797	
4.188	4.711	4.673	4.637	4.787	4.790	4.797	4.463	42
3.727	4.970	5.043	4.841	4.684	4.085	4.078	3.535	
3.729	4.736	4.969	4.996	4.897	4.655	4.151	3.875	
4.240	4.840	4.846	4.842	4.888	4.882	4.887	4.518	43
3.760	5.097	5.211	4.970	4.741	4.133	4.127	3.585	
3.688	4.711	4.830	4.749	4.614	4.413	4.049	3.842	
4.237	4.816	4.812	4.757	4.631	4.542	4.550	4.244	44
3.711	5.078	5.188	4.919	4.601	4.048	4.047	3.533	
3.600	4.567	4.648	4.564	4.455	4.309	3.970	3.705	
4.146	4.567	4.569	4.497	4.313	4.176	4.185	4.016	45
3.603	4.915	5.019	4.782	4.410	3.961	3.962	3.422	
3.504	4.401	4.487	4.500	4.487	4.355	3.981	3.559	
4.071	4.406	4.457	4.405	4.218	4.123	4.137	4.051	46
3.538	4.840	5.016	4.810	4.352	3.899	3.900	3.382	
3.497	4.417	4.514	4.514	4.555	4.409	4.004	3.532	
4.072	4.499	4.545	4.470	4.295	4.270	4.281	4.174	47
3.600	4.850	5.151	4.995	4.470	3.924	3.921	3.444	
3.592	4.431	4.588	4.583	4.590	4.386	3.989	3.590	
4.010	4.501	4.641	4.588	4.489	4.417	4.422	4.257	48
3.672	4.816	5.178	5.155	4.689	4.014	4.013	3.541	

3.652	4.322	4.495	4.599	4.675	4.528	4.053	3.625	
3.908	4.351	4.636	4.706	4.701	4.557	4.555	4.381	49
3.642	4.704	5.028	5.118	4.774	4.082	4.074	3.593	
3.601	4.306	4.497	4.690	4.808	4.680	4.120	3.646	
3.885	4.315	4.635	4.794	4.765	4.583	4.589	4.421	50
3.546	4.626	4.863	4.898	4.619	4.025	4.023	3.561	
3.545	4.413	4.631	4.698	4.708	4.596	4.106	3.702	
3.923	4.486	4.738	4.851	4.697	4.468	4.467	4.262	51
3.474	4.588	4.782	4.724	4.421	3.951	3.953	3.468	
3.536	4.426	4.647	4.579	4.444	4.304	3.965	3.727	
3.921	4.621	4.852	4.859	4.648	4.302	4.291	4.017	52
3.479	4.572	4.787	4.699	4.410	3.904	3.906	3.404	
3.536	4.351	4.607	4.504	4.355	4.204	3.906	3.640	
3.882	4.632	4.879	4.778	4.523	4.202	4.186	3.945	53
3.517	4.525	4.844	4.790	4.462	3.855	3.845	3.390	
3.500	4.323	4.659	4.602	4.480	4.275	3.917	3.540	
3.856	4.618	4.798	4.622	4.329	4.144	4.137	3.973	54
3.533	4.497	4.856	4.814	4.421	3.797	3.780	3.415	
3.460	4.320	4.706	4.674	4.533	4.322	3.932	3.565	
3.855	4.605	4.646	4.459	4.217	4.103	4.109	3.980	55
3.529	4.462	4.740	4.684	4.282	3.754	3.735	3.461	
3.459	4.295	4.662	4.568	4.372	4.204	3.891	3.654	
3.820	4.529	4.523	4.361	4.212	4.082	4.089	3.940	56
3.501	4.356	4.544	4.484	4.122	3.728	3.715	3.492	
3.513	4.235	4.554	4.377	4.149	4.055	3.841	3.689	
3.748	4.388	4.443	4.356	4.237	4.077	4.075	3.923	57
3.459	4.212	4.384	4.326	3.971	3.714	3.706	3.481	
3.555	4.162	4.457	4.324	4.078	4.021	3.824	3.658	
3.681	4.280	4.345	4.349	4.203	4.080	4.072	3.913	58
3.449	4.160	4.303	4.200	3.857	3.684	3.681	3.448	
3.537	4.148	4.467	4.381	4.143	4.078	3.825	3.661	
3.652	4.250	4.244	4.255	4.106	3.994	3.992	3.795	59
3.499	4.183	4.258	4.116	3.811	3.620	3.621	3.406	
3.483	4.188	4.575	4.465	4.281	4.124	3.817	3.703	
3.665	4.299	4.239	4.171	4.051	3.893	3.898	3.665	60
3.575	4.205	4.239	4.125	3.837	3.557	3.555	3.347	

J.1.2 31 PIPE DIFFUSER, 100% SPEED, DESIGN MASS FLOW

2.974	3.955	4.212	4.197	4.149	4.043	3.497	3.077	
3.522	3.995	3.943	3.915	3.909	3.894	3.797	2.994	1
3.003	3.837	3.846	3.907	3.765	3.636	3.453	3.025	

2.982	4.064	4.338	4.330	4.312	4.163	3.553	3.132	
3.613	4.171	4.101	4.112	4.152	4.141	3.981	3.056	2
3.025	3.968	3.988	4.040	3.914	3.781	3.539	3.085	
2.983	4.143	4.393	4.370	4.311	4.124	3.561	3.198	
3.679	4.273	4.217	4.252	4.269	4.222	4.038	3.072	3
3.050	4.049	4.066	4.095	3.959	3.785	3.558	3.112	
2.948	4.148	4.334	4.302	4.212	4.064	3.541	3.205	
3.690	4.214	4.225	4.245	4.183	4.069	3.939	3.031	4
3.029	4.032	4.024	4.017	3.872	3.662	3.523	3.088	
2.892	4.065	4.164	4.175	4.134	4.045	3.543	3.150	
3.678	4.054	4.095	4.124	4.003	3.871	3.815	2.962	5
2.966	3.986	3.940	3.874	3.754	3.534	3.489	3.040	
2.882	4.016	4.101	4.118	4.125	4.066	3.573	3.115	
3.686	3.990	3.985	4.011	3.904	3.792	3.750	2.918	6
2.932	4.015	3.993	3.863	3.784	3.539	3.492	3.011	
2.955	4.065	4.246	4.263	4.280	4.232	3.665	3.160	
3.704	4.070	4.027	4.042	4.042	3.978	3.894	2.950	7
2.978	4.105	4.183	4.032	3.990	3.717	3.580	3.035	
3.062	4.124	4.362	4.403	4.453	4.414	3.772	3.250	
3.736	4.218	4.188	4.210	4.298	4.294	4.173	3.051	8
3.080	4.220	4.407	4.263	4.244	3.939	3.705	3.120	
3.130	4.116	4.295	4.365	4.442	4.428	3.814	3.313	
3.775	4.345	4.336	4.352	4.451	4.473	4.342	3.135	9
3.172	4.330	4.577	4.446	4.418	4.014	3.776	3.203	
3.134	4.106	4.205	4.235	4.276	4.277	3.772	3.290	
3.800	4.395	4.385	4.339	4.348	4.332	4.248	3.131	10
3.206	4.392	4.635	4.506	4.442	3.948	3.767	3.212	
3.105	4.056	4.156	4.205	4.209	4.199	3.739	3.191	
3.778	4.311	4.325	4.211	4.122	4.066	4.075	3.069	11
3.170	4.356	4.559	4.432	4.324	3.839	3.735	3.150	
3.073	3.968	4.065	4.151	4.183	4.177	3.725	3.108	
3.748	4.222	4.282	4.146	3.990	3.935	3.990	3.025	12
3.141	4.291	4.498	4.372	4.193	3.766	3.684	3.107	
3.091	3.942	4.001	4.026	4.056	4.059	3.674	3.124	
3.751	4.284	4.338	4.160	3.969	3.919	3.939	3.020	13
3.182	4.306	4.568	4.428	4.172	3.778	3.657	3.130	
3.151	3.902	3.993	4.025	4.013	3.973	3.635	3.182	
3.727	4.332	4.427	4.248	4.070	3.968	3.922	3.019	14
3.261	4.319	4.659	4.566	4.313	3.937	3.718	3.204	
3.179	3.889	4.102	4.252	4.256	4.152	3.671	3.204	
3.664	4.270	4.437	4.357	4.265	4.136	4.045	3.027	15
3.274	4.251	4.630	4.623	4.423	4.078	3.777	3.273	

3.170	3.964	4.297	4.480	4.468	4.316	3.737	3.208	
3.660	4.283	4.477	4.466	4.412	4.300	4.183	3.074	16
3.212	4.180	4.499	4.501	4.304	4.013	3.753	3.274	
3.172	4.019	4.376	4.462	4.418	4.282	3.740	3.240	
3.706	4.429	4.557	4.491	4.356	4.248	4.134	3.144	17
3.145	4.176	4.444	4.353	4.063	3.885	3.691	3.199	
3.167	3.964	4.309	4.341	4.253	4.135	3.672	3.252	
3.710	4.489	4.581	4.451	4.272	4.090	3.925	3.140	18
3.139	4.193	4.459	4.322	3.972	3.876	3.664	3.119	
3.128	3.919	4.273	4.292	4.208	4.074	3.621	3.210	
3.658	4.412	4.528	4.408	4.213	4.010	3.813	3.056	19
3.167	4.138	4.460	4.378	3.962	3.853	3.613	3.083	
3.095	3.919	4.305	4.300	4.226	4.080	3.618	3.173	
3.623	4.362	4.475	4.351	4.087	3.951	3.802	2.994	20
3.174	4.085	4.423	4.385	3.906	3.769	3.575	3.085	
3.096	3.933	4.329	4.275	4.187	4.058	3.614	3.209	
3.614	4.372	4.382	4.228	3.946	3.881	3.784	2.998	21
3.164	4.098	4.355	4.265	3.784	3.725	3.560	3.125	
3.124	3.930	4.289	4.153	4.054	3.979	3.583	3.273	
3.608	4.355	4.260	4.103	3.935	3.877	3.773	3.012	22
3.155	4.080	4.232	4.079	3.654	3.682	3.542	3.165	
3.152	3.894	4.192	3.991	3.915	3.883	3.551	3.283	
3.584	4.273	4.181	4.084	4.008	3.920	3.802	3.014	23
3.119	3.961	4.076	3.934	3.526	3.568	3.484	3.166	
3.138	3.838	4.114	3.924	3.880	3.884	3.547	3.229	
3.551	4.164	4.149	4.135	4.016	3.923	3.826	3.034	24
3.061	3.836	3.935	3.810	3.441	3.471	3.423	3.133	
3.080	3.839	4.132	3.987	3.943	3.915	3.541	3.183	
3.521	4.076	4.068	4.099	3.935	3.882	3.770	3.060	25
3.038	3.796	3.843	3.708	3.414	3.457	3.367	3.098	
3.028	3.869	4.183	4.081	4.037	3.916	3.514	3.164	
3.508	4.026	3.979	3.985	3.855	3.831	3.682	3.044	26
3.063	3.780	3.781	3.647	3.422	3.472	3.348	3.064	
3.019	3.882	4.218	4.136	4.083	3.914	3.486	3.145	
3.506	3.991	3.934	3.895	3.818	3.829	3.681	3.000	27
3.076	3.729	3.740	3.660	3.449	3.480	3.334	3.047	
3.032	3.867	4.184	4.113	4.064	3.946	3.492	3.138	
3.491	3.964	3.949	3.893	3.822	3.883	3.776	2.983	28
3.034	3.667	3.720	3.725	3.517	3.532	3.353	3.067	
3.028	3.844	4.061	4.015	3.987	3.925	3.499	3.192	
3.473	3.960	3.977	3.941	3.845	3.944	3.859	3.004	29
2.973	3.671	3.756	3.808	3.610	3.625	3.397	3.117	

3.007	3.813	3.933	3.916	3.940	3.861	3.490	3.266	
3.457	3.925	3.949	3.968	3.907	3.950	3.823	3.004	30
2.935	3.711	3.790	3.822	3.630	3.657	3.432	3.144	
2.978	3.773	3.872	3.906	3.959	3.844	3.473	3.270	
3.434	3.834	3.853	3.944	3.961	3.907	3.739	2.962	31
2.942	3.714	3.776	3.781	3.592	3.633	3.434	3.117	
2.950	3.753	3.867	3.930	3.975	3.855	3.454	3.193	
3.412	3.764	3.787	3.879	3.919	3.837	3.692	2.911	32
2.967	3.702	3.740	3.760	3.575	3.583	3.408	3.060	
2.946	3.772	3.914	3.972	3.963	3.840	3.434	3.103	
3.432	3.808	3.811	3.843	3.802	3.762	3.669	2.902	33
3.001	3.735	3.751	3.804	3.602	3.537	3.382	3.020	
2.967	3.847	4.059	4.094	4.058	3.936	3.460	3.061	
3.479	3.934	3.915	3.891	3.810	3.796	3.738	2.945	34
3.028	3.813	3.829	3.904	3.699	3.588	3.422	3.015	
2.993	3.957	4.243	4.288	4.270	4.143	3.538	3.089	
3.558	4.093	4.066	4.062	4.045	4.040	3.959	3.022	35
3.043	3.927	3.949	4.025	3.866	3.760	3.529	3.060	
3.007	4.075	4.387	4.415	4.413	4.238	3.589	3.168	
3.644	4.246	4.229	4.250	4.283	4.264	4.122	3.074	36
3.052	4.043	4.080	4.114	4.015	3.885	3.596	3.122	
2.994	4.142	4.424	4.404	4.349	4.157	3.578	3.219	
3.697	4.303	4.311	4.326	4.327	4.255	4.112	3.065	37
3.054	4.101	4.128	4.095	4.005	3.832	3.593	3.138	
2.938	4.118	4.314	4.285	4.210	4.082	3.551	3.188	
3.687	4.191	4.260	4.252	4.176	4.055	3.980	3.003	38
3.028	4.056	4.048	3.966	3.871	3.665	3.549	3.090	
2.880	4.035	4.131	4.134	4.108	4.053	3.552	3.115	
3.666	4.042	4.118	4.119	3.984	3.871	3.852	2.943	39
2.981	4.005	3.986	3.870	3.791	3.557	3.525	3.034	
2.895	4.017	4.107	4.117	4.127	4.100	3.593	3.098	
3.665	4.040	4.061	4.057	3.943	3.856	3.822	2.928	40
2.971	4.040	4.095	3.964	3.915	3.629	3.543	3.021	
2.992	4.070	4.254	4.278	4.318	4.310	3.700	3.172	
3.682	4.160	4.156	4.136	4.125	4.096	4.030	2.989	41
3.030	4.119	4.289	4.190	4.179	3.852	3.651	3.068	
3.095	4.107	4.331	4.392	4.474	4.473	3.802	3.276	
3.707	4.297	4.315	4.295	4.377	4.402	4.302	3.091	42
3.116	4.203	4.466	4.416	4.434	4.042	3.751	3.158	
3.142	4.088	4.248	4.314	4.387	4.404	3.811	3.328	
3.749	4.396	4.437	4.404	4.471	4.486	4.380	3.148	43
3.176	4.274	4.562	4.564	4.574	4.085	3.784	3.219	

3.130	4.066	4.167	4.189	4.190	4.204	3.755	3.276	
3.765	4.411	4.462	4.375	4.322	4.252	4.198	3.118	44
3.179	4.293	4.546	4.578	4.550	4.020	3.743	3.195	
3.093	3.995	4.103	4.138	4.123	4.128	3.728	3.167	
3.738	4.308	4.408	4.289	4.123	3.992	4.016	3.057	45
3.146	4.239	4.440	4.473	4.407	3.935	3.692	3.126	
3.072	3.936	4.029	4.062	4.084	4.098	3.710	3.100	
3.716	4.257	4.393	4.279	4.047	3.913	3.932	3.028	46
3.136	4.211	4.427	4.412	4.278	3.875	3.630	3.095	
3.119	3.932	4.019	3.990	3.967	3.952	3.642	3.136	
3.716	4.337	4.471	4.346	4.080	3.922	3.866	3.027	47
3.193	4.251	4.528	4.483	4.271	3.913	3.624	3.134	
3.186	3.895	4.064	4.089	4.009	3.896	3.604	3.186	
3.671	4.358	4.550	4.452	4.215	3.986	3.833	3.010	48
3.254	4.251	4.587	4.615	4.390	4.052	3.699	3.208	
3.197	3.903	4.222	4.359	4.280	4.111	3.656	3.191	
3.615	4.291	4.555	4.529	4.396	4.171	3.972	3.016	49
3.227	4.180	4.516	4.638	4.416	4.119	3.738	3.268	
3.166	3.987	4.408	4.570	4.463	4.244	3.722	3.199	
3.640	4.362	4.612	4.583	4.466	4.313	4.090	3.086	50
3.150	4.128	4.403	4.496	4.236	3.999	3.691	3.244	
3.154	4.026	4.462	4.523	4.365	4.145	3.704	3.248	
3.687	4.498	4.661	4.554	4.359	4.213	3.991	3.155	51
3.109	4.147	4.392	4.388	4.028	3.873	3.637	3.162	
3.137	3.986	4.390	4.384	4.216	3.978	3.610	3.260	
3.675	4.516	4.625	4.488	4.269	4.029	3.774	3.120	52
3.133	4.147	4.413	4.379	3.973	3.841	3.602	3.089	
3.109	3.969	4.366	4.326	4.196	3.938	3.563	3.198	
3.633	4.437	4.540	4.422	4.185	3.952	3.705	3.020	53
3.155	4.083	4.404	4.428	3.965	3.787	3.545	3.058	
3.102	3.986	4.386	4.329	4.230	3.988	3.574	3.156	
3.620	4.415	4.491	4.344	4.042	3.883	3.709	2.973	54
3.145	4.056	4.372	4.391	3.898	3.720	3.518	3.057	
3.120	3.999	4.387	4.292	4.188	3.991	3.575	3.207	
3.624	4.419	4.404	4.215	3.940	3.830	3.687	2.987	55
3.136	4.075	4.300	4.239	3.787	3.694	3.501	3.101	
3.136	3.992	4.319	4.147	4.053	3.913	3.543	3.278	
3.615	4.369	4.281	4.098	3.965	3.856	3.680	2.999	56
3.123	4.030	4.178	4.057	3.671	3.636	3.460	3.131	
3.139	3.944	4.210	3.991	3.923	3.816	3.508	3.278	
3.593	4.256	4.200	4.087	4.028	3.913	3.718	3.001	57
3.087	3.905	4.028	3.922	3.559	3.517	3.399	3.121	

3.101	3.902	4.151	3.963	3.912	3.847	3.511	3.219	
3.558	4.134	4.136	4.117	4.002	3.920	3.736	3.019	58
3.047	3.818	3.899	3.816	3.499	3.454	3.355	3.091	
3.047	3.909	4.184	4.062	3.985	3.895	3.502	3.176	
3.531	4.036	4.032	4.047	3.911	3.877	3.671	3.040	59
3.051	3.796	3.815	3.735	3.494	3.465	3.332	3.073	
3.012	3.934	4.235	4.157	4.068	3.898	3.472	3.157	
3.517	3.985	3.947	3.918	3.842	3.824	3.602	3.024	60
3.083	3.767	3.760	3.699	3.508	3.481	3.320	3.049	

J.1.3 31 PIPE DIFFUSER, 100% SPEED, NEAR CHOKE

1.3904	3.5537	3.6967	3.6503	3.6376	3.6288	2.6626	1.4908	
2.9312	3.6874	3.6699	3.6589	3.6136	3.6001	3.5119	1.565	1
1.4702	3.6492	3.8281	3.6704	3.8182	3.5456	2.7476	1.2254	
1.4078	3.6001	3.7565	3.7167	3.7184	3.689	2.691	1.5047	
2.9576	3.7999	3.7739	3.7314	3.6597	3.6279	3.5463	1.548	2
1.4721	3.7615	3.8891	3.7067	4.0167	3.7249	2.7708	1.2143	
1.4274	3.6218	3.7906	3.7657	3.7669	3.7302	2.7208	1.5173	
2.9649	3.8654	3.8841	3.8129	3.6939	3.63	3.5429	1.536	3
1.4744	3.8482	3.9192	3.7495	4.1273	3.8987	2.7924	1.1968	
1.4467	3.5684	3.7179	3.7172	3.725	3.6947	2.7347	1.5322	
2.9445	3.8405	3.9384	3.8697	3.7077	3.5914	3.4901	1.5223	4
1.4707	3.8727	3.9547	3.8356	4.1104	3.9584	2.812	1.1835	
1.4695	3.4696	3.5811	3.5876	3.6011	3.5797	2.7272	1.5488	
2.9123	3.7811	3.9314	3.8949	3.7088	3.5289	3.3999	1.5076	5
1.4669	3.8379	3.9835	3.9473	4.0053	3.8553	2.8202	1.1715	
1.4996	3.3866	3.4647	3.4672	3.4628	3.4368	2.7069	1.5654	
2.899	3.7748	3.9305	3.933	3.74	3.509	3.3284	1.4991	6
1.4646	3.7898	3.9937	4.0352	3.8957	3.6806	2.8094	1.1607	
1.5332	3.3646	3.4487	3.4396	3.4133	3.3661	2.6957	1.5827	
2.9056	3.841	3.9884	4.0202	3.8462	3.5843	3.3142	1.5024	7
1.4716	3.7767	4.0333	4.0897	3.8229	3.5486	2.7971	1.1588	
1.5644	3.4066	3.5679	3.5657	3.533	3.4251	2.6987	1.5993	
2.9392	3.9634	4.1085	4.1646	4.0237	3.7471	3.3854	1.5116	8
1.4875	3.8313	4.1386	4.1615	3.8136	3.4994	2.8022	1.1653	
1.5932	3.5179	3.81	3.8389	3.8109	3.6201	2.725	1.6153	
2.9869	4.1006	4.2477	4.2965	4.177	3.9248	3.5167	1.5244	9
1.5124	3.899	4.2457	4.2479	3.8118	3.4981	2.8233	1.1724	
1.6056	3.6103	4.0382	4.1298	4.1066	3.8582	2.7583	1.631	
3.0205	4.1294	4.305	4.3407	4.2348	4.0523	3.6604	1.5346	10
1.5317	3.9064	4.2557	4.2729	3.7279	3.4446	2.829	1.1809	

1.5977	3.6509	4.138	4.2494	4.2064	3.9441	2.7648	1.6352	
3.0344	4.0761	4.258	4.2231	4.0912	3.9553	3.6405	1.5294	11
1.5501	3.8692	4.2194	4.2437	3.5548	3.3078	2.8015	1.1846	
1.5951	3.6519	4.1271	4.1513	4.05	3.8228	2.7263	1.6201	
3.0505	4.0468	4.1437	4.0101	3.8182	3.6682	3.4631	1.5134	12
1.5771	3.8683	4.2089	4.1789	3.364	3.1555	2.7545	1.1906	
1.5879	3.6355	4.1061	4.0739	3.9937	3.8054	2.6993	1.5927	
3.0448	3.9973	4.0374	3.9024	3.6485	3.4462	3.3278	1.5126	13
1.6002	3.8476	4.1637	4.0925	3.2664	3.0956	2.7242	1.2118	
1.5706	3.6604	4.1881	4.1768	4.1696	3.984	2.7055	1.5783	
3.0245	3.9261	3.9897	3.9683	3.7043	3.4827	3.3955	1.5324	14
1.6158	3.7623	4.0419	4.005	3.3078	3.1307	2.7128	1.2492	
1.5659	3.7386	4.3135	4.3044	4.3307	4.1592	2.7415	1.5786	
3.0384	3.9741	3.9939	4.0099	3.7757	3.5954	3.536	1.5568	15
1.6445	3.6887	3.8979	3.8733	3.3757	3.1954	2.7158	1.2821	
1.5477	3.7902	4.3197	4.2818	4.2947	4.1793	2.757	1.5761	
3.0817	4.0909	4.0389	3.9886	3.7837	3.6526	3.6544	1.5681	16
1.675	3.6588	3.8042	3.7459	3.4164	3.2561	2.7232	1.3029	
1.5116	3.7582	4.1771	4.1364	4.1498	4.1109	2.7663	1.5571	
3.0895	4.0832	4.0245	3.9697	3.8295	3.6865	3.7149	1.5703	17
1.6941	3.6554	3.7761	3.699	3.4483	3.2606	2.712	1.3021	
1.4796	3.7133	4.0561	4.0257	4.0387	4.0269	2.7719	1.5403	
3.0672	3.9572	3.9475	3.9442	3.8833	3.7394	3.732	1.5768	18
1.688	3.6063	3.7353	3.6969	3.4989	3.2183	2.6823	1.2898	
1.4693	3.6888	4.0112	4.0099	4.0062	3.9611	2.7755	1.5319	
3.0338	3.8391	3.8483	3.8698	3.8449	3.7253	3.6871	1.5857	19
1.6668	3.5276	3.6704	3.6763	3.5455	3.2129	2.6817	1.2852	
1.4669	3.6755	4.0287	4.0154	3.9607	3.8543	2.7733	1.53	
3.0022	3.7832	3.7874	3.7804	3.7516	3.6783	3.6129	1.5924	20
1.6569	3.4758	3.5996	3.6062	3.5828	3.2579	2.7054	1.3004	
1.4726	3.6709	4.0342	3.9572	3.8601	3.7426	2.7608	1.524	
2.9855	3.7843	3.7409	3.713	3.6917	3.6537	3.5513	1.5925	21
1.6589	3.4385	3.5184	3.5106	3.5952	3.2747	2.7233	1.3122	
1.4763	3.6583	3.9736	3.8406	3.7496	3.6617	2.7503	1.5145	
2.9815	3.794	3.7044	3.6689	3.6519	3.6208	3.4749	1.5982	22
1.6483	3.3732	3.4307	3.424	3.548	3.2259	2.7036	1.323	
1.4669	3.6156	3.8909	3.7603	3.6999	3.6286	2.7332	1.5001	
2.9641	3.7718	3.6912	3.6745	3.6035	3.5182	3.3705	1.6013	23
1.6307	3.3122	3.365	3.3486	3.464	3.1583	2.6651	1.3295	
1.4409	3.576	3.8724	3.7545	3.6854	3.5952	2.7133	1.4864	
2.938	3.7159	3.6774	3.6633	3.5474	3.4111	3.2686	1.5955	24
1.6121	3.2811	3.3174	3.2782	3.3801	3.0947	2.6291	1.3358	

1.4257	3.5716	3.8782	3.7594	3.6643	3.547	2.6813	1.4659	
2.9202	3.6566	3.62	3.6021	3.4992	3.3477	3.2039	1.5885	25
1.5929	3.2519	3.2535	3.2085	3.3082	3.0368	2.5956	1.3489	
1.4156	3.5764	3.8484	3.7172	3.6088	3.4839	2.6536	1.444	
2.9095	3.5918	3.5303	3.5058	3.4497	3.3214	3.1856	1.5944	26
1.5635	3.1948	3.1518	3.1351	3.2439	2.9767	2.5682	1.3605	
1.4061	3.5439	3.7562	3.6225	3.5227	3.4361	2.6322	1.432	
2.8892	3.5076	3.4377	3.4134	3.3756	3.3024	3.2167	1.6037	27
1.5254	3.1247	3.0595	3.0822	3.207	2.9468	2.5634	1.3589	
1.3962	3.4871	3.6368	3.5329	3.4595	3.4275	2.6249	1.4342	
2.8615	3.4384	3.3817	3.3537	3.318	3.3245	3.2877	1.6177	28
1.4997	3.084	3.0125	3.0714	3.2071	2.9646	2.5831	1.3495	
1.3932	3.4607	3.5884	3.5179	3.4816	3.4599	2.6237	1.4356	
2.8458	3.4195	3.377	3.3723	3.3425	3.3979	3.3579	1.6215	29
1.4932	3.1053	3.0345	3.1001	3.2361	3.0151	2.6121	1.3376	
1.3906	3.4875	3.6534	3.5987	3.5666	3.5065	2.6227	1.4328	
2.8495	3.4742	3.4479	3.4775	3.4663	3.4832	3.3919	1.6169	30
1.4997	3.1863	3.132	3.1867	3.2851	3.0607	2.6393	1.3123	
1.3875	3.5331	3.7559	3.6884	3.6181	3.5253	2.6159	1.4289	
2.8719	3.577	3.5455	3.592	3.5861	3.5217	3.3833	1.6011	31
1.5047	3.3022	3.2936	3.3204	3.353	3.109	2.6602	1.279	
1.3857	3.5513	3.7897	3.7085	3.6194	3.5259	2.6161	1.4342	
2.8956	3.6603	3.6309	3.6478	3.6222	3.5184	3.3781	1.5902	32
1.4988	3.4197	3.4658	3.4533	3.4283	3.1654	2.6856	1.2506	
1.3856	3.5417	3.7446	3.6803	3.6144	3.5449	2.6246	1.4497	
2.9121	3.6786	3.6632	3.6526	3.6031	3.5292	3.4147	1.5805	33
1.4832	3.5047	3.6154	3.5551	3.5165	3.2629	2.7239	1.2342	
1.3918	3.5455	3.7032	3.6557	3.6331	3.5858	2.6435	1.4731	
2.9298	3.693	3.6936	3.6714	3.6302	3.5841	3.4751	1.5716	34
1.4701	3.5749	3.7521	3.6417	3.6397	3.4035	2.7728	1.2299	
1.4066	3.5785	3.7238	3.679	3.6776	3.642	2.6721	1.4917	
2.959	3.7604	3.7652	3.7349	3.696	3.6467	3.5131	1.5525	35
1.4676	3.6701	3.8639	3.7213	3.8152	3.5745	2.8172	1.2262	
1.4243	3.6162	3.7734	3.7357	3.7332	3.6841	2.7015	1.5069	
2.9767	3.8482	3.8735	3.8312	3.7557	3.6835	3.5323	1.5396	36
1.4696	3.7776	3.9086	3.7856	3.9952	3.7578	2.8508	1.2143	
1.4407	3.6114	3.7715	3.7524	3.7403	3.691	2.7223	1.5202	
2.9731	3.886	3.9494	3.9151	3.7914	3.6671	3.5036	1.5251	37
1.4719	3.8384	3.9032	3.8444	4.1048	3.9181	2.8742	1.2023	
1.4603	3.5476	3.6847	3.6815	3.6753	3.6298	2.7283	1.5369	
2.949	3.8622	3.965	3.9474	3.7827	3.5949	3.4173	1.512	38
1.4644	3.8281	3.8823	3.9188	4.105	3.9591	2.8833	1.1887	

1.4837	3.4671	3.5826	3.5816	3.5699	3.5195	2.7179	1.5559	
2.923	3.8216	3.9446	3.9298	3.7511	3.5003	3.3015	1.5	39
1.4587	3.7635	3.8739	3.9836	4.0344	3.8645	2.8665	1.1725	
1.5088	3.4222	3.5422	3.5333	3.4888	3.4272	2.7006	1.5741	
2.9123	3.8177	3.9631	3.9515	3.7701	3.4642	3.2214	1.4961	40
1.457	3.7073	3.8972	4.023	3.9494	3.7203	2.834	1.1623	
1.537	3.43	3.6052	3.5942	3.5147	3.4261	2.6945	1.5872	
2.927	3.8699	4.0368	4.0564	3.8873	3.5297	3.2117	1.4993	41
1.468	3.7078	3.9795	4.0813	3.8873	3.6195	2.8118	1.1636	
1.5666	3.499	3.791	3.8081	3.7019	3.535	2.707	1.5987	
2.9675	3.9857	4.1749	4.2213	4.0647	3.6873	3.2845	1.5131	42
1.4867	3.7823	4.1285	4.1891	3.8666	3.5801	2.8103	1.1681	
1.5914	3.6008	4.0458	4.1251	4.0062	3.7456	2.7382	1.6086	
3.0104	4.0982	4.2905	4.3537	4.2069	3.8587	3.4129	1.5267	43
1.5133	3.8444	4.2404	4.2796	3.8305	3.5432	2.8165	1.1779	
1.5998	3.6541	4.225	4.375	4.2503	3.9212	2.7647	1.6166	
3.0283	4.0938	4.2976	4.3763	4.2255	3.9498	3.5156	1.5383	44
1.5297	3.8353	4.2364	4.2738	3.7056	3.44	2.8039	1.1866	
1.5973	3.6608	4.2419	4.374	4.2436	3.9118	2.7505	1.6135	
3.0362	4.0302	4.1859	4.2175	4.0428	3.8102	3.453	1.5304	45
1.546	3.8132	4.2098	4.2061	3.5208	3.2752	2.7586	1.1942	
1.5986	3.6586	4.188	4.2129	4.0785	3.805	2.7076	1.5956	
3.0436	3.9958	4.0702	4.0215	3.7826	3.5449	3.2756	1.5169	46
1.5714	3.8146	4.194	4.1028	3.3548	3.1398	2.7058	1.2025	
1.5884	3.6423	4.1529	4.1549	4.0969	3.8908	2.6878	1.5732	
3.0289	3.9325	4.0083	3.9846	3.6921	3.4072	3.1956	1.5217	47
1.5862	3.7867	4.135	4.0249	3.3077	3.1053	2.6795	1.2255	
1.5739	3.6853	4.2578	4.2815	4.2902	4.0938	2.7027	1.5675	
3.0127	3.893	3.9908	4.0496	3.7601	3.502	3.3092	1.5458	48
1.6025	3.7233	4.0184	3.9436	3.3502	3.1602	2.6737	1.2579	
1.5671	3.7561	4.3582	4.3802	4.4109	4.2561	2.7395	1.5694	
3.0376	3.9816	3.9976	4.0562	3.8023	3.6027	3.4585	1.5654	49
1.6369	3.6782	3.881	3.8196	3.3994	3.2319	2.6884	1.2876	
1.5388	3.7764	4.3068	4.3207	4.3453	4.262	2.7532	1.5606	
3.0695	4.0776	4.0108	4.019	3.8122	3.6513	3.5786	1.5683	50
1.6637	3.649	3.7988	3.7406	3.4278	3.2713	2.6921	1.2997	
1.4981	3.7199	4.1309	4.163	4.2022	4.1954	2.7696	1.5414	
3.0618	4.0298	3.9745	4.0089	3.8917	3.699	3.6392	1.5694	51
1.6737	3.617	3.7525	3.7219	3.4692	3.2452	2.6756	1.2905	
1.4694	3.6828	4.0309	4.0688	4.1097	4.1151	2.7798	1.5279	
3.0302	3.8914	3.884	3.9431	3.9351	3.7608	3.647	1.5744	52
1.6637	3.5529	3.6931	3.6933	3.5171	3.2138	2.6513	1.2754	

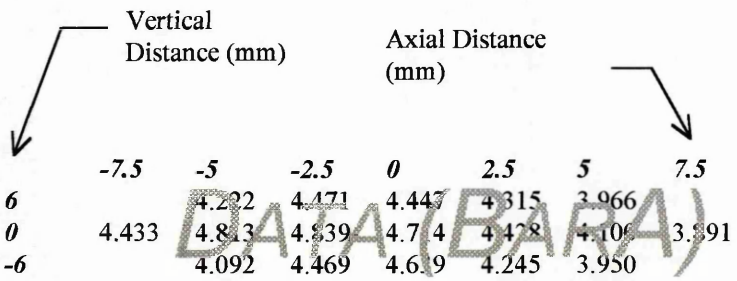
1.4602	3.6625	4.0134	4.05	4.0792	4.0292	2.7893	1.5223	
2.9946	3.778	3.7943	3.8367	3.8741	3.7522	3.6074	1.5825	53
1.6421	3.4827	3.6185	3.6225	3.5613	3.239	2.6597	1.2734	
1.4605	3.6528	4.0317	4.0368	4.0074	3.892	2.785	1.52	
2.9594	3.7214	3.7291	3.7322	3.7751	3.7119	3.5515	1.5839	54
1.6374	3.4322	3.5314	3.5288	3.5845	3.2884	2.6834	1.2829	
1.4646	3.6467	4.0101	3.9496	3.874	3.7545	2.7695	1.5169	
2.9398	3.7185	3.6823	3.6566	3.7107	3.686	3.5105	1.588	55
1.6371	3.3683	3.4284	3.4354	3.5698	3.2804	2.6869	1.2957	
1.463	3.6335	3.945	3.8288	3.7509	3.6679	2.7509	1.5078	
2.9285	3.7304	3.6535	3.6126	3.655	3.6284	3.4309	1.5934	56
1.6274	3.286	3.3475	3.3584	3.4946	3.2168	2.6617	1.3051	
1.448	3.609	3.9048	3.7703	3.7044	3.6224	2.727	1.4988	
2.908	3.711	3.6517	3.6136	3.5972	3.5048	3.3218	1.5971	57
1.612	3.2339	3.288	3.2891	3.4029	3.1418	2.63	1.3104	
1.4252	3.6019	3.9287	3.789	3.6908	3.5782	2.7002	1.4833	
2.8887	3.6661	3.6162	3.5916	3.5385	3.3853	3.213	1.5902	58
1.5975	3.2185	3.2407	3.2164	3.3258	3.093	2.5982	1.3192	
1.4061	3.6139	3.9402	3.79	3.6684	3.5244	2.6634	1.4625	
2.8797	3.6244	3.5346	3.5256	3.4831	3.2987	3.1532	1.5906	59
1.5743	3.1873	3.162	3.1353	3.2639	3.0489	2.5659	1.3323	
1.398	3.6157	3.8942	3.7333	3.6002	3.4553	2.6322	1.4407	
2.8685	3.5678	3.4198	3.4284	3.4105	3.2409	3.144	1.6004	60
1.5421	3.1244	3.0706	3.0658	3.2109	3.0179	2.541	1.3392	

J.2. 22 CIRCULAR PIPE DIFFUSER

Table J.2 Operating Conditions for 22 Pipe Diffuser Traverses

Flow Condition	m_{corr} (kg/sec)	Corr. Speed (rpm)	$P_{tot\ out}$ (Pa)*	$P_{tot\ in}$ (Pa)	$T_{tot\ out}$ (K)	$T_{tot\ in}$ (K)
At Surge	3.523	34923	488728	79130	488.44	275.37
Near Surge	3.750	34943	468792	76783	483.71	275.22
Design	3.930	34950	451370	74877	480.67	274.95
Near Choke	4.154	34965	423291	72247	477.45	275.18

* At impeller discharge



DATA (BARA)

Figure J.3 Designations for 22 Circular Pipe Diffuser Data

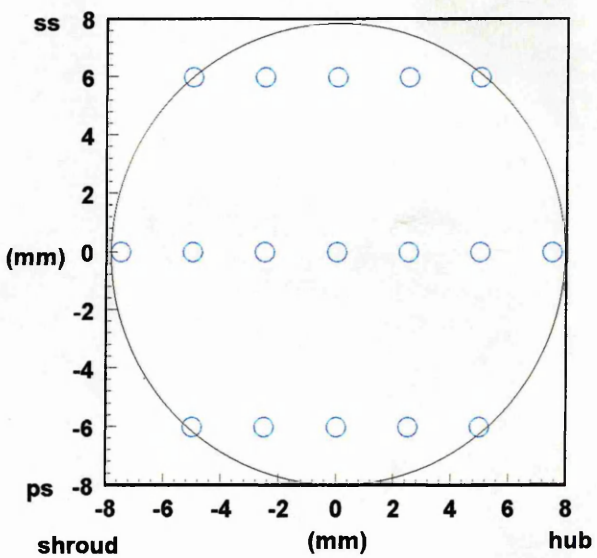


Figure J.4 Measurement Locations for 22 Circular Pipe Diffuser Unsteady Total Pressure Traverses

J.2.1 22 CIRCULAR PIPE DIFFUSER, 100% SPEED 'AT SURGE'

	4.048	4.3976	4.3325	4.0541	3.7895		
4.1476	4.5894	4.4399	4.3048	4.098	3.8066	3.8358	1
	4.0196	4.253	4.3278	4.019	3.7922		
	4.0432	4.3293	4.2463	4.0075	3.7387		
4.2475	4.518	4.3375	4.2683	4.073	3.8221	3.8356	2
	3.9846	4.1119	4.1621	3.8996	3.7502		
	4.0134	4.1941	4.0856	3.9431	3.7108		
4.3866	4.558	4.3336	4.2078	4.0622	3.8406	3.8056	3
	3.9712	4.0656	4.083	3.8528	3.7285		
	4.0477	4.2154	4.0674	3.9401	3.7157		
4.5505	4.7589	4.4457	4.2374	4.0993	3.8435	3.7446	4
	3.9959	4.1434	4.1522	3.9003	3.7534		
	4.1843	4.5128	4.4108	4.1859	3.8149		
4.6929	5.0061	4.712	4.4691	4.2491	3.8831	3.704	5
	4.0314	4.2394	4.3101	4.031	3.8384		
	4.3735	4.8581	4.8262	4.5815	4.0436		
4.7909	5.2053	5.0577	4.8173	4.5736	4.1477	3.8201	6
	4.0447	4.2719	4.4486	4.1961	3.9811		
	4.4849	4.9967	4.9815	4.7491	4.2046		
4.8593	5.332	5.3374	5.1117	4.9201	4.5308	4.0675	7
	4.08	4.3201	4.5689	4.3747	4.1613		
	4.5157	4.9168	4.7786	4.5303	4.1407		
4.8855	5.3301	5.3765	5.1824	5.0171	4.7033	4.1703	8
	4.1398	4.4546	4.7307	4.5504	4.3031		
	4.4641	4.7684	4.579	4.3006	3.9385		
4.8449	5.1139	5.1463	4.9736	4.7828	4.4377	4.0343	9
	4.1591	4.5646	4.8146	4.5075	4.2058		
	4.3545	4.6267	4.5032	4.227	3.8451		
4.7198	4.8438	4.8208	4.6524	4.4294	4.0484	3.8303	10
	4.1	4.5247	4.6622	4.1722	3.9065		
	4.2139	4.4813	4.4756	4.2451	3.8303		
4.5435	4.6417	4.5585	4.3829	4.1422	3.8183	3.7577	11
	4.0076	4.3694	4.3685	3.8334	3.6691		
	4.099	4.3262	4.3942	4.2202	3.8169		
4.3697	4.5057	4.429	4.2116	3.9591	3.7838	3.8128	12
	3.9507	4.2331	4.2152	3.7475	3.629		
	4.0432	4.1891	4.2744	4.16	3.8072		
4.3442	4.5585	4.5137	4.1766	3.9398	3.8687	3.8616	13
	4.0111	4.3109	4.3738	3.9029	3.7088		

	4.1435	4.3051	4.3218	4.1773	3.8571		
4.454	4.8691	4.8363	4.4221	4.1172	3.983	3.8159	14
	4.1252	4.5632	4.7217	4.1746	3.8518		
	4.3534	4.7199	4.7466	4.5698	4.0654		
4.5649	5.2056	5.2111	4.8295	4.4694	4.1326	3.7365	15
	4.2288	4.8127	5.0683	4.4857	4.0536		
	4.5665	5.0795	5.1636	5.0007	4.2901		
4.6521	5.43	5.5568	5.2821	4.9033	4.5377	3.9521	16
	4.3012	4.9568	5.3244	4.7384	4.2595		
	4.6079	5.045	5.199	5.1164	4.3842		
4.7079	5.4563	5.8077	5.6985	5.3001	4.9643	4.1845	17
	4.3789	5.0596	5.5263	4.9159	4.4131		
	4.5409	4.767	4.8512	4.8002	4.262		
4.6856	5.2985	5.8558	5.9153	5.3676	4.9617	4.1952	18
	4.399	5.1139	5.6882	4.9751	4.3896		
	4.4635	4.5656	4.596	4.566	4.1872		
4.6308	5.0664	5.5994	5.7046	5.0261	4.4798	3.9688	19
	4.3846	5.0761	5.6478	4.8246	4.2321		
	4.4099	4.5474	4.5667	4.518	4.1919		
4.5589	4.853	5.1833	5.2499	4.5944	4.0953	3.9354	20
	4.3047	4.903	5.3163	4.5144	4.0223		
	4.3223	4.5105	4.5416	4.4831	4.1501		
4.4651	4.7024	4.8425	4.8861	4.3442	3.9755	4.0456	21
	4.195	4.7116	4.9293	4.2584	3.8592		
	4.1854	4.3197	4.3577	4.2924	4.0093		
4.342	4.617	4.6466	4.6251	4.2329	3.9385	4.1009	22
	4.1287	4.6195	4.6706	4.1116	3.7756		
	4.0843	4.0861	4.0585	4.0219	3.8908		
4.2512	4.5669	4.4907	4.3586	4.1296	3.912	4.0293	23
	4.1137	4.5684	4.5244	4.0574	3.8206		
	4.0768	4.041	3.8944	3.8609	3.8584		
4.2014	4.4499	4.3185	4.1756	4.0685	3.8891	3.9035	24
	4.1068	4.5099	4.4517	4.1168	3.9354		
	4.0988	4.1009	3.9312	3.9018	3.8477		
4.2174	4.3817	4.2562	4.2149	4.1454	3.8751	3.7447	25
	4.103	4.439	4.4403	4.2442	4.0131		
	4.0723	4.1785	4.0936	4.0572	3.8197		
4.2561	4.4209	4.3433	4.3554	4.2688	3.9103	3.6819	26
	4.0766	4.3457	4.4161	4.3254	4.0265		
	4.0259	4.2409	4.2755	4.2684	3.8556		
4.2567	4.4854	4.4606	4.4511	4.375	4.0414	3.7843	27
	3.9985	4.2286	4.3461	4.2926	3.9966		

	4.0284	4.3278	4.4775	4.4678	3.9444		
4.252	4.5351	4.5468	4.5298	4.4757	4.2378	3.9643	28
	3.9234	4.1525	4.335	4.1926	3.9334		
	4.075	4.4439	4.6481	4.6066	4.0623		
4.3038	4.6346	4.6572	4.7386	4.6443	4.3355	4.0238	29
	3.8903	4.1485	4.4177	4.1351	3.8796		
	4.131	4.5657	4.6743	4.5819	4.1484		
4.3666	4.7812	4.8455	4.9551	4.6989	4.2755	3.9264	30
	3.8903	4.2315	4.5012	4.1808	3.892		
	4.1904	4.5685	4.5359	4.3918	4.0991		
4.3071	4.88	5.0404	5.0506	4.6101	4.0737	3.8095	31
	3.9286	4.3669	4.5746	4.2528	3.931		
	4.2168	4.4257	4.3137	4.1484	3.9521		
4.1653	4.8536	5.1125	4.9578	4.4095	3.8942	3.7505	32
	4.0189	4.5036	4.6369	4.2628	3.9383		
	4.1776	4.2903	4.13	4.0102	3.8678		
4.0476	4.7521	4.9981	4.7378	4.215	3.818	3.7547	33
	4.0915	4.5202	4.6448	4.2361	3.9022		
	4.0954	4.262	4.1058	4.0171	3.8457		
4.0198	4.6599	4.7404	4.4903	4.1169	3.8099	3.7784	34
	4.0942	4.432	4.5645	4.2008	3.8647		
	4.0328	4.2807	4.1991	4.0362	3.8154		
4.0652	4.5907	4.4937	4.3543	4.1098	3.8137	3.8012	35
	4.039	4.276	4.4064	4.1086	3.8183		
	3.9987	4.2503	4.2153	3.9992	3.7482		
4.1417	4.5202	4.3488	4.2975	4.0827	3.8133	3.8121	36
	3.9838	4.1234	4.2196	3.9829	3.7736		
	3.9707	4.1447	4.0879	3.9454	3.7019		
4.2423	4.5109	4.3346	4.2506	4.0517	3.8239	3.803	37
	3.9469	4.0341	4.1016	3.9013	3.7367		
	3.9861	4.0807	3.9822	3.9136	3.6841		
4.4056	4.6401	4.4236	4.227	4.0561	3.8308	3.767	38
	3.9433	4.077	4.1347	3.9176	3.7468		
	4.1141	4.2963	4.1685	4.0634	3.7477		
4.5845	4.903	4.6425	4.3831	4.1613	3.8401	3.7061	39
	3.9919	4.2114	4.2973	4.0316	3.8101		
	4.2933	4.6414	4.5895	4.4577	3.9636		
4.7152	5.1523	4.9551	4.7003	4.431	3.9926	3.7287	40
	4.0318	4.2848	4.4641	4.2167	3.9537		
	4.4258	4.8497	4.8711	4.7153	4.1695		
4.7637	5.2874	5.2668	5.0431	4.8033	4.3655	3.9663	41
	4.0635	4.3039	4.593	4.4199	4.1634		

	4.4653	4.7903	4.7751	4.585	4.1877		
4.7777	5.2824	5.3862	5.2262	5.0505	4.6855	4.155	42
	4.1016	4.3778	4.7477	4.6372	4.3743		
	4.4483	4.6828	4.5517	4.311	3.9889		
4.7483	5.1407	5.2646	5.15	4.9445	4.5911	4.1004	43
	4.1309	4.5114	4.893	4.6981	4.3577		
	4.3836	4.5928	4.4251	4.1864	3.8411		
4.6841	4.9081	4.9931	4.8527	4.5939	4.1828	3.8619	44
	4.1018	4.5525	4.8399	4.4153	4.0795		
	4.2633	4.5014	4.3982	4.1815	3.792		
4.5581	4.706	4.7221	4.5314	4.2369	3.8566	3.7436	45
	4.0158	4.4371	4.5606	4.0103	3.783		
	4.1268	4.3725	4.3489	4.1734	3.7851		
4.4041	4.5637	4.5185	4.2666	3.9899	3.7401	3.7682	46
	3.9133	4.261	4.316	3.8115	3.669		
	4.0159	4.2123	4.2444	4.1186	3.773		
4.2793	4.5202	4.4933	4.124	3.892	3.7812	3.8283	47
	3.8872	4.2242	4.3484	3.8687	3.6916		
	4.0201	4.1581	4.1608	4.0538	3.7849		
4.3553	4.7259	4.7244	4.242	3.99	3.8868	3.8096	48
	3.998	4.4278	4.6404	4.085	3.7959		
	4.2099	4.4976	4.4392	4.3059	3.9255		
4.4664	5.0486	5.0731	4.5996	4.2773	4.005	3.719	49
	4.1193	4.695	5.0148	4.3931	3.9676		
	4.4338	4.9044	4.9015	4.7713	4.1776		
4.6004	5.3416	5.3909	5.0159	4.6899	4.289	3.7869	50
	4.1857	4.8647	5.3315	4.7008	4.1629		
	4.5411	5.0455	5.1685	5.0778	4.348		
4.6364	5.4077	5.608	5.4147	5.1312	4.7638	4.0867	51
	4.2292	4.9603	5.5631	4.9598	4.3609		
	4.4989	4.804	4.9399	4.8922	4.2918		
4.657	5.302	5.6984	5.7203	5.3866	5.0594	4.2399	52
	4.2764	5.0286	5.7424	5.1563	4.4398		
	4.4399	4.5984	4.6602	4.6478	4.1808		
4.6281	5.1183	5.6013	5.7388	5.2071	4.7672	4.0879	53
	4.291	5.0407	5.785	5.1666	4.3378		
	4.3884	4.5528	4.5751	4.5798	4.1649		
4.5996	4.9743	5.3387	5.4171	4.749	4.2469	3.8984	54
	4.2477	4.9256	5.544	4.9102	4.1273		
	4.3242	4.5723	4.6093	4.5915	4.159		
4.5446	4.8461	5.0117	5.0126	4.342	3.9533	3.9308	55
	4.1694	4.754	5.1398	4.5747	3.9444		

	4.2274	4.4598	4.5152	4.4455	4.0565		
4.4599	4.745	4.7584	4.7099	4.1373	3.8893	4.0305	56
	4.0965	4.6308	4.8146	4.3315	3.8227		
	4.1314	4.2244	4.2527	4.185	3.9192		
4.355	4.6763	4.5917	4.4517	4.0269	3.8824	4.0418	57
	4.0695	4.5672	4.5897	4.1787	3.815		
	4.0918	4.0827	3.992	3.9513	3.8585		
4.2779	4.5759	4.4317	4.2293	3.9467	3.8889	3.9619	58
	4.0548	4.4795	4.4333	4.1189	3.8963		
	4.0888	4.088	3.9209	3.9179	3.8706		
4.2651	4.4706	4.3154	4.1644	3.9696	3.8509	3.7942	59
	4.0561	4.4036	4.3615	4.1738	3.9746		
	4.0795	4.1489	4.0131	4.0383	3.8552		
4.2945	4.4847	4.3396	4.2587	4.1022	3.8159	3.6474	60
	4.0516	4.3372	4.3606	4.2745	3.9888		

J.2.2 22 CIRCULAR PIPE DIFFUSER, 100% SPEED 'NEAR SURGE'

	3.9484	4.3488	4.2442	3.9181	3.6429		
3.9654	4.3657	4.3323	4.286	4.1196	3.8684	3.7613	1
	3.7852	3.9263	4.0131	3.7401	3.5298		
	3.925	4.3113	4.2056	3.9252	3.6185		
4.0253	4.3882	4.292	4.2038	4.0369	3.8789	3.7983	2
	3.7243	3.8545	3.9432	3.6485	3.4789		
	3.8888	4.2278	4.1386	3.9205	3.5933		
4.1358	4.4339	4.2774	4.1601	4.0324	3.9238	3.7685	3
	3.718	3.8294	3.911	3.6082	3.459		
	3.8986	4.2372	4.1764	3.9337	3.6116		
4.2951	4.5718	4.3356	4.2453	4.1277	3.9564	3.726	4
	3.7822	3.9162	3.9687	3.6658	3.5025		
	4.0357	4.5201	4.4852	4.1558	3.7154		
4.4519	4.803	4.5879	4.5022	4.3279	4.0312	3.7315	5
	3.88	4.084	4.1416	3.8405	3.6122		
	4.2182	4.8654	4.8829	4.5569	3.9169		
4.566	5.0195	4.9394	4.8467	4.6539	4.2825	3.8605	6
	3.9537	4.1997	4.3401	4.0836	3.783		
	4.3444	5.0146	5.0648	4.7667	4.0633		
4.6104	5.1235	5.2059	5.1302	5.0021	4.6463	4.0638	7
	3.9879	4.2333	4.4818	4.3155	3.984		
	4.3794	4.9316	4.8887	4.5561	4.0182		
4.624	5.0791	5.2698	5.229	5.1047	4.8039	4.1333	8
	4.0016	4.2468	4.5826	4.4552	4.0983		

	4.3602	4.7852	4.6337	4.2709	3.8502		
4.6071	4.9074	5.1061	5.0763	4.8529	4.5417	4.0012	9
	4.0049	4.252	4.5823	4.3631	3.9863		
	4.3085	4.6358	4.4403	4.1453	3.7542		
4.5721	4.721	4.8555	4.7901	4.4691	4.1588	3.8226	10
	3.9769	4.1908	4.4306	4.0828	3.7494		
	4.2189	4.4643	4.3203	4.1021	3.709		
4.4553	4.592	4.6714	4.5509	4.1939	3.945	3.7921	11
	3.9031	4.0945	4.2576	3.8454	3.6083		
	4.1086	4.2944	4.2185	4.0541	3.665		
4.3073	4.5534	4.6082	4.4	4.0711	3.9172	3.8683	12
	3.8545	4.0596	4.2331	3.7905	3.601		
	4.0271	4.161	4.1548	4.0296	3.6654		
4.2887	4.674	4.7093	4.3505	4.09	3.986	3.9287	13
	3.9219	4.1638	4.3792	3.8863	3.6501		
	4.1017	4.2769	4.2604	4.1045	3.7463		
4.3956	4.9652	5.0143	4.5586	4.252	4.1077	3.9302	14
	4.0606	4.3459	4.6558	4.0946	3.7448		
	4.2358	4.6164	4.6453	4.4684	3.9553		
4.5009	5.2499	5.3426	4.9374	4.5931	4.3346	3.9655	15
	4.1962	4.5071	4.9505	4.3866	3.9097		
	4.3576	4.8896	4.9821	4.8578	4.1817		
4.6116	5.4378	5.5661	5.3075	5.0129	4.7315	4.1964	16
	4.3201	4.6267	5.1699	4.6763	4.1157		
	4.3765	4.8439	4.9704	4.9555	4.2697		
4.6824	5.4708	5.6817	5.5902	5.334	5.0192	4.3292	17
	4.4067	4.6773	5.2379	4.8499	4.2448		
	4.3252	4.5799	4.6561	4.6494	4.15		
4.6216	5.2916	5.6793	5.7719	5.3859	4.8695	4.2179	18
	4.4208	4.6544	5.1967	4.8502	4.1926		
	4.2418	4.3694	4.4125	4.3848	4.0711		
4.5321	5.0092	5.4441	5.6678	5.1748	4.4966	4.0179	19
	4.4126	4.6655	5.0845	4.7425	4.0794		
	4.1764	4.345	4.3838	4.3318	4.0574		
4.5112	4.8295	5.0936	5.3031	4.8217	4.2543	4.0017	20
	4.3702	4.6324	4.8686	4.533	3.9689		
	4.0804	4.3135	4.3496	4.277	3.9937		
4.4667	4.7571	4.8664	4.9614	4.5357	4.1227	4.0271	21
	4.2603	4.4918	4.6167	4.2733	3.8165		
	3.9721	4.1568	4.157	4.0605	3.834		
4.3258	4.693	4.7916	4.7824	4.4224	4.0462	3.9825	22
	4.1413	4.36	4.443	4.0597	3.6642		

	3.9076	4.004	3.9015	3.8037	3.7205		
4.1743	4.5861	4.7087	4.6033	4.3946	4.0747	3.9465	23
	4.0847	4.3347	4.3677	3.9749	3.6388		
	3.9222	4.0156	3.8136	3.7136	3.7046		
4.0954	4.4761	4.5473	4.419	4.3488	4.1392	3.9499	24
	4.0699	4.3301	4.3466	3.9996	3.706		
	3.9271	4.1015	3.9039	3.8343	3.7361		
4.1332	4.4813	4.4622	4.3627	4.3346	4.157	3.9309	25
	4.0228	4.2728	4.3132	4.0359	3.7575		
	3.9485	4.2146	4.0923	4.0251	3.7749		
4.2057	4.5734	4.5207	4.4383	4.3842	4.1593	3.9027	26
	3.9371	4.1967	4.2482	4.0428	3.7673		
	3.9523	4.305	4.2747	4.2073	3.8313		
4.2215	4.5764	4.5699	4.5176	4.4635	4.2397	3.9312	27
	3.8684	4.1149	4.1583	4.0046	3.7506		
	3.9586	4.3454	4.436	4.3126	3.8885		
4.1986	4.5449	4.5968	4.5949	4.5915	4.3725	3.9863	28
	3.8318	4.0266	4.112	3.9609	3.7093		
	3.957	4.4126	4.5344	4.3742	3.9707		
4.2198	4.6352	4.6928	4.7419	4.717	4.4381	3.972	29
	3.8082	3.9948	4.1332	3.924	3.6787		
	3.9672	4.5149	4.5503	4.3724	4.0141		
4.2698	4.7731	4.8349	4.8606	4.7208	4.3949	3.9041	30
	3.819	4.0498	4.1851	3.9291	3.6806		
	3.9574	4.524	4.4602	4.2344	3.9385		
4.2558	4.7989	4.9085	4.9268	4.6381	4.2748	3.8772	31
	3.8547	4.1726	4.2766	3.9836	3.7165		
	3.954	4.3908	4.2906	4.0157	3.8087		
4.1486	4.7289	4.8846	4.8797	4.5419	4.153	3.847	32
	3.8906	4.2518	4.3336	4.0337	3.7443		
	3.9546	4.27	4.1298	3.8854	3.7083		
4.0234	4.5951	4.7798	4.7234	4.4017	4.0616	3.7904	33
	3.8937	4.2292	4.3175	4.0289	3.7231		
	3.9418	4.2477	4.1066	3.8733	3.6654		
3.9336	4.4372	4.5815	4.5371	4.2894	3.9967	3.7462	34
	3.8691	4.1116	4.2111	3.9572	3.6465		
	3.9156	4.2766	4.1523	3.8901	3.6451		
3.9158	4.355	4.3944	4.3929	4.1979	3.9379	3.7623	35
	3.8119	3.9802	4.0912	3.8406	3.5634		
	3.8953	4.2661	4.1613	3.9073	3.6308		
3.9386	4.3635	4.3149	4.273	4.1044	3.9074	3.8	36
	3.7524	3.8803	3.9809	3.7354	3.5063		

	3.8571	4.1945	4.1042	3.9099	3.5995		
4.0225	4.412	4.3174	4.1803	4.0341	3.9297	3.8044	37
	3.7235	3.8355	3.9331	3.675	3.4815		
	3.833	4.1463	4.088	3.8979	3.5919		
4.1699	4.5164	4.3309	4.1768	4.0699	3.9637	3.7595	38
	3.7563	3.867	3.9547	3.6862	3.4939		
	3.9315	4.3343	4.2782	3.9971	3.6483		
4.368	4.7204	4.4935	4.3628	4.2253	3.9966	3.7324	39
	3.8524	4.019	4.1036	3.7892	3.561		
	4.1064	4.6755	4.6711	4.3467	3.8194		
4.5148	4.9476	4.8194	4.7027	4.5127	4.1574	3.7831	40
	3.945	4.1772	4.3093	4.0028	3.7045		
	4.2642	4.9383	4.9781	4.681	4.0052		
4.5891	5.0874	5.1382	5.0517	4.8951	4.5069	3.9861	41
	3.9968	4.2531	4.473	4.2623	3.9133		
	4.3179	4.9376	4.9384	4.6738	4.0792		
4.5989	5.077	5.2978	5.264	5.1792	4.8328	4.151	42
	4.0169	4.2662	4.5874	4.4942	4.1185		
	4.3196	4.8279	4.6827	4.3639	3.9355		
4.592	4.9434	5.2476	5.2595	5.0954	4.7793	4.1276	43
	4.0301	4.292	4.6629	4.5203	4.1154		
	4.2874	4.6827	4.4485	4.142	3.7855		
4.5597	4.7715	5.039	5.025	4.7245	4.3884	3.9142	44
	4.0092	4.2702	4.5986	4.2597	3.8857		
	4.2297	4.5244	4.312	4.052	3.6962		
4.4884	4.6349	4.8126	4.7116	4.3445	4.0441	3.7746	45
	3.9485	4.1774	4.4269	3.9477	3.6596		
	4.1294	4.3455	4.2217	4.0254	3.66		
4.3491	4.557	4.665	4.4743	4.1083	3.9111	3.7902	46
	3.8715	4.0803	4.342	3.8402	3.6153		
	4.0259	4.1827	4.1606	4.0108	3.6379		
4.2516	4.5852	4.6757	4.3444	4.0244	3.9334	3.8863	47
	3.8656	4.1215	4.4317	3.9167	3.6698		
	4.0293	4.1766	4.1757	4.0357	3.6859		
4.3162	4.8005	4.9109	4.4208	4.1048	4.0465	3.9317	48
	3.9757	4.2997	4.6698	4.0969	3.7488		
	4.1644	4.467	4.4683	4.2861	3.8394		
4.4194	5.0897	5.254	4.7281	4.3518	4.2256	3.9409	49
	4.1135	4.4621	4.9629	4.3654	3.862		
	4.3057	4.7985	4.8386	4.6869	4.0788		
4.5358	5.367	5.5263	5.1128	4.7439	4.5517	4.0483	50
	4.2421	4.5871	5.2228	4.7007	4.0322		

	4.37	4.8984	5.001	4.9432	4.2375		
4.6186	5.5118	5.6555	5.4193	5.1194	4.9507	4.2969	51
	4.3554	4.687	5.3639	5.0042	4.2368		
	4.3336	4.6874	4.8	4.7974	4.2019		
4.6289	5.4324	5.6567	5.6381	5.2951	5.0617	4.3379	52
	4.4093	4.7085	5.3682	5.1505	4.2956		
	4.2888	4.4684	4.5419	4.5208	4.0959		
4.5617	5.1743	5.5158	5.7022	5.1907	4.729	4.1348	53
	4.4108	4.6842	5.2806	5.0641	4.1905		
	4.2424	4.4307	4.4541	4.3799	4.0635		
4.5465	4.9711	5.2372	5.4782	4.9102	4.359	4.0069	54
	4.408	4.7036	5.1045	4.8417	4.0835		
	4.1757	4.4273	4.4472	4.3646	4.0335		
4.551	4.8687	4.9548	5.0818	4.5534	4.1364	4.0182	55
	4.3593	4.6379	4.8281	4.5603	3.9732		
	4.0691	4.3042	4.3206	4.2251	3.924		
4.4568	4.7839	4.7913	4.7772	4.3242	3.9905	4.0079	56
	4.2279	4.4891	4.567	4.2704	3.8071		
	3.9925	4.1453	4.0957	3.9801	3.7794		
4.2992	4.6901	4.7374	4.6199	4.2967	3.9523	3.932	57
	4.113	4.3795	4.3973	4.0792	3.7059		
	3.9764	4.1175	3.943	3.7919	3.7132		
4.1789	4.5963	4.634	4.4467	4.2995	4.0343	3.9324	58
	4.0723	4.3605	4.355	4.0324	3.752		
	3.9699	4.1507	3.941	3.8221	3.7321		
4.1649	4.5517	4.5069	4.3147	4.2648	4.0847	3.9265	59
	4.0516	4.3164	4.3212	4.0381	3.8119		
	3.9798	4.2264	4.0562	3.9765	3.7692		
4.2124	4.6004	4.508	4.3336	4.2734	4.0728	3.8889	60
	3.9841	4.2423	4.2858	4.0305	3.8172		

J.2.3 22 CIRCULAR PIPE DIFFUSER, 100% SPEED 'DESIGN

	3.8309	4.1865	4.1235	3.9387	3.5293		
3.9852	4.2617	4.1414	4.2111	4.1208	3.897	3.6275	1
	3.7728	3.8558	3.8262	3.56	3.382		
	3.8135	4.1766	4.1029	3.9322	3.505		
4.0146	4.2628	4.1054	4.0961	4.0157	3.8942	3.6345	2
	3.706	3.7773	3.7598	3.4879	3.3232		
	3.7906	4.1744	4.0742	3.9146	3.4837		
4.093	4.2971	4.131	4.0322	3.9577	3.9286	3.6411	3
	3.6684	3.7191	3.7134	3.4395	3.2751		

	3.7859	4.2062	4.1121	3.9301	3.4982		
4.1803	4.3373	4.149	4.0452	3.9667	3.9453	3.6379	4
	3.6983	3.741	3.7208	3.433	3.2452		
	3.8672	4.3976	4.3195	4.0686	3.5764		
4.3002	4.5006	4.2479	4.1711	4.0543	3.9989	3.6687	5
	3.7817	3.8699	3.848	3.5576	3.3022		
	4.0192	4.7259	4.6675	4.3675	3.7175		
4.3987	4.7105	4.4958	4.4251	4.2832	4.1728	3.766	6
	3.8502	4.0226	4.0716	3.8047	3.4539		
	4.1473	4.9306	4.9274	4.6325	3.8641		
4.4288	4.8142	4.747	4.7306	4.6014	4.4934	3.9559	7
	3.8917	4.1123	4.271	4.0622	3.6541		
	4.1859	4.8411	4.8501	4.6233	3.9157		
4.4006	4.7752	4.8852	4.9595	4.8348	4.7425	4.0864	8
	3.8977	4.134	4.3927	4.2338	3.7744		
	4.1622	4.639	4.5653	4.3869	3.8602		
4.3689	4.6716	4.882	5.0007	4.8315	4.686	4.1074	9
	3.8938	4.1337	4.4033	4.2112	3.7321		
	4.1012	4.4607	4.3483	4.2082	3.7823		
4.3133	4.5302	4.751	4.8364	4.6113	4.399	4.0277	10
	3.8914	4.082	4.2868	4.0644	3.6095		
	4.0076	4.3041	4.2454	4.1315	3.7421		
4.2335	4.412	4.5835	4.6153	4.3439	4.1503	3.9742	11
	3.8612	3.9896	4.1528	3.9445	3.5564		
	3.9083	4.135	4.1622	4.094	3.7013		
4.1489	4.3679	4.4887	4.4765	4.1872	4.0492	3.9641	12
	3.8137	3.9375	4.1266	3.9293	3.5507		
	3.8429	4.0267	4.0868	4.0418	3.6569		
4.0959	4.4295	4.5481	4.469	4.1776	4.071	3.9878	13
	3.8391	4.0123	4.236	3.9962	3.5767		
	3.8791	4.128	4.1394	4.0732	3.6698		
4.126	4.6234	4.7556	4.5966	4.3084	4.2181	4.0284	14
	3.9574	4.2025	4.4362	4.1714	3.6617		
	3.9832	4.3968	4.3995	4.3152	3.796		
4.2006	4.8988	5.0626	4.8674	4.5774	4.4662	4.1153	15
	4.1209	4.4525	4.7019	4.4493	3.8009		
	4.0862	4.5829	4.6186	4.5558	3.922		
4.3125	5.1414	5.2987	5.1433	4.8827	4.7874	4.2702	16
	4.3014	4.6972	4.9439	4.7891	3.9924		
	4.1217	4.5522	4.5687	4.5559	3.9527		
4.3831	5.2498	5.4159	5.3207	5.057	4.9068	4.3318	17
	4.4326	4.8323	5.0425	5.0058	4.1074		

	4.1018	4.4015	4.3635	4.3759	3.9156		
4.3877	5.1581	5.387	5.422	5.0939	4.7262	4.272	18
	4.4634	4.8156	4.9962	4.9659	4.0853		
	4.0669	4.3183	4.2667	4.2849	3.9111		
4.3489	4.9374	5.2293	5.4052	5.0385	4.4831	4.2066	19
	4.4685	4.7899	4.9352	4.8013	4.0273		
	4.0207	4.3022	4.2691	4.218	3.8585		
4.3482	4.7713	4.9887	5.1782	4.831	4.2893	4.157	20
	4.4561	4.7502	4.8283	4.5895	3.9828		
	3.9194	4.2131	4.1844	4.0646	3.7506		
4.3431	4.7238	4.7971	4.8513	4.542	4.1052	4.0719	21
	4.3599	4.5948	4.6364	4.3229	3.8826		
	3.8023	4.073	4.0201	3.8647	3.6395		
4.2933	4.7235	4.7129	4.6157	4.336	3.9819	3.9663	22
	4.2242	4.4358	4.4636	4.1028	3.7665		
	3.7521	4.025	3.9001	3.7252	3.5704		
4.213	4.6712	4.6543	4.4832	4.3075	4.009	3.9019	23
	4.1624	4.3803	4.384	3.9825	3.685		
	3.7627	4.1222	3.9235	3.6866	3.5195		
4.1402	4.6043	4.5736	4.4036	4.3343	4.1347	3.9004	24
	4.1407	4.3692	4.3587	3.957	3.6334		
	3.788	4.283	4.0341	3.7543	3.5036		
4.118	4.6271	4.5186	4.3371	4.3375	4.22	3.9048	25
	4.0725	4.2739	4.2968	3.9282	3.6164		
	3.8231	4.4065	4.1696	3.9005	3.5381		
4.1388	4.6684	4.5089	4.3153	4.2394	4.1713	3.924	26
	3.9717	4.1405	4.1854	3.866	3.615		
	3.8495	4.4553	4.3002	4.0518	3.5941		
4.1634	4.6143	4.4817	4.3279	4.1954	4.171	3.9552	27
	3.9023	4.0479	4.0759	3.7737	3.571		
	3.8712	4.4568	4.4019	4.1383	3.6504		
4.1588	4.5371	4.4578	4.3768	4.2625	4.1923	3.9477	28
	3.8561	4.0031	4.0201	3.7042	3.5035		
	3.9036	4.4937	4.4648	4.1669	3.661		
4.1771	4.5405	4.5103	4.4548	4.3622	4.2037	3.9053	29
	3.826	3.9839	4.0144	3.6578	3.4455		
	3.9041	4.5284	4.4627	4.1466	3.6657		
4.2017	4.6039	4.5848	4.5694	4.4014	4.2052	3.8962	30
	3.8147	4.0003	4.015	3.6289	3.4162		
	3.8761	4.4857	4.4055	4.108	3.6689		
4.1966	4.6506	4.6639	4.6468	4.3933	4.2393	3.9188	31
	3.8399	4.079	4.064	3.6545	3.4313		

	3.8512	4.3867	4.3385	4.0826	3.6409		
4.1492	4.6586	4.6869	4.5964	4.345	4.204	3.8975	32
	3.8728	4.145	4.1173	3.7032	3.4726		
	3.8508	4.3212	4.2674	4.0096	3.578		
4.1054	4.5725	4.6071	4.4592	4.2611	4.1208	3.8121	33
	3.8736	4.1297	4.1135	3.7291	3.5027		
	3.846	4.2967	4.1894	3.9304	3.539		
4.0576	4.4082	4.422	4.364	4.1965	4.0087	3.7208	34
	3.8457	4.0431	4.0248	3.6762	3.4722		
	3.8414	4.2636	4.1332	3.9081	3.5304		
4.0109	4.2653	4.2211	4.2752	4.1477	3.9148	3.6664	35
	3.8138	3.9462	3.9033	3.5756	3.4016		
	3.8388	4.244	4.1182	3.9206	3.5213		
4.0055	4.2229	4.1241	4.1667	4.0606	3.8851	3.666	36
	3.7589	3.8462	3.7924	3.4787	3.3307		
	3.8257	4.2366	4.1041	3.9237	3.4973		
4.07	4.2646	4.1473	4.0802	4.0112	3.9477	3.6869	37
	3.6999	3.7706	3.7334	3.4295	3.2908		
	3.8161	4.236	4.1148	3.9267	3.5071		
4.1615	4.3223	4.2017	4.0742	4.0202	3.9913	3.6881	38
	3.7049	3.7502	3.7383	3.4083	3.2672		
	3.8721	4.3242	4.2391	3.996	3.56		
4.2828	4.4602	4.2656	4.1785	4.084	4.0226	3.6981	39
	3.7835	3.846	3.8296	3.463	3.2745		
	4.0139	4.6112	4.5381	4.2322	3.6887		
4.4027	4.6707	4.4606	4.3884	4.2508	4.1373	3.7655	40
	3.8695	4.0173	4.0312	3.655	3.3793		
	4.1616	4.8811	4.8483	4.5416	3.8435		
4.468	4.8075	4.7064	4.6892	4.5736	4.4311	3.9295	41
	3.9174	4.1387	4.2414	3.9311	3.5778		
	4.2357	4.9041	4.8993	4.6655	3.943		
4.4509	4.7955	4.8903	4.9642	4.8854	4.7646	4.1033	42
	3.9302	4.1595	4.3773	4.14	3.7605		
	4.2322	4.7125	4.6441	4.4768	3.9057		
4.4039	4.7058	4.9433	5.1023	5.0118	4.8499	4.1727	43
	3.9236	4.1497	4.4325	4.2054	3.7922		
	4.1788	4.5084	4.3624	4.218	3.8082		
4.3376	4.5983	4.9014	5.0227	4.8338	4.5974	4.1102	44
	3.9125	4.1213	4.3948	4.0858	3.67		
	4.0811	4.3194	4.1923	4.0686	3.7404		
4.252	4.4907	4.7553	4.8116	4.5299	4.2771	4.0238	45
	3.8945	4.0521	4.2692	3.937	3.5568		

	3.9637	4.1465	4.1021	4.0204	3.7012		
4.1549	4.4209	4.6145	4.6189	4.2863	4.0925	3.991	46
	3.8516	3.9699	4.1907	3.8889	3.5317		
	3.8663	4.0181	4.0498	3.9877	3.6452		
4.0806	4.4361	4.5891	4.5274	4.197	4.0635	4.0016	47
	3.8305	3.9706	4.2235	3.959	3.559		
	3.8513	4.0335	4.0535	3.9621	3.6162		
4.0788	4.5859	4.7479	4.5731	4.2293	4.1644	4.0266	48
	3.908	4.095	4.3718	4.1221	3.6287		
	3.9343	4.2576	4.2459	4.1262	3.7009		
4.1407	4.8413	5.0134	4.7814	4.4013	4.3615	4.0788	49
	4.043	4.3057	4.5716	4.3811	3.7489		
	4.0299	4.4704	4.4928	4.3967	3.8374		
4.2479	5.1128	5.2724	5.066	4.69	4.6505	4.2058	50
	4.212	4.5422	4.8037	4.7273	3.915		
	4.1062	4.545	4.5865	4.5322	3.919		
4.3537	5.2859	5.3912	5.2681	4.9266	4.8592	4.3503	51
	4.3721	4.7368	4.9805	5.0401	4.0947		
	4.1206	4.4583	4.4677	4.4106	3.8934		
4.4095	5.2829	5.3837	5.3663	5.0207	4.7712	4.3217	52
	4.4556	4.7756	5.017	5.1171	4.1377		
	4.1063	4.3681	4.3328	4.2793	3.8717		
4.3938	5.1224	5.2782	5.3895	5.0186	4.4647	4.2264	53
	4.4572	4.721	4.9629	4.9832	4.0882		
	4.0759	4.3533	4.2942	4.2202	3.8476		
4.4068	4.9595	5.1129	5.2593	4.9298	4.2567	4.1541	54
	4.4692	4.7166	4.9026	4.7971	4.0505		
	4.0114	4.3223	4.2551	4.134	3.7784		
4.4248	4.8703	4.9305	4.9556	4.671	4.0912	4.107	55
	4.4299	4.6588	4.7657	4.5658	3.9926		
	3.9003	4.1996	4.1358	3.9565	3.6636		
4.3837	4.8212	4.7975	4.6507	4.3966	3.9496	3.9866	56
	4.3049	4.4885	4.5695	4.2923	3.8644		
	3.8187	4.1122	3.9979	3.791	3.5761		
4.2895	4.7605	4.7164	4.4768	4.2622	3.8805	3.8729	57
	4.187	4.3493	4.4142	4.0935	3.7644		
	3.8006	4.1394	3.9497	3.7086	3.527		
4.2054	4.6777	4.6139	4.3741	4.259	3.9809	3.8359	58
	4.1506	4.3516	4.386	4.0218	3.7095		
	3.8128	4.2547	4.0195	3.7281	3.4988		
4.1602	4.6407	4.5119	4.3042	4.289	4.1185	3.8586	59
	4.1037	4.3268	4.3618	3.9861	3.6836		

	3.8449	4.3858	4.1427	3.8399	3.5115		
4.1712	4.6764	4.4889	4.2719	4.2523	4.1604	3.8656	60
	4.0182	4.2135	4.2729	3.9247	3.6656		

J.2.4 22 CIRCULAR PIPE DIFFUSER, 100% SPEED 'NEAR CHOKE'

	3.3163	4.0777	4.0142	3.8862	3.2097		
3.4689	3.6224	3.7322	3.778	3.6407	3.6758	3.5761	1
	2.9461	3.3597	3.4501	3.6297	2.9696		
	3.3085	3.9503	3.8681	3.7739	3.1968		
3.4541	3.5256	3.6719	3.7737	3.6585	3.6606	3.5935	2
	2.9894	3.403	3.432	3.6364	2.9946		
	3.3062	3.8691	3.7787	3.7028	3.1743		
3.4058	3.442	3.5817	3.7291	3.6691	3.6347	3.6258	3
	3.0137	3.3713	3.3373	3.5648	2.9866		
	3.3138	3.8546	3.7732	3.6777	3.166		
3.3575	3.3821	3.522	3.6861	3.6738	3.6272	3.6456	4
	3.0072	3.3087	3.235	3.5018	2.9821		
	3.3276	3.8771	3.8093	3.683	3.163		
3.3277	3.3499	3.5058	3.7408	3.7164	3.6842	3.6722	5
	3.0062	3.3048	3.225	3.5255	2.9966		
	3.391	3.9296	3.8657	3.7251	3.1799		
3.3241	3.3606	3.5274	3.8702	3.8598	3.82	3.7361	6
	3.0448	3.4206	3.3121	3.6316	3.0345		
	3.5078	4.119	4.0458	3.8993	3.2419		
3.3517	3.4475	3.6382	4.0457	4.0956	4.0067	3.8155	7
	3.1159	3.6185	3.4627	3.8076	3.0954		
	3.6118	4.3019	4.2831	4.145	3.3489		
3.4768	3.6403	3.827	4.2268	4.2943	4.1677	3.829	8
	3.1979	3.7918	3.6433	4.0255	3.2037		
	3.6377	4.267	4.3368	4.2643	3.4399		
3.6121	3.8364	4.0108	4.3472	4.365	4.226	3.766	9
	3.2676	3.8595	3.8399	4.1717	3.2841		
	3.5772	3.9799	4.0782	4.0896	3.4496		
3.6975	3.8609	4.0553	4.3586	4.3616	4.2008	3.6579	10
	3.3107	3.8304	3.9879	4.1007	3.2573		
	3.4883	3.6968	3.7611	3.7984	3.3963		
3.6615	3.6761	3.9505	4.2897	4.3585	4.1523	3.5452	11
	3.3195	3.7691	4.0525	3.8752	3.1385		
	3.3963	3.5325	3.5431	3.5507	3.3215		
3.5867	3.4829	3.8196	4.2077	4.3522	4.117	3.4753	12
	3.314	3.7525	4.0427	3.6539	3.0265		

	3.3397	3.5259	3.4926	3.4453	3.2596		
3.5402	3.4025	3.7974	4.2054	4.3744	4.1355	3.4882	13
	3.2985	3.7782	4.0015	3.4958	2.9393		
	3.3276	3.6408	3.6065	3.5227	3.2478		
3.5457	3.4642	3.9097	4.304	4.3999	4.1778	3.5239	14
	3.2767	3.7972	3.9515	3.3821	2.895		
	3.3373	3.7697	3.765	3.698	3.2642		
3.5866	3.6668	4.1351	4.4496	4.4299	4.205	3.562	15
	3.2858	3.8577	3.9686	3.3299	2.8884		
	3.3812	3.8955	3.8466	3.781	3.2788		
3.6062	3.8544	4.2824	4.5063	4.473	4.3128	3.681	16
	3.3554	4.0457	4.1159	3.3744	2.9135		
	3.4496	4.0851	3.935	3.7783	3.2713		
3.5193	3.9174	4.31	4.4932	4.5551	4.496	3.8191	17
	3.4299	4.1982	4.2573	3.4696	2.9646		
	3.5174	4.2903	4.1327	3.9128	3.3066		
3.4714	3.9449	4.3569	4.5298	4.6376	4.5602	3.8732	18
	3.4358	4.1452	4.2752	3.5116	2.9887		
	3.57	4.493	4.3872	4.1006	3.3319		
3.4787	4.0384	4.4094	4.499	4.5555	4.4401	3.8532	19
	3.4154	3.9827	4.1791	3.4823	2.9755		
	3.5843	4.572	4.5105	4.1316	3.3027		
3.4887	4.0453	4.2807	4.2812	4.2857	4.3045	3.8726	20
	3.4124	3.8394	4.0128	3.4537	2.9639		
	3.5587	4.4757	4.4222	4.016	3.232		
3.4363	3.8555	3.9638	3.9983	4.0691	4.2568	3.8945	21
	3.3848	3.7108	3.8867	3.4655	2.9664		
	3.4881	4.2702	4.2412	3.9328	3.1782		
3.3895	3.6674	3.7445	3.9267	4.0311	4.2351	3.8502	22
	3.3343	3.6437	3.8012	3.4807	2.9625		
	3.4142	4.0873	4.1154	3.8735	3.1283		
3.3706	3.6195	3.7729	4.0716	4.1009	4.1608	3.768	23
	3.3099	3.6358	3.7366	3.4811	2.9382		
	3.3704	3.9916	4.056	3.8469	3.0827		
3.3437	3.6506	3.8487	4.1338	4.0972	4.0884	3.6954	24
	3.2606	3.5841	3.6613	3.4642	2.9153		
	3.3595	3.9927	4.0269	3.8503	3.06		
3.3441	3.659	3.8113	4.0025	4.0085	4.0239	3.6227	25
	3.1584	3.4483	3.5446	3.4147	2.9042		
	3.349	4.0254	4.0094	3.8542	3.0671		
3.3535	3.6402	3.6969	3.8469	3.9188	3.9623	3.5812	26
	3.064	3.2819	3.3811	3.356	2.8767		

	3.3213	4.0033	3.9884	3.8618	3.0723		
3.3328	3.5708	3.5831	3.7691	3.8371	3.9015	3.5605	27
	2.9973	3.1529	3.2437	3.2823	2.8347		
	3.304	3.9383	3.927	3.8161	3.0508		
3.3114	3.5309	3.5442	3.692	3.7499	3.8779	3.5442	28
	2.9353	3.0923	3.1667	3.1863	2.7674		
	3.2991	3.8761	3.8134	3.713	3.0378		
3.2804	3.5233	3.5709	3.623	3.684	3.8393	3.525	29
	2.8803	3.0646	3.1224	3.1029	2.7183		
	3.2772	3.8096	3.704	3.6582	3.042		
3.2868	3.5378	3.595	3.6475	3.6582	3.792	3.5307	30
	2.855	3.0571	3.0899	3.0657	2.6868		
	3.2651	3.7977	3.7268	3.7065	3.07		
3.3064	3.5477	3.5865	3.6814	3.6705	3.7909	3.5488	31
	2.8518	3.059	3.0828	3.0598	2.6776		
	3.2812	3.9182	3.899	3.8161	3.0987		
3.346	3.6002	3.6302	3.6776	3.6892	3.8499	3.571	32
	2.8502	3.0861	3.1298	3.1027	2.6944		
	3.3329	4.0819	4.0816	3.9175	3.1424		
3.4032	3.6634	3.6985	3.6963	3.6944	3.8579	3.5937	33
	2.8474	3.1233	3.2366	3.2212	2.7599		
	3.3651	4.166	4.1424	3.9676	3.1908		
3.4675	3.705	3.751	3.7571	3.6635	3.7783	3.6069	34
	2.8546	3.1832	3.3468	3.3771	2.8454		
	3.3663	4.0998	4.0554	3.923	3.2172		
3.5317	3.6937	3.7711	3.8172	3.6562	3.7122	3.6126	35
	2.8852	3.26	3.424	3.5043	2.9159		
	3.3459	3.9724	3.8929	3.8051	3.212		
3.5446	3.6217	3.7222	3.8333	3.6754	3.7015	3.6174	36
	2.9326	3.343	3.454	3.5362	2.9474		
	3.3305	3.8477	3.7555	3.7145	3.1971		
3.5057	3.5171	3.6119	3.7939	3.6947	3.6938	3.638	37
	2.9697	3.3758	3.4079	3.4988	2.949		
	3.322	3.7974	3.7189	3.6809	3.1818		
3.4511	3.4325	3.5334	3.7241	3.7037	3.6769	3.674	38
	2.9844	3.3434	3.3148	3.4668	2.9412		
	3.33	3.8173	3.7578	3.6718	3.1805		
3.4143	3.3827	3.5277	3.7494	3.7356	3.6997	3.699	39
	2.9861	3.3032	3.2553	3.5076	2.9514		
	3.3691	3.8723	3.8204	3.7039	3.1914		
3.4081	3.3971	3.5825	3.8893	3.8579	3.8048	3.7443	40
	3.016	3.3705	3.2884	3.6321	2.9921		

	3.4658	4.0143	3.9448	3.8213	3.2422		
3.4254	3.4841	3.7163	4.0791	4.0872	3.9781	3.8183	41
	3.0856	3.5585	3.4029	3.8206	3.0544		
	3.5752	4.2161	4.165	4.0513	3.3369		
3.5063	3.6579	3.9398	4.2816	4.3061	4.1535	3.8494	42
	3.1789	3.7781	3.5784	4.0428	3.1417		
	3.6328	4.2705	4.288	4.219	3.4306		
3.6486	3.8762	4.175	4.4293	4.3937	4.2486	3.8049	43
	3.2631	3.9104	3.8015	4.2242	3.2482		
	3.6035	4.0738	4.1338	4.1487	3.4677		
3.7424	3.9623	4.2684	4.4738	4.4035	4.2555	3.7169	44
	3.3244	3.9321	4.0092	4.2225	3.275		
	3.5231	3.8034	3.8376	3.8881	3.419		
3.7117	3.813	4.1593	4.4138	4.4105	4.2231	3.6257	45
	3.3449	3.8926	4.1204	4.0244	3.1985		
	3.4401	3.6327	3.6145	3.6362	3.3501		
3.5952	3.568	3.9616	4.3102	4.4127	4.1894	3.5518	46
	3.3374	3.8598	4.1075	3.7645	3.0847		
	3.3768	3.5933	3.5323	3.4905	3.2831		
3.5002	3.4057	3.83	4.2344	4.4066	4.1947	3.5406	47
	3.321	3.8401	4.0246	3.5532	2.9931		
	3.3601	3.69	3.6126	3.5193	3.263		
3.471	3.3895	3.8392	4.2575	4.4266	4.2459	3.5768	48
	3.3008	3.8192	3.9252	3.4107	2.9362		
	3.3632	3.8257	3.7783	3.6805	3.271		
3.4968	3.5195	3.9964	4.3642	4.4335	4.2732	3.609	49
	3.292	3.8228	3.8535	3.3266	2.9196		
	3.3947	3.9373	3.8931	3.8161	3.294		
3.5612	3.7301	4.1763	4.4301	4.464	4.3264	3.6933	50
	3.3311	3.9392	3.8972	3.3192	2.9314		
	3.4502	4.0928	3.9707	3.8388	3.2896		
3.5358	3.8366	4.25	4.4152	4.5224	4.468	3.8362	51
	3.4141	4.141	4.0311	3.3837	2.9612		
	3.5118	4.2667	4.1168	3.8913	3.3044		
3.4631	3.8313	4.2754	4.4402	4.6277	4.5751	3.9329	52
	3.4627	4.2245	4.1302	3.4436	2.9874		
	3.5669	4.452	4.3596	4.0635	3.3286		
3.4642	3.87	4.3514	4.4903	4.6291	4.5049	3.9042	53
	3.4259	4.1044	4.1144	3.417	2.976		
	3.6062	4.5893	4.5546	4.1839	3.3243		
3.4809	3.9423	4.3321	4.3795	4.4035	4.3057	3.8681	54
	3.4048	3.9197	4.0036	3.3604	2.9417		

	3.5997	4.5599	4.5325	4.1342	3.2536		
3.4293	3.8586	4.1013	4.1087	4.1351	4.1859	3.8649	55
	3.3787	3.7459	3.8834	3.3594	2.9273		
	3.5388	4.3502	4.3168	4.0177	3.1881		
3.3285	3.6492	3.8121	3.9436	4.0619	4.1633	3.8371	56
	3.3187	3.6279	3.7961	3.3762	2.9203		
	3.4465	4.1042	4.1068	3.9275	3.133		
3.2986	3.5634	3.7586	4.0668	4.1484	4.1406	3.7455	57
	3.281	3.5958	3.7312	3.3803	2.9041		
	3.375	3.9404	3.9879	3.8706	3.1027		
3.2861	3.6032	3.8495	4.1922	4.1933	4.0639	3.6495	58
	3.2603	3.5857	3.6685	3.3671	2.8781		
	3.3431	3.8983	3.9506	3.8601	3.0702		
3.2727	3.6499	3.8733	4.1175	4.0954	3.9982	3.5725	59
	3.1862	3.5088	3.5956	3.3585	2.8726		
	3.3431	3.9453	3.9571	3.8613	3.0688		
3.2942	3.6604	3.7748	3.9245	3.9482	3.9384	3.5095	60
	3.0887	3.3549	3.4698	3.3322	2.8654		

J.3. 13 CIRCULAR PIPE DIFFUSER TRAVERSES

Table J.3 Operating Conditions for 13 Circular Pipe Diffuser Traverses

Flow Condition	m_{corr} (kg/sec)	Corr. Speed (rpm)	$P_{tot\ out}$ (Pa)*	$P_{tot\ in}$ (Pa)	$T_{tot\ out}$ (K)	$T_{tot\ in}$ (K)
Near Surge	3.444	34933	491318	79240	508.30	284.64
Design	3.749	34941	453966	75749	502.56	284.84
Near Choke	4.212	34892	398088	70199	494.42	285.14

* At impeller discharge

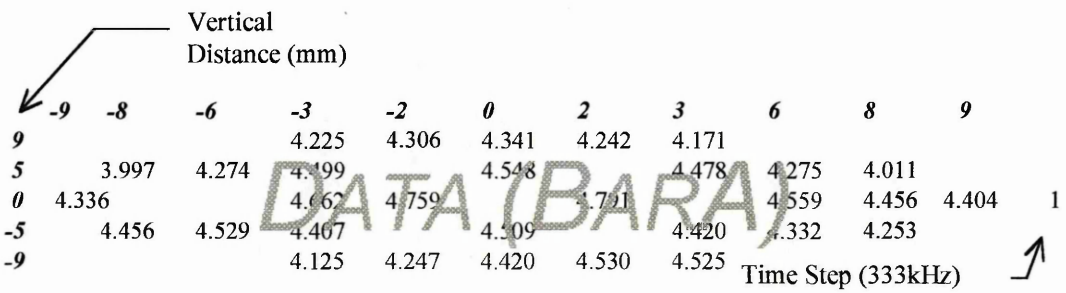


Figure J.5 Designations for 13 Circular Pipe Diffuser Data

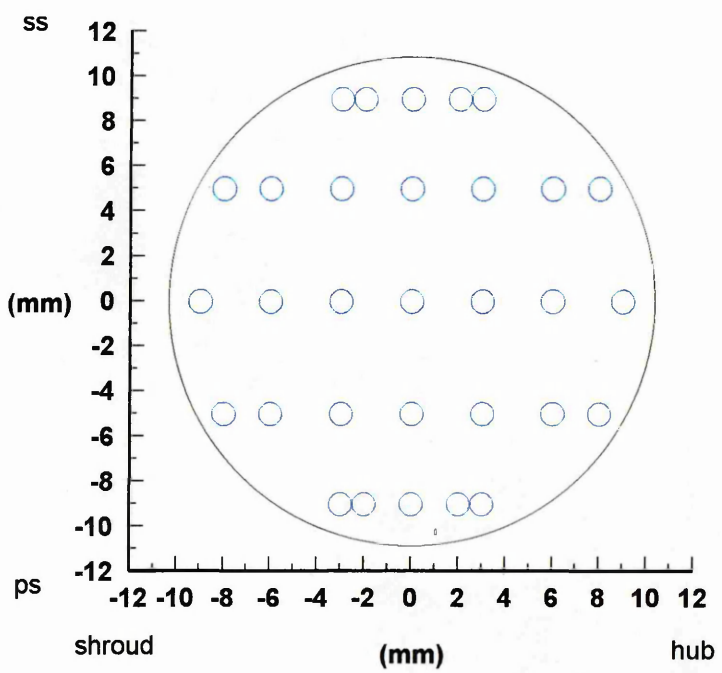


Figure J.6 Measurement Locations for 13 Circular Pipe Diffuser Data

J.3.1 13 (CIRCULAR) PIPE DIFFUSER, 100% SPEED, NEAR SURGE

			4.225	4.306	4.341	4.242	4.171				
	3.997	4.274	4.499		4.548		4.478	4.275	4.011		
4.336		4.662	4.759		4.791		4.559	4.456		4.404	1
	4.456	4.529	4.407		4.509		4.420	4.332	4.253		
			4.125	4.247	4.420	4.530	4.525				
			4.049	4.117	4.192	4.167	4.121				
	3.878	4.099	4.455		4.620		4.508	4.195	3.994		
4.291		4.712	4.790		4.821		4.653	4.526		4.496	2
	4.574	4.648	4.529		4.639		4.582	4.419	4.298		
			4.234	4.327	4.529	4.615	4.612				
			3.956	4.033	4.136	4.166	4.141				
	3.684	3.881	4.367		4.671		4.531	4.175	4.004		
4.055		4.598	4.772		4.795		4.651	4.481		4.425	3
	4.449	4.514	4.505		4.615		4.550	4.287	4.177		
			4.152	4.200	4.396	4.476	4.494				
			4.009	4.072	4.144	4.189	4.162				
	3.658	3.868	4.347		4.665		4.543	4.215	4.044		
3.857		4.412	4.750		4.801		4.564	4.350		4.293	4
	4.191	4.234	4.329		4.496		4.422	4.131	4.071		
			4.000	4.020	4.189	4.337	4.373				
			4.085	4.126	4.137	4.154	4.134				
	3.837	4.051	4.390		4.627		4.532	4.284	4.103		
3.865		4.309	4.711		4.823		4.481	4.217		4.205	5
	3.987	4.006	4.114		4.339		4.265	4.021	4.010		
			3.882	3.915	4.090	4.298	4.350				
			4.073	4.105	4.091	4.075	4.049				
	4.016	4.223	4.425		4.591		4.537	4.340	4.141		
3.988		4.295	4.625		4.720		4.348	4.122		4.162	6
	3.927	3.927	3.982		4.173		4.097	3.919	3.928		
			3.836	3.879	4.047	4.263	4.321				
			3.974	4.012	4.026	3.998	3.981				
	4.023	4.209	4.394		4.504		4.503	4.327	4.124		
4.039		4.287	4.462		4.466		4.104	4.003		4.086	7
	4.014	3.991	3.938		3.996		3.926	3.838	3.845		
			3.864	3.899	3.994	4.137	4.204				
			3.837	3.893	3.945	3.929	3.923				
	3.871	4.017	4.274		4.336		4.344	4.225	4.074		
3.955		4.207	4.244		4.161		3.855	3.831		3.939	8
	4.106	4.085	3.930		3.880		3.802	3.759	3.776		
			3.880	3.882	3.900	3.969	4.033				
			3.717	3.788	3.850	3.854	3.867				
	3.718	3.792	4.081		4.131		4.112	4.088	4.013		
3.818		4.063	4.023		3.928		3.744	3.705		3.752	9
	4.094	4.117	3.975		3.899		3.740	3.654	3.662		
			3.784	3.767	3.785	3.833	3.892				

			3.664	3.730	3.778	3.783	3.810				
	3.630	3.683	3.909		3.984		3.952	3.988	3.950		
3.720		3.923	3.879		3.772		3.717	3.669		3.632	10
	3.978	4.053	3.986		3.936		3.702	3.518	3.510		
			3.641	3.645	3.697	3.769	3.806				
			3.669	3.719	3.755	3.744	3.785				
	3.636	3.686	3.822		3.918		3.941	3.968	3.919		
3.689		3.874	3.834		3.690		3.671	3.636		3.583	11
	3.863	3.940	3.902		3.868		3.632	3.416	3.412		
			3.565	3.591	3.659	3.736	3.763				
			3.700	3.731	3.752	3.736	3.772				
	3.680	3.735	3.819		3.908		3.998	3.990	3.917		
3.688		3.865	3.839		3.656		3.558	3.529		3.552	12
	3.821	3.854	3.780		3.746		3.568	3.413	3.426		
			3.566	3.576	3.625	3.718	3.757				
			3.731	3.747	3.764	3.746	3.771				
	3.708	3.768	3.856		3.917		4.008	3.984	3.871		
3.691		3.856	3.826		3.691		3.440	3.415		3.529	13
	3.829	3.813	3.702		3.691		3.573	3.519	3.541		
			3.567	3.558	3.583	3.704	3.775				
			3.773	3.788	3.809	3.808	3.827				
	3.672	3.796	3.951		3.982		3.973	3.930	3.739		
3.709		3.897	3.861		3.772		3.429	3.397		3.542	14
	3.843	3.814	3.714		3.730		3.636	3.643	3.679		
			3.537	3.534	3.563	3.704	3.787				
			3.946	4.002	4.063	4.088	4.084				
	3.712	3.932	4.172		4.210		4.165	4.011	3.704		
3.785		4.070	4.050		3.946		3.651	3.582		3.641	15
	3.936	3.948	3.851		3.846		3.729	3.719	3.772		
			3.559	3.594	3.648	3.772	3.823				
			4.345	4.440	4.516	4.483	4.427				
	4.039	4.368	4.668		4.696		4.640	4.411	3.969		
4.082		4.480	4.473		4.291		4.086	4.021		3.981	16
	4.267	4.349	4.160		4.051		3.918	3.882	3.932		
			3.772	3.828	3.893	3.997	3.986				
			4.655	4.764	4.848	4.701	4.607				
	4.443	4.893	5.209		5.203		5.109	4.818	4.265		
4.539		5.031	5.020		4.777		4.578	4.521		4.370	17
	4.749	4.918	4.681		4.471		4.299	4.236	4.207		
			4.223	4.295	4.347	4.436	4.383				
			4.653	4.767	4.861	4.679	4.577				
	4.546	5.046	5.434		5.430		5.276	4.916	4.396		
4.797		5.384	5.386		5.134		4.897	4.793		4.541	18
	5.022	5.317	5.205		4.989		4.738	4.487	4.328		
			4.713	4.804	4.869	4.929	4.843				

			4.502	4.635	4.763	4.655	4.550				
	4.297	4.726	5.246		5.346		5.215	4.791	4.379		
4.619		5.243	5.277		5.104		4.902	4.731		4.426	19
	4.861	5.169	5.292		5.276		4.974	4.448	4.220		
			4.848	4.941	5.053	5.116	5.061				
			4.457	4.563	4.669	4.604	4.522				
	4.147	4.494	4.960		5.140		5.080	4.705	4.348		
4.360		4.938	5.013		4.877		4.726	4.610		4.356	20
	4.570	4.719	4.892		5.033		4.884	4.370	4.198		
			4.489	4.557	4.697	4.851	4.898				
			4.446	4.499	4.536	4.471	4.412				
	4.212	4.562	4.788		4.925		4.914	4.647	4.317		
4.300		4.710	4.822		4.686		4.542	4.531		4.436	21
	4.347	4.352	4.447		4.602		4.595	4.401	4.349		
			4.117	4.164	4.295	4.494	4.614				
			4.377	4.393	4.387	4.304	4.256				
	4.325	4.687	4.726		4.750		4.726	4.550	4.270		
4.358		4.562	4.659		4.566		4.400	4.457		4.534	22
	4.214	4.194	4.217		4.315		4.304	4.365	4.432		
			4.013	4.076	4.184	4.309	4.395				
			4.310	4.336	4.330	4.227	4.170				
	4.357	4.689	4.712		4.626		4.575	4.467	4.262		
4.366		4.468	4.462		4.413		4.246	4.360		4.509	23
	4.141	4.149	4.130		4.128		4.066	4.114	4.234		
			4.057	4.132	4.184	4.193	4.220				
			4.275	4.331	4.366	4.279	4.220				
	4.315	4.548	4.625		4.491		4.436	4.415	4.266		
4.314		4.424	4.285		4.232		4.060	4.223		4.331	24
	4.116	4.130	4.043		3.933		3.865	3.809	3.906		
			4.026	4.078	4.062	4.019	4.038				
			4.267	4.352	4.427	4.371	4.306				
	4.247	4.407	4.505		4.375		4.325	4.423	4.277		
4.245		4.380	4.161		3.998		3.876	4.074		4.119	25
	4.069	4.078	3.910		3.767		3.689	3.618	3.654		
			3.834	3.848	3.808	3.811	3.852				
			4.210	4.298	4.378	4.350	4.300				
	4.193	4.324	4.382		4.292		4.251	4.426	4.243		
4.208		4.346	4.093		3.788		3.709	3.939		3.941	26
	4.018	4.010	3.785		3.683		3.603	3.619	3.629		
			3.601	3.600	3.600	3.674	3.735				
			4.105	4.159	4.213	4.213	4.203				
	4.150	4.274	4.281		4.232		4.222	4.371	4.192		
4.170		4.308	4.036		3.642		3.573	3.810		3.826	27
	3.964	3.954	3.709		3.666		3.632	3.729	3.744		
			3.468	3.485	3.554	3.656	3.726				

			3.989	3.995	4.025	4.060	4.076				
	4.142	4.223	4.156		4.134		4.160	4.234	4.105		
4.121		4.255	3.971		3.589		3.487	3.692		3.762	28
	3.924	3.914	3.696		3.702		3.730	3.835	3.867		
			3.481	3.518	3.621	3.718	3.781				
			3.928	3.899	3.896	3.948	3.976				
	4.111	4.151	4.033		3.982		4.023	4.062	3.988		
4.063		4.173	3.928		3.617		3.458	3.613		3.730	29
	3.891	3.862	3.712		3.746		3.789	3.830	3.872		
			3.586	3.623	3.701	3.772	3.818				
			3.907	3.871	3.834	3.881	3.909				
	4.022	4.069	3.963		3.851		3.866	3.923	3.879		
3.997		4.104	3.955		3.719		3.472	3.584		3.701	30
	3.870	3.810	3.715		3.758		3.757	3.762	3.803		
			3.668	3.699	3.735	3.764	3.802				
			3.921	3.912	3.867	3.866	3.867				
	3.870	3.970	3.979		3.863		3.782	3.856	3.825		
3.923		4.072	4.070		3.907		3.565	3.603		3.678	31
	3.850	3.790	3.696		3.751		3.677	3.689	3.726		
			3.666	3.681	3.728	3.753	3.787				
			4.009	4.042	4.048	3.976	3.930				
	3.765	3.943	4.083		4.053		3.895	3.930	3.851		
3.884		4.130	4.234		4.155		3.769	3.726		3.723	32
	3.838	3.829	3.724		3.792		3.693	3.671	3.725		
			3.625	3.656	3.755	3.828	3.855				
			4.160	4.237	4.290	4.171	4.083				
	3.806	4.070	4.283		4.336		4.165	4.132	3.946		
3.994		4.305	4.442		4.422		4.066	3.998		3.920	33
	3.922	3.980	3.885		3.954		3.858	3.788	3.846		
			3.678	3.754	3.889	4.031	4.045				
			4.243	4.346	4.391	4.275	4.173				
	3.931	4.244	4.485		4.557		4.432	4.294	4.007		
4.182		4.520	4.637		4.647		4.355	4.310		4.201	34
	4.168	4.276	4.149		4.223		4.144	4.085	4.094		
			3.869	3.985	4.153	4.315	4.311				
			4.160	4.247	4.271	4.208	4.133				
	3.972	4.269	4.560		4.665		4.553	4.276	3.987		
4.310		4.695	4.794		4.798		4.552	4.507		4.410	35
	4.417	4.555	4.381		4.477		4.433	4.361	4.272		
			4.093	4.210	4.408	4.548	4.542				

J.3.2 13 CIRCULAR PIPE DIFFUSER 100% SPEED, DESIGN MASS FLOW

			3.951	4.065	4.080	4.064	3.969				
	3.733	3.996	4.297		4.424		4.341	4.189	3.787		
4.133		4.460	4.577		4.552		4.202	4.006		4.001	1
	4.376	4.399	4.371		4.326		4.263	4.084	3.989		
			3.776	3.733	3.710	3.797	3.777				
			3.886	3.991	4.054	4.063	3.975				
	3.804	4.055	4.378		4.569		4.516	4.244	3.836		
4.232		4.644	4.695		4.666		4.353	4.185		4.110	2
	4.468	4.583	4.548		4.530		4.461	4.258	4.101		
			3.921	3.895	3.909	4.003	3.969				
			3.722	3.824	3.964	3.989	3.922				
	3.675	3.891	4.269		4.608		4.572	4.163	3.791		
4.073		4.613	4.700		4.653		4.343	4.136		3.969	3
	4.301	4.517	4.596		4.633		4.471	4.138	3.993		
			3.965	3.943	3.984	4.081	4.035				
			3.666	3.755	3.904	3.934	3.893				
	3.485	3.670	4.132		4.578		4.535	4.116	3.764		
3.749		4.410	4.699		4.609		4.244	3.968		3.771	4
	4.033	4.242	4.462		4.622		4.420	3.999	3.908		
			3.840	3.814	3.874	4.033	3.996				
			3.758	3.830	3.869	3.886	3.868				
	3.421	3.619	4.095		4.498		4.431	4.110	3.770		
3.568		4.194	4.696		4.615		4.165	3.845		3.691	5
	3.832	3.980	4.225		4.456		4.347	3.995	3.940		
			3.663	3.635	3.708	3.920	3.929				
			3.824	3.865	3.783	3.790	3.775				
	3.474	3.725	4.136		4.403		4.311	4.091	3.782		
3.564		4.059	4.590		4.588		4.113	3.823		3.747	6
	3.735	3.855	4.058		4.238		4.180	3.969	3.966		
			3.571	3.564	3.612	3.798	3.840				
			3.750	3.782	3.685	3.684	3.654				
	3.546	3.829	4.172		4.313		4.233	4.020	3.759		
3.640		3.995	4.387		4.441		4.000	3.821		3.832	7
	3.754	3.882	3.961		4.012		3.938	3.848	3.934		
			3.586	3.571	3.551	3.680	3.739				
			3.634	3.668	3.625	3.623	3.570				
	3.603	3.870	4.162		4.216		4.163	3.925	3.712		
3.692		4.003	4.174		4.170		3.806	3.745		3.809	8
	3.870	3.954	3.849		3.810		3.738	3.718	3.850		
			3.579	3.522	3.438	3.547	3.620				
			3.569	3.620	3.598	3.596	3.534				
	3.636	3.868	4.092		4.120		4.086	3.853	3.664		
3.679		4.010	4.000		3.898		3.621	3.564		3.671	9
	3.950	4.008	3.798		3.710		3.637	3.581	3.680		
			3.496	3.403	3.308	3.400	3.478				

			3.553	3.626	3.595	3.595	3.533				
	3.634	3.845	4.001		4.030		3.983	3.827	3.644		
3.595		3.945	3.841		3.688		3.507	3.425		3.525	10
	3.920	3.998	3.835		3.702		3.590	3.432	3.475		
			3.411	3.330	3.243	3.289	3.341				
			3.578	3.668	3.633	3.630	3.575				
	3.608	3.850	3.976		3.962		3.894	3.849	3.659		
3.558		3.827	3.714		3.550		3.422	3.391		3.482	11
	3.845	3.945	3.849		3.689		3.553	3.319	3.338		
			3.380	3.320	3.239	3.254	3.281				
			3.632	3.719	3.675	3.676	3.618				
	3.604	3.872	4.003		3.914		3.848	3.867	3.695		
3.608		3.750	3.641		3.474		3.335	3.399		3.538	12
	3.807	3.874	3.788		3.630		3.520	3.317	3.346		
			3.341	3.276	3.203	3.250	3.286				
			3.679	3.749	3.685	3.682	3.633				
	3.666	3.916	4.017		3.890		3.836	3.823	3.698		
3.715		3.752	3.637		3.448		3.265	3.379		3.586	13
	3.815	3.828	3.706		3.575		3.550	3.444	3.484		
			3.308	3.219	3.133	3.203	3.279				
			3.715	3.766	3.697	3.684	3.641				
	3.760	3.996	4.041		3.939		3.854	3.762	3.640		
3.843		3.863	3.684		3.496		3.269	3.392		3.565	14
	3.843	3.836	3.719		3.601		3.605	3.603	3.668		
			3.332	3.232	3.127	3.163	3.236				
			3.794	3.853	3.819	3.802	3.745				
	3.896	4.179	4.158		4.091		3.977	3.783	3.571		
4.037		4.032	3.809		3.629		3.377	3.460		3.514	15
	3.926	3.939	3.859		3.745		3.684	3.680	3.748		
			3.456	3.377	3.281	3.256	3.279				
			4.101	4.200	4.193	4.176	4.093				
	4.223	4.609	4.545		4.461		4.363	4.088	3.711		
4.401		4.366	4.107		3.900		3.661	3.684		3.594	16
	4.181	4.229	4.110		3.953		3.807	3.684	3.700		
			3.679	3.615	3.537	3.503	3.474				
			4.486	4.621	4.534	4.518	4.402				
	4.559	5.122	5.068		4.945		4.863	4.567	4.031		
4.792		4.829	4.585		4.345		4.113	4.139		3.959	17
	4.599	4.705	4.502		4.276		4.090	3.881	3.827		
			4.051	3.997	3.921	3.872	3.823				
			4.637	4.778	4.619	4.598	4.475				
	4.573	5.232	5.329		5.267		5.192	4.878	4.278		
4.918		5.141	4.991		4.816		4.527	4.576		4.320	18
	4.866	5.075	4.920		4.720		4.491	4.233	4.083		
			4.439	4.430	4.395	4.328	4.244				

			4.445	4.583	4.536	4.515	4.387				
	4.291	4.820	5.048		5.165		5.119	4.778	4.294		
4.697		5.031	5.076		4.944		4.601	4.652		4.395	19
	4.779	5.035	5.074		5.041		4.767	4.420	4.215		
			4.578	4.598	4.613	4.531	4.415				
			4.301	4.427	4.502	4.480	4.361				
	4.129	4.445	4.698		4.928		4.911	4.616	4.226		
4.481		4.801	4.949		4.756		4.420	4.442		4.249	20
	4.591	4.729	4.815		4.926		4.640	4.265	4.115		
			4.321	4.308	4.331	4.285	4.180				
			4.285	4.370	4.390	4.369	4.277				
	4.094	4.315	4.533		4.744		4.725	4.507	4.142		
4.393		4.681	4.846		4.552		4.247	4.250		4.174	21
	4.430	4.418	4.413		4.559		4.313	4.065	4.017		
			4.037	3.980	4.010	3.994	3.927				
			4.272	4.315	4.203	4.178	4.129				
	4.096	4.303	4.483		4.628		4.597	4.430	4.090		
4.353		4.619	4.808		4.494		4.116	4.140		4.207	22
	4.326	4.223	4.152		4.291		4.031	3.953	3.987		
			3.890	3.843	3.937	3.947	3.861				
			4.192	4.217	4.062	4.030	3.995				
	4.081	4.292	4.416		4.482		4.456	4.356	4.070		
4.300		4.565	4.793		4.540		3.996	4.025		4.204	23
	4.272	4.128	4.048		4.143		3.866	3.874	3.946		
			3.858	3.844	3.944	3.950	3.850				
			4.102	4.149	4.029	3.987	3.945				
	4.057	4.231	4.304		4.304		4.300	4.282	4.076		
4.228		4.533	4.720		4.607		3.925	3.886		4.145	24
	4.227	4.095	3.997		4.010		3.738	3.725	3.808		
			3.837	3.799	3.815	3.816	3.729				
			4.079	4.134	4.064	4.018	3.959				
	4.019	4.164	4.185		4.131		4.146	4.188	4.026		
4.136		4.489	4.587		4.544		3.874	3.734		3.980	25
	4.151	4.055	3.930		3.893		3.646	3.579	3.649		
			3.728	3.633	3.571	3.588	3.537				
			4.040	4.090	4.055	4.012	3.946				
	3.970	4.118	4.123		4.030		4.028	4.097	3.949		
4.040		4.413	4.448		4.372		3.827	3.650		3.836	26
	4.106	4.037	3.852		3.802		3.580	3.529	3.586		
			3.548	3.412	3.331	3.375	3.359				
			3.908	3.946	3.944	3.911	3.863				
	3.893	4.041	4.085		3.986		3.904	3.991	3.856		
3.963		4.321	4.315		4.172		3.789	3.599		3.748	27
	4.093	3.999	3.762		3.738		3.587	3.607	3.617		
			3.387	3.261	3.216	3.295	3.307				

			3.745	3.763	3.791	3.773	3.752				
	3.862	3.954	4.020		3.941		3.775	3.889	3.793		
3.907		4.197	4.151		4.005		3.746	3.552		3.748	28
	4.084	3.947	3.660		3.685		3.637	3.702	3.664		
			3.293	3.196	3.202	3.311	3.330				
			3.637	3.623	3.665	3.646	3.642				
	3.856	3.901	3.920		3.836		3.657	3.755	3.699		
3.862		4.067	3.998		3.895		3.690	3.523		3.745	29
	4.059	3.887	3.603		3.646		3.666	3.708	3.668		
			3.262	3.187	3.205	3.309	3.338				
			3.612	3.589	3.573	3.557	3.538				
	3.817	3.876	3.832		3.723		3.549	3.586	3.586		
3.808		3.972	3.895		3.847		3.633	3.497		3.719	30
	4.019	3.847	3.602		3.632		3.647	3.614	3.621		
			3.261	3.174	3.142	3.230	3.270				
			3.627	3.629	3.512	3.507	3.449				
	3.699	3.790	3.790		3.683		3.482	3.444	3.475		
3.749		3.971	3.887		3.868		3.634	3.474		3.648	31
	3.954	3.811	3.637		3.665		3.630	3.533	3.552		
			3.279	3.171	3.092	3.166	3.199				
			3.676	3.690	3.540	3.537	3.441				
	3.581	3.694	3.795		3.755		3.524	3.417	3.418		
3.750		4.038	3.985		3.966		3.713	3.491		3.574	32
	3.901	3.820	3.723		3.746		3.680	3.527	3.508		
			3.336	3.228	3.171	3.233	3.232				
			3.773	3.790	3.701	3.685	3.571				
	3.551	3.717	3.894		3.952		3.738	3.582	3.455		
3.843		4.170	4.191		4.172		3.882	3.605		3.577	33
	3.976	3.950	3.905		3.898		3.819	3.604	3.541		
			3.461	3.392	3.361	3.414	3.392				
			3.871	3.919	3.916	3.895	3.784				
	3.617	3.861	4.101		4.206		4.041	3.885	3.622		
3.994		4.382	4.445		4.458		4.115	3.834		3.754	34
	4.181	4.207	4.174		4.135		4.063	3.826	3.747		
			3.622	3.566	3.547	3.621	3.610				
			3.923	4.003	4.054	4.041	3.937				
	3.759	4.024	4.316		4.433		4.319	4.126	3.778		
4.169		4.610	4.653		4.674		4.367	4.093		3.993	35
	4.393	4.466	4.408		4.391		4.349	4.135	4.016		
			3.763	3.716	3.718	3.831	3.818				

J.3.3 13 CIRCULAR PIPE DIFFUSER, 100% SPEED, NEAR CHOKE

			3.588	3.713	3.702	3.481	3.383				
	3.499	3.949	4.130		3.880		3.651	3.539	3.246		
3.397		3.671	3.747		3.533		3.285	3.173		3.211	1
	3.809	3.964	3.781		3.899		3.740	3.352	3.375		
			3.765	3.505	3.280	3.380	3.304				
			3.757	3.896	3.899	3.642	3.522				
	3.694	4.221	4.416		4.134		3.890	3.835	3.466		
3.677		3.989	4.066		3.795		3.446	3.387		3.467	2
	4.067	4.261	4.018		4.097		3.864	3.482	3.478		
			4.024	3.745	3.493	3.554	3.450				
			3.733	3.852	3.879	3.625	3.513				
	3.712	4.191	4.420		4.179		3.942	3.915	3.575		
3.849		4.126	4.173		3.944		3.511	3.494		3.565	3
	4.148	4.403	4.165		4.189		3.887	3.443	3.402		
			4.287	4.005	3.749	3.745	3.603				
			3.613	3.683	3.730	3.532	3.439				
	3.547	3.914	4.169		4.045		3.876	3.812	3.538		
3.752		3.963	3.984		3.877		3.472	3.450		3.486	4
	3.962	4.283	4.186		4.194		3.817	3.318	3.288		
			4.387	4.091	3.851	3.800	3.644				
			3.514	3.564	3.611	3.451	3.376				
	3.392	3.691	3.922		3.920		3.847	3.722	3.465		
3.547		3.719	3.714		3.720		3.446	3.419		3.466	5
	3.715	4.043	4.044		4.100		3.755	3.294	3.310		
			4.223	3.914	3.669	3.613	3.495				
			3.448	3.497	3.516	3.368	3.298				
	3.298	3.598	3.772		3.839		3.838	3.705	3.448		
3.367		3.543	3.543		3.580		3.425	3.435		3.561	6
	3.536	3.804	3.785		3.883		3.665	3.272	3.310		
			3.978	3.634	3.371	3.343	3.259				
			3.401	3.460	3.461	3.297	3.229				
	3.295	3.618	3.698		3.731		3.790	3.722	3.458		
3.316		3.468	3.479		3.498		3.366	3.450		3.656	7
	3.460	3.646	3.567		3.652		3.508	3.228	3.278		
			3.717	3.378	3.140	3.149	3.076				
			3.364	3.435	3.442	3.279	3.199				
	3.306	3.678	3.672		3.640		3.713	3.712	3.447		
3.398		3.470	3.515		3.484		3.295	3.410		3.657	8
	3.492	3.607	3.456		3.474		3.380	3.207	3.262		
			3.538	3.224	3.021	3.051	2.976				
			3.326	3.399	3.435	3.300	3.218				
	3.303	3.680	3.625		3.599		3.634	3.637	3.395		
3.515		3.482	3.547		3.514		3.258	3.334		3.570	9
	3.557	3.653	3.436		3.371		3.331	3.190	3.205		
			3.490	3.206	3.005	3.007	2.903				

			3.294	3.364	3.438	3.328	3.246				
	3.288	3.628	3.538		3.568		3.594	3.572	3.331		
3.545		3.447	3.499		3.502		3.220	3.257		3.465	10
	3.554	3.667	3.420		3.309		3.287	3.098	3.059		
			3.541	3.256	3.016	2.934	2.800				
			3.274	3.346	3.439	3.307	3.235				
	3.304	3.609	3.446		3.508		3.569	3.554	3.287		
3.539		3.383	3.380		3.422		3.185	3.200		3.382	11
	3.501	3.603	3.350		3.268		3.236	2.976	2.930		
			3.542	3.243	2.975	2.841	2.692				
			3.251	3.331	3.389	3.248	3.192				
	3.331	3.616	3.413		3.446		3.523	3.537	3.251		
3.552		3.342	3.295		3.322		3.162	3.161		3.343	12
	3.437	3.484	3.236		3.216		3.215	2.952	2.902		
			3.470	3.150	2.885	2.786	2.666				
			3.219	3.280	3.294	3.183	3.144				
	3.365	3.624	3.417		3.373		3.420	3.456	3.222		
3.591		3.365	3.326		3.276		3.136	3.137		3.362	13
	3.408	3.413	3.147		3.156		3.229	3.055	2.978		
			3.340	3.013	2.779	2.783	2.705				
			3.195	3.233	3.221	3.149	3.104				
	3.369	3.589	3.406		3.297		3.295	3.350	3.171		
3.584		3.433	3.443		3.307		3.111	3.115		3.384	14
	3.432	3.409	3.068		3.087		3.242	3.185	3.090		
			3.255	2.924	2.711	2.789	2.731				
			3.193	3.217	3.209	3.155	3.097				
	3.350	3.520	3.409		3.275		3.207	3.249	3.122		
3.520		3.534	3.610		3.429		3.147	3.096		3.370	15
	3.504	3.454	3.041		3.069		3.247	3.257	3.186		
			3.220	2.900	2.714	2.797	2.735				
			3.250	3.284	3.299	3.263	3.197				
	3.402	3.551	3.523		3.408		3.258	3.220	3.089		
3.547		3.772	3.873		3.674		3.305	3.132		3.327	16
	3.661	3.602	3.122		3.152		3.306	3.291	3.218		
			3.288	2.971	2.811	2.872	2.803				
			3.606	3.663	3.712	3.652	3.547				
	3.760	3.957	3.903		3.771		3.599	3.498	3.266		
3.913		4.273	4.345		4.096		3.652	3.321		3.404	17
	3.997	3.959	3.416		3.412		3.502	3.424	3.346		
			3.507	3.185	2.992	3.023	2.941				
			3.974	4.051	4.094	3.963	3.834				
	4.122	4.410	4.375		4.225		4.046	3.962	3.589		
4.360		4.834	4.853		4.557		4.124	3.746		3.774	18
	4.322	4.342	3.792		3.772		3.873	3.763	3.637		
			3.919	3.595	3.371	3.380	3.267				

			4.054	4.121	4.128	3.963	3.852				
	4.179	4.536	4.596		4.471		4.319	4.327	3.882		
4.511		5.055	5.124		4.863		4.520	4.146		4.172	19
	4.433	4.488	4.142		4.141		4.226	4.049	3.890		
			4.242	3.929	3.719	3.699	3.568				
			3.799	3.818	3.836	3.754	3.689				
	3.874	4.193	4.371		4.317		4.153	4.186	3.818		
4.307		4.896	5.049		4.891		4.593	4.254		4.234	20
	4.382	4.373	4.194		4.253		4.380	4.092	3.955		
			4.222	3.946	3.770	3.742	3.636				
			3.613	3.609	3.622	3.603	3.554				
	3.574	3.841	4.078		4.087		3.896	3.859	3.652		
4.020		4.604	4.820		4.797		4.454	4.098		3.964	21
	4.257	4.189	4.061		4.136		4.274	3.976	3.911		
			4.026	3.741	3.513	3.489	3.426				
			3.463	3.477	3.487	3.470	3.420				
	3.369	3.612	3.892		3.956		3.693	3.543	3.449		
3.792		4.367	4.587		4.692		4.320	3.960		3.716	22
	4.118	4.066	3.941		3.959		4.069	3.826	3.805		
			3.857	3.551	3.295	3.298	3.274				
			3.287	3.323	3.331	3.306	3.260				
	3.208	3.447	3.754		3.915		3.630	3.379	3.321		
3.587		4.188	4.422		4.527		4.118	3.778		3.568	23
	3.980	3.993	3.902		3.901		3.893	3.683	3.673		
			3.740	3.445	3.210	3.216	3.184				
			3.139	3.178	3.206	3.192	3.148				
	3.090	3.307	3.621		3.861		3.650	3.359	3.284		
3.479		4.085	4.295		4.311		3.844	3.515		3.401	24
	3.897	3.961	3.887		3.837		3.708	3.520	3.549		
			3.672	3.403	3.194	3.192	3.124				
			3.055	3.109	3.154	3.144	3.100				
	3.031	3.232	3.532		3.796		3.708	3.447	3.339		
3.431		4.002	4.141		4.111		3.628	3.289		3.221	25
	3.829	3.912	3.856		3.766		3.557	3.398	3.456		
			3.640	3.366	3.156	3.119	3.019				
			3.068	3.136	3.203	3.150	3.106				
	3.073	3.255	3.487		3.723		3.718	3.483	3.319		
3.467		3.923	3.978		4.002		3.550	3.153		3.066	26
	3.781	3.869	3.830		3.754		3.507	3.337	3.369		
			3.600	3.299	3.056	3.002	2.900				
			3.103	3.180	3.231	3.142	3.103				
	3.119	3.319	3.492		3.699		3.722	3.474	3.237		
3.508		3.810	3.845		3.935		3.493	3.106		2.974	27
	3.717	3.802	3.769		3.795		3.528	3.354	3.342		
			3.586	3.273	3.002	2.953	2.840				

			3.084	3.143	3.174	3.100	3.077				
	3.102	3.355	3.520		3.663		3.676	3.436	3.167		
3.520		3.736	3.743		3.845		3.401	3.073		2.911	28
	3.674	3.729	3.684		3.807		3.528	3.348	3.302		
			3.556	3.222	2.949	2.955	2.851				
			3.029	3.064	3.094	3.078	3.072				
	3.061	3.376	3.559		3.588		3.590	3.396	3.141		
3.489		3.726	3.677		3.704		3.275	2.998		2.858	29
	3.654	3.662	3.565		3.744		3.495	3.278	3.220		
			3.493	3.136	2.865	2.926	2.847				
			3.022	3.036	3.085	3.096	3.079				
	3.082	3.398	3.545		3.484		3.471	3.320	3.078		
3.457		3.710	3.634		3.548		3.165	2.893		2.835	30
	3.653	3.645	3.457		3.624		3.464	3.171	3.125		
			3.412	3.047	2.773	2.902	2.855				
			3.063	3.085	3.116	3.106	3.059				
	3.171	3.435	3.481		3.411		3.382	3.223	2.999		
3.419		3.619	3.580		3.421		3.105	2.832		2.823	31
	3.656	3.649	3.390		3.519		3.435	3.108	3.094		
			3.368	3.012	2.730	2.908	2.882				
			3.115	3.146	3.155	3.077	3.003				
	3.245	3.476	3.452		3.373		3.303	3.137	2.943		
3.354		3.496	3.490		3.335		3.090	2.838		2.845	32
	3.642	3.652	3.381		3.483		3.432	3.095	3.110		
			3.390	3.046	2.772	2.961	2.945				
			3.187	3.240	3.216	3.086	3.011				
	3.286	3.538	3.534		3.403		3.254	3.096	2.927		
3.277		3.428	3.425		3.283		3.101	2.881		2.888	33
	3.619	3.672	3.435		3.560		3.479	3.114	3.132		
			3.454	3.142	2.894	3.067	3.044				
			3.343	3.410	3.382	3.237	3.155				
	3.363	3.697	3.751		3.557		3.334	3.195	2.996		
3.262		3.491	3.487		3.333		3.170	2.969		3.005	34
	3.673	3.792	3.588		3.731		3.585	3.209	3.213		
			3.606	3.340	3.094	3.234	3.190				
			3.580	3.679	3.653	3.474	3.370				
	3.592	4.021	4.098		3.846		3.591	3.480	3.198		
3.458		3.782	3.784		3.528		3.325	3.182		3.248	35
	3.901	4.070	3.848		3.950		3.716	3.395	3.402		
			3.798	3.546	3.287	3.391	3.335				